Contents

Deposits of coal slurry as secondary resources of hard coal

***Wiesław Blaschke*[1], *Ireneusz Baic*[2], *Wojciech Sobko*[3] *and* *Beata Witkowska-Kita*[4]**

The article describes comprehensively, on the basis of inventoried sites, issues related to the suitability of coal slurry deposits for the energetic and economical application. The effect of inventory was the localisation of 62 coal-slurry deposits in which almost 16,5 mln Mg of coal slurry was stored. Due to the fact that part of the sites, on which coal slurry was stored, were subject to anthropogenic transformation a mathematical formula was developed that allows determining with the assumed accuracy the amounts of coal slurry produced and environmentally stored. The conducted estimated analysis, using this formula, showed that since 1945, there have been nearly 120 mln Mg of coal slurry stored in the environment that is eight times more than it was inventoried and what is currently recognised in official statistics. In order to develop the most cost-effective beneficiation technology of inventoried coal slurry deposits, detailed qualitative studies were conducted afterwards. They were carried out on the basis of an authorial research methodology which defines the scope of necessary physical and chemical parameters that must be determined for the particular samples of coal slurry. The obtained results show significant diversification in the quality of coal slurries stored in the particular settling ponds. The reason for this is the diversification of types of technological coal that come from the particular coal mines that used these settling ponds, as well as the efficiency of the technological solutions in terms of preparation processes applied by the particular coal mines. For this reason, there was an individual approach necessary to develop technologies of their preparation in order to obtain a full value fuel that meets the requirements set by the power sector. In the paper, the results of the analysis of the energetic potential of identified coal slurry deposits before and after the preparation process are also presented. Estimation of energetic potential was made using the authorial double-option algorithm. The presented results of coal slurry preparation studies and the analysis of their energetic potential have shown that as a result of preparation a significant amount of this potential is lost. This is the effect of movement of the finest grain of coal grains to refuse. The most favourable results, meaning the smallest losses of energetic potential according to the preparation results, were obtained using flotation technology. The conducted tests enable one to conclude that there is a possibility of preparation of coal slurry stored in the deposits. However, considerable losses of the energetic potential of these materials should be expected.

Keywords: *coal slurry deposits, coal waste, settling ponds, waste treatment technology, preparation of coal*

Introduction

Run-of-mine coal is a mixture of coal and waste rock particles which is of virtually no usable value on the market. In order to obtain a commercial product, run-of-mine coal is subjected to preparation processes in coal preparation plants. In industrial conditions, this process is based on methods of gravity preparation in a water medium or dense (magnetite) media. Methods for production of commercial coal that have been established and modified for years generate a considerable amount of by-products in the form of coal slurry.

Issues of processing and preparation of coal slurry deposits were the subject of many tests and analysis in Poland (Białas et al., 2001; Gawlik, 2005; Lorenz and Ozga-Blaschke, 2005) and other countries (Hlavata and Cablik, 2012; Rotunajanu and Lazar, 2014). However, they concerned only certain aspects like chemical properties, physical characteristics and economic application (Aghazadeh, Gharabaghi and Azadmehr, 2016; Galos and Szlugaj, 2014; Grudziński, 2005). Also carried out research on the content of heavy metals in sludge and their impact on the environment (Białecka, Grabowski and Bajerski, 2016; Yilmaz, 2011).

In 2009–2012, the Centre for Waste Management and Environmental Management, a Branch of the Institute of Mechanised Construction and Rock Mining, together with the Department of Mineral Processing and Waste Utilisation of The Silesian University of Technology implemented research and development project no. N R09 0006 06/2009 entitled "Identification of coal slurry deposits in Poland's fuel balance and technological development strategy for their utilisation" (Development Project No. N R09 006, 2009).

The main objective of the project was to determine the possibility of integrating the existing deposits of coal slurry, directly or through appropriate preparation processes, into Poland's fuel balance.

The first thing done as part of the project mentioned above was an inventory of the existing slurry deposits and their quantitative and qualitative assessment. Then, a mathematical model was developed to calculate the energy potential of each of the deposits, which will make it possible in the future to identify potential customers

[1] *Wiesław Blaschke*, Institute of Mechanised Construction and Rock Mining, Branch in Katowice, Al. W Korfantego 193A 40-157 Katowice, Poland wsblaschke@gmail.com

[2] *Ireneusz Baic*, Institute of Mechanised Construction and Rock Mining, Branch in Katowice, Al. W Korfantego 193A 40-157 Katowice, Poland i.baic@imbigs.pl

[3] *Wojciech Sobko*, Institute of Mechanised Construction and Rock Mining, Branch in Katowice, Al. W Korfantego 193A 40-157 Katowice, Poland w.sobko@imbigs.pl

[4] *Beata Witkowska-Kita*, Institute of Mechanised Construction and Rock Mining, Branch in Katowice, Al. W Korfantego 193A 40-157 Katowice, Poland b.witkowska@imbigs.pl

and the quantities of possible supplies. On the basis of the assessment of the impact of the listed coal slurry deposits on various components of the environment and considering the score evaluation system developed, a ranking list of the deposits with potentially the greatest threat to the environment was compiled: the list takes into account the current status of the deposit, the phase of its possible exploitation and the status after completion of the exploitation. Also determined were future trends, scope and design guidelines for prospective reclamation of land left after exploitation of coal slurry deposits (Brenek, Santarius and Hudecek; 2014). For the coal slurry deposits that were inventoried and characterised qualitatively and quantitatively, technologies were developed to prepare them up to fully usable fuel for utility power plants. These technologies take into account the diverse physical structure and chemical properties of these slurries. Areas of potential utilisation of waste produced during preparation of coal slurry deposits were identified.

The final stage of the project comprised proposals of technical, organisational and legal solutions – along with the strategy of technological development – aimed at using in domestic power industry the coal slurries inventoried quantitatively and qualitatively (Baic, 2015; Blaschke and Baic, 2012; Development Project No. N R09 006, 2009). This article presents the results of quantitative and qualitative analysis of the chemical, physical and energy properties of the coal slurry deposits inventoried in the Silesian Province.

The methodology of identification of coal slurry deposits in the Upper Silesian coal basin

In order to identify existing coal slurry deposits, information from the following databases and documents was analysed: Register of Mining Areas (ROG), the MIDAS Database, and Regional Geographical Information System for the province of Silesia (RSIP) and other planning documents, such as reports on implementation of waste management plans, environmental protection programs, environmental surveys and others. It has been found from the scope of this information that it is too general and can only provide an indication as to the information about the owner and the location of a given deposit of coal slurry. Also, it has been found that the information about the amount of coal slurry deposited is not regularly updated, which in the current market situation (change of ownership, exploitation, and land reclamation) prevents their utilisation (Baic, Blaschke and Sobko, 2011; Baic, Sobko and Łukowska, 2012; Lutyński, A., Suponik and Lutyński, M., 2013).

Therefore a questionnaire was carried out among selected business entities currently producing coal slurry, which control lands on which deposits of coal slurry are located, and among the institutions which may store archival documents. As a result of the questionnaire and numerous site visits, 62 settling ponds were located, where nearly 16.5 million Mg of coal slurry is deposited. A summary of the coal slurry deposits inventoried (without information about their location or the users, due to confidentiality clauses with the owners of these facilities), is shown in Table 1 (Baic, Blaschke and Sobko, 2011; Baic, Sobko and Łukowska, 2012).

Tab. 1. A list of coal slurry deposits inventoried.

No.	**Deposit No.**	**Number of ponds**	**Mass of coal slurry deposited** [Mg]
1.	K18	1	200000
2.	K4/1-19	19	1102000
3.	K11/1-3	3	1521000
4.	K12/1-5	5	65000
5.	K1/1-2	2	228000
6.	K17	1	130000
7.	K2/1-2	2	460000
8.	K3/1-2	2	1293000
9.	K6	1	163000
10.	K7	1	644000
11.	K5/1-4	4	620000
12.	K9/1-2	2	560000
13.	K10	1	100000
14.	K8	1	150000
15.	K13	1	670000
16.	K14	1	221000
17.	K15	1	42250
18.	K16	1	25000
19.	K19/1-3	3	580000
20.	K20	1	800000
21.	K21	1	40000
22.	K22/1-2	2	1261600
23.	K23	1	1365000
24.	K24/1-2	2	100000
25.	W1/1	1	1629000
26.	W2/2-3	2	2498000
TOTAL		**62**	**16467850**

Due to the fact that some of the areas in which coal slurry was deposited in the 1990s have been anthropogenically transformed into recreational areas, industrial sites, water reservoirs, etc., a mathematical formula was developed which makes it possible to estimate the amount of coal slurry produced between 1945 and 1989. An estimate analysis conducted using the mathematical formula showed that almost 120 million Mg of coal slurry had been deposited in the environment since 1945, which is eight times more than inventoried and is now reported in the official statistics.

Chemical properties of coal slurry deposits

In order to develop the most cost-effective preparation technology, chemical properties of coal slurry samples from the inventoried deposits were studied. For this purpose, a research algorithm was developed and the scope of necessary properties defined. First of all, the chemical composition of coal slurry samples was analysed for the content of SiO_2, Al_2O_3, TiO_2, Fe_2O_3, CaO, MgO, K_2O, Na_2O, S_c, C, P_2O_5 in order to characterise them qualitatively (Baic, 2013; Baic, 2015; Baic et al., 2012; Blaschke W. and Blaschke Z., 2005). Limiting the results of the chemical composition analysis of coal slurry from all the deposits studied are shown in Table 2. This table also gives the research method used to investigate the chemical composition of the coal slurry samples.

Tab. 2. Results of the chemical composition of coal slurry samples.

No.	Component	Limiting content [%]	The method according to Polish Standard
1.	SiO_2	27.81–63.96	PN-G-04528/03:1977
2.	Al_2O_3	4.83–10.26	PN-G-04528/04:1977
3.	TiO_2	0.01–0.30	PN-G-04528/08:1978
4.	Fe_2O_3	0.46–1.78	PN-G-04528/04:1977
5.	CaO	0.01–0.14	PN-G-04528/06:1977
6.	MgO	0.35–1.20	PN-G-04528/07:1977
7.	K_2O	1.19–2.98	PN-G-04528/10:1998
8.	Na_2O	0.32–1.33	
9.	S_c	0.57–2.98	PN-90/G04514/16
10.	C	11.15–31.80	PN-B-04481:1988
11.	P_2O_5	0.001–0.015	PN-G-04528/11:1979

Based on these studies, it was found that the main constituents of coal slurry samples are silica (27.81–63.96 %) and carbon (11.15–31.80 %). Such a composition is typical of a fine-grained waste of this type. The values that deviate from the data reported in the literature are very low Al_2O_3 and TiO_2 contents.

Direct analysis of slurry samples covered tests for the presence of such metals as arsenic, barium, chromium, tin, zinc, aluminium, cadmium, cobalt, magnesium, manganese, copper, molybdenum, nickel, lead, mercury, vanadium and calcium. The contents of these metals were determined by atomic emission spectrometry with inductively coupled plasma (ICP-AES) using a JY 2000 spectrometer. Table 3 shows the results for barium, zinc, cobalt and nickel, the content of which exceeded the maximum permissible concentrations in soils, according to the regulation by the Minister of Environment of 1 September 2016 (Dz. U. 2016, item. 1395).

Tab. 3. Results of the determination of selected metals in coal slurry samples.

Deposit No.	Metals			
	Barium	Zinc	Cobalt	Nickel
	[mg/kg dry weight]			
MPC[1)]	**200.00**	**300.00**	**20.00**	**100.00**
K18	417.92	499.69	92.67	178.98
K11	877.98	601.27	184.03	102.10
K3	1123.4	405.96	144.23	156.08
K4	n.e.	n.e.	85.67	n.e.
K6	534.67	n.e.	n.e.	n.e.
K2	333.24	n.e.	55.68	n.e.
K17	777.27	n.e.	49.35	n.e.
K1	422.37	n.e.	38.55	n.e.
K5/1	423.91	n.e.	55.22	n.e.
K5/4	599.06	n.e.	20.33	n.e.

MPC [1)]– maximum permissible concentrations of heavy metals in the soil - land II-1 (Dz.U. 2016, item. 1395)
n.e. - not exceeded

It was found that the cases of exceeded permissible concentrations of the metals mentioned above are not only due to their presence in the exploited deposit but also to anthropogenic pollutants and their presence in the land surrounding the area of the deposits studied. The results for the other metals did not exceed the permissible values of concentrations in soil (land II-1) in accordance with this Regulation.

Also analysed water extracts of coal slurry samples, which were prepared in accordance with PN - EN 12457-4:2006 standard. The scope of the study included the following basic properties: conductivity, pH, TDS, COD_{Cr}, phenols, ammonium nitrogen, nitrates(V), nitrates(III), cyanides, chlorides, sulphates(VI), sulphides, chromium(VI). Determination of metal content (the list of metals similar as in the case of direct analysis) of the waters extracts was performed by atomic emission spectrometry with inductively coupled plasma (ICP-AES) using a JY 2000 spectrometer.

Table 4 shows the results of the analysis of aqueous extracts of the slurry deposit samples for metals whose maximum permissible values were exceeded (barium, zinc, cobalt and nickel).

Tab. 4. Results of the analysis of water extracts of coal slurry deposit samples.

Deposit No.	Metals			
	Barium	Zinc	Cobalt	Nickel
	[mg/l]			
MPV[1)]	**2.000**	**2.000**	**1.000**	**0.500**
K18	0.880	0.055	0.088	0.440
K11	0.068	0.108	0.183	0.440
K3	0.633	1.220	0.177	1.020
K4	0.055	0.102	0.067	0.009
K6	1.550	0.089	0.011	0.010
K2	0.777	0.022	0.022	0.011
K17	1.120	0.011	0.980	0.055
K1	0.858	0.009	0.013	0.009
K5/1	0.023	0.089	0.022	0.098
K5/4	0.010	0.033	0.032	0.011

MPV[1)] - maximum permissible value, (Dz.U. 2014, item. 1800)

Analysis of water extracts of coal slurry samples for all basic properties and all analysed metals showed no exceeded maximum permissible values of substances harmful to the water environment in accordance with the Regulation of the Minister of Environment of 18 November 2014 (Dz.U. 2014, item. 1800). Consequently, it was concluded that the metals whose concentrations were found by direct analysis to be exceeded occur in bound forms, thus posing no threat to the environment.

Physical characteristics of coal slurry deposits

Coal slurry from the identified sedimentary ponds was studied in accordance with the methodology adopted. Basic scope of qualitative analysis was performed to determine (Baic, 2013; Baic, 2015; Baic, Blaschke and Grudziński, 2011; Lutyński and Szpyrka, 2012):

- surface moisture content W_{ex} and hygroscopic moisture content W_h (PN-80/G-04511, PN-80/G-04511, PN-G-04560:1998, PN-80/G-04511),
- ash content of the slurry on an air-dried basis A^a, on an "as-received" basis A^r and a dry basis A^d, (PN-G-04560:1998, PN-80/G-04512),
- sulphur content of the slurry on an air-dried basis S_t^a, on an "as-received" basis S_t^r and on a dry basis S_t^d (PN-90/G-04514/16),
- volatile matter content of the slurry on an air-dried basis V^a, on an "as-received" basis V^r and on a dry basis V^d (PN-G-04516:1998, PN-G-04560:1998, PN-ISO 562:2000)
- net calorific value of the slurry on an air-dried basis Q^a, on an "as-received" basis Q^r and on a dry basis Q^d (PN-81/G-04513).

Next, grain size analysis and densimetric analysis were performed on averaged samples. For each grain size fraction and density fraction, the following quantities were determined:

- yield,
- hygroscopic moisture W_h,
- ash content of the slurry on an air-dried basis A^a and a dry basis A^d,
- sulphur content of the slurry on an air-dried basis S_t^a and on a dry basis S_t^d,
- volatile matter content of the slurry on an air-dried basis V^a on a dry basis V^d,
- the calorific value of the slurry on an air-dried basis Q^a and on a dry basis Q^d.

The samples were prepared for the analysis in accordance with PN-90/G-04502. The results of the analysis of physical properties carried out on coal slurry samples of the slurry are shown in Tables 5 and 6. Table 5 presents a summary of the results of the physical properties of coal slurry on an air-dried basis as statistical averages and the standard deviation of these averages for each deposit. Table 6 presents the results of the

physical properties of the coal slurry on an air-dried basis and dry basis in the grain size fraction <0.1 mm, as this grain fraction has the greatest share in the coal slurries analysed.

Tab. 5. Summary of the results of the physical properties of coal slurry on an air-dried basis.

Deposit No.	**Ash content** [%]	**Standard deviation of the ash content** [%]	**Total sulphur content** [%]	**Standard deviation of the total sulphur content** [%]	**Volatile matter content** [%]	**Standard deviation of the volatile matter content** [%]	**Net calorific value** [MJ/Mg]	**Standard deviation of the net calorific value** [MJ/Mg]
K13	27.47	2.99	1.90	0.84	28.50	4.32	15096	1509
K14	32.98	2.58	0.72	0.03	23.85	0.41	15646	829
K12	41.36	1.41	0.86	0.10	21.31	1.25	14813	581
K18/1	63.96	9.06	0.57	0.16	14.38	2.55	9325	2052
K18/2	63.04	17.76	0.64	0.25	14.39	5.47	10073	2746
K11/1	49.48	5.39	0.88	0.34	18.50	1.76	13297	2413
K3/1	60.43	10.56	0.70	0.20	16.41	3.13	9265	3498
K3/2	45.90	12.59	2.98	1.27	18.01	2.23	14877	5976
K2	58.34	8.24	2.26	0.67	14.29	1.17	12304	2803
K17	28.41	4.23	0.95	0.11	23.47	1.33	22807	1538
K1	26.98	3.46	0.95	0.15	23.77	0.75	23293	1444
K4/1	27.89	0.32	0.97	0.13	23.79	0.71	22941	590
K4/2	47.22	2.55	0.59	0.11	18.89	0.29	15813	937
K4/3	31.84	4.51	0.79	0.13	23.85	1.25	20828	2065
K5/1	53.79	5.17	1.21	0.19	16.99	1.52	12051	1504
K5/2	42.86	13.10	1.09	0.38	16.89	2.30	17802	5351
K5/3	37,59	1.44	0.94	0.08	20.64	0.87	19402	646
K5/4	35.22	1.28	0.97	0.02	21.54	0.40	20351	844
K11/2	37.33	1.29	0.92	0.06	20.72	0.54	19672	767
K6	38.83	5.88	0.94	0.15	20.16	2.12	18887	1834
Average	42.55	-	1.09	-	20.02	-	16427	-
Standard deviation	12.28	-	0.60	-	3.85	-	4520	-

Tab. 6. Summary of the results of the physical properties of coal slurry grain fraction <0.1 mm on an air-dried basis and on a dry basis.

Deposit No.	**Yield of size fraction < 0.1 mm** [%]	**Hygr. moisture** [%]	**Ash content** [%]		**Total sulphur content** [%]		**Volatile matter content** [%]		**Net calorific value** [MJ/Mg]	
	γ	W_h	A^a	A^d	S_t^a	S_t^d	V^a	V^d	Q^a	Q^d
K13	27.90	4.30	53.00	55.38	1.21	1.26	17.21	17.98	12753	13326
K14	60.79	3.97	55.64	57.94	0.66	0.69	12.66	13.19	10185	10606
K12	70.16	4.61	53.02	55.58	0.86	0.90	15.20	15.94	11224	11766
K18/1	69.33	2.99	73.49	75.75	0.44	0.45	10.60	10.93	1684	1736
K18/2	54.75	2.13	77.23	78.91	0.47	0.48	7.92	8.09	6195	6330
K11/1	67.87	4.07	58.94	61.44	0.74	0.77	16.25	16.94	10680	11133
K3/1	28.43	1.51	57.73	58.62	4.15	4.21	15.62	15.86	8914	9051
K3/2	48.36	1.38	67.20	68.14	2.49	2.52	13.56	13.75	6791	6886
K2	57.23	2.56	52.49	53.87	0.67	0.69	16.21	16.63	12386	12712
K17	77.58	2.87	64.43	66.33	1.29	1.33	14.37	14.80	8540	8792
K1	65.75	1.57	49.91	50.71	1.36	1.38	16.15	16.40	15272	15515
K4/1	67.76	2.07	37.03	37.81	0.21	0.21	22.27	22.74	18704	19099
K4/2	54.80	1.92	41.19	42.00	0.38	0.39	20.02	20.41	16406	16727
K4/3	57.57	1.83	39.75	40.49	1.36	1.39	19.91	20.29	17271	17593
K5/1	75.76	1.64	45.53	46.29	0.96	0.98	17.83	18.13	15682	15943
K5/2	72.87	2.03	44.20	45.12	1.00	1.02	18.00	18.37	15464	15784
K5/3	68.53	1.24	42.58	43.11	1.05	1.06	17.98	18.21	16055	16257
K5/4	68.12	2.08	43.01	43.92	1.04	1.06	18.42	18.81	18118	18503
K11/2	78.93	2.57	63.13	64.80	0.69	0.71	14.30	14.68	7388	7583
K6	72.97	1.33	57.24	58.01	0.61	0.62	16.36	16.58	11855	12015
Average	62.27	2.43	53.84	55.21	1.09	1.11	16.04	16.44	12078	12368
Standard deviation	14.26	1.05	11.31	11.71	0,88	0,89	3,30	3,34	4580	4658

Based on the analysis of the results of the qualitative studies it can be stated that:

- the average net calorific value of the coal slurries (on an air-dry basis) deposited in individual settling ponds ranges from 9265 to 23293 MJ/Mg, and the standard deviation of this parameter is in the range from 581 to 5976 MJ/Mg
- the average ash content of the coal slurries (on an air-dried basis) deposited in individual settling ponds ranges from 26.98 to 63.96 % and the standard deviation of this parameter is in the range from 1.28 to 17.76 %,

- the average total sulphur content (on an air-dried basis) of the coal slurries deposited in individual settling ponds ranges from 0.57 to 2.98 % and the standard deviation of this parameter is in the range from 0.03 to 1.27 %,
- the average surface moisture content of the coal slurries deposited in individual settling ponds ranges from 11.69 to 34.48 % and the standard deviation of this parameter is in the range from 1.07 to 4.89 %,
- the average hygroscopic moisture content of the coal slurries deposited in individual settling ponds ranges from 1.04 to 7.92 % and the standard deviation of this parameter is in the range from 0.07 to 2.40 %,
- the average volatile matter content of the coal slurries deposited in individual settling ponds ranges from 14.29 to 28.50 % and the standard deviation of this parameter is in the range from 0.40 to 5.47 %,
- the grain size analysis of the coal slurry has shown that most particles are in the grain-size fraction below 0.1 mm. The average share of grains sized below 0.1 mm in all settling ponds amounts to 62.27 % and ranges for individual ponds ranges from 27.90 % to 78.93 % with a standard deviation of 14.26 % and only three settling ponds contained less than 50 % of this grain size fraction,
- the average net calorific value of the coal slurry (on an air-dried basis) in the grain size fraction below 0.1 mm deposited in individual settling ponds is in the range from 6184 to 18704 MJ/Mg with a standard deviation of 4580 MJ/Mg,
- the grain-size fraction below 0.1 mm, has higher ash and sulphur contents.

The energy potential of coal slurry deposits

The quantitative and qualitative analysis of coal slurry deposits made it possible to estimate the energy potential of these slurries. For this purpose, an algorithm was developed for estimating the energy potential of the deposits inventoried. Two ways of estimating the energy potential were proposed (Baic, 2015; Baic, Lutyński A. and Lutyński M., 2012; Lutyński A. and Lutyński M., 2014). The first of these options is a rough estimate of the energy potential of a deposit, which is based on:

- the estimated mass of coal slurries in the deposit,
- the average net calorific value determined in a qualitative analysis of individual samples collected from the deposit.

This method is used to estimate the average approximate value of the energy potential of the deposit, which is most commonly used and reported in relevant studies. Although this is undoubtedly important information, to make this preliminary information more complete it is also important to specify the limits between which the energy potential of the coal slurry may fluctuate. For this purpose, in addition to the average value of the energy potential, also its limiting values are given, the lower and upper ones, based on the estimated standard deviation of the net calorific value determined for each sample. It is known from the theory of probability that 68 % of the individual estimates obtained from individual samples lie between these limiting values.

Thus, the average approximate value of the energy potential of a deposit (on an as-received basis or an air-dried basis) is estimated from the relationship:

$$E_{av} = M \bullet Q^{rva}_{av} \bullet 10^{-3}, \text{ [GJ]} \quad (1)$$

where:

E_{av} average value of the energy potential of the deposit, [GJ]

M is estimated mass of coal slurries in the deposit, [Mg]

Q^{rva}_{av} average net calorific value (on an as-received basis or an air-dried basis) determined by qualitative analysis of individual samples collected from a deposit, which is estimated from the relationship:

$$Q^{rva}_{av} = \frac{1}{n}\sum_{i=1}^{n} Q^{r}_{i} \text{ [kJ/kg]} \quad (2)$$

The limiting values of the energy potential of a deposit are estimated from the relationships:

$$E_{max} = M \bullet (Q^{rva}_{av} + S_Q) \bullet 10^{-3}, \text{[GJ]} \quad (3)$$

and

$$E_{min} = M \bullet (Q^{rva}_{av} - S_Q) \bullet 10^{-3}, \text{[GJ]} \quad (4)$$

where:

S_Q standard deviation of the net calorific value estimated from the relationship:

$$S_Q = \sqrt{\frac{1}{n-1}\sum_{i=1}^{n}\left(Q^{rva}{}_i - Q^{rva}{}_{av}\right)} \qquad [GJ] \tag{5}$$

The results of the estimation are shown in Tables 7 and 8.

Tab. 7. The energy potential of coal slurry (on dry basis) deposited in settling ponds.

Deposit No.	Approx. weight of the deposit	Average net calorific value	Standard deviation of the net calorific value	Energy potential (as received basis)		
				average	maximal	minimal
	[Mg]	[MJ/Mg]	[MJ/Mg]	[GJ]	[GJ]	[GJ]
K13	1000000	12380	674	12380000	13053891	11706109
K14	300000	12552	607	3765600	3947736	3583463
K12	1000.000	12179	568	12178667	12748949	11610385
K18/1	100000	7737	1673	773747	941065	606428
K18/2	100000	8587	2369	858675	1095554	621796
K11/1	640000	11087	2324	7095825	8583052	5608598
K3/1	1521000	6874	2270	10455354	13907739	7002969
K3/2	176000	13115	4655	2308240	3127660	1488819
K2	1117000	10213	1975	11408107	13614438	9201776
K17	155000	18979	1732	2941794	3210402	2673187
K1	153000	19352	1062	2284311	2409719	2158902
K4/1	345600	19285	1290	6664939	7110828	6219049
K4/2	163000	12038	724	1962221	2080363	1844078
K4/3	460000	16155	1394	7431258	8072425	6790091
K5/1	130000	8256	967	1073316	1199042	947589
K5/2	228000	13648	3628	3111873	3938967	2284779
K5/3	106000	14869	680	1576075	1648248	1503903
K5/4	102000	15385	763	1569270	1647164	1491375
K11/2	176000	15057	464	2650090	2731792	2568388
K6	236000	14636	1268	3453624	3753031	3154214

Tab. 8. The energy potential of coal slurry (on an air-dried basis) deposited in settling ponds.

Deposit No.	Approximate weight of the deposit	Average net calorific value	Standard deviation of the net calorific value	Energy potential (air-dried basis)		
				average	maximal	minimal
	[Mg]	[MJ/Mg]	[MJ/Mg]	[GJ]	[GJ]	[GJ]
K13	1000000	15096	1509	15095667	16604265	13587068
K14	300000	15646	830	4693800	4942657	4444943
K12	1000000	14813	581	14812667	15393327	14232006
K18/1	100000	9325	2052	932547	1137768	727326
K18/2	100000	10073	2747	1007325	1281976	732674
K11/1	640000	13297	2413	8509964	10054237	6965690
K3/1	1521000	9265	3498	14092825	19413371	8772280
K3/2	176000	14877	5976	2618308	3670019	1566597
K2	1117000	12304	2803	13743987	16874910	10613064
K17	155000	22807	1538	3535074	3773403	3296745
K1	153000	23293	1444	3563810	3784749	3342871
K4/1	345600	22941	590	7928525	8132297	7224753
K4/2	163000	15813	937	2577600	2730378	2424822
K4/3	460000	20829	2065	9581173	10530941	8631404
K5/1	130000	12051	1504	1566590	1762060	1371119
K5/2	228000	17802	5351	4058928	5279050	2838807
K5/3	106000	19402	646	2056612	2125131	1988132
K5/4	102000	20351	844	2075761	2161898	1989625
K11/2	176000	19672	767	3462345	3597362	3327329
K6	236000	18887	1834	4457435	4890353	4024518

The second variant of estimating the energy potential of the deposits is based on a deeper knowledge of the material accumulated in the deposit, including knowledge of the future utilisation of the slurry and method of its preparation. The energy potential is estimated based on:

- the defined mass of coal slurries in the deposit,
- the yield of the concentrate obtained using the selected preparation technology,
- the average net calorific value determined for the concentrates obtained from samples prepared by individual technologies.

Because of the need to compare the energy potentials of slurries prepared using different technologies, net calorific values on the air-dried basis were used in the estimation.

The average value of the energy potential of the deposit was estimated from the relationship:

$$E_{av} = M \bullet U \bullet Q^{a}_{av} \bullet 10^{-3} \quad [GJ] \tag{6}$$

where:

E_{av} average estimated value of the energy potential of the deposit [GJ]

M estimated mass of the coal slurries in the deposit, [Mg]

Q^{a}_{av} average net calorific value (on an air-dried basis) determined by qualitative analysis of individual samples prepared using the preparation technology selected, [MJ/Mg]

U yield of the concentrate obtained using the selected preparation technology

The results of the estimation of the energy potential on an air-dried basis for four preparation methods along with the expected loss of this potential are shown in Tables 9, 10, 11 and 12 (Baic, 2015; Baic, Blaschke and Grudziński, 2011; Lutyński A. and Lutyński M., 2014).

Methods used in the study:

- preparation in hydrocyclone with a diameter 150 mm; feed density of 150 g/l,
- preparation in a centrifugal drainer, feed density of 150 g/l; preliminary de-sliming on sieve 0.1 mm,
- preparation in Reichert 5 -spiral of LD 4 type; feed density 400 g/l; preliminary de-sliming on sieve 0.1 mm,
- preparation in flotation machine; feed density 100 g/l; flotation reagent type MONTANOL 505, dose of flotation reagent 0.6 kg/l (Fećko et al., 2011; Szpyrka and Lutyński, 2012; Wang et al., 2014).

Tab. 9. The energy potential of coal slurry in individual deposits *as a result of preparation* in hydrocyclone.

Deposit No.	Raw deposit data			Hydrocyclone			
	Weight	Net calorific value	Potential E_{av}	Recovery	Net calorific value	Potential E_{av}	Loss of potential
	[Mg]	[MJ/Mg]	[GJ]	[-]	[MJ/Mg]	[GJ]	[%]
K13	1000000	15096	15095667	0.47	18121	8516870	44
K14	300000	15646	4693800	0.56	20362	3420816	27
K12	1000000	14813	14812667	0.50	17281	8640500	42
K18/1	100000	9325	932547	0.50	9295	464750	50
K18/2	100000	10073	1007325	0.60	8576	514560	49
K11/1	640000	13297	8509964	0,51	15990	5219136	39
K3/1	1521000	9265	14092825	0.57	16277	12377730	12
K3/2	176000	14877	2618308	0.63	12027	1333553	49
K2	1117000	12304	13743987	0.58	14234	9221639	33
K17	155000	22807	3535074	0.44	13444	916880	74
K1	153000	23293	3563810	0.52	17972	1429852	60
K4/1	345600	22941	7928525	0.51	24363	4294124	49
K4/2	163000	15813	2577600	0.59	24557	2073136	20
K4/3	460000	20828	9581173	0.57	25501	6686362	30
K5/1	130000	12051	1566590	0.46	21415	1180617	25
K5/2	228000	17802	4058928	0.48	21085	2307542	43
K5/3	106000	19402	20566631	0.50	21161	1121533	45
K5/4	102000	20351	2075761	0.51	21844	1136324	45
K11/2	176000	19672	3462345	0.44	12008	92999	97
K6	236000	18887	4457435	0.47	18022	1999000	55
av.	-	16427	-	0.53	16950	-	44

Tab. 10. The energy *potential of coal slurry in individual deposits as a result of preparation in a centrifugal drainer with preliminary de-sliming.*

Deposit No.	Raw deposit data			Centrifugal drainer			
	Weight	Net calorific value	Potential E_{av}	Recovery	Net calorific value	Potential E_{av}	Loss of potential
	[Mg]	[MJ/Mg]	[GJ]	[-]	[MJ/Mg]	[GJ]	[%]
K13	1000000	15096	15095667	0.23	18916	4350680	71
K14	300000	15646	4693800	0.36	20654	2230632	52
K12	1000000	14813	14812667	0.10	22042	2204200	85
K18/1	100000	9325	932547	-	-	-	-
K18/2	100000	10073	1007325	-	-	-	-
K11/1	640000	13297	8509964	0.04	21043	538700	94
K3/1	1521000	9265	14092825	0.14	25840	5502369	61
K3/2	176000	14877	2618308	-	-	-	-
K2	1117000	12304	13743987	0.48	24104	11923600	13
K17	155000	22807	3535074	0.03	18965	88187	97

Deposit No.	Raw deposit data			Centrifugal drainer			
	Weight	Net calorific value	Potential E_{av}	Recovery	Net calorific value	Potential E_{av}	Loss of potential
	[Mg]	[MJ/Mg]	[GJ]	[-]	[MJ/Mg]	[GJ]	[%]
K1	153000	23293	3563810	0.08	25046	306000	91
K4/1	345600	22941	7928525	0.28	24095	2331625	71
K4/2	163000	15813	2577600	0.47	24164	1851204	28
K4/3	460000	20828	9581173	0.52	24315	5816148	39
K5/1	130000	12051	1566590	0.25	24430	793975	49
K5/2	228000	17802	4058928	0.22	24043	1205997	70
K5/3	106000	19402	20566631	0,26	23802	655983	68
K5/4	102000	20351	2075761	0.22	24281	544865	74
K11/2	176000	19672	3462345	0.02	18519	65187	98
K6	236000	18887	4457435	0.08	24124	455461	90
av.	-	16427	-	0.22	22846	-	68

Tab. 11. The energy potential of coal slurry in individual deposits as a result of preparation in Reichert spiral with preliminary de-sliming.

Deposit No.	Raw deposit data			Reichert spiral			
	Weight	Net calorific value	Potential E_{av}	Recovery	Net calorific value	Potential E_{av}	Loss of potential
	[Mg]	[MJ/Mg]	[GJ]	[-]	[MJ/Mg]	[GJ]	[%]
K13	1000000	15096	15095667	0.29	18825	5459250	64
K14	300000	15646	4693800	0.41	20271	2493333	47
K12	1000000	14813	14812667	0.18	21523	3874140	74
K18/1	100000	9325	932547	0.04	21042	92585	90
K18/2	100000	10073	1007325	-	-		-
K11/1	640000	13297	8509964	0.15	20760	1992960	77
K3/1	1521000	9265	14092825	0.23	25843	9040657	36
K3/2	176000	14877	2618308	0.06	24258	150564	94
K2	1117000	12304	13743987	0.50	24335	12602267	9
K17	155000	22807	3535074	0.09	19136	266947	92
K1	153000	23293	3563810	0.14	24241	519000	85
K4/1	345600	22941	7928525	0.30	24459	2535909	68
K4/2	163000	15813	2577600	0.50	23763	1936684	25
K4/3	460000	20828	9581173	0.52	24333	5820454	39
K5/1	130000	12051	1566590	0.30	23352	910728	42
K5/2	228000	17802	4058928	0.27	23666	1456879	64
K5/3	106000	19402	20566631	0.30	24035	764313	63
K5/4	102000	20351	2075761	0.27	24195	666330	68
K11/2	176000	19672	3462345	0.07	18756	231074	93
K6	236000	18887	4457435	0.14	24256	801000	82
av.	-	16427	-	0.25	22687	-	64

Tab. 12. The energy potential of coal slurry in individual deposits as a result of preparation in a flotation machine.

Deposit No.	Raw deposit data			Flotation machine			
	Weight	Net calorific value	Potential E_{av}	Recovery	Net calorific value	Potential E_{av}	Loss of potential
	[Mg]	[MJ/Mg]	[GJ]	[-]	[MJ/Mg]	[GJ]	[%]
K13	1000000	15096	15095667	-	-	-	-
K14	300000	15646	4693800	-	-	-	-
K12	1000000	14813	14812667	-	-	-	-
K18/1	100000	9325	932547	-	-	-	-
K18/2	100000	10073	1007325	-	-	-	-
K11/1	640000	13297	8509964	-	-	-	-
K3/1	1521000	9265	14092825	-	-	-	-
K3/2	176000	14877	2618308	0.45	24687	1955210	25
K2	1117000	12304	13743987	0.41	20670	9466240	31
K17	155000	22807	3535074	0.74	27620	3168014	10
K1	153000	23293	3563810	0.80	27120	3319488	7
K4/1	345600	22941	7928525	0.81	26880	7524680	5
K4/2	163000	15813	2577600	0.65	21525	2280574	11
K4/3	460000	20828	9581173	0.41	24520	4624472	51
K5/1	130000	12051	1566590	-	-		
K5/2	228000	17802	4058928	0.58	24670	3262361	20
K5/3	106000	19402	20566631	0.72	25875	1974780	4
K5/4	102000	20351	2075761	0.71	25810	1869160	10
K11/2	176000	19672	3462345	0.70	25845	3184104	8
K6	236000	18887	4457435	0.72	25465	4327013	3
av.	-	16427	-	0.64	25057	-	15

The results of coal slurry preparation by four methods are shown in Tables 9, 10, 11 and 12, and the analysis of their energy potential showed that a significant part of this potential is lost during the preparation process.

During the preparation process of coal slurry, the smallest losses of energy potential were obtained using flotation machine. In this case, the average loss of the energy potential was 15 %. However, for individual settling ponds, this losses ranged between 3 and 51 %. The average net calorific value of the flotation concentrates obtained by this preparation method was 25,057 MJ/Mg. It was the highest value of all analysed preparation methods. Unfortunately not all coal slurries were sensitive to preparation in flotation machine with the use of flotation reagent type MONTANOL 505 for this studies.

The preparation in a centrifugal drainer with preliminary de-sliming on sieve 0.1 mm turned out less preferred method. In this case, the average losses of the energy potential were 68 %. These losses ranged from 13 % up to 98 % for individual settling ponds. On the other hand, the net calorific value of the concentrates obtained by this preparation method was 22,864 MJ/Mg.

These results were similar to the results obtained by preparation in Reichert spirals with preliminary de-sliming of the feed on sieve 0.1 mm. In this case, the average losses of the energy potential were 64 %, and the average net calorific value of the concentrates was 22,678 MJ/Mg.

During the preparation process of coal slurry in hydrocyclone net calorific value of the concentrate (16,950 MJ/Mg) increased slightly in relation to the net calorific value of the raw slurry (16,427 MJ/Mg). In this case, the average losses of the energy potential were 44 %. For individual settling ponds, the losses of the energy ranged from 12 % up to 97 %. This method should not be used for preparing the coal slurries deposited in the settling ponds.

Based on these studies it can be concluded that it is possible to prepare coal slurry deposited in settling ponds. Most favourable results were obtained using the flotation method. Good quality concentrates one can obtained during the preparation in Reichert spirals and centrifugal drainer. However, in these methods, the average loss of the energy potential is much higher than for flotation.

Discussion of the results

Summing up:

- The inventory of coal slurry deposits has shown that more than 16.5 million Mg of coal slurry is deposited into the environment. When used directly, or after employing an appropriate preparation technology, these slurries can become a valuable fuel for the power industry.
- Estimation analysis employing a mathematical formula presented here showed that almost 120 million Mg of this feedstock had been deposited into the environment since 1945, which is eight times more than evidenced by physical inventory and currently reported in the official statistics.
- Most of the land into which coal slurry was deposited in the 20th century has undergone an anthropogenic transformation, thus preventing exploitation and utilisation of the coal slurry deposited. These areas have been reclaimed, in part or in whole, to become recreational areas or areas with industrial or service facilities.
- The main components of coal slurry samples are silica (27.81-63.96 %) and carbon (11.15-31.80 %). This composition is typical of a fine-grained waste of this type. The values that deviate from the data reported in the literature are very low Al_2O_3 and TiO_2 contents.
- Direct analysis of chemical properties of slurry samples from the inventoried settling ponds showed permissible concentrations of metals such as barium, zinc, cobalt and nickel were exceeded. This is not only due to their presence in the deposit, but also most likely to anthropogenic pollutants, and the presence of these metals in the land surrounding the settling ponds studied.
- Analysis of water extracts of coal slurry samples for basic properties and metals showed no exceeded maximum permissible value of substances harmful to the water environment. This means that the metals present in coal slurry, including those for which the permissible limiting values were found to be exceeded, occur in chemically bonded forms. Consequently, they neither pose a threat to the environment nor do they restrict possible areas of their utilisation.
- The results of physical properties of coal slurry samples studied show a considerable variation in the quality of slurry deposited in individual settling ponds, which is obvious due to the varied geological and mining conditions of individual mines which deposited coal slurry in these ponds.
- The qualitative and quantitative results of coal slurry deposits indicate a significant energy potential, which can be effectively used of appropriate preparation technologies.
- The results of coal slurry preparation by four methods and the analysis of their energy potential have shown that a large amount of this potential is lost as a result of preparation. It is the result of the smallest coal particles passing through to the tailings. Most favourable results were obtained using the flotation method.

- The analysis showed that industrial use of coal slurry would be effective if the method devoided of any additional preparation operations is applied, such as pelletizing (Borowski and Hycnar, 2013; Hycnar and Borowski, 2016; Hycnar and Bugajczyk, 2004).

References

Aghazadeh S., Gharabaghi M., Azadmehr A. (2016). Increasing the useful heating value of coal using a physico-chemical process. *International Journal of Coal Preparation and Utilization, 36(4), s. 175–191*.

Baic I. (2013) Analiza parametrów chemicznych, fizycznych i energetycznych depozytów mułów węglowych zinwentaryzowanych na terenie województwa śląskiego; *Annual Set The Environment Protection, Vol. 15, , Part 2, pp. 1511-1524, Koszalin*

Baic I. (2015) Analiza wielokierunkowego wykorzystania depozytów mułów węglowych wraz z ocena oddziaływania na środowisko*; Studia, Rozprawy, Monografie Nr 191, Wyd. IGSMiE PAN Kraków, s. 1-234, Krakow*

Baic I., Blaschke W., Grudziński Z. (2011) Wstępne badania nad możliwością przewidywania parametrów jakościowych odpadów powstających w procesach wzbogacania węgli kamiennych; *Annual Set The Environment Protection, Vol. 13, Part 2, pp. 1373-1383, Koszalin* .

Baic I., Blaschke W., Sobko W. (2011) Depozyty mułów węglowych – inwentaryzacja i identyfikacja ilościowa; *Annual Set The Environment Protection, Vol. 13, Part 2, pp. 1405-1415, Koszalin* .

Baic I., Lutyński A., Lutyński M. (2012) Potencjał energetycznych zdeponowanych mułów węglowych. *Polityka Energetyczna Vol. 15, issue 3, pp. 259–271, Krakow*

Baic I., Sobko W., Łukowska M. (2012) Inwentaryzacja szacunkowa i in situ depozytów mułów węglowych. *Polityka Energetyczna Vol. 15, issue 3, pp. 221–229, Krakow 2012*.

Baic I. Witkowska-Kita B., Lutyński A., Suponik T. (2012) Parametry chemiczne depozytów mułów węglowych. Baza danych DMW. Polityka Energetyczna Vol. 15, issue 3, pp. 231–245, Kraków 2012

Białas M., Białas J., Lutyński A., Kasztan A., Narloch G. (2001). Wydzielanie ziaren węglowych z zawiesin odpadowych. *Gospodarka Surowcami Mineralnymi, 17, z spec.*

Białecka B., Grabowski J., Bajerski A. (2016) Assessment of the mercury emission from burning mining waste dumps. *Acta Montanistica Slovaca Vol.21, issue 1, pp.29-36. Kosice 2016*

Blaschke W., Baic I. (2012) Problematyka depozytów mułów węglowych w Polsce. *Polityka Energetyczna Vol. 15, issue 3, pp. 211–219, Kraków* .

Blaschke W. Blaschke Z. (2005) Preparation of coal slurries deposited in ground settling ponds. *Acta Montanistica Slovaca Vol 10, special issue 1, pp. 17-21, Kosice 2005.*

Borowski G., Hycnar J.J. (2013). Utilization of fine coal waste as a fuel briquettes. *International Journal of Coal Preparation and Utilization, 33(4), s. 194–204.*

Brenek R., Santarius A., Hudecek V. (2014) Decontamination of waste dumpside of s.p. Diamo. *Acta Montanistica Slovaca Vol.19, issue 1, pp.6-14, Kosice*

Development Project No. N R09 006 06/2009. „Identyfikacja potencjału energetycznego depozytów mułów węglowych w bilansie paliwowym kraju oraz strategia rozwoju technologicznego w zakresie ich wykorzystania. IMBiGS. Warsaw 2009.

Fećko P., Hlavatá M., Podešvová M., Mucha N., Király A. (2011) New flotation agents on a slurry sample from Darkov Mine. *Journal of the Polish Mineral Engineering Society, No 1(27), p. 27–38. Kraków*

Galos K., Szluga J. (2014). Management of hard coal mining and processing wastes in Poland. *Gospodarka Surowcami Mineralnymi – Mineral Resources Management, 30(4).*

Gawlik L. (2005) Prawne aspekty wykorzystania mułów węglowych zdeponowanych w osadnikach. Zeszyty Naukowe Politechniki Koszalińskiej. Zeszyt Nr 22, Seria: Inżynieria Środowiska. Issue 22 , *pp.377-386, Koszalin*

Grudziński Z. (2005) Analiza porównawcza jakości mułów węgla kamiennego pochodzących z bieżącej produkcji i zdeponowanych w osadnikach ziemnych. *Zeszyty Naukowe Politechniki Koszalińskiej. Zeszyt Nr 22, Seria: Inżynieria Środowiska. Issue 22 (2005), pp.671-679, Koszalin*

Hlavata M., Cablik V. (2012) Application of Fine Tailings from Coal Preparation in the Ostrava - Karvina District. Rocznik Ochrona Środowiska - *Annual Set the Environment Protection, Vol. 14, pp. 285-289, Koszalin*

Hycnar J.J., Borowski G. (2016) Metody podwyższenia kaloryczności drobnoziarnistych odpadów węglowych. Monografia, Politechnika Lubleska, s.156, Lublin

Hycnar J.J., Bugajczyk M. (2004) Kierunki racjonalnego zagospodarowania drobnoziarnistych odpadów węglowych. Polityka Energetyczna - Energy Policy Journal, Vol. 7 special issue, Kraków

Lorenz U., Ozga-Blaschke U. (2005) Muły węgla kamiennego - produkt czy odpad. Zeszyty Naukowe Politechniki Koszalińskiej. Zeszyt Nr 22, Seria: Inżynieria Środowiska. Issue 22 , *pp. 682-691, Koszalin 2005*

Lutyński A, Lutyński M. (2014) Assessment of coal slurry deposits energetic potential and possible utilization paths; *Physicochemical Problems of Mineral Processing, Vol. 50,Issue 1, pp. 159-168, Wrocław.*

Lutyński A, Suponik T., Lutyński M. (2013) Investigation of coal slurry properties deposited at impoundments; *Physicochemical Problems of Mineral Processing, Vol. 49,Issue 1, pp. 22-35, Wrocław.*

Lutyński A., Szpyrka J. (2012) Analiza własności fizykochemicznych depozytów mułów węglowych na Górnym Śląsku. *Polityka Energetyczna Vol. 15, issue 3, pp. 273–285, Krakow*

Szpyrka J., Lutyński A. (2012) Badania wzbogacania depozytów mułów węglowych. *Polityka Energetyczna - Energy Policy Journal, Vol. 15, issue 3, pp. 247-258, Kraków*

Rotunajanu I., Lazar M. (2014) Hydrogeological classification and evaluation of coal deposits. *Mining Revue Vol.20, No 2/2014, pp. 7-14, University of Petrosani, Romania,*

Wang Ch., Harbottle D., Liu Q., Xu Z. (2014). Current State of fine mineral tailings treatment: A critical review on theory and practice. *Minerals Engineering, 58, s. 113–131.*

Yilmaz E. (2011). Advances in reducing large volumes of environmentally harmful mine waste rocks and tailings. *Gospodarka Surowcami Mineralnymi, 27(2).*

Implemented stage fracturing technique to improve oil production in Nubian sandstone of North Gialo, Libya

***Emad I. M. Fandi*[1], *Branko Leković*[2], *Badees Gazal*[3], *Elnori Elhaddad*[4] *and* *Abdulbaset Al Saghr*[5]**

This paper is an investigation on North Gialo Field to enhance the oil recovery by stimulating the main reservoir, the Upper Nubian Sandstone, which is affected by pervasive diagenetic modifications of porosity and permeability. The significant increase in the production rate after hydraulic fracturing treatment shows the importance of implementing this method for this formation in Libya for optimising production. And moreover, to gain better recovery of the stored hydrocarbon in this reservoir. The sensitivity of this case that is required a critical treatment with a precaution investigation during the operation such as High Strength Proppant, type of proppant, sieve size, conductivity indication, production estimation, Net Present Value, and the comparison between treated and untreated cases. Furthermore, deeper Nubian Sandstone formation and the treatment temperature up to 149 °C. Therefore, choosing the delayed borate crosslinked fluid by using Hydroxy Propyl Guar (HPG), gelling agent and special additives designed to enhance the viscosity at a higher temperature, to break the viscosity at the end of the end of the pump time and good proppant transport. Another benefit of the additives is stable fluid rheology, low fluid loss properties, and good cleanup properties. Post-stimulation data were collected, and the evaluation was performed in order to calibrate and improve the current models and future stimulation treatment within the North Nubian Sandstones.

Keywords: *Nubian Sandstone, High Strength Proppant, Fracture Conductivity, Improve Oil Production, Hydroxy Propyl Guar (HPG), Borate Gel (HPGuar)*

Introduction

This paper evaluates the implementation of fracturing stimulation on Upper Nubian sandstone formation, which is classified as tight formation. However, the main purpose is to mitigate some formation damage issues should be operationally tested and evaluated to determine the cost-to-benefit ratio for improved well productivity.

As a general consideration at the Oil and Gas Industry, low permeability is limited to 10 mD for oil reservoir and 1 mD for the gas reservoir. For this case, fractures observed within the cores were largely closed and mineralised with quartz cementation and/or were clay-filled. On observation, open fractures appear to be localised. This investigation placed uncertainty regarding the potential effect of fracturing within the reservoir.

Nubian sandstone formation can be deep, high stress, high temperature, homogenous and can contain multiple layers. After that, the Stimulation objective is to increase the Productivity Index. Thus, this facet of the Structure process actively and positively affects the reservoir's productivity, whereas most of the other operations in this process are aimed at minimising reservoir damage, eliminating production problems, and flow paths by which hydrocarbon are efficiently extracted for low permeability rocks.

Hydraulic fracturing has experienced even more dramatic improvements since the introduction of crosslinked polymer fluids, High-Strength Proppants (HSP), and analytical techniques, such as the matching pressure plot to reduce the risk. Such techniques have enabled engineers to improve the flow from both low-permeability and high-permeability reservoirs substantially.

To evaluate the stimulation effectiveness, it is essential to estimate mechanical rock properties and hydraulic fracture properties, such as fracture half-length and fracture conductivity.

This paper discusses and presents a field case in Upper Nubian Sandstone (UNS), reservoir treated with a polymer as HPGuar with a delayed crosslinked borate and selected various proppant types, sieve sizes, and areal concentration of proppant (kg/m²) to compare. This paper will also cover steps of the stimulation procedure for the 6J9 well, including major operational issues and present decisions made while composing the procedure.

Post-stimulation data were collected and evaluation performed in order to calibrate and improve current models and future stimulation treatment within the North Nubian Sandstones.

Finally, recommendations will be made based on the results to be applied in the future in order to obtain the maximum value of treatment for this formation.

[1] *Emad I. M. Fandi*, Faculty of Mining and Geology, University of Belgrade. emad.fandi@liboaljadeeda-oil.ly; emad.fandi77@gmail.com
[2] *Branko Leković,* Faculty of Mining and Geology, University of Belgrade. branko.lekovic@rgf.bg.ac.rs
[3] *Badees Gazal*, Hess Libya Exploration Limited. badees2@gmail.com
[4] *Elnori Elhaddad*, Faculty of Mining and Geology, University of Belgrade. norimab2014@gmail.com
[5] *Abdulbaset Al Saghr*, General Gas Transmission and Distribution Company. a.alsaghr@gasly.ly

Fracturing Fluids and Sirte Basin Literature Overview

Fracturing fluids are technological advances in the petroleum industry proceed in incremental steps, not in the leaps and bounds associated with emerging technologies (Kevin and Norm, 2012). However, the importance of incremental advances should not be overlooked. Their impact can be measured in the production gains from wells that in the past would be shut-in because of poor economic performance or not even drilled because the technology was not present to safely complete the well. Therefore, Incremental advances have occurred in every aspect of the petroleum industry, ranging from the techniques and equipment to locate and extract hydrocarbons to the methods used to increase production and maximize recoverable reserves (Economides and Nolte, 2000).

Gray (2006) argue that Halliburton Oil Well Company as the exclusive licensee. In 1949, the process was first made available to the industry, the exclusive licensing agreement was terminated, and the fracturing process was licensed to other qualified service companies, including BJ Services since 1953 (Droegemueller and Leonhardt, 2005).

In 1955, an estimated 4,500 fracturing jobs were performed per month. In 1957, mathematical fracture models were introduced, forerunners of today's fracture simulators. Water-based fluids based on guar polymers were used by the early 1960s. Moreover, cross-linked water-based fluids had been introduced.

By the early 1970s, water-based systems replaced oil base fluids during 1970s, and 1980s water-based polymers evolved Lower residue became important with Hydroxy Propyl Guar (HPG), replacing Guar Later Carboxy Methyl Hydroxy Propyl Guar (CMHPG) replaced HPG. By the 1990s, the industry had returned to Guar for cheaper fluids, as mentioned by Abhinav et al. (2017) and Elsarawy and Naser-El-Din (2012).

Rheology testing of fracturing fluid is important in evaluating and characterising the viscosity profile Fracturing fluid in the fracture at simulated fracturing conditions. Thus the frequently, of additives may reduce the pump pressure required to move the fluid downhole (Vispy, 2004; Xu and Fu, 2012; Li et al., 2015).

The fracture fluid system has been used successfully around the globe over the last 15 years. The main reason for the global use is the HPG delayed crosslinked borate system can be prepared from nearly any type of source water. The system is used for this range of temperature 51.6° to 148.9 °C (Duenckel et al., 2016).

Thus HPG delayed crosslinked borate system fracture is used in Libya, Algeria, Egypt, Europe, Oman, Russia, and Saudi. Therefore, hydraulic fracturing history in Sirte basin started in 1993 in well C217, table 1. Since that year a total number of eight wells were fractured, these wells are C304, C217, C316, C303, C040, C313, C238, C059, and C139.

In the recent study by Mei Y. et al. (2013), an equally important function of fracturing fluids is the transport of proppant into the fracture. Various mechanisms can be responsible for the transport of the proppant that when the setting velocity of the proppant is negligible, the slurry behaves as a "perfect suspension," and the solid moves effectively with the slurry fluid velocity. Therefore, when the setting velocity of the proppant is significant, a proppant bank is created, and its top is continuously sheared off by the high- velocity slurry above the bank, and low-reservoir permeability, allowing for lower proppant-pack permeability. So the solid moves towards the fracture tip with a slower mean velocity.

The transition between the two mechanisms depends mainly on two factors the apparent viscosity of the fluid (at the settling conditions) and the density difference between the proppant material and the fluid (Aboud and Melo, 2007). In low - viscosity fluids, proppant is transported by "stationary bed saltation" flow, which is characterised by the deposition of a bed of proppant followed by saltation flow of the proppant slurry above the proppant bed. Laboratory evaluations indicate that building a proppant bank occurs in three consecutive phases.

Several authors (Gandler, 2010; Ribeiro and Sharma, 2013; Xu and Fu, 2012; Liang et al., 2016) argued that during the first phase, the bank builds up gradually as a function of time until an equilibrium height is reached near the wellbore. The bank stops growing at this point as a result of the erosion caused by the increased fluid drag forces on the proppant particles. During the second phase, that bank grows only in height until it reaches equilibrium height over its full length.

Raimbay A. et al. study (2017) shows that in the third phase, the bank grows only in length, and the injected proppant saltates over the full the length of the bank toward the bank`s front, where it settles, increasing the length of the bank in the direction of flow.

The analytical relations derived for each of these phases are to provide permeability flow paths for hydrocarbon in low sandstone formation and permanence this permeable flow path can be achieved by proppant agents that are injected with treated water.

Water frac (using slick water or water with friction reducer instead of gel to transport proppant) have been a successful fracturing technique in some tight gas reservoir.

Proppant placement is an essential factor that determines the effectiveness of such hydraulic fracture treatment and Prediction of resulting proppant distribution after the proposed preliminary main treatment. (Liu and Sharma, 2002; LaFollette and Carman, 2010).

Tab. 1. Fracture History in Sirte Basin.

Wells	**C304**	**C217**	**C316**	**C303**	**L040**	**C313**	**C238**	**L059**	**C139**
Field Name	C-North	C-Main	C-Main	C-Main	L-Field	C-Main	C-Main	L-Field	C-Main
Frac Date	3/1/1996	2/1/1993	11/1/2005	1/1/2006	11/6/2006	10/1/2007	10/1/2007	10/2/2007	10/1/2007
Fracturing Parameters									
Instantaneous Shut-In Pressure ISIP [kPa]	38004	40976	36597	36487	45188	36825	43589	33839	-
Closure pressure [kPa]	33970	33026	33474	32833	36590	33012	38025	32943	32819
Frac Gradient [kPa/m]	12.4	12.4	12.4	12.2	13.6	12.4	14.5	12	12.2
Fluid Efficiency [%]	21	30	14	12	17	20	-	29	-
Proppant In Formation [Kg]	9,072.0	5,896.7	18,143.7	17,418.0	18,279.7	15,831.0	13,607.7	128,366.6	24947.6
Instantaneous Production									
Oil [m³/day]	Before	0	23.8	28	0	31.6	46.6	73	26.5	73
	After	95.4	218.4	161	91	40.1	95.6	88	53.4	116.1
Water Cut [%]	Before	0	0	0	0	0	0	0	0	0
	After	0	4	0	0	0	24	0	16	0

Field Description

North Gialo Discovered in 2002 with the drilling of the 6J1 well exploratory well and tested the Nubian sandstone at rates up to 795 m³/day, resulting in the discovery of the field. An additional 14 appraisal wells were drilled revealing a large areal extent, low porosity (10 %), low permeability (1 mD) reservoir with a 670.56 meter hydrocarbon column of volatile oil. Initial DST rates of the appraisal wells varied widely, from 32 - 1590 m³/day. The discovery was based on the interpretation of the 3D seismic survey, data obtained by the 1970s four exploratory wells and the Farigh Field to the Northwest.

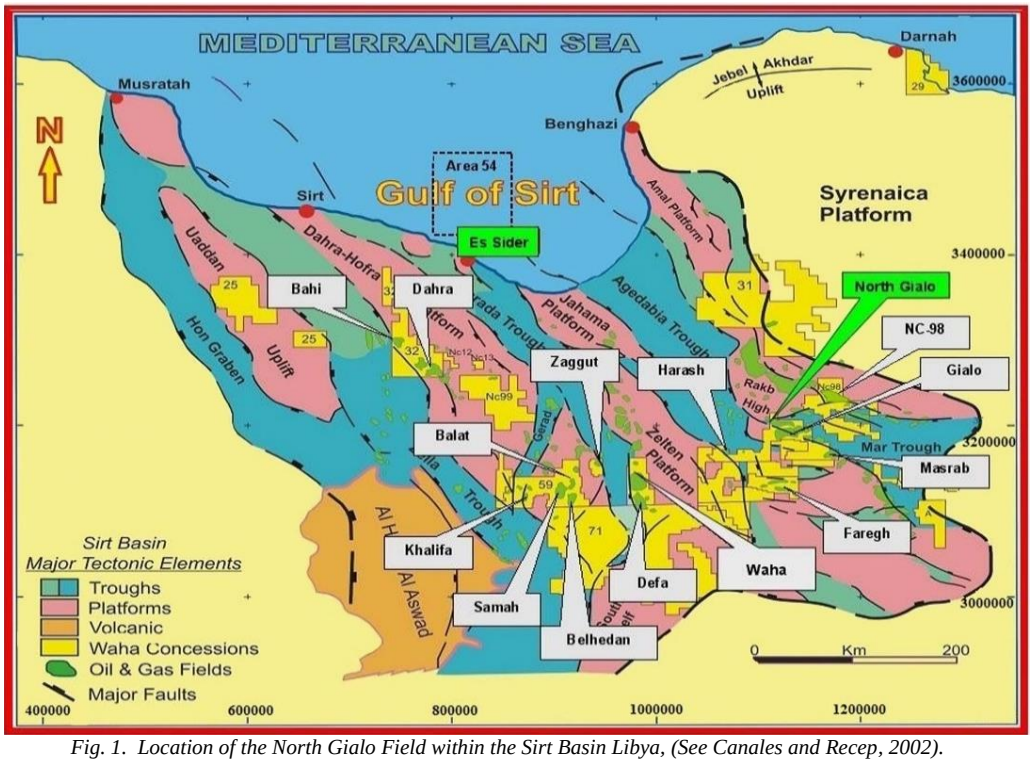

Fig. 1. Location of the North Gialo Field within the Sirt Basin Libya, (See Canales and Recep, 2002).

North Gialo is a new oil field estimated to contain 0.64 billion cubic meters of light oil and 0.187 trillion cubic meters of associated gas. The North Gialo Field is located in the SE portion of the Sirte Basin encompassing over 307,561056 m² with approximately 101,171400 productive square meters as shown in Figure 1 (see Canales and Recep, 2002).

North Gialo field lies at the intersection of the Hameimat and Ajdabaiya troughs of the Sirte Basin, southeast of the Farigh Field (Veba, Nubian, 0.191 billion cubic meter Original Oil In Place - OOIP) and north of the Gialo Field (Waha, 2.05 billion cubic meter OOIP), as argued by Liu and Sharme (2002), and Canales and Recep (2002).

Candidate Selection

The target zone for the treatment is the Upper Nubian Sandstone (UNS), for 6J9 well, located in a very heterogeneous reservoir with three multilayered producing sand. The candidate well is currently completed as an oil producer well with sets of perforations from 3743 m to 3788 m and low permeability. Thus HPGuar fluid system and High Strength Proppant fractured have been used in this study.

An average Young's Modulus throughout the upper Nubian sandstone formation is 49.6 GPa, with Poisson ratio of 0.1672 in the competent sand. The stresses across the upper Nubian sandstone formation have some contrast between the consolidated and unconsolidated rock depending on the degree of cementation and presence of shale. The in-situ stress indicated about 57,226 kPa.

Pressure and stress analysis starts with overburden stress and pore pressure estimates provided by the ConocoPhillips Middle East-North Africa Business as argued by Philivan (2008), and Silva (2010). The Nubian section is primarily clean, quartz-rich sandstones (quartz arenites). The reservoir quality of the sands has been negatively affected by pervasive diagenetic modifications of porosity and permeability with a high degree of rock consolidation and high-temperature conditions. The treatment was done for upper Nubian sand, and the cross thickness is about 45 meter. 6J9 well Completion and reservoir data listed in table 2.

Tab. 2. 6J9 well completion and reservoir data.

Well	6J9 -59E
Formation	UNS
Interval Depth (m)	3743 – 3887.4
Frac Design (m)	3743 – 3788
Reservoir Pressure (kPa)	42058
Production Rate (m³/day)	342.6
Choke size (cm)	2.45
Reservoir Temperature (°C)	143
Permeability (mD)	4.8
Porosity (%)	10
Tubing (cm)	OD 8.89
Casing	OD 24.45
Water Saturation (%)	35
Perforation Density (shut/m)	16

Methodology and Procedures

Implementation was done by two method analyses, which were run within Production Simulator, from Stim-Lab - Baseline conductivity analysis and production analysis. Production Simulator has the capability of producing predicted production rate and net present value (NPV) curve. All inputs for these curves related to costs, however, are the only estimate and all NPV curves should be used as qualitative comparisons, not quantitative.

The simulation study is comprised of major steps completed by a different technology. Therefore, the programs used for modelling were Production Simulator and Fracture Simulator. Hence, Rheology Fluid Software Application and Fracture Simulator, these programs use known rheology, viscosity, reservoir, and mechanical rock properties along with a user-created pump schedule to produce optimised fracture geometry, conductivity, and areal concentration of proppant (kg/m²).

Hydraulically fracture was done for 6J9 well, Upper Nubian Sandstone within the perf intervals 3,743- 3,788 meter and temperature is 143°C so selected fluid system such as HPGuar delayed crosslinked Borate that this fluid system have to crosslink, the primary is water-based slurry of borate mineral, provide delayed borate crosslink fluids and the secondary is an instantaneous. HPGuar delayed crosslinked borate system is recommended for wells with bottom hole static temperatures (BHST) of 51.7° to 149 °C.

Therefore, the linear polymer solution is referred to as water frac, which is typically prepared from guar-based polymers for pre-pad and displacement. Water frac is very important and a widely - used component of the hydraulic fracture. Preparing water frac from a guar-based polymer is a two-step process. First, the gelling agent must be dispersed in water. Then, the gelling agent (polymer) must hydrate to obtain the desired increase in fluid viscosity.

6J9 Treatment Design Considerations

The stage treatment starts with filling the well with Linear Gel (water Frac) prepared with HPG to minimise friction pressures during the breakdown followed by pumping a Breakdown/Stepdown test. This test is used to evaluate bottom hole treating pressures and to determine friction pressures at the perforation and/or near wellbore area. The breakdown phase followed by a Stepdown test. The Stepdown test is used to quantify perforation and near wellbore friction (Tortuosity) which will help to determine whether fracture entrance problems are present.

Minifrac treatment is a stage to determine the fracture closure stress and the fluid leak-off parameters at in-situ conditions. Once the fractures have closed, the pumps should be brought back on as quickly as possible to try to establish one dominant fracture (the sand slug will help screen-off the other small fractures that were forming).

Larger pad volumes and fluid leak-off additives (Sand Slug), should be considered to address and negate the problem. When the treating pressure rises after a breakdown that should make run a sand slug during Pad to see how the formation would react. As the treatment will be conducted through a part of the existing perforations, included proppant slug of 120 kg/m³ depending on the formation during pumping mini-frac to verify if proppant can be placed in the formation.

Therefore, if competing multiple fractures exist, it is best to place proppant into the fracture(s) and shutdown. The mini-frac treatment provides the collection and interpretation of many valuable reservoir and stimulation characteristics which permit stimulation optimisation for each individual well. Some of these factors include average permeability, fracturing pressures, fracture extension pressure, fluid leak-off values, mechanical properties, and fracture closure pressure. The Main Treatment is designed to place 120,875 Kg of 20/40, mesh (High strength Proppant) with a proppant concentration up to 839 kg/m³.

Chemical Compositional Selection

A delayed crosslinked borate gel provides the following characteristics as shown in the tables (3 - 6)

Tab. 3. 22.7 kg Water Frac HPG composition.

Description	Additive name	Concentration
Liquid Gel Concentration	HPG	11.35 L/m³
Lower PH Buffer	A weak acid solution	0.2 L/m³
Breaker	An oxidant breaker	0.24 kg/m³

Tab. 4. 22.7 kg Water Frac HPG additional to an additive to enhancement the fluid recovery and product formation from clay swelling.

Description	Additive name	Concentration
Clay control	Clays stabiliser (Organic Polymer)	4.0 L/m³
Surfactant	A no ionic surfactant	2.0 L/m³
Breaker	A high-temperature oxidant breaker	2.0 L/m³
Biocide	A biocide (Short Action)	0.018 kg/m³

Tab. 5. Cross-Linked Gel Composition.

Description	Additive name	Concentration
Liquid Gel Concentration	HPG	11.35 L/m³
Lower PH Buffer	A weak acid solution	0.2 L/m³
Cross-linker	A primary delayed crosslinker (base oil solution)	4.2 L/m³
Cross-linker	A secondary instantaneous crosslinker (high pH, water base)	0.5 L/m³
Gel Stabilizer	A gel stabiliser for high temperature (solid)	0.48 kg/m³
High pH Buffer	A high pH control, is not strictly a buffer is pH control solution	2.72 L/m³
Breaker	A breaker activator (catalyst)	0.06 kg/m³
Breaker	an oxidant breaker	0.24 kg/m³

Tab. 6. 22.7 kg Cross-Linked Gel additional to an additive to enhancement the fluid recovery and product formation from clay swelling.

Description	Additive name	Concentration
Clay control	Clays Stabilizer (Organic Polymer)	4.0 L/m³
Surfactant	A no ionic surfactant	2.0 L/m³
Biocide	A biocide (Short Action)	0.018 kg/m³
Breaker	A high - temperature an oxidant breaker	2.0 L/m³
Breaker	An oxidant breaker	0.24 kg/m³

Frac Fluid Rheology Selection

Fluid rheology and major viscosity requirements for proppant transport at a given gel loading, and temperature based on a best-fit curve calculated values based on the software application for the rheology fracture fluid model to measured data. Almost every Halliburton stimulation field lab can generate data on fracturing fluid viscosity versus time, also called a Break Profile. The proppant in suspension and settle with the fluid an apparent viscosity up 250 mPa*s depends on the proppant laden fluid on the pump schedule and the minimum acceptable viscosity to carry the proppant is 200 mPa*s as shown in Fig. 2.

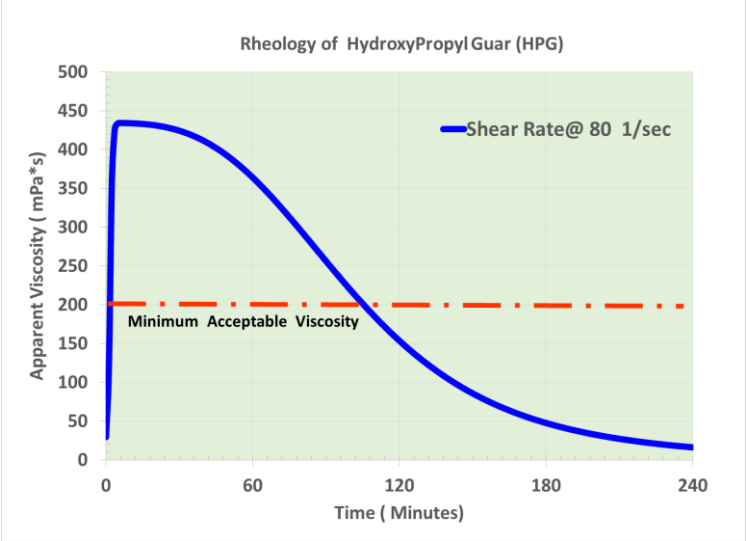

Fig. 2. Breaking Profile.

The shear rate of the fluid has been subjected for which the fluid property is desired. It is typically reported for linear gels at 300 rotation per minute (rpm) on Fann Model- 35, a viscometer equipped with a Bob size, B1 bob, this bob is the large bob. It is usually used to determine the base gel viscosity of frac fluids, which produces a shear of 511 1/sec (reciprocal seconds), as shown in Fig. 3.

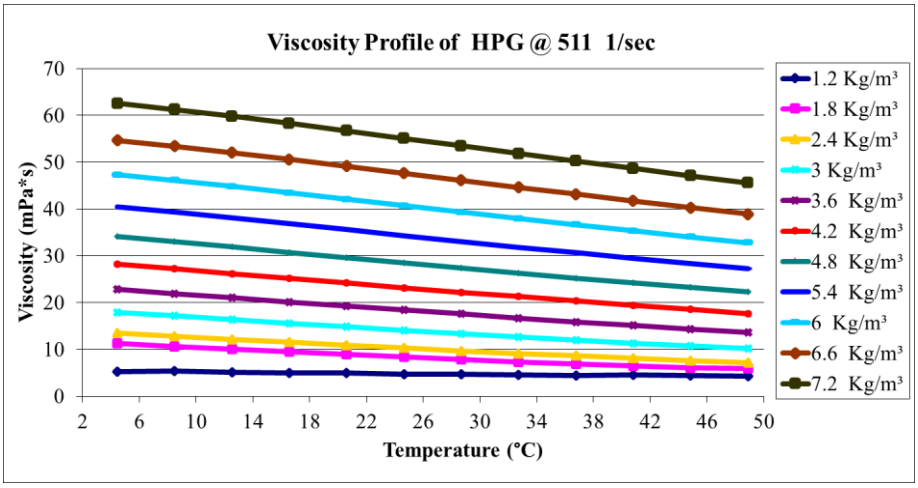

Fig. 3. Viscosity profile for several HPG concentrations Vs Temperature.

Therefore, the rheological properties of the fracturing fluid play a crucial part because they directly affect the performance of the fluid with respect to almost all the fluid functions. Thus can be directly used to calculate frictional pressure losses in the wellbore, perforations, and fracture. Several industry tests have concluded, based on laboratory proppant transport testing, that cross-linked borate fluids were perfect proppant transport fluids.

Proppant Analysis

Twelve treatments were initially compared in the Baseline Analysis. The treatment contained High Strength Proppant (HSP), and Intermediate Height Strength Proppant (IHSP), with 20/40, 16/20 and /or 16/30 sieve sizes at 5, 10 and 15 Kg/m² areal proppant concentration. The properties of these twelve treatments are listed below in table 7. Figure (4), shows the results of the Baseline Analysis, conductivity vs stress and the well has expected minimum horizontal stresses range, the 6J9-59E well has expected through the targeted perforation intervals, of 46,884 – 55,158 kilopascals, (kPa). This range is represented by the Red Vertical Lines on the plot.

At 48,263 kilopascals, (kPa) the plot shows 16/20 -HSP at 15 Kg/m² , 16/20 -HSP at 10 Kg/m², and 16/30- HSP at 15 Kg/m² having the top three conductivity values: 3,810 md*m, 2,590 md*m, and 3,000 md*m. 16/20 -HSP was chosen as the optimised proppant type and sieve size. Eliminating all other proppants, a plot was created with only 16/20-HSP at three areal proppant concentration values: 5 Kg/m², 10 Kg/m², and 15 Kg/m².

Tab. 7. 6J9 Proppant properties for Baseline Analysis.

Type	Sieve Size	Areal Concentration	Colour on Graph
HSP	20/40	5 kg/m²	
HSP	20/40	10 kg/m²	
HSP	20/40	15 kg/m²	
HSP	16/20	5 kg/m²	
HSP	16/20	10 kg/m²	
HSP	16/20	15 kg/m²	
HSP	16/30	5 kg/m²	
HSP	16/30	10 kg/m²	
HSP	16/30	15 kg/m²	
IHSP	16/30	5 kg/m²	
IHSP	16/30	10 kg/m²	
IHSP	16/30	15 kg/m²	

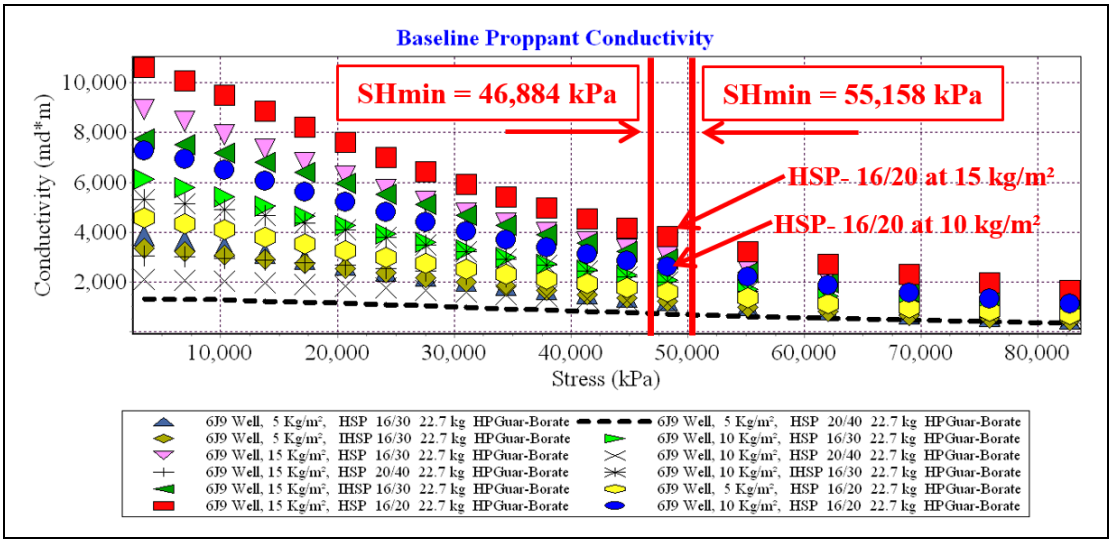

Fig. 4. 6J9 Well Baseline Analysis Results.

Production Analysis

The next analysis was Production Analysis. This analysis provides production and NPV profiles based on the well properties and costs entered by the user.

An untreated well is also analysed and compared to the treated well profiles. The production analysis incorporates damage effects caused by non-Darcy flow, multi-phase flow, and gel damage into its production calculations. It also provides corrected permeability, width, and conductivity values based on the damage effects.

Table 8 below shows the damage effect results of the production analysis run for 16/20 -HSP proppant in the 6J9 well after 2 years of production. The table shows that as proppant areal concentration increases, so do

conductivity and % available width. Permeability, however, decreased as proppant areal concentration increase, but the difference is very small. The highest conductivity and % available width is seen in the 15 Kg/m² areal concentration, but the largest conductivity and % available width improvement is from 5 Kg/m² to 10 Kg/m².

Tab. 8. 6J9 Production Analysis Damage Effects.

Areal Concentration	Conductivity	Available Width	Corrected Permeability
5 Kg/m²	64.05 md*m	61.16%	42.25 darcy
15 Kg/m²	122.3 md*m	77.62%	34.40 darcy
20 Kg/m²	190.1 md*m	84.21%	32.85 darcy

The production analysis uses the above-corrected values and other reservoir and well properties to create production and NPV profiles for 6J9 well. Figures 5, 6, and 7 show estimated cumulative production, production rate, and NPV profiles, respectively, for 6J9 well. The plots contain profiles for 16/20 -HSP at 5, 10, and 15 Kg/m² proppant areal concentration as well as an untreated well.

At the end of two years, the following values in Table 9 were calculated. Again, the highest cumulative production occurs with 15 Kg/m² areal concentration, but the largest improvement is seen when going from 5 Kg/m² to 10 Kg/m² proppant areal concentration.

Tab. 9. 6J9 Estimate Cumulative Production Values after 2 years.

Areal Concentration	Cumulative Production
5 Kg/m²	270600 m³
10 Kg/m²	279500 m³
15 Kg/m²	285100 m³
Untreated Well	**165400 m³**

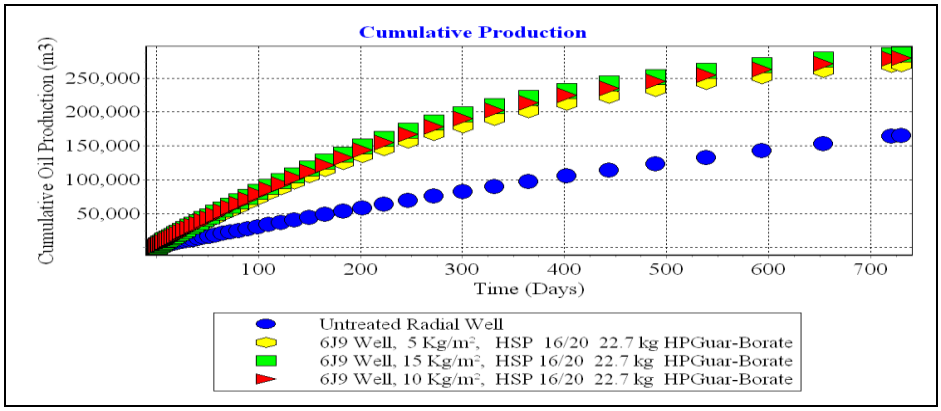

Fig. 5. 6J9 Well Estimated Cumulative Production – 2 years.

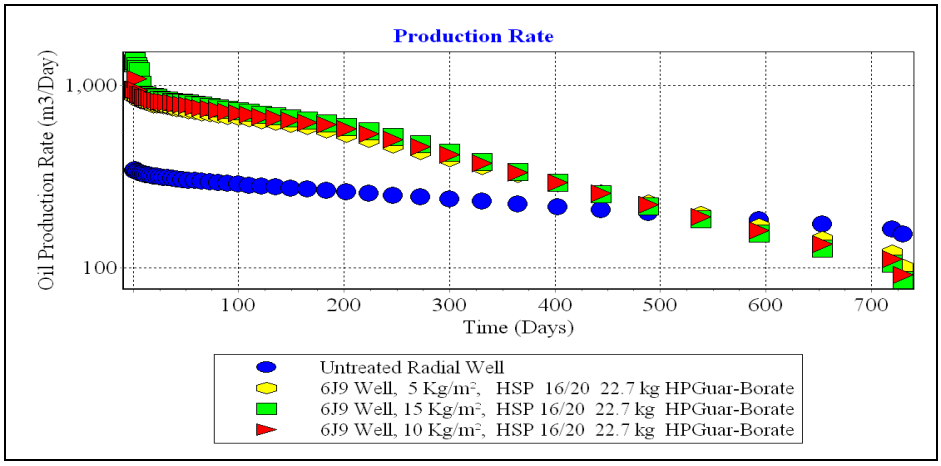

Fig. 6. 6J9 Well Estimated Production Rate – 2 years.

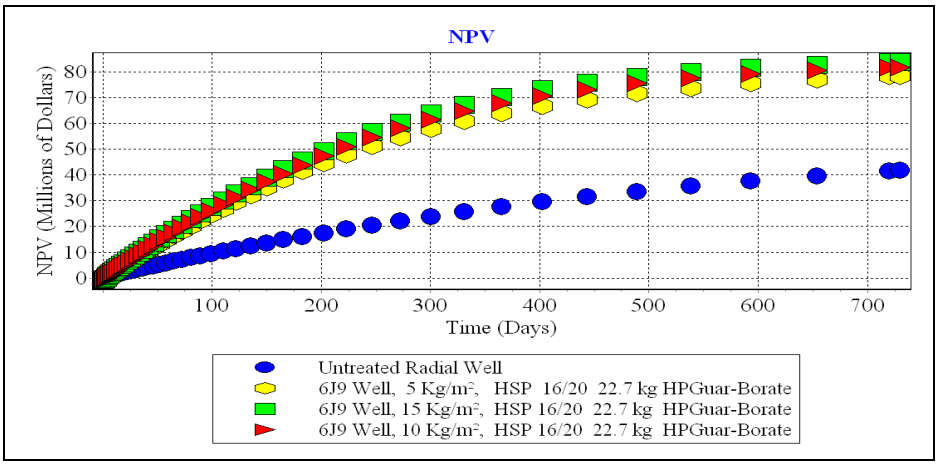

Fig. 7. 6J9 Well Estimated NVP – 2 years.

Initial and final (after 2 years) production rates are listed below in Table 10. When comparing initial production rates, 15 Kg/m² shows the highest initial production rate. Therefore, the largest improvement is seen when going from 10 Kg/m² to 15 Kg/m² proppant areal concentration. The Production rate plot also shows that after approximately one year, the production rate of the treated wells drops but the above the rate of the untreated well.

Tab. 10. 6J9 Estimated Production Rates, Initial and after 2 years production.

Areal Concentration	Initial production rate	2 years production rate
5 Kg/m²	881.7 m³/day	100.5 m³/day
10 Kg/m²	951.7 m³/day	91.88 m³/day
15 Kg/m²	1331 m³/day	85.93 m³/day
Untreated Well	**342.6 m³/day**	**153.7 m³/day**

The Net Present Value (NPV), values after two years are shown below in Table 11. Again, the highest NPV occurs at 15 Kg/m² areal concentration, but the largest improvement is seen when going from 5 Kg/m² to 10 Kg/m² proppant areal concentration.

Tab. 11. 6J9 Estimated NPV after 2 years.

Areal Concentration	NPV
5 Kg/m²	$78.34 Million
10 Kg/m²	$81.65 Million
15 Kg/m²	$83.82 Million
Untreated Well	**$41.80 Million**

6J9 Stage Fracturing Design

The design run within Fracture Simulators for 6J9 well, the target zone for treatment is 3,743 meter to 3788 meters, and the candidate well is currently completed as an oil producer well with sets of perforations through the mentioned formation. Based on the data provided, the formation characteristics and reservoir data show a very low permeability formation to cover this long interval with a hydraulic fracturing it requires fracture height controlling by pumping large quantities of slurry volume, pad volume, slurry injection rate, amount of proppants, and net pressure between the minimum in-situ stress of the formation and treating pressure.

The cross thickness was 45 meter, where the treatment contained High Strength Proppant, HSP- 16/20, 16/30 and 20/40.

One of the Fracture Simulator Module estimates the Folds-Of-Increase (FOI) which may result from various combinations of proppant volumes. It considers each proppant type independently.

The calculations interactively determine the best possible fracture. FOI Module is a very powerful tool to predict the potential of post-frac productivity in low permeability reservoirs. This would be significant in terms of total well life. This design considers proppant type and mass of proppant, where the mass of proppant varies from 100,000 kg to 150,000 kg per stage.

As shown in Fig. 8, the combination of the proppant types with an increase of proppant mass, and the acceleration of the Folds of increase values — the best result of Fold Of Increase (FOI), which would increase in HSP- 16/20. However, the type of sieve sizes and proppant will be investigated to see the effect on FOI. The following tables 12 through 13 shows - Pumping Schedule for the Fracture Simulator schedule and main treatment design results. Figures 9 through 10 show matching pressure and fracture conductivity profile. Post Fracture job might be considered to achieve better production when compared with pre-job.

This research will mostly focus on proppant section design that should be performed with several proppants and evaluated based on the predicted performance from the well and economics of the treatment. Therefore, the material selection is a key factor design. Not only proppant but the fracturing fluids have a great impact in fracture conductivity. The fluid viscosity being the most important property will dictate several conditions during the frac job (friction, fracture width, and proppant transport).

The bottom of the targeted zone for stimulation is located 17 meters above the oil-water contact. Therefore, a decision has been taken to limit the treatment zone between 3,743 to 3,788 meter. For practical considerations, and to ensure that the entire targeted zone is fractured, avoid screen out if taken place and eliminate an increase in water cut. The optimum model of Fracture Simulator is 9 to 18 meter.

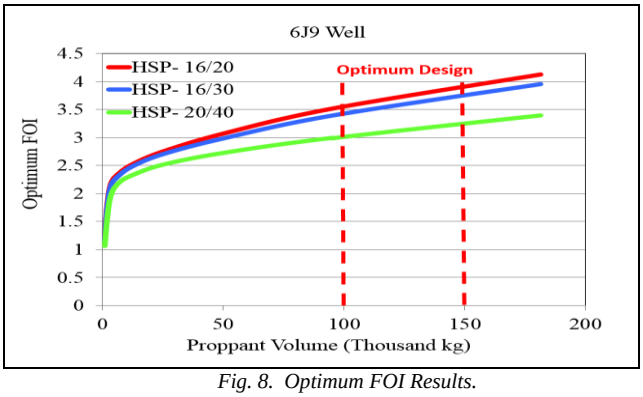

Fig. 8. Optimum FOI Results.

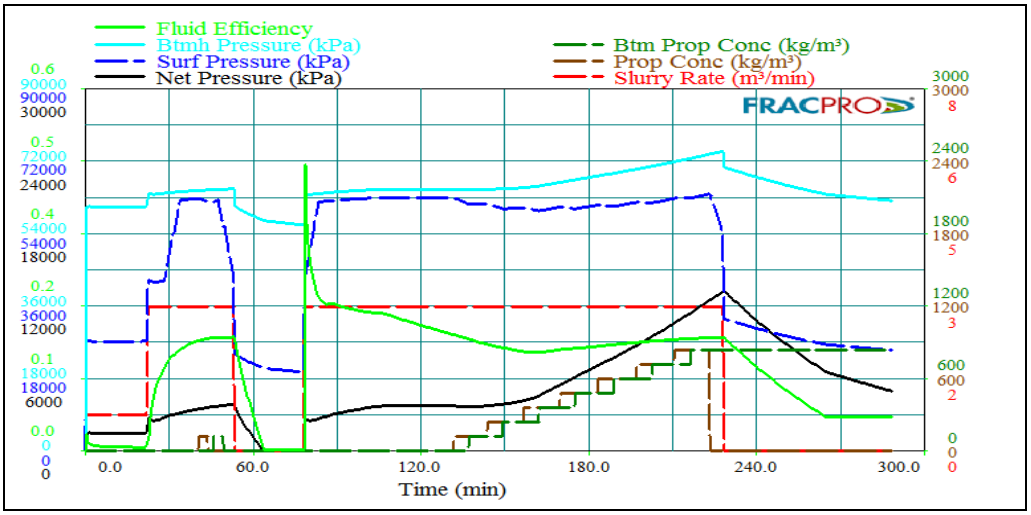

Fig. 9. Preliminary main treatment design.

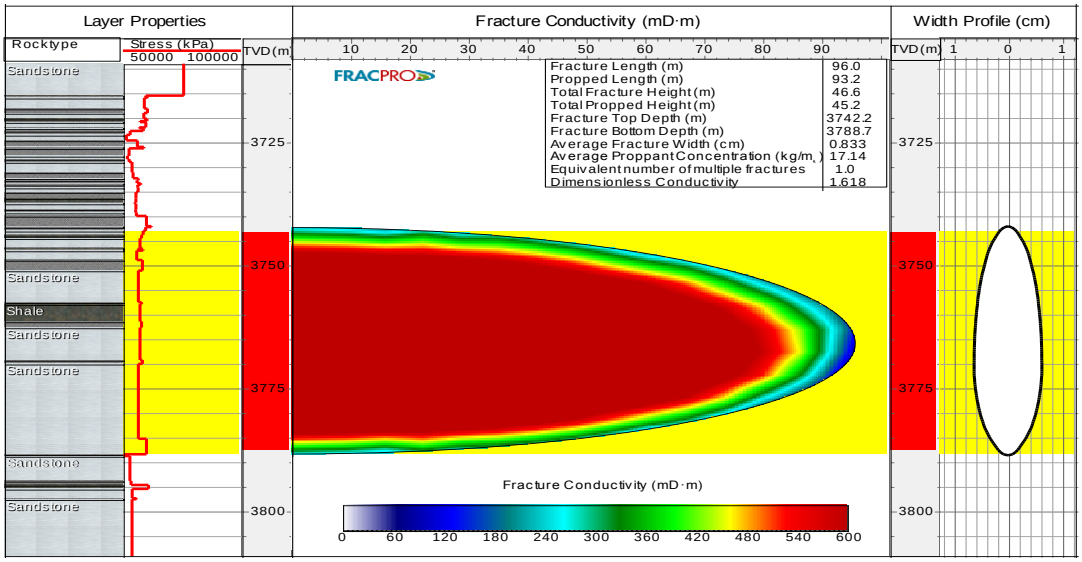

Fig. 10. Main Treatment Fracture Conductivity.

Tab. 12. Pump Schedule for MiniFrac and Main Treatment.

WELL NAME: 6J9-59E **22.7 KG WATER FRAC (HPG)**: 71 m³
JOB NAME: Stage 1 **BORATE GEL (HPG) 22.7 KG:** 488 m³
NO. OF PERFS: 736 **HSP 20/40:** 122,238 kg
MID PERF DEPTH: 3765.5 m
ESTIMATED PUMP TIME: 3.39 hrs.
BHST: 143 degC
FRAC GRADIENT: 15.2 kP/m

Frac the Upper Nubian interval with 428 cubic meters of Borate Gel (HPG) (45 mPa*s) carrying 120,875 Kilograms of 20/40 -HSP. Treat down 8.89 cm tubing at 3.18 m³/min with an anticipated wellhead treatment pressure of 61,301 kPa. Use following schedule:

TUBING (SURFACE)									
STAGE NO.	**STAGE DESCRIPTION**	**ELAPSED TIME MIN:SEC**	**FLUID DESCRIPTION**	**SLURRY RATE (M³/MIN)**	**CLEAN VOLUME (M³)**	**PROPPANT TYPE**	**PROP. CONC. (KG/M³)**	**PROP. MASS (KG)**	**COMMENT**
1	Load Well	22:22	22.7 Kg Water Frac (HPG)	0.79	17.791		0.0	0.0	load Hole
2	Shut-In	22:22	0.000	0.00	0.000		0.0	0.0	
3	Step Rate Test	28:20	22.7 Kg Water Frac (HPG)	3.18	18.927		0.0	0.0	Step Rate
4	Shut-In	28:20	0.000	0.00	0.000		0.0	0.0	
5	Fluid Efficiency Test	40:14	Borate Gel (HPG) 22.7 Kg	3.18	37.854		0.0	0.0	Mini Frac
6	Sand slug	43:55	Borate Gel (HPG) 22.7 Kg	3.18	11.356	HSP- 20/40	120	1362.72	Sand Slug
7	Fluid Efficiency Test	47:30	Borate Gel (HPG) 22.7 Kg	3.18	11.356		0.0	0.0	Displace
8	Fluid Efficiency Test	53:05	22.7 Kg Water Frac (HPG)	3.18	17.791		0.0	0.0	Over Displace
9	Shut-In for FET Analysis	78:05	0.000	0.00	0.000		0.0	0.0	
10	Pad	131:40	Borate Gel (HPG) 22.7 Kg	3.18	170.344		0.0	0.0	
11	Proppant Laden Fluid	143:58	Borate Gel (HPG) 22.7 Kg	3.18	37.854	HSP- 20/40	120	4542.48	
12	Proppant Laden Fluid	156:40	Borate Gel (HPG) 22.7 Kg	3.18	37.854	HSP- 20/40	240	9084.96	
13	Proppant Laden Fluid	169:46	Borate Gel (HPG) 22.7 Kg	3.18	37.854	HSP- 20/40	359	13589.586	
14	Proppant Laden Fluid	183:17	Borate Gel (HPG) 22.7 Kg	3.18	37.854	HSP- 20/40	479	18132.066	
15	Proppant Laden Fluid	197:11	Borate Gel (HPG) 22.7 Kg	3.18	37.854	HSP- 20/40	599	22674.546	
16	Proppant Laden Fluid	210:46	Borate Gel (HPG) 22.7 Kg	3.18	35.961	HSP- 20/40	719	25855.959	
17	Proppant Laden Fluid	223:16	Borate Gel (HPG) 22.7 Kg	3.18	32.176	HSP- 20/40	839	26995.664	
18	Flush	228:23	22.7 Kg Water Frac (HPG)	3.18	16.277		0.0	0.0	
Total					**559.103**			**122,237.98**	

Tab. 13. Main Treatment Design Results.

DESCRIPTION	
Propped Fracture Half Length	96 [m]
Propped Fracture Top Height	3742 [m]
Propped Fracture Bottom Height	3789 [m]
Average Fracture Width	0.83 [cm]
Fracture Average Proppant Concentration	17.13 [Kg/m²]
Dimensionless Conductivity	1.24
Fracture Average Proppant Conductivity	554.1 [mD·m]

6J9 Post Frac

The treatment has performed the Stage 1, 22.7 kilograms — a delayed cross-linked borate gel treatment on the North Gialo Field, 6J9 well. A pre-job safety meeting was held on the location, where the details of the job

were discussed, and potential safety hazards were reviewed, and environmental compliance procedures were outlined. The maximum pressure for the treatment was set at 68,948 kPa. The treatment was designed at 3.18 m³/min, with 427.752 m³ of 22.7 Kg.

A delayed cross-linked borate gel is carrying 120,882.4 kg of 20/40 -HSP. The job was pumped at an average treating rate and pressure of 4.8 m³/min and 55,158 kPa respectively.

Initially, the well was loaded with 22.7 Kg Water Frac (HPG) at a rate of 0.795 - 3.18 m³/min. Once the well was loaded and the pressure stabilised, the pumps were shut down. The ISIP after Shutting down was 19,691 kPa.

Secondly, the fluid efficiency test was pumped at maximum rate and pressure of 4.83 m³/min and 53,779 kPa.

However, for more details see mini-frac job summary in table 14. Figures 11 and 12 shows a chemical job summary for all the treatments performed, and the main treating frac job summary.

Tab. 14. Mini Frac Job Summary.

Pump Time	49.28	Minute
Max Treating Pressure	53,779	kPa
Max Slurry Rate	4.8	m³/min
Max Prop Concentration	132	kg/ m³
Clean Volume	111.4	m³
Slurry Volume	111.88	m³
Prop Mass	1270	Kg
Load to Recover	111.4	m³
Perforation frictions	1813	kPa
Near wellbore (NWB) frictions	4847	kPa
BH ISIP	58,550	kPa
Frac gradient	15.6	kPa/m
Closure gradient	14	kPa/m
Fluid Efficiency	49.6	%

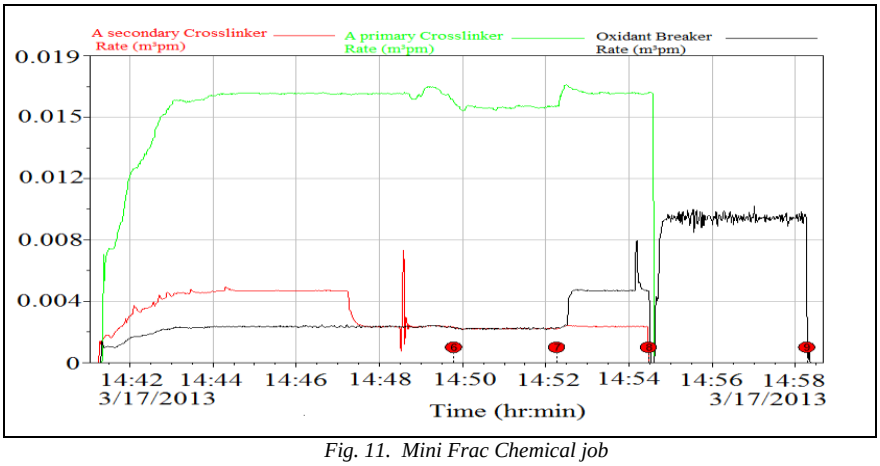

Fig. 11. Mini Frac Chemical job

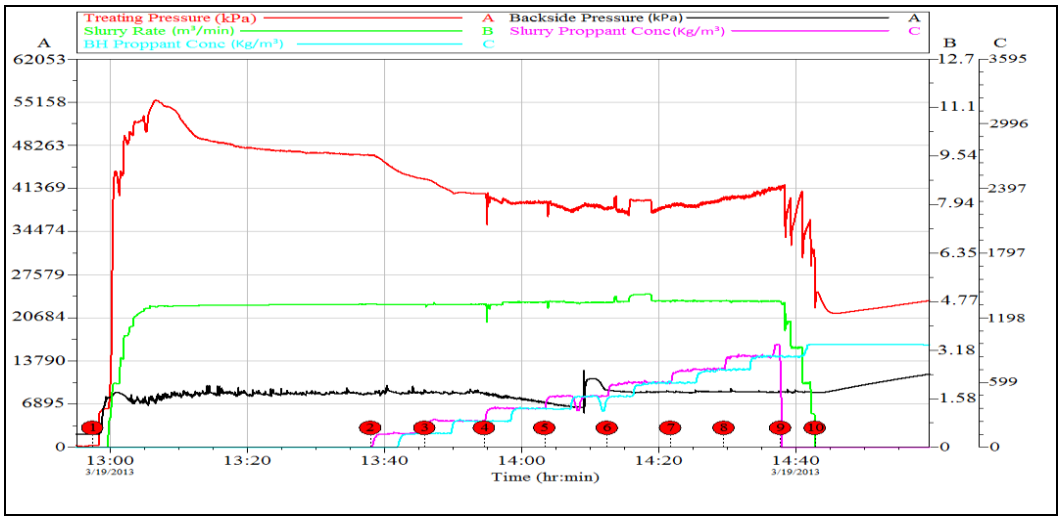

Fig. 12. Main treating Frac job Summary.

6J9 Pre and Post Stage Fracturing Treatment

The post-treatment performance provides a good indication of stimulation success, for 6J9 well and the best-applied method to determine with Production Simulator and Fracture Simulator Models. The Initial production was 342.6 m³/day when compared with the Post-stim production was 1112.4 m³/day (3.247 FOI). Therefore, this analysis is a key element for the optimisation of the hydraulic fracturing process, forecasting well performance.

Thus the treatment paid-out in 3 days and over $ 22 million in additional revenue over 60 days as shown in figure 13.

Post-stimulation data collection and evaluation will be used to calibrate and improve current models for future stimulation treatments within the North Gialo Nubian sandstone.

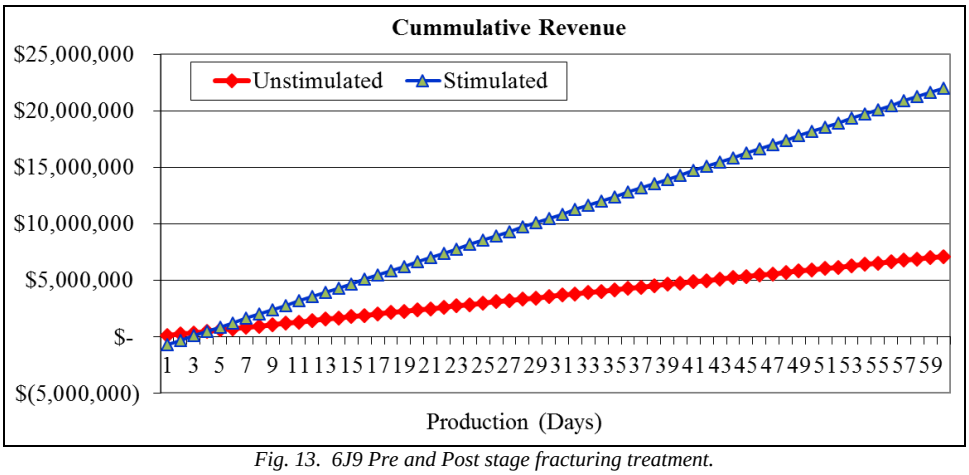

Fig. 13. 6J9 Pre and Post stage fracturing treatment.

Discussion

Fracture stimulation has been considered to enhance oil recovery for the Gialo field located in Libya. For such fracturing treatments, a reliable and combatable fracturing fluid is required to provide adequate rheological performance at a high temperature up to 146 ºC for pump during 2 hours. However, some tests were conducted on location to evaluate fluid formulations response using Services Company.

In this case, a crosslinked fluid was used in fracturing treatments to compensate the high-temperature reservoirs (bottom hole temperature > 93ºC) in order to the improved proppant transport compared to linear polymer systems.

Alternative options are available regarding fracturing fluids such as polymer and crosslinker combinations for high-temperature applications. However, it was recommended to use guar-based polymers crosslinked with either borate or zirconium compounds, which gave the best results compared to the other fluids.

An investigation of prop mesh size was performed, which showed that HSP- 16/20 had the best results with maximum performance. However, practically another size was used (HSP- 20/40) regarding two reasons: Firstly, the only prop at the stock was HSP- 20/40 at that time, and the second was no investigation was done for the size of the prop. Such analysis can lead to having a better vision for making decisions. Even though, HSP- 20/40 mesh size, which is high strength proppant, it will provide sufficient conductivity contrast between the formation matrix and the fracture.

The simulation shows that it is possible to forecast the oil production of low permeability in Upper Nubian sandstone formation. However, the results of the analysis by a combination of Production Simulator and Fracture

Simulator modelling improved an excellent accuracy to the results which is good indication comparing to deduction of actual results of the fracturing practice.

On the other hand, applied these models are not only forecasting the performance, but it also compares well performance using various proppants, fluid rheology, fracture length, fracture heights, fracture geometrics, and proppant concentration. The value of Fold of Increase (FOI) is 3.06 for the model, as shown in figure 8, where the actual stimulation result is 3.247. After that, the oil production rate was increased by a ratio of 224.7 %.

Rheology testing of fracturing fluid candidates for the Gialo field was conducted to determine the optimum fluid composition. As a result, the candidates were selected water-based, crosslinked fluid is Borate Crosslinked Guar. However, 6J9 well was responded positively to the fractured hydraulic technique by implemented HPG Fluid System. This method was applied for high temperature as well as including (HSP- 20/40).

Conclusion

The Baseline Analysis results show HSP- 16/20 proppant provides the highest conductivity, under the predicted well stress conditions, the proppant type and size was selected for the stimulation. Thus results show that the borate crosslinked fluids with HSP- 16/20 provide the highest conductivity at 15 Kg/m² proppant areal concentration.

The Production Analysis results show that stimulating the well more than doubles the cumulative production after 2 years when compared to the well unstimulated. This analysis also shows that 15 Kg/m² proppant areal concentration with borate crosslinked fluids will provide the highest cumulative production after 2 years as well as the highest initial production rate just after stimulation, 28, 5100 m³ and 1,331 m³/day, respectively.

When comparing these values to 5 and 10 Kg/m² areal concentration results as seen in table 9 the most improvement is shown when going from 5 and 10 Kg/m² rather than when going from 10 to 15 Kg/m², but table 10 the most improvement is shown when going from 10 to 15 Kg/m² rather than when going from 5 to 10 Kg/m².

The percentage increase of initial production rate with 5 to 10 Kg/m² increasing 7.94 % and 10 to 15 Kg/m² increasing only 39.85 %.

The percentage increase in cumulative production after 2 years from 5 to 10 Kg/m² is 3.29 % where from 10 to 15 Kg/m² is only 2 %.

The same increase pattern is seen when comparing the different proppant areal concentration to the final NPV after 2 years.

References

Abhinav M. et al. (2017) Sondergeld. A Study of Propped-Fracture Conductivity: Impairment Mechanisms Under Laboratory Conditions. Presented at the SPWLA 58th Annual Logging Symposium held in Oklahoma City, *Oklahoma, USA*,

Aboud, S. and Melo, B. (2007) Past Technologies Emerge Due to Lightweight Proppant Technology: Case Histories Applied on Mature Field, *paper SPE 107184*

Canales, H. and Recep S. (2002) Concession 59 North Gialo. *Presentation. Waha Oil Company Exploration Department, ESG, Powerpoint Presentation.*

Droegemueller, B. and Leonhardt, B. (2005) Hydraulic Frac Stimulations in a Libyan Oil Field, A Case History. Society of Petroleum Engineers, *SPE European Formation Damage Conference, pp. 25-27*.

Duenckel, R. et al. (2016) The Science of proppant Conductivity Testing-Lessons Learned and Best Practices. *Society of Petroleum Engineers. doi: 10.2118/179125-MS*.

Economides, J. and Nolte, G. (2000) Reservoir Stimulation, 3rd ed. New York: *John. Wiley & Sons*.

Elsarawy, A. and Naser-El-Din, H. (2016) Laboratory Study on using produced in high PH Borate Gels Used in Hydraulic Fracturing. SPE-179553-MS. *Presented at the SPE Improved Oil Recovery Conference held in Tulsa, Oklahoma, USA, pp.2-17.*

Gandler, L. (2010) North Gialo Unitization Impact, *Presentation, Hess Corporation Libya Subsurface Team, Powerpoint Presentation.*

Gray, S. (2006) BJ Services Technology Center. ENG103 fundamentals of fracturing engineering version 2.0. *Report No. 06-05-0411*.

Kevin, F. and Norm, W. (2012) Hydraulic – Fracture- Height Growth: Real Data. SPE 145949. *Pinnacle, A Halliburton Service, pp.8- 19.*

Liang, T. et al. (2016) Identifying and Evaluating Surfactant Additives to Reduce Water Blocks after Hydraulic Fracturing for Low Permeability Reservoirs. Presented at the SPE Improved for Oil Recovery Conference, Tulsa, SPE- 179601-MS.https://doi.org/10.2118/179601-MS .

Li, Q. et al. (2015) How Extremely High-TDS Produced Water Compositions Affect Selection of Fracturing Fluid Additives. Presented at the SPE International Symposium on Oilfield Chemistry, The Woodlands, Texas, SPE-173746-MS. http://dx.doi.org/10.2118/173746-MS .

Liu, Y. and Sharme, M. (2002) Effect of Fracture Width and Fluid Rheology on Proppant Setting and Retardation: *An Experimental Study, paper SPE 96208*.

Mei, Y. et al. (2013) Hydraulic Fracture Design Flaws- Proppant Selection. *Presented at the SPE Annual Technical Conference and Exhibition, New Oleans. SPE-166299-MS.https://doi.org/10.2118/166299-MS , pp. 1-10.*

Raimbay, A. et al. (2017) Effective of Fracture Roughness, Shear Displacement, Fluid Type, and Proppant on the Conductivity of a single Fracture: A Visual and Quantitative Analysis. *Presented at the SPE/CSUR 171577) Unconventional resources Conference – Canada, pp. 446-470.*

Ribeiro, H. and Sharma, M. (2013) Fluid Selection for Energized Fracture Treatments. *Presented at the SPE hydraulic Fracture Technology Conference, the Woodlands, Texas, 4 – 6. SPE-163867-MS.https://doi.org/10.2118/163867-MS.*

Vispy F. (2004) Rheological Study of HydroxyPropyl Guar (HPG) Slurries. *Msc. Thesis. Norman. The University of Oklahoma.*

Xu, L. and Fu, Q. (2012) Proper Selection of Surfactant Additive Ensure Better Well Stimulation in Unconventional Oil and Gas Formations. *Paper SPE- 153265-MS presented at the SPE Middle East Unconventional Gas Conference and Exhibition, Abu Dhabi, UAE, 23-25, http://dx.doi.org/10.2118/153265-MS* .

Philipvan, D. (2008) North Gialo Well Log-Based Mechanical Properties & Stress Estimates for Application to Hydraulic Fracture Design. Petrophysical Analysis: *Report WNT.530405.IF-2008-1. Houston, Texas.*

Silva, M. (2010) MGP SVP Development Production, Hess Corporation Libya Subsurface Team, *PowerPoint Presentation.*

LaFollette, .F. and Carman, S., 2010. Proppant Diagnosis; Results So Far, *Paper SPE 131782-MS, SPE Unconventional Oil Conference and Exhibition, Denver, Colorado, May, 18.*

Registering the underground objects in the 3D cadastre: a case study of wine cellar located in the vineyard area Tokaj

Karel Janečka[1] *and* ***Diana Bobíková***[2]

The paper explores the way in which the underground objects can be measured, modelled, stored in spatial database and visualised for purposes of the 3D cadastre. The underground objects can be represented as 3D consolidated parcels representing an independent property that is not related to the surface parcel boundaries. The proposed solution is demonstrated for the wine cellar located in the vineyard area Tokaj. Since the international standard ISO 19152 Land Administration Domain Model exists and allows for the registration of 3D parcels, it is important that the used data model for storage of 3D underground parcels is based upon this standard. To model the 3D underground parcels the LADM boundary face concept with topological encoding is used. To visualise the 3D underground cadastral map, a new visualisation tool has been developed. The tool enables the visualisation of spatial data directly from the spatial database. When working with a huge amount of spatial data, it is necessary to optimise the way the data in the database are queried. To optimise the loading of data from the spatial database the vector tiles were created.

Keywords: *3D cadastre, underground objects, wine cellar, LADM, 3D visualisation.*

Introduction

The main purpose of the cadastral system is to support the registration of a title with a legally binding digital cadastral map (Falzon and Williamson, 2001). People want to have the legal status of their property clearly defined in the cadastre. That gives a clear and serious responsibility to cadastre to define the boundaries of the property in all dimensions. Also, the third dimension is a source of income and a criterion which increases the land value (Aydin, 2008). The current 2D cadastral systems cannot support the description of underground parcels (Sandberg, 2001). Kim and Heo (2017) argue that an advanced cadastral system is required for management of the physical and legal statuses of underground parcels. 3D cadastre then registers and gives insight into rights and restrictions not only on 2D parcels but also on 3D property units (Stoter and Oosterom, 2006).

In 2012 an international standard ISO 19152:2012 Land Administration Domain Model (LADM) was accepted. Domain-specific standardisation is needed to capture the semantics of the land administration domain on top of the agreed foundation of basic standards for geometry, temporal aspects, metadata and also observations and measurements from the field (Lemmen et al., 2015). LADM supports cadastral data exchange with and from the distributed land administration, for example, legal data related to cadastral objects with data from other sources describing physical objects as utilities (Janečka and Souček, 2017). It means that the concepts presented in LADM can be used in the building of Spatial Data Infrastructure (Čada and Janečka, 2016).

LADM also allows for the registration of 3D parcels and therefore has to be considered for establishing of the 3D cadastre including the registration of underground objects. The registration of underground objects has been recently studied. A volume of papers discuss the registration of underground utilities in the 3D cadastre (Cevdet (2008), Ghawana et al. (2013), Spirou-Sioula et al. (2013), Shoajei et al. (2013), Pouliot et al. (2015), Hashim et al. (2016)). In some countries (for example Serbia) the utilities are considered to be separate subjects of law which can be sold or bought and therefore there is a reason for their future registration using 3D spatial units (Radulović et al., 2018). This paper is more about the underground objects characterised by separate special-purpose use (typically wine cellars). Karabin et al. (2018) and Kitsakis et al. (2018) explored that in many countries around the world such underground objects (like wine cellars, metros, underground buildings) are considered to be real estates. However, they are not registered nor displayed on a cadastral map. Also, the legal and organisational aspects need to be considered, however, these are out of the scope of this paper.

Regarding the current manners in which the underground constructions are nowadays displayed on the 2D cadastral map, an example is illustrated in Figure 1. This approach is also applicable to the wine cellars (Janečka and Souček, 2017). Aydin (2008) argues that it is anticipated that without planning of underground spaces for supporting surface life city in the years and generations to come, there will be serious and unavoidable problems with growing populations and emphasizes the need to register the underground objects, but the wine cellars, metros or mining objects are not mentioned. However, it is obvious that also such objects need to be registered in the cadastre. Kim et al. (2015) introduced a concept of a 3D underground cadastral system based on data

[1] *Karel Janečka,* University of West Bohemia, Technická 8, 306 14 Pilsen, Czech Republic, kjanecka@kgm.zcu.cz
[2] *Diana Bobíková,* Technical University of Košice, Letná 9, 042 00 Košice, Slovakia, diana.bobikova@tuke.sk

acquisition with terrestrial laser scanning and proposed 3D underground property mapping with an indoor mapping method designed for as-built BIM. They defined the concepts of 3D underground parcels by the representation of survey measurements through the creation of new classes and attributes for the existing ISO 19152:2012 LA_SpatialUnit package and LA_Surveying and Representation package. The paper aims to demonstrate another suitable data acquisition method for the underground objects like wine cellars, the storage of the selected underground object in the LADM compliant data model and its visualisation using the own newly developed tool enabling basic visualisation directly from the Oracle Spatial database. This is in accordance with the general requirements for the establishment of 3D cadastre as defined (together with the need of 3D property registration laws) by Aien et al. (2013). The main advantage of the proposed solution is a possibility to model and store the existing 2D parcels and newly created 3D underground parcels in one environment. The newly created visualisation tool also enables to visualise such data directly from the spatial database without a necessity of their conversion into another data format.

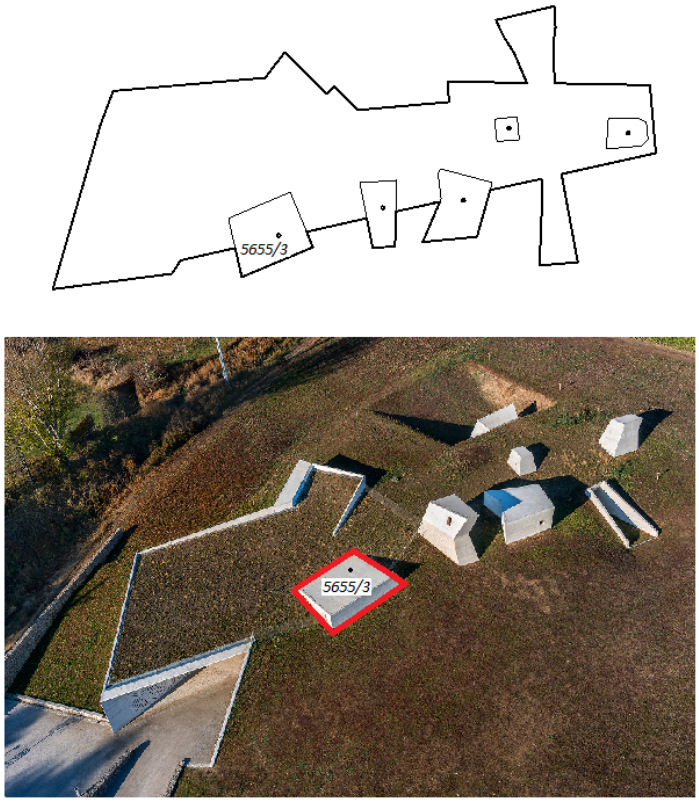

Fig. 1. (top) 2D visualisation of the boundaries of underground construction (Archeopark Pavlov, Czech Republic) on the cadastral map. Every component of the construction located above ground is displayed on a "separate" building parcel. However, in fact, only one building parcel is registered in the cadastre (here with parcel number 5665/3). (down) The photography of the underground object with components located above the ground. Highlighted in red is the part of the underground object corresponding to the building parcel 5655/3 (source of photography: http://alesjungmann.cz/project/archeopark-pavlov).

Due to the fact that the data model presented in the paper is based on LADM, it can serve as a base for extension of other LADM based models. In the last years, several LADM based country profiles have been proposed, i.e. for Poland (Bydłosz, 2015), Czech Republic (Janečka and Souček, 2017), Serbia (Radulović et al., 2017) or Croatia (Vučić et al., 2015). For example, the Czech LADM based country profile currently does not include the LADM class LA_BoundaryFace. The Czech cadastre still retains the 2D paradigm. The Czech LADM based country profile contains all of the classes and code lists required for Level 2 compliance. Moreover, it also contains some Level 3 classes. The Czech cadastre is based on the registration of 2D parcels, and therefore (for example), the Level 3 class LA_BoundaryFace is not integrated into the Czech profile. If the necessity for the further development of 3D systems arises within the Czech cadastre (e.g. advanced registration of underground objects), then the profile can be expanded precisely to support 3D parcels modelled using LA_BoundaryFace in the way as presented in this article.

The rest of the paper is structured as follows: The used research methodology is described in the section Methodology. The data acquisition method and creation of the 3D underground parcel is in detail described in the section Creation of a 3D model of the wine cellar. The paper intended that the proposed solution has to be in accordance with the ISO 19152:2012 (LADM) international standard. The section Registration of the

underground objects considering LADM introduces the data model and its fulfilling by the data. Furthermore, this section contains a description of the developed tool which enables the basic visualisation and first attempts towards the optimisation of the visualisation. The paper ends with the conclusions.

Methodology

The vineyard Tokaj is located to the southeast of Slovakia. This area, especially due to the high-quality and character of the land, is suitable for wine production. The storage of wine is one of the most important fact affecting its final quality. The wine cellars in this area are well-known for their macro- and microclimatic conditions. The wine cellars are located below the ground, only the entrance portals are located above the ground, as depicted in Figure 2. Nowadays, to register the wine cellars in the cadastre the survey sketch has to be created. The graphical part of the survey sketch is shown in Figure 3. To know the exact legal and physical extent of wine cellars in a given area is a necessary condition for the further 3D development of the area including the property rights. The paper assumes that the legal extent of the 3D underground parcel representing wine cellar is defined by its physical boundaries. If there is a necessity to store some protected area around the wine cellar, then the physical boundaries will be different from the legal boundaries including the protected area.

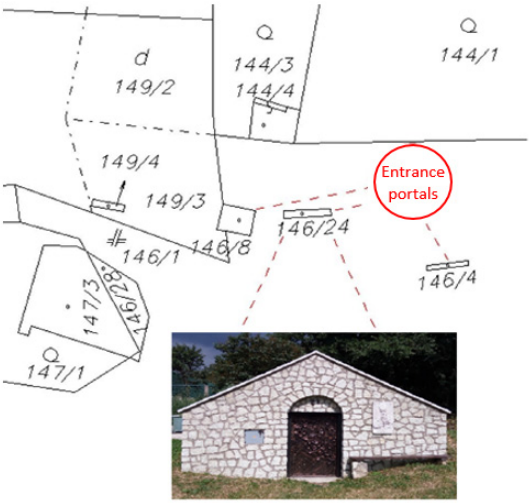

Fig. 2. The entrance portals of wine cellars (vineyard area Tokaj, cadastral unit Veľká Tŕňa) and their displaying on the 2D cadastral map. In this case, every entrance portal is established on separate building parcel.

Fig. 3. Demonstration of the graphical part of the technical background (survey sketch – for measurement of the entrance portal, underground cellars and passages marked with letters A-K) serving to register a legal act (from a letter - contract) into cadastre of real estates (Bobíková and Janečka, 2017).

Regarding the registration and modelling of 3D parcel representing the underground construction, there are in principle two main basic principles (which are also applicable for underground utilities). The 3D underground parcel can be split into several smaller 3D spatial units with respect to the surface parcel partition. Such an approach was demonstrated, for example, by Thompson et al. (2017). All these smaller 3D parcels then together form the whole 3D underground parcel which represents the underground construction. The conception of 3D underground parcel representing the wine cellar used in this paper is as given by Karki et al. (2013) and Van Oosterom (2013), i.e. the 3D underground consolidated parcel representing an independent property that is not related to the surface parcel boundaries. The latter approach still enables the user to ask the queries like finding all the surface parcels below which the 3D underground parcel is located and is quite independent on the situation (partition of parcels) on the surface. Döner et al. (2011) recommend using the absolute heights for geometries of 3D underground parcels. In such case, the geometry of the 3D underground parcel is not related to the surface. Therefore, to model the 3D underground parcel representing the underground wine cellar the consolidated parcel with absolute heights was used. Furthermore, Thompson et al. (2015) introduced a categorisation of 3D spatial units consisting of several categories. Among others, there is the category of general 3D spatial units, which can be potentially used also for representation of underground objects. The category of general 3D spatial units contains the spatial units whose geometries are formed by general faces. From the LADM perspective, such 3D spatial units can be modelled using the LADM boundary face concept. As recognised by Janečka et al. (2017), to store the geometries of such 3D spatial units into the spatial database management system, the freeform faces need to be appropriately approximated by planar faces. This is also the case of the 3D underground parcel representing the wine cellar which is described in the paper as in the reality the wine cellar's ceiling is shaped like an arc.

The used data model is based on the model proposed by Thompson (2013). The data model follows the LADM concepts and enables storing both 2D (using boundary face strings concept) and 3D (using boundary face concept) spatial units, i.e. the boundaries of 2D surface parcels above the wine cellar were stored in the same data model as the 3D underground parcel representing the wine cellar. Furthermore, a precise Digital Terrain Model (DTM) was available for the territory of the study area. The paper presents three types of underground cadastral mapping for the wine cellar, according to Kim et al. (2015):

1. An isometric view of the 3D underground cadastral map. This is used to describe the geometric information of a 3D underground parcel separately from the surface parcel.
2. A 2D surface parcel with footprints of the 3D underground cadastral map, which is used to represent the 3D underground property with corresponding surface parcels.
3. A 3D surface and 3D underground cadastral map, which are used to represent the location of 3D underground properties with regard to real-world situations. They are able to register and manage depth information, which represents the difference between 3D surface and 3D underground property.

In order to optimise the way in which data are retrieved for visualisation the data model was extended for the classes storing the vector tiles.

Creation of a 3D model of the wine cellar

Data acquisition

A geometrical model of the 3D parcel is required for registration of 3D properties (Kim et al., 2015). To create the model of the wine cellar the data with appropriate accuracy are needed. Nowadays, there are a lot of different methods that are suitable for surveying 3D objects. However, they are effective for 3D above-ground cadastral systems and are not well suitable to 3D underground cadastral systems.

The used method to capture the detail data for creation of the 3D model of wine cellar was tacheometry. Using tacheometry, one can determine the position and height of the point (X, Y, and Z point coordinates) in the defined coordinate system. Principle lies in measurements of oblique length, horizontal and height (zenith) angle simultaneously by one instrument – universal measuring station (UMS) (Blišťan and Kovanič, 2012). The accuracy of tacheometry using UMS is sufficient also for the needs of precise documentation of various underground geo-objects (for example wine cellars).

Creation of the 3D wire-frame model

Upon the measured points, the 3D wire-frame model was created. The creation of the 3D wire-frame model of wine cellar was done in MicroStation Descartes software and stored in DGN file format. For the visualisation purposes (see Figure 4) the "faces" were classified (floors, walls, ceilings).

Fig. 4. The 3D model of the wine cellar. The floors are highlighted in green, walls are brown, and ceilings are blue (Janičková et al., 2016).

Registration of the underground objects considering LADM

The data model

To store the 3D model representing the wine cellar in the spatial database the data model based on the model by Thompson (2013) was proposed. The used data model is based on the LADM and is able to accommodate full 3D parcels. It also supports all level of encodings defined in ISO 19152:2012 (ISO-TC211, 2012). In case of wine cellar topology based encoding was used, i.e. adjacency is directly encoded in the database. Another advantage of the data model is that is also able to combine 2D and 3D spatial data seamlessly. To model the 3D boundaries of underground objects the boundary face concept presented in ISO 19152:2012 is used. The principle of the concept is captured in Figure 5. The corresponding class for modelling boundary faces is LA_BoundaryFace. An instance of class LA_BoundaryFace is a boundary face. Another LADM class used in the research is LA_BoundaryFaceString to model 2D parcels (which could be theoretically interpreted as unbounded volumes). The principle of the boundary face string concept is demonstrated in Figure 6. The physical data model for storing the 2D and 3D spatial units is captured in Figure 7.

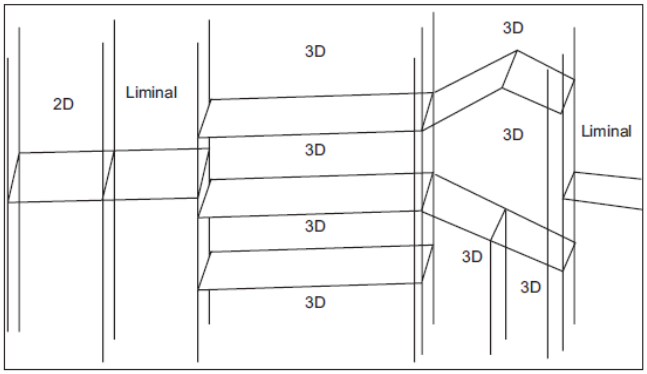

Fig. 5. The side view showing the mixed use of boundary face strings and boundary faces to define both bounded and unbounded 3D volumes (according to ISO-TC211 (2012)).

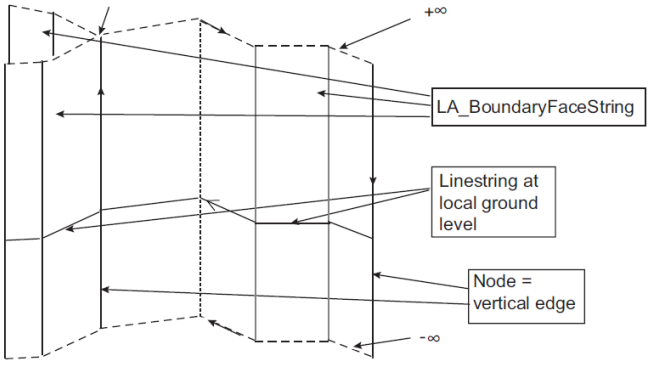

Fig. 6. Boundary face string concept (according to ISO-TC211 (2012)).

From the wire-frame model to the boundary representation

The original 3D wire-frame model of the wine cellar was stored in the DGN file format. Using the FME software the data was transformed into the Object File (OBJ) in ASCII format. The OBJ file then contains a list of vertex indices and triangle face elements. These triangle face elements represent the boundary of the wine cellar. According to the boundary face concept defined in LADM (ISO-TC211, 2012), the ordering of the vertices describing a particular face (triangle) must guarantee that the normal vector of that face is pointing to the exterior of the object. As the next step, the Java utility was created. This utility has the OBJ file as an input and returns the text files with SQL INSERT statements. For every table to be filled a separate text file is created. Furthermore, using the SQL Developer client, the data was imported from the text files into the Oracle Spatial database. To store the X and Y coordinates of the points the SDO_GEOMETRY data type is used. The Z coordinate is stored in the CORNER table (attribute elevation).

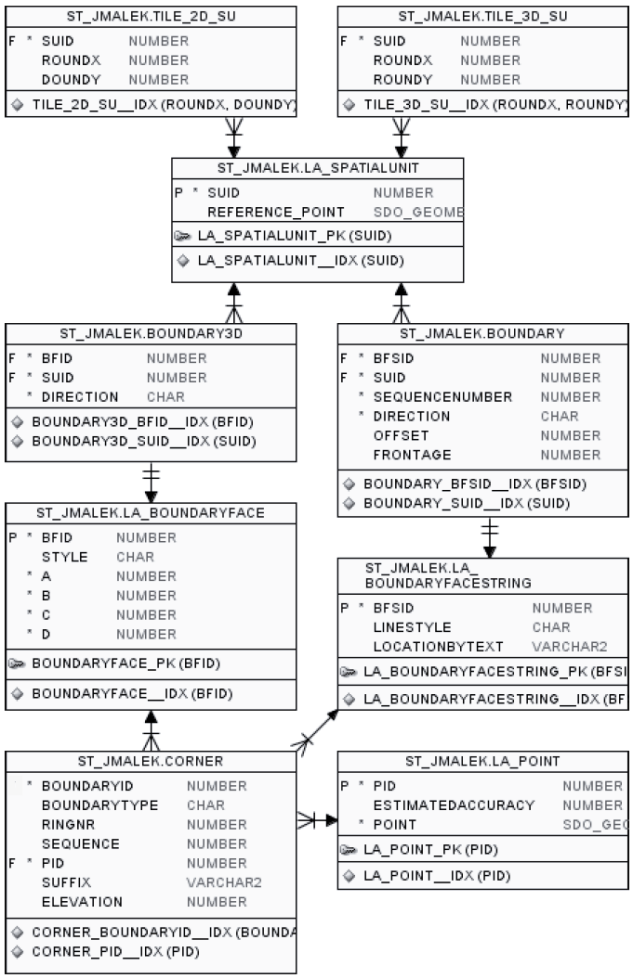

Fig. 7. The physical data model for storing the 2D and 3D spatial units. The model is in accordance with the one defined in Thompson (2013). The newly added tables are TILE_2D_SU and TILE_3D_SU to store the vector tiles.

Figure 8 illustrates the overall used data workflow. Existing 2D cadastral data were imported into the proposed data model together with the 3D model of the underground object and stored in an Oracle Spatial database.

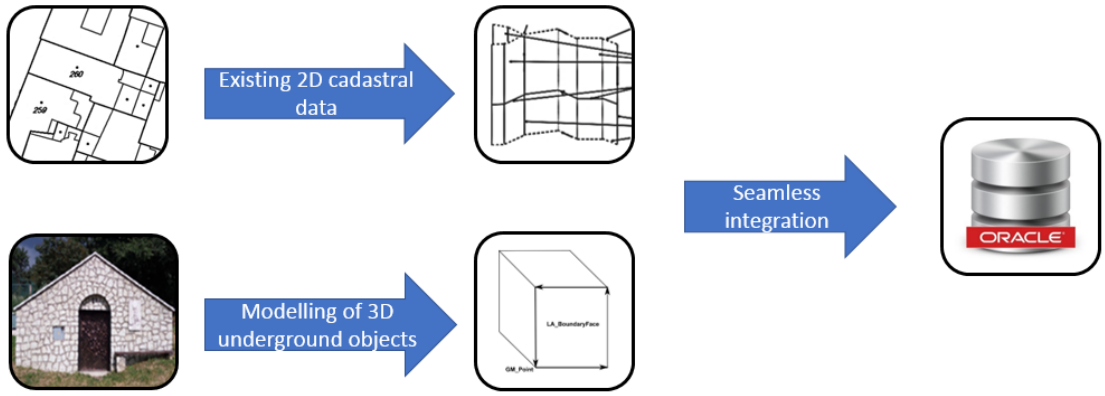

Fig. 8. Existing 2D cadastral data were imported into the data model according to the boundary face string concept. The 3D model of the wine cellar was stored using a boundary face concept.

Visualisation

After the data had been loaded into the database, the remaining task was to visualise the integrated 2D parcels (2,5D respectively) and 3D underground parcel. The intention was to make a program that would load the data directly from the database from the implemented data model, without the need of any middleware or transformation into another data format. To create the visualisation tool, C# has been used instead of previously intended Java, since it offers better performance and seemingly better engines, although it is not as portable. In particular, a 3D game engine called Unity (Agugiaro et al., 2011; Ruzinoor et al., 2015) has been used, which comes with its own programming environment. So instead of writing a complete program, the solution was to write scripts that create and manipulate elements in this environment. This proved to be useful as extensions such as camera movement, or object colouring can be added easily.

The trouble was encountered when trying to load the cadastral data from the database because Unity engine does not support the .NET version needed for the usage of ODBC (Open database connectivity). To solve this issue, an executable programme ParcelLoader.exe was created in C# using Oracle.ManagedDataAccess library. The created executable programme then runs with specific parameters within the Unity environment to retrieve the requested data (parcels) from the database as depicted in Figure 9. The developed tool for visualisation is currently able to load and visualise 2D and 3D parcels directly from the Oracle Spatial database.

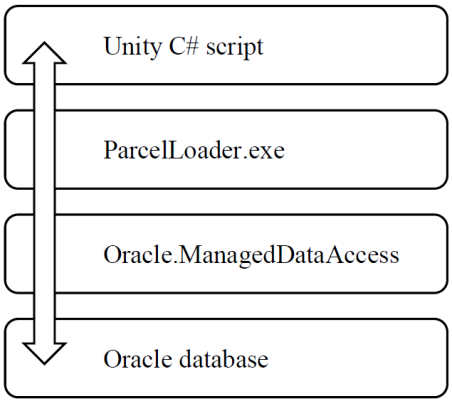

Fig. 9. The principle of using Unity C# script to receive the data from Oracle database.

Figure 10 presents the isometric view of wine cellar using the developed visualisation tool. This tool serves as a proof of concept of visualisation of the data directly from the Oracle Spatial database from the data model presented in Figure 7.

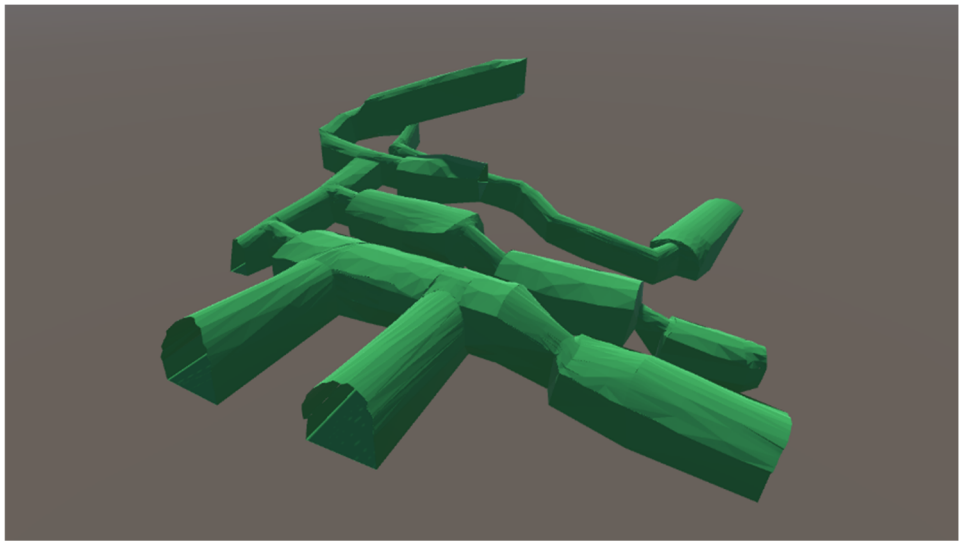

Fig. 10. Isometric view of a 3D underground cadastral map of wine cellar using the developed visualisation tool.

Figure 11 demonstrates the combination of 2D surface parcels with footprints of the wine cellar.

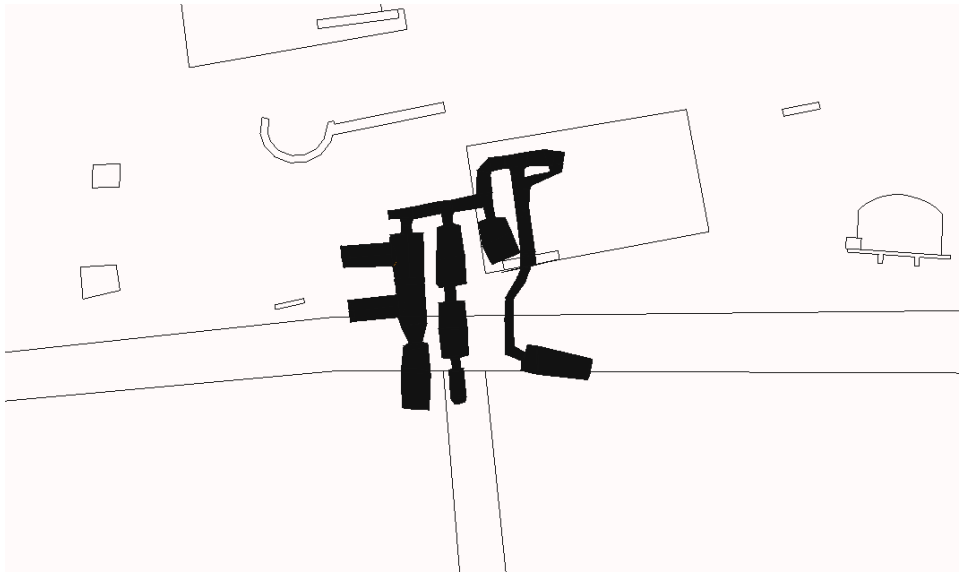

Fig. 11. 2D surface parcel with footprints of a 3D underground cadastral map of the wine cellar.

The developed visualisation tool does not allow for displaying DTM. Therefore, to visualise 3D surface (DTM) and 3D underground cadastral map ArcScene software was used (see Figure 12).

In case that one would like to visualise 2,5D parcels (2D parcels projected onto the DTM) using the developed visualisation tool, then the further development is needed. If the DTM is stored in the spatial database together with 2D and 3D parcels, then it would be theoretically possible to compute the projection of the boundaries of the 2D parcels onto the DTM directly at the side of a spatial database and then visualise them. Another approach could be to compute the projection at the side of the visualisation tool. To enable this computation, the capabilities of the tool has to be extended in the future also to support the loading (and visualisation) of DTM.

Fig. 12. 3D surface and 3D underground cadastral map.

Vector tiles for database query optimisation

The tool which has been developed aims to visualise the stored data from the spatial database. The main intention (from the paper's perspective) was to make a direct visualisation without conversion of the data into other format and to visualise the data from the LADM compliant data model containing both 2D and 3D topologically structured geometries. First, to retrieve the data from the database faster, the R-tree spatial indices were created upon the spatial attributes.

When working with a database with huge amount of spatial data it is necessary to optimise the way the data in the database are queried. Therefore the vector tiles (200x200 meters) related to spatial units were created. The indexing tables (TILE_2D_SU and TILE_3D_SU) store the identifier of the spatial unit and XY coordinates of the centre (s) of corresponding vector tile(s). This way only spatial units on nearby tiles are loaded while browsing the data. The principle of creation of vector tile is captured in Figure 13.

Fig. 13. The principle of how the vector tile is created. The grey highlighted parcels are associated with the particular tile.

Conclusions

The paper explored important aspects of the building of the 3D underground cadastre – the data acquisition, data modelling and 3D visualisation. The further work will also focus on the proposal of 3D property registration laws dealing with underground objects. The data model presented in figure 7 could be easily extended to support both the legal and physical boundaries of underground objects.

At the moment 2D and 3D parcels are stored in the spatial database in LADM based data model. The digital terrain model is stored outside the database in the DGN file format. In the further research, DTM will be stored in the spatial database; the first attempt is given for example in Janečka and Kára (2012).

The visualisation tool developed in this research is able to load and visualise 2D and 3D parcels directly from the Oracle Spatial database. Currently, the spatial database contains only a testing dataset consisting of

several tens of geometries. In the future work, the larger datasets will be imported into the database and performance analysis will be done.

The visualisation tool will be further developed in order to support also visualisation of DTM stored in the spatial database and 2,5D parcels in combination with 3D parcels.

The used approach for the 3D data acquisition, 3D modelling of the underground object and its 3D visualisation is applicable also on other types of underground objects, i.e. mining objects and is fully conformant with LADM.

Acknowledgement: *The first author of this publication was supported by the project LO1506 of the Czech Ministry of Education, Youth and Sports.*

References

Agugiaro, G., Remondino, F., Girardi, G., von Schwerin, J., Richards-Rissetto, H., De Amicis, R. (2011) A Web-Based Interactive Tool for Multi-Resolution 3d Models of a Maya Archaeological Site, ISPRS Trento 2011 Workshop, Trento, Italy.

Aien, A., Kalantari, M., Rajabifard, A., Williamson, I., Wallace, J. (2013) Towards integration of 3D legal and physical objects in cadastral data models. Land Use Policy, 35, 140–154.

Aydin, C., C. (2008) Usage of Underground Space for 3D Cadastre Purposes and Related Problems in Turkey. Sensors, 8, 6972-6983.

Blišťan, P., Kovanič, Ľ. ml. (2012) Geodetic methods for efficient spatial data collection. Egrse. Vol. 19, 1.

Bobíková, D., Janečka, K. (2017) Evidovanie podzemných objektov v trojrozmernom priestore budúceho katastra nehnuteľností. In: Proceedings of 10th International Scientific and professional Conference Geodesy, Cartography and Geoinformatics. Repiská, Slovakia, ISBN 978-80-553-2814-0.

Bydłosz, J. (2015). The application of the Land Administration Domain Model in building a country profile for the Polish cadastre. Land Use Policy, 49, 598–605.

Cevdet, C. A. (2008) Usage of Underground Space for 3D Cadastre Purposes and Related Problems in Turkey. Sensors. 8, 11, s. 6972–6983.

Čada, V., Janečka, K. (2016) The Strategy for the Development of the Infrastructure for Spatial Information in the Czech Republic. ISPRS Inter. J. Geo-Inf., 5, 33.

Döner, F., Thompson, R., Stoter, J., Lemmen, C., Ploeger, H., van Oosterom, P., Zlatanova, S. (2011) Solutions for 4D Cadastre–With a Case Study on Utility Networks. International Journal of Geographical Information Science. 25, 7, s. 1173–1189.

Falzon, K., Williamson, I. (2001) Digital lodgement of cadastral survey data in australia-issues and options. Aust. Surv., 46, 62–71.

Ghawana, T., Hespanha, J., Khandelwal, P., van Oosterom, P. (2013) 3D Cadastral Complexities in Dense Urban Areas of Developing countries: Case Studies from Delhi and Satellite Towns. In: Proceedings of FIG Working Week. Abuja, Nigeria.

Hashim, M., Jaw, S. W., Marghany, M. (2010) Subsurface Utility Mapping for Underground Cadastral Infrastructure. In: Proceedings of 31st Asian Conference on Remote Sensing (ACRS), Volume: 2.

ISO-TC211 (2012) Geographic Information - Land Administration Domain Model (LADM). ISO 19152.

Janečka, K., Kára, M. (2012) Advanced Data Structures for Surface Storage. In: Proceedings of GIS Ostrava 2012 – Surface models for geosciences. VŠB-TUO, Ostrava, ISBN 978-80-248-2667-7.

Janečka, K., Souček, P. (2017) A Country Profile of the Czech Republic Based on an LADM for the Development of a 3D Cadastre. ISPRS Int. J. Geo-Inf., 6, 143.

Janečka, K., Karki, S., van Oosterom, P., Zlatanova, S, Kalantari, M., Ghawana, T. (2018) Chapter 4. 3D Spatial DBMS for 3D Cadastres. In: Best Practises 3D Cadastres - Extended version. Editor: Peter van Oosterom. International Federation of Surveyors (FIG), 133–182, ISBN: 978-87-92853-64-6.

Janičková, I., Kovanič, Ľ, Blišťan, P. (2016) Dokumentácia skutočného stavu vínnej pivnice v obci Veľká Tŕňa. Bachelors work. Faculty of Mining, Ecology, Process Control and Geotechnologies, Technical University of Košice, Košice.

Karabin, M., Kitsakis, D., Koeva, M., Navratil, G., Paasch, J., Paulsson, J., Vučić, N., Janečka, K., Lisec, A. (2018) Layer Approach to ownership in 3D cadastre – a subway case. In: Proceedings of the 6th International FIG Workshop on 3D Cadastres 2-4 October 2018, Delft, the Netherlands. Peter van Oosterom and Dirk Dubbeling (eds.). International Federation of Surveyors (FIG), 111-136, ISBN: 978-87-92853-80-6.

Karki, S., Thompson, R., McDougall, K. (2013) Development of validation rules to support digital lodgement of 3D cadastral plans. Comput. Environ. Urban Syst. 40, 34–45.

Kim, S., Heo, J. (2017) Development of 3D underground cadastral data model in Korea: Based on land administration domain model. Land Use Policy, 60, 123-138.

Kim, S., Kim, J. Jung, J., Heo, J. (2015) Development of a 3D Underground Cadastral System with Indoor Mapping for As-Built BIM: The Case Study of Gangnam Subway Station in Korea. Sensors, 15.

Kitsakis, D., Paasch, J. M., Paulsson, J., Navratil, G., Vucic, N., Karabin, M., El-Makawy, M., Koeva, M., Janečka, K., Erba, D., Alberdi, R., Kalantari, M., Yang, Z., Pouliot, J., Roy, F., Montero, M., Alvarado, A., Karki, S. (2018) Chapter 1. Legal foundations. In: Best Practises 3D Cadastres – Extended version. Editor: Peter van Oosterom. International Federation of Surveyors (FIG), 1–66, ISBN: 978-87-92853-64-6.

Lemmen, Ch., van Oosterom, P., Benett, R. (2015) The Land Administration Domain Model. Land Use Policy, 49, 535-545.

Pouliot, J., Bordin, P., Cuissard, R. (2015) Cadastral Mapping for Underground Networks: A Preliminary Analysis of User Needs. In: Proceedings of the International Cartographic Conference, Brazil.

Radulović, A., Sladić, D., Govedarica, M. (2017) Towards 3D Cadastre in Serbia: Development of Serbian Cadastral Domain Model. ISPRS Int. J. Geo-Inf., 6, 312.

Radulović, A., Sladić, D., Govedarica, M., Ristić, A., Jovanović, D. (2018) Towards 3D Utility Network Cadastre: Extended Serbian LADM Country Profile. In: Proceedings of the 6th International FIG Workshop on 3D Cadastres 2-4 October 2018, Delft, the Netherlands. Peter van Oosterom and Dirk Dubbeling (eds.). International Federation of Surveyors (FIG), 95-110, ISBN: 978-87-92853-80-6.

Ruzinoor C., M., Zulkifli, A., N., Nordin, N., Mohd Yusof, S., A. (2015) Online 3D Oil Palm Plantation Management Based on Game Engine: A Conceptual Idea, Jurnal Teknologi, volume 78.

Sandberg, H. (2001) Three-dimensional division and registration of title to land: legal aspects. Proceedings of the Registration of Properties in Strata-International Workshop on 3D Cadastres, 201–209.

Shojaei, D., Kalantari, M., Bishop, I. D., Rajabifard, A., Aien, A. (2013) Visualization Requirements for 3D Cadastral Systems. Computers, Environment and Urban Systems. 39–54.

Spirou-Sioula, K., Ioannidis, C., Potsiou, C. (2013) Technical Aspects for 3D Hybrid Cadastral Model. Survey Review. 45, s. 419–427.

Stoter, J., E., van Oosterom, P. (2006) 3D Cadastre in an International Context: Legal, Organizational, and Technological Aspects; Crc Press: Boca Raton, FL, USA.

Thompson, R. J. (2013) Progressive Development of a Digital Cadastral Data Base, 5th Land Administration Domain Model Workshop, Kuala Lumpur, Malaysia.

Thompson, R., van Oosterom, P., Karki, S., Cowie, B. A (2015) Taxonomy of Spatial Units in a Mixed 2D and 3D Cadastral Database. In: Proceedings of the FIG Working Week. Sofia, Bulgary, ISBN: 978-87-92853-35-6.

Thompson, R., van Oosterom, P., Soon, K. H. (2017) LandXML Encoding of Mixed 2D and 3D Survey Plans with Multi - Level Topology. ISPRS Int. J. Geo-Inf., 6, 6.

Van Oosterom, P. (2013) Research and development in 3D cadastres. Comput. Environ. Urban Syst. 40, 1–6.

Vučić, N., Markovinović, D., Mičević, B. (2013). LADM in the Republic of Croatia-making and testing country profile. In Proceedings of the 5th FIG International Land Administration Domain Model Workshop 2013, Kuala Lumpur, Malaysia, 24–25 September 2013.

Automated Separation of Basalt Fiber and Other Earth Resources by the Means of Acoustic Vibrations

***Anri Elbakian*[1], *Boris Sentyakov*[1], *Pavol Božek*[2], *Ivan Kuric*[3] *and* *Kirill Sentyakov*[1]**

The production of a composite nanostructured polymer reinforced with basalt fiber requires precise and fine separation of non-fibrous inclusions. The unique properties of such material predetermine it for use in various sectors, but especially in mining (safer for mining purposes, for example, drilling without sparkle occurrence, lower production price than metal mining tools, etc.) (Kemal Ozfirat, 2015). Basalt fiber is a material from which products with excellent thermal conductivity, hygroscopicity, and chemical resistance are obtained, in addition, they do not burn. Used in many industries, including mechanical engineering, as well as heat insulation material in the construction and other human activities. However, in the production of basalt fiber cloths, non-fibrous inclusions are formed. These inclusions reduce the quality of the products and, due to their barbs, can lead to injuries, especially of the mucous membrane. It was found in research (Timoshenko et al., 1985) that when affecting basalt fiber canvases by sound waves of the acoustic field, non-fibrous inclusions are falls from them. The task of modeling this phenomenon and process is worthwhile.

Keywords: *basalt fiber, non-fiber inclusion, frequency, vibrations, sound, precise separation, mining*

Introduction

Recently, continuous filaments extruded from naturally flame-retardant basalt beads were examined as substitutes for asbestos fibers in almost all their applications. It is claimed that basalt fiber products offer similar properties to S-2 glass fibers at a price between glass S-2 and E glass and can offer manufacturers a cheaper alternative to carbon fiber products.

Basalt is an igneous volcanic rock. It is used as a raw material for the production of basalt fiber (for the production of heat and sound insulating materials, composite basalt reinforcement, for example). Mats of basalt fiber have an excellent thermal conductivity, hygroscopicity, and chemical resistance; in addition, it does not burn. Used in many industries, including mechanical engineering, as well as heat insulation material in the construction and other human activities (Kim and Lee, 2010; Asdrubali et al., 2014; Wand and Torng, 2001; Pompoli, 2004; Papadopoulos, 2005; Timoshenko et al., 1985). Materials reinforced with basalt fiber are highly resistant to weathering (including ultraviolet light), crashes (in crushed form, basalt fiber is also a part of mixture in concrete), corrosion with prolonged lifespan compared to steel, creating more durable structures with lower transportation costs due to lighter materials (lighter than reinforced concrete or metal poles) and easier handling which is suitable for mining industry, for example, for creating reinforcements for mining shafts (Lopresto et al., 2011). These features open up access to new technologies, results of scientific studies with these materials are applicable at world level.

The competitive advantages of materials reinforced with basalt fiber include:

- three times more durable than steel;
- no corrosion of the material;
- one-quarter of steel weigh;
- lower shipping costs;
- more economical to build high constructions;
- material lifespan is over 100 years;
- heat resistance 700 ° C and short-term, up to 1000 ° C (Buratti et al., 2013; Moretti et al., 2014; Buratti et al., 2014; Fabian et al., 2015; ASTM C518-10, 2003; EN ISO 12667, 2001; ISO 10534-2, 1998)

Areas of the usage of the basalt fiber are mainly the construction industry and especially mining. However, in the production of basalt fiber cloths, so-called non-fibrous inclusions are formed, which are bunches of molten original basalt filament. Their quantitative content depends on the perfection of the technological process of obtaining basalt fiber. In any case, these inclusions reduce the quality of the products and, due to their barbs, can

[1] *Anri Elbakian, Boris Sentyakov, Kirill Sentyakov***,** Department of Mechatronic Systems, Faculty of Quality Management, Kalashnikov Izhevsk State Technical University, Studencheskaya street, 7, 426069, Izhevsk, Russia, henry25@mail.ru, sentyakov@inbox.ru, la1030@mail.ru

[2] *Pavol Božek,* Institute of Production Technologies, Faculty of Materials Science and Technology in Trnava, Slovak University of Technology in Bratislava, Jána Bottu street, 25, 917 24, Trnava, Slovak Republic, pavol.bozek@stuba.sk

[3] *Ivan Kuric,* Department of Automation and Production Systems, Faculty of Mechanical Engineering, University of Žilina, Univerzitná 8215/1, 010 26 Žilina, Slovak Republic, ivan.kuric@fstroj.utc.sk

lead to injuries, especially of the mucous membrane. It was found in research (Biderman, 1980) that affecting basalt fiber canvases by sound waves of the acoustic field, non-fibrous inclusions are falls from them. The task of modeling this phenomenon and process is worthwhile.

Figure 1 shows the scheme of basalt fiber in the form of an oscillatory system. The elementary fiber can be mistaken for an elastic beam located on adjacent curved fibers. Let us assume that on such fibers the non-fibrous excess inclusions having different geometric shapes and different masses are held by the forces of natural adhesion. Moreover, elementary fibers with non-fibrous inclusions attached to them are affected by the acoustic field. This research is done on the basis of the considered general theoretical principles of the investigation of the oscillatory system (Biderman, 1980; Bolotin, 1978; Makarov, 1982; Mensky, 1982; Uysal, 2013; Cavus, 2013).

Further below we will build a mathematical model of the process of sound impact on the considered system of interacting bodies connected by an elastic coupling (Figure 1).

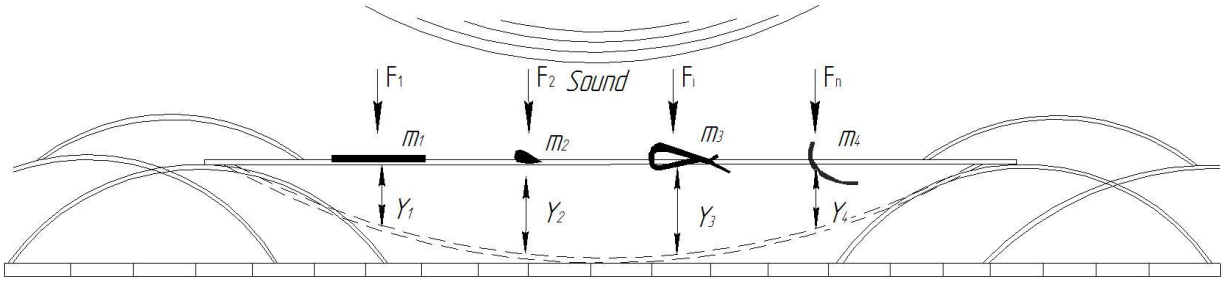

Fig. 1. The calculation scheme.

In Figure 1: m is the mass of non-fibrous inclusion, kg; c is the adhesion stiffness, $N.m^{-1}$; a is the damping coefficient (for energy losses due to viscous friction), kg. s^{-1}; y is the displacement of non-fibrous inclusions from the static equilibrium position, m; x is the displacement of the elastic base under the action of the driving force of the sound wave, m.

Consider the balance of power, acting on each of the four masses. We take Newton's second law as a basis. In this model, two forces are defined:

- the force of elastic resistance proportional to the movement,
- proportional to the speed of movement the force of elastic resistance.

According to the scheme for calculating the equilibrium equation of four forces (figure 1), we obtain a system of four differential equations in Eq. 1.

$$\begin{cases} m_1 y_1'' = c(x - y_1) + c(y_2 - y_1) + a(x' - y_1') + a(y_2' - y_1') \\ m_2 y_2'' = c(y_1 - y_2) + c(y_3 - y_2) + a(y_1' - y_2') + a(y_3' - y_2') \\ m_3 y_3'' = c(y_2 - y_3) + c(y_4 - y_3) + a(y_2' - y_3') + a(y_4' - y_3') \\ m_4 y_4'' = c(x - y_4) + c(y_3 - y_4) + a(x' - y_4') + a(y_3' - y_4') \end{cases} \quad (1)$$

The following second-order differential equations Eq. 2 can describe the free movement of each mass separately.

$$m_i y_i'' + a y_i' + c y_i = 0 \quad (2)$$

Or in the form of a typical oscillatory link (Makarov, 1982) of the dynamic system (Eq. 3).

$$T_i^2 y_i'' + 2T_i \xi_i y_i' + y_i = 0 \quad (3)$$

Where T_i is the period of free oscillations (or time constant), s;

ξ_i - the damping coefficient ($0 < \xi_i < 1$).

These parameters in the joint consideration of Eq. 2 and Eq. 3 are the following (Eq. 4, Eq. 5):

$$T_i = \sqrt{\frac{m_i}{c}} \quad (4)$$

$$a = 2T_i \xi_i c \quad (5)$$

Then the fundamental frequency of each of the four elements is determined from the known formula (Makarov, 1982):

$$\omega_i = \frac{\sqrt{1-\xi_i^2}}{T_i} = \frac{\sqrt{4m_i c - a^2}}{2m_i} \tag{6}$$

Using an analytical method for solving the system of Eq. 1, we get one linear differential equation. It has constant coefficients of the eighth order. The further task causes certain difficulties, since it involves the consideration of various solutions for real and complex roots, finding the roots of the characteristic equation of the eighth degree.

It is necessary to investigate the object in the frequency domain, as well as to consider alternative ways to solve the system (Eq. 1). It is proposed to use the methods of Makarov (Makarov, 1982) Automatic Control Theory (TAU). Applying the Laplace transforms, and going over to the images (Eq. 7), the system (Eq. 1) can be represented in the form (Eq. 8):

$$\begin{cases} y_i'' \to p^2 Y_i \\ y_i' \to p Y_i \end{cases} \tag{7}$$

$$\begin{cases} m_1 p^2 Y_1 + 2apY_1 + 2cY_1 = (c + ap)(X + Y_2) \\ m_2 p^2 Y_2 + 2apY_2 + 2cY_2 = (c + ap)(Y_1 + Y_3) \\ m_3 p^2 Y_3 + 2apY_3 + 2cY_3 = (c + ap)(Y_2 + Y_4) \\ m_4 p^2 Y_4 + 2apY_4 + 2cY_4 = (c + ap)(Y_3 + X) \end{cases} \tag{8}$$

Or as a system of operator equations with transfer functions (Eq. 9):

$$\begin{cases} Y_1 = W_1(X + Y_2) \\ Y_2 = W_2(Y_1 + Y_3) \\ Y_3 = W_3(Y_2 + Y_4) \\ Y_4 = W_4(Y_3 + X) \end{cases} \tag{9}$$

The following equation (Eq. 10) expresses a mathematical model of the structural elements of a dynamic system by defining the transfer function of the operator.

$$\begin{cases} W_1 = \frac{c+ap}{m_1 p^2 + 2ap + 2c} \\ W_2 = \frac{c+ap}{m_2 p^2 + 2ap + 2c} \\ W_3 = \frac{c+ap}{m_3 p^2 + 2ap + 2c} \\ W_4 = \frac{c+ap}{m_4 p^2 + 2ap + 2c} \end{cases} \tag{10}$$

Then, solving the system (Eq. 9) about Y_i for a given X, we obtain a system solution (Eq. 1) for all masses in the following operator form (Eq. 11).

$$Y_i = W_{pi}(p)X \tag{11}$$

We can obtain an analytical solution to the problem through the inverse Laplace transform.

Applying a complex transfer function (Eq. 12), according to the known formulas (Makarov, 1982; Sentyakov, 2004; Timofeev, 2004; Jasenek et al., 2012) we have the amplitude-frequency $A(\omega)$ and the phase-frequency $\varphi(\omega)$ characteristics (Eq. 12):

$$\begin{cases} W_P(\omega i) = Re(\omega) + Im(\omega) \cdot i \\ A(\omega) = |W_P(\omega i)| = \sqrt{Re(\omega)^2 + Im(\omega)^2} \\ \varphi(\omega) = arg\ (W_P(\omega i)) = arctg(Im(\omega)/Re(\omega)) \end{cases} \tag{12}$$

As the square roots of the eigenvalues of the matrix (Eq. 13) coefficients of the original (Eq. 1) undamped ($\xi_i = 0$, $a_i = 0$) differential equations system, the critical frequencies can be calculated without amplitude response.

$$\begin{bmatrix} \frac{-2c}{m_1} & \frac{c}{m_1} & 0 & 0 \\ \frac{c}{m_2} & -\frac{2c}{m_2} & \frac{c}{m_2} & 0 \\ 0 & \frac{c}{m_3} & -\frac{2c}{m_3} & \frac{c}{m_3} \\ 0 & 0 & \frac{c}{m_4} & \frac{-2c}{m_4} \end{bmatrix} \quad (13)$$

Material and Methods

Calculate the eigenvalues of the matrix of the fourth order. This will again require the solution of high order algebraic equations. We will use one of the many application software solutions for such tasks (Shaiks, 2018; Haque, 2018; Kuzmin et al., 2015).

The dynamic characteristic of the system is obtained in accordance with the proposed model. The following physical quantities are used:

- elementary fiber diameter d = 0.003 mm;
- elementary fiber length L = 35 mm;
- size (the ball diameter) of inclusions v_1 = 0.3, v_2 = 0.1, v_3 = 0.5, v_4 = 0.2 mm;
- Basalt densityp = 2300 kg . m^{-3} = 2.3 mg . mm^{-3};
- Basalt elasticity modulus E = 100 GPa.

Then the fiber rigidity coefficient is the following (Eq. 14):

$$c = E \cdot \frac{S}{L} = 20.20 \frac{\text{Н}}{\text{м}} = 2020\, mg\, .mm^{-1} \quad (14)$$

Where S - the elementary fiber cross-sectional area for the known d.

The inclusion masses for known v and pareрespectively equal to m_1 = 0.01035, m_2 = 0.00038, m_3 = 0.04792, m_4 = 0.00307 mg.

The damping coefficient affects the amplitude of the mass oscillation and is assumed to be a = 1 mg . s^{-1}. It does not affect the critical frequency.

The following critical frequencies of the system have been obtained with respect to the matrix (13) were thus ωK_1 = 517, ωK_2 = 86, ωK_3 = 29, ωK_4 = 183 Hz.

The natural frequencies of the individual masses according to the formula (6) are respectively equal to ω_1 = 70, ω_2 = 301, ω_3 = 33, ω_4 = 127 Hz.

Figure 2 shows the system solution (Eq. 1) with frequency impact at the lower critical frequency x = sin (29t).

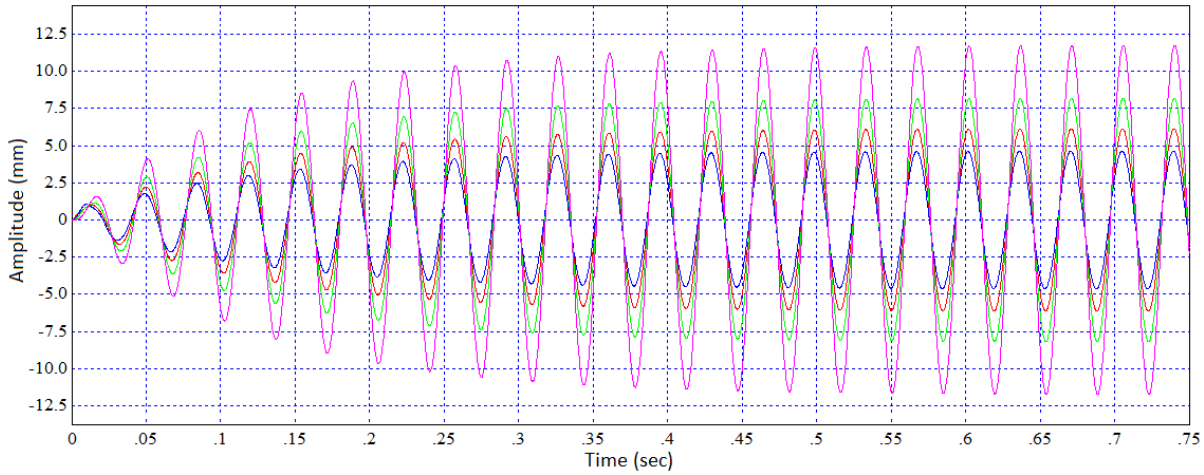

Fig. 2. Amplitude mode for x = sin(29t).

Figure 3 shows the system solution (Eq. 1) with frequency impact at the second critical frequency x = sin (86t).

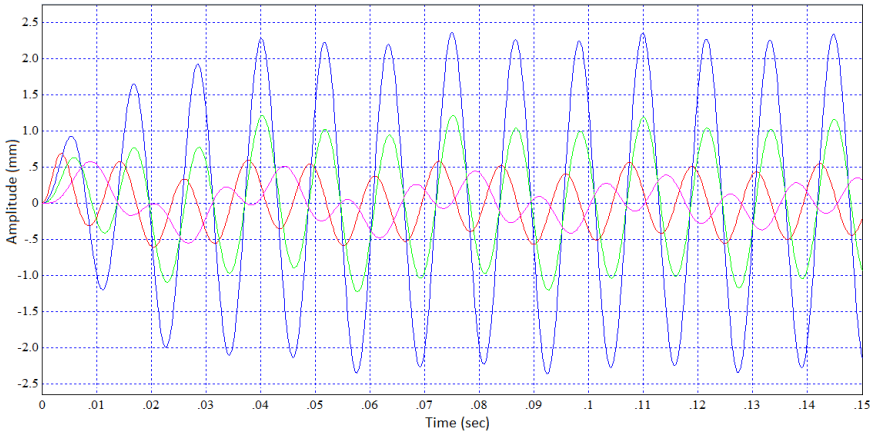

Fig. 3. Amplitude mode for x = sin (86t).

Figure 4 shows the system solution (Eq. 1) with frequency impact at the next critical frequency $x = \sin(183t)$.

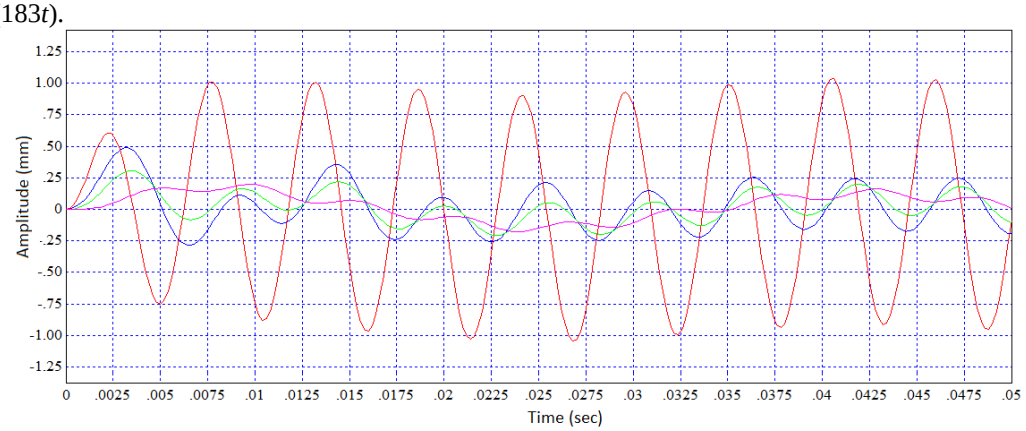

Fig. 4. Amplitude mode x = sin(183t).

The amplitude-frequency characteristics for all masses, calculated from formulas (Eq. 12) is shown in Figure 5.

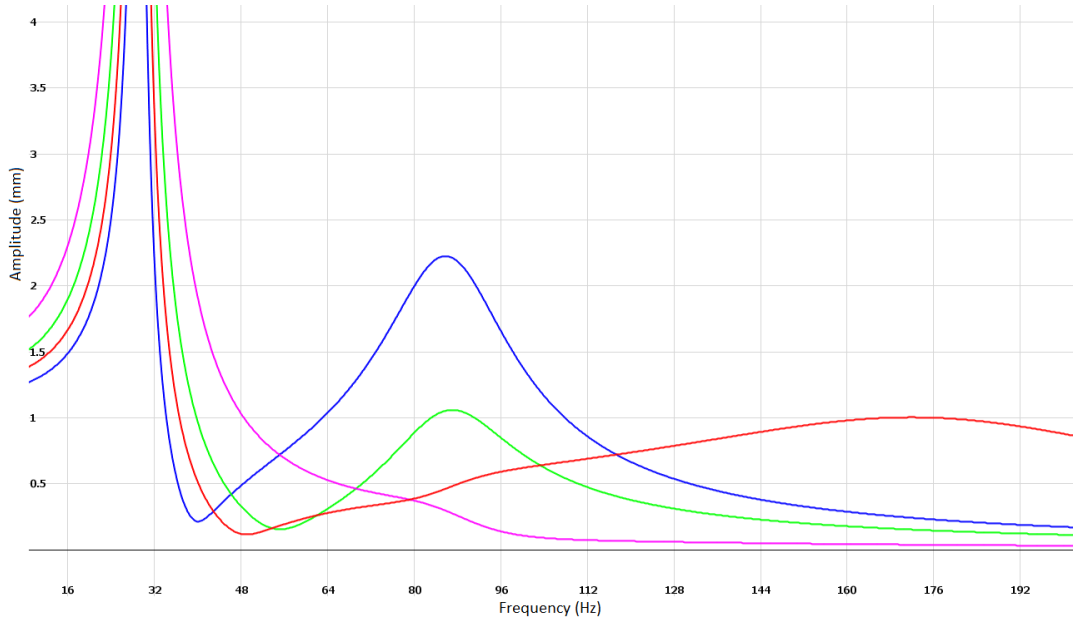

Fig. 5. Frequency dependence of the amplitude.

The largest resonance amplitude is observed at the very first (lowest) critical frequency of the system as shown in Figures 2 and 5.

The inertia force that detaches the inclusion from the fiber depends not only on the amplitude but also on the oscillation frequency (Bury et al., 2017; Akhmatova, 1980):

$$F_i = m_i A_i \omega^2 \tag{15}$$

The dependence of the detachment force of all masses on the frequency, calculated by the formula (Eq. 15) is shown in Figure 6.

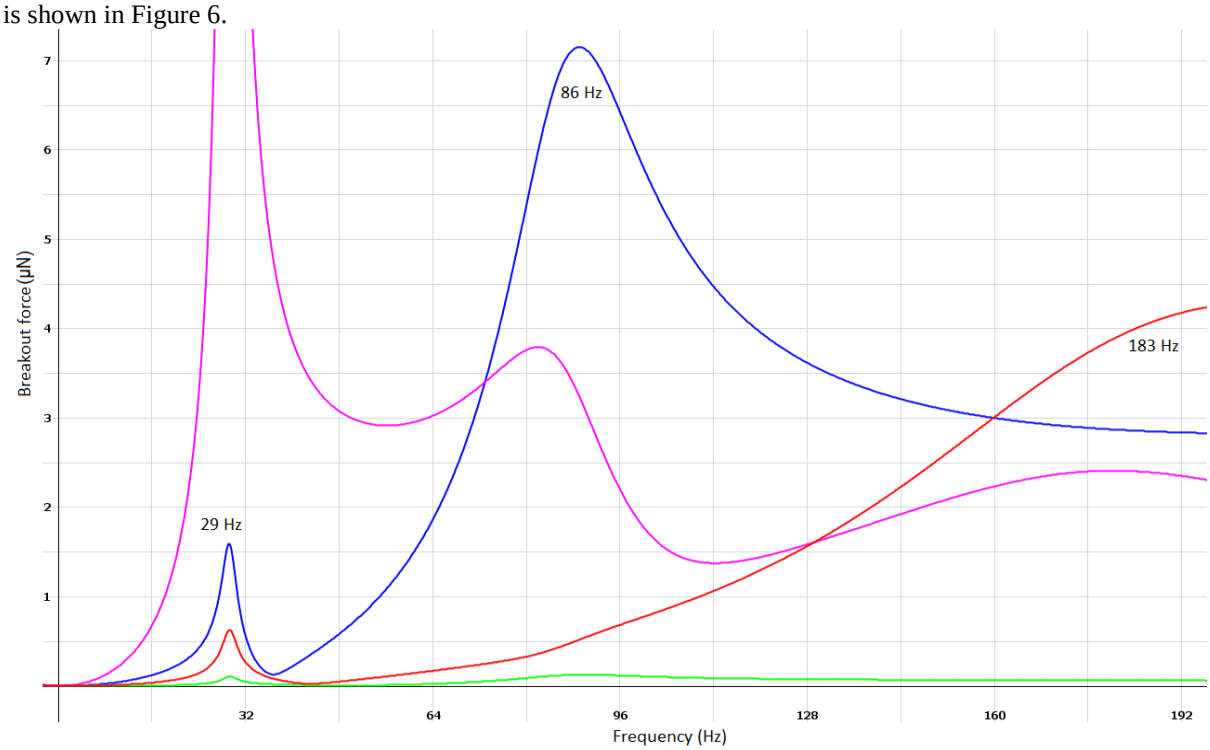

Fig. 6. Dependence of separation force on the frequency.

So, for example, for the first mass (the blue line in the graphs), the amplitudes at first (ascending) three critical frequencies will be 5, 2.3 and 0.2 mm (Fig. 2, 3, 4 and 5). The corresponding detachment forces (Fig. 6) will be 2.5, 7 and 3 μN. The greatest detachment force corresponds to the highest value of the product of mass, amplitude, and the square of cyclic frequency (Eq. 15). Therefore, it appears not at the largest amplitude and not the highest frequency.

Experimental study for the acoustical treatment process of the superthin basalt fiber canvas (Boczar, 2003; Ribero, 2003; Kriven, 2016).This research aims to confirm the benefits and find rational parameters of the acoustical treatment process of the formed primary canvases. The reasons for the formation of non-fibrous inclusions in canvases made from superthin basalt fiber obtained by duplex technology are known from (Jasenek et al. 2012). Below in Figure 7 is the experimental installation scheme for studying the acoustic field effect on superthin basalt fiber samples. The sound source is a loudspeaker 1 type BD 93, with a diffuser 120 mm in diameter, power 40 W and a working frequency range of generated sound vibrations from 38 to 18000 Hz. The loudspeaker is connected to a sound generator of type G3-33, providing a frequency change in the audio range from 20 to 20,000 Hz with an output voltage of up to 14 V.

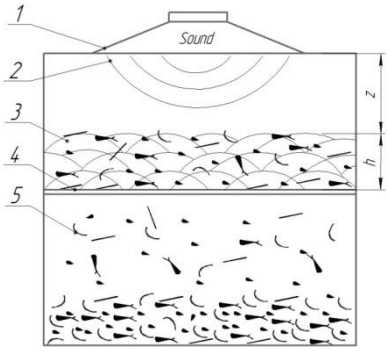

Fig. 7. Installation for acoustic treatment of basalt fiber canvas samples:
1 - sound source, 2 - sound wave, 3 - basalt canvas, 4 - grid, 5 - non-fibrous inclusions, h - the thickness of canvas, z-distance from the sound source.

To measure the weight of samples of superthin basalt fiber canvases and the mass of non-fibrous inclusions falling out of them under the sound influence, electronic laboratory scales GH-252 with a division value of 0.1 mg were used. The test samples had the same thickness h and were located at a distance z from the loudspeaker on a wire grid with a diameter of 2 mm in increments of 20 mm in one direction and 40 mm in the other 4 (Fiore et al., 2015).

In Figure 7, the tests were carried out as follows. Under the influence of sound vibrations 2 from the lower surface of the basalt fiber canvas sample 3, non-fibrous inclusions 5 did actually begin to separate.

The first preliminary experiments showed that non-fibrous inclusions do not fall out of the canvas under the sound influence in the frequency range from 260 Hz to 20 kHz, and an essential reaction is observed only in the sound frequency range from 40 to 160 Hz. The sound level was 118 ± 2 dB.

Sixty-five samples of superthin basalt fiber canvases with sizes 150 x 150 x 8 to 10 mm and density 13.2 to 15.1 kg.m^{-3} were prepared for further experiments. All experiments were carried out in five series - when every five samples were exposed to sound of different frequencies - from 40 Hz every 10 Hz to 160 Hz. The sound level was 118 ± 2 dB. In these experiments, the total mass of all non-fibrous inclusions fallen out under the influence of sound from each sample was measured without differentiating them by mass and shape (Fig. 8).

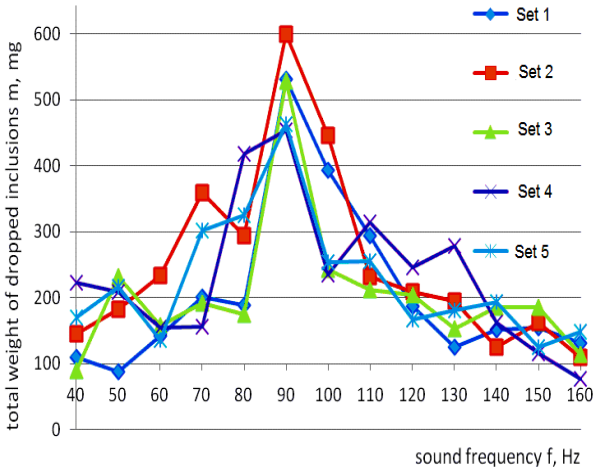

Fig. 8. The total mass dependence of all non-fibrous inclusions, fallen out under the sound field influence, on the sound frequency.

Results and Discussion

The results of the experiments are shown in Figure 8, from which it follows that the largest number of non-fibrous inclusions, according to their total mass, are separated from the canvas samples under the sound influence at a frequency of 90 Hz.

It should be noted that the total mass of the fallen non-fibrous inclusions determined in these experiments does not allow us to judge with confidence the optimal parameters of acoustic processing-the frequency and the sound level at which the greatest number of inclusions from the canvas falls out since the inclusions proportion in different samples vary. It was not possible to prepare canvas samples with the same number of non-fibrous inclusions contained in them due to the fact that the processes of inclusions formation have a random character.

Strictly speaking, the acoustic treatment efficiency of the considered articles can be judged if the mass fractions of the non-fibrous inclusions contained in the samples before and after the acoustic treatment are determined (Timoshenko et al., 1985). For this purpose, the efficiency index of the basalt fiber canvases acoustic treatment is introduced - the reduction coefficient of the non-fibrous inclusions content in the canvas sample KNI determined by the ratio:

$$K_{NI} = \frac{\omega_0}{\omega_1}, \tag{16}$$

Tab. 1. Mass fraction of non-fibrous inclusions (NI) in superthin basalt fiber canvases before and after acoustic treatment.

No. Experiment	The canvas mass before treatment M_0, (mg)	The fallen outNI mass m_2(mg)	The canvas mass after treatment M_1, (mg)	The remaining NI mass m1, (mg)	Mass fraction of NI in the canvas before treatment ω_0, %	Mass fraction of NI in the canvas after treatmentω_1, %	The reduction coefficient of NI mass fraction KNI	The average value <KNI>
Sound frequency 70 Hz level 100 dB, generator voltage U = 12 V, exposure time t = 40 s								
1	998.7	5.8	992.9	76.3	8.22	7.68	1 070	1 087
2	897.9	4.5	893.4	64.3	7.66	7.20	1 064	
3	639.5	8.0	631.5	64.6	11.35	10.23	1 109	
4	1501.6	22.9	1478.7	187.1	14.02	12.69	1 105	
Sound frequency 90 Hz level 100 dB, generator voltage U = 12 V, exposure time t = 40 s								
5	1126.2	14.6	1111.6	88.8	9.18	7.99	1 149	1 145
6	773.3	7.1	766.2	40.8	6.19	5.32	1 164	
7	771.2	3.7	767.5	29.5	4.30	3.84	1 120	
8	682.0	13.1	668.7	78.18	13.41	11.69	1 147	
Sound frequency 110 Hz, level 100 dB, generator voltage U = 12 V, exposure time t = 40 s								
9	425.1	4.0	421.1	39.7	10.28	9.43	1 090	1 070
10	960.6	4.1	956.5	70.2	7.73	7.34	1 053	
11	825.2	4.5	820.7	54.3	7.13	6.62	1 077	
12	1037.2	4.3	1032.9	84.2	8.63	8.15	1 059	
Sound frequency 70 Hz, level 118 dB, generator voltage U = 12 V, exposure time t = 40 s								
13	606.0	41.7	564.3	42.7	13.93	7.57	1 840	1 723
14	1045.8	73.4	972.4	86.4	15.28	8.89	1 719	
15	434.7	24.3	410.4	37.8	14.29	9.21	1 552	
16	448.5	34.6	413.9	37.2	16.00	8.99	1 780	
Sound frequency 90 Hz level 118 dB, generator voltage U = 12 V, exposure time t = 40 s								
17	582.9	42.4	540.5	29.8	12.39	5.5	2 253	2 368
18	996.9	44.3	952.3	53.6	9.82	5.63	1 744	
19	704.9	37.7	667.2	32.2	9.92	4.83	2 054	
20	482.7	85.1	397.6	27.0	23.22	6.79	3.42	
Sound frequency 110 Hz, level 118 dB, generator voltage U = 12 V, exposure time t = 40 s								
21	805.1	40.3	764.8	29.8	8.71	3.90	2.233	1 850
22	545.2	16.4	528.8	22.3	7.10	4.22	1 682	
23	648.3	26.8	621.5	33.3	9.27	5.36	1 729	
24	697.1	40.6	656.5	47.0	12.57	7.16	1 756	

where ω_0 and ω_1- the mass fraction of non-fibrous inclusions in the sample before and after treatment (%), respectively, which are in turn determined by the expressions:

$$\omega_0 = 100 * \frac{m_0}{M_0}, \qquad \omega_1 = 100 * \frac{m_1}{M_1}, \tag{17}$$

Where m_0 and m_1 are respectively the mass of non-fibrous inclusions in the sample before and after treatment, M_0 and M_1 are, respectively, the mass of the sample before and after treatment. The values of m_0, m_1, M_0, M_1 were obtained using the electronic laboratory scale GH-252 with a division value of 0.1 mg.

For the next series of experiments twenty-four samples with dimensions of 150x150x8 to 10 mm and a density of 13.2 ... 15.1 kg / m^3 were prepared in order to determine the reduction coefficient of the non-fibrous inclusion content in the canvas sample *KNI* (Eq. 16, Eq. 17) at the frequencies of the applied sound field f = 70 Hz, f = 90 Hz and f = 100 Hz and the sound level is L = 100 dB and L = 118 dB, respectively. The measurements results of m_0, m_1, M_0, M_1, and calculations of ω_0, ω_1, and m_2 (the mass of non-fibrous inclusions fallen out from the superthin basalt fiber canvas in the process of acoustic treatment) are presented in Table 1.

As can be seen from the Table 1, the mass of non-fibrous inclusions fallen out of the samples under the sound influence is proportional to the sound level L, since the *KNI* index at a sound level of L = 118 dB is much higher in comparison with the analogous index at a sound level of L = 110 dB. Just as in the previous experiments, the maximum decrease in the non-fibrous inclusions content in the samples after acoustic treatment with a frequency of 90 Hz is observed, while the mass fraction of non-fibrous inclusions in basaltic fiber canvases at an L = 118 dB sound level decreases by an average of 2.4 times.

For a better understanding of the acoustic treatment practical benefits, we introduce one more efficiency indicator - the mass fraction percentage of non-fibrous inclusions fallen out during processing, from the mass of all inclusions in the sample before treatment with $NI_{\%}$:

$$NI_{\%} = 100 * \frac{m_2}{m_1 + m_2}, \tag{18}$$

where m_1 is the mass of non-fibrous inclusions in the sample remaining after processing, m_2 is the mass of non-fibrous inclusions fallen out during processing.

Using the known formulas (Eq. 19, Eq. 20, Eq. 21, Eq. 22, Eq. 23) for processing the results and determining the error (Sentyakov, 2004; Timofeev, 2004) and formula 3, we can calculate the limits of the $NI_{\%}$ value for each of the six combinations (f = 70 Hz and L = 110 dB , f = 79 Hz and L = 110 dB, f = 110 Hz and L = 110 dB, f = 70 Hz and L = 118 dB, f = 90 Hz and L = 118 dB, f = 110 Hz and L = 118 dB) of the sound field output parameters, presented in Table 1.

$$< NI_{\%} >= \frac{\Sigma NI_{\%i}}{n}, \tag{19}$$

where $<NI_{\%}>$ is the arithmetic average of the mass fraction percentage of non-fibrous inclusions fallen out during processing, on the mass of all inclusions in the sample before processing, $\Sigma\, NI_{\%i}$ is the sum of the values of all the experiments, n is the number of experiments,

$$\Delta NI_{\%i} =< NI_{\%} > - NI_{\%i}, \tag{20}$$

where $\Delta NI_{\%i}$ – the deviation of each experiment value from the average,

$$S_{<NI_{\%}>} = \sqrt{\frac{\Sigma(\Delta NI_{\%i})^2}{n(n-1)}}, \tag{21}$$

where $S_{<NI\%>}$ – confidence interval,

$$\Delta NI_{\%} = S_{<NI_{\%}>} \times t, \tag{22}$$

where $\Delta NI_{\%}$ is the deviation, t is the coefficient of the student (3.2 for reliability p = 0.95), that is, how many times it is necessary to increase the standard confidence interval, so that for a certain number of tests n get the reliability of p,

$$NI_{\%} =< NI_{\%} > \pm \Delta NI_{\%}, \tag{23}$$

The results of the calculations are listed in Table 2.

Tab. 2. The mass fraction percentage of non-fibrous inclusions $NI_{\%}$ fallen out during acoustic processing of basalt fiber canvases.

No. of experiments	Sound level L, dB	Soundwave frequency f, Hz	$NI_{\%}$, %
1, 2, 3, 4	100	70	5-12
5, 6, 7, 8	100	90	11-16
9, 10, 11, 12,	110	110	3,5-10
13,14,15,16	118	70	38-53
17,18,19,20	118	90	38-79
21,22,23,24	118	110	37-58

Conclusions

The widespread of the $NI_{\%}$ is explained by the different samples heterogeneity; it is impossible to select two samples even with an approximate identical content of the amount or mass fraction of non-fibrous inclusions. However, a certain regularity is observed (Biderman, 1980). As can be seen from Table 2, the mass fraction of the fallen non-fibrous inclusions $NI_{\%}$ in the acoustic treatment process from the total mass of non-fibrous inclusions, that were contained in the sample before processing, is proportional to the sound level L. In the concluded experiments, the maximum number of $NI_{\%}$ heavily depended on the exposed sound frequency, at f = 90 Hz which was achieved at a sound level of L = 118 dB the fraction of inclusions can reach up to 80 %.

Thus, as a result of an experimental study of the acoustic treatment process, the application of this treatment process for reduction of the non-fibrous inclusions content in primary superthin basalt fiber canvases has been confirmed, which also improves the working conditions for people working with basalt fiber canvases. Following recommendations for further study of non-fibrous inclusions separation by means of acoustic vibrations and determination of rational parameters for the application of the acoustic treatment process into the mining industry are suggested:

- investigation of the sound field distribution based on its distance from the acoustic vibrations source;
- investigation of the necessary processing time depending on the created sound level at the interaction point of the sound field with the primary canvas;
- further study of the vibrational properties of individual particles in non-fibrous inclusion separation from the basalt fiber canvas using acoustic vibrations, in order to accurately estimate the reason for the mass of the individual inclusions to differ greatly among themselves at a certain frequency level, even though the sound effect frequency coincides with the natural frequency of oscillation of non-fibrous inclusions by the appearance of a physical resonance;
- the most effective acoustic processing in this study has been found to be at a frequency of 90 Hz;
- the design of acoustic processing equipment has to provide the possibility to adjust the distance from the sound source to the sample surface within a distance that will provide a sound level at the interaction point at a level not lower than 118 dB;
- the conveyor speed and the number of loudspeakers must allow for the sample surface to be exposed to the sound for 20 to 40s.

Acknowledgment: *The contribution is sponsored by the project 015STU-4/2018: Specialised laboratory supported by multimedia textbook for subject "Production systems design and operation" for STU Bratislava.*

References

Akhmatova, A. S. (1980). Laboratorniy practicum pofizike (Laboratory practical work on physics). *Moscow: Vishayashkolaizdt.*

Asdrubali, F., D'Alessandro, F., Mencarelli and Horoshenkov, K. V. (2014). Sound absorption properties of tropical plants for indoor applications. The 21st International Congress on Sound and Vibration, 13-17 July 2014, Beijing, *China.*

ASTM C518-10. (2003). Standard Test Method for Steady-State Thermal Transmission Properties by Means of the Heat Flow Meter Apparatus; ASTM: USA: West Conshohocken, PA.

Biderman V.L. (1980) Theory of Mechanical Oscillations: A Textbook for High Schools. *M: High School, 408 p., Ill.*

Biderman, V. L. (1980). Theory of Mechanical Oscillations: *A Textbook for High Schools*.

Boczar, T. (2003) Time-Frequency Analysis of Acoustic Emission Pulses Generated by Partial Discharges, *Journal of Electrical Engineering, (54) 63-68.*

Bolotin, V. V. (1987). Vibrations in technology: Handbook. In six Volumes. *Moscow: Mashinostroenie*.

Buratti, C., Moretti, E., Belloni, E. and Agosti, F. (2014). Development of Innovative Aerogel Based Plasters: Preliminary Thermal and Acoustic Performance Evaluation. Sustainability 2014(6) 5839-5852. [online]. [2015-02-03]. Available at : http://www.enea.it/it/produzione-scientifica/EAI/anno-2011/indice-world-view-3-2011/basalt-fiber-from-earth-an-ancient- material-for innovative-and-modern-application//

Buratti, C., Moretti, E., Belloni, E. and Cotana, F. (2013). Unsteady simulation of energy performance and thermal comfort in non-residential buildings. *Building and Environment 2013(59) 482-491*.

Bury, P., Hardoň, Š., Kobayashi, H. and Imamura K. (2017). Investigation of deep defects in nanocrystalline-Si/Si interfaces using acoustic spectroscopy. *Journal of Electrical Engineering 2017(68) 1335 – 3632*.

E N ISO 12667. (2001). Thermal Performance of Building Materials and Products-Determination of Thermal Resistance by Means of Guarded Hot Plate and Heat Flow Meter Methods-Products of High and Medium Thermal Resistance; *ISO: Geneva, Switzerland*.

Fabian, M., Boslai, R., Ižol, P., Janeková, J., Fabianová, J., Fedorko, G., and Božek, P. (2015). Use of parametric 3D modelling - tying parameter values to spreadsheets at designing molds for plastic injection. *Manufacturing Technology 2015 (15) 24-31*

Fiore, V., Scalici, T., Di Bella, G., Valenza, A. (2015). A review on basalt fibre and its composites. Composites Part B*: Engineering Volume 74, 1 June 2015, Pages 74-94*.

Huang, S. Z. C and Pan, Y-Ch. (2015). Automated visual inspection in the semiconductor industry: A survey. *Computers in Industry, 2015 (66) 1-10*.

ISO 10534-2. (1998). Acoustics-Determination of Sound Absorption Coefficient and Impedance in Impedance Tubes-Part 2: Transfer-Function Method*; ISO: Geneva, Switzerland*.

Jasenek, J., Korenko, B. and Červeňová, J. (2012). Fiber optic sensor for the space distribution measurement of magnetic field. *Journal of Electrical Engineering 2012 (63) 23-26*.

Kemal Ozfirat, M. (2015). Selection of tunneling machines in soft ground by fuzzy analytic hierarchy process. *Acta Montanistica Slovaca 2015(20) 98-109*.

Kim, H. K. and Lee, H. K. (2010). Influence of cement flow and aggregate type on the mechanical and acoustic characteristics of porous concrete. *Applied Acoustics 2010(71) 607-615*.

Kuzmin, K. L., Gutnikov, S. I., Zhukovskaya, E. S. and Lazoryak, B. I. (2017). Basaltic glass fibers with advanced mechanical properties. *Journal of Non-Crystalline Solids 2017(476) 144-150*.

Lopresto, V., Leone, C. and De Iorio, I. (2011). Mechanical characterisation of basalt fibre reinforced plastic. *Composites Part B: Engineering 2011(42) 717-723*.

Makarov, I. M. and Mensky, B. M. (1981). Linear automatic systems. *Mechanical Engineering 1981(23) 221-232*.

Moretti, E., Zinzi, M. and Belloni, E. (2014). Polycarbonate panels for buildings: Experimental investigation of thermal and optical performance. *Energy and Building 2014(70) 23-35*.

Papadopoulos, A. M. (2005). State of the art in thermal insulation materials and aims for future developments. *Energy Build. 2005(37) 77-86.*

Pompoli, F. (2004). Studio di modelli di previsione delle proprietà fisico-acustiche, di materiali in lana di roccia Rockwool, *Relazione Tecnica*.

Ribero, D., Kriven, W.M. (2016) Properties of Geopolymer Composites Reinforced with Basalt Chopped Strand Mat or Woven Fabric. *Journal of the American Ceramic Society Volume 99, Issue 4, 1 April 2016, Pages 1192-1199.*

Sentyakov, B. A. and Timofeev, L. V. (2004). Tehnologia proizvodstva teploizolyacionnih materialov na osnove basaltovogo volokna (Technology of production of thermal insulation materials based on basalt fiber). *Izhevsk: ISTU* .

Shaikh, F. and Haque, S. (2018). Behaviour of Carbon and Basalt Fibres Reinforced Fly Ash Geopolymer at Elevated Temperatures. *International Journal of Concrete Structures and Materials. 2018 (12) 35.*

Timoshenko S.P, Young D.H. and Weaver, U. (1985). Oscillations in engineering. / Transl. from English. Korneyuchuk, L. G., Ed. Grigoluk, E. I. - M. (1985). *Mechanical Engineering 1985(27) 243-254.*

Uysal, O., Cavus, M.: Effect of a pre-split plane on the frequencies of blast induced ground vibrations. *Acta Montanistica Slovaca 2013(18) 101-109.*

Wang, C. N. and Torng, J. H. (2001). Experimental study of the absorption characteristics of some porous fibrous materials. *Applied Acoustics 2001 (62) 447- 459*.

Process innovations in the mining industry and the effects of their implementation presented on the example of longwall milling heads

Łukasz Bołoz[1] *and* ***Katarzyna Midor***[2]

In Poland, the mining industry is one of the branches, in which innovation improvement activities must be undertaken, as it is still a strategic industrial branch. Process innovation is one of the innovation types allowing the improvement of the production process, as well as the improvement of the product quality.

In extractive processes, mechanical mining based on hard coal milling in longwall excavations is related to the development of a considerable amount of unneeded fractions, i.e., fine coal and dust. In consequence, it results in a reduction of mined material value, development of dustiness, as well as a hazard of coal dust explosion. Moreover, there is the necessity of efficient spraying system application. The appearance of a larger amount of coarse grade allows reduction of mentioned problems what increases mining efficiency. It is possible when the process of constructional and kinematic milling parameters of worm-type cutting heads is designed properly. The procedure of selection of these parameters proposed in this study supported with experiment executed in industrial conditions allows obtaining the targeted aim, i.e., increase of the amount of coarser fractions in case of mining with use of worm-type milling heads, what constitutes an excellent example of process innovations implemented in the Polish mining industry.

Keywords: *innovation, process, cutting heads, cutting head designing, coarse grade, longwall shearers*

Introduction

Hard coal mining is considered as traditional industry boomed in Poland in time of the centrally controlled economic system. From the macro-economical point of view, a drop of the hard coal output is considered as a natural and positive state indicating the development of Polish economy according to Hirsch's theory of the branch lifetime cycle indicating, that in given stage of economy development different branches play a various role in the total state economy. This means that economic growth results in the meaning of branches belonging to the traditional industry is weakened and meaning of branches using advanced technologies growths. Traditional industry is characterized by low market dynamism, and in consequence, innovations occur in a small degree. However, Polish hard coal mining is still a strategic branch of the state industry. With respect to the hard coal output, Poland is placed on the 10-th position in worldwide rankings, and 1-st position in the European Union. Hard coal assures energy safety guaranty actually being major source of the electric energy generation (Midor, 2015), (Kołodziej et al., 2015), (Gembalska-Kwiecień, 2016), (Zasadzień et al., 2015), (Drucker, 1992), (Borowiecki, 2011). Thus action allowing economic reinforcement should be undertaken in order to prolong the lifetime of the mining industry branch in Poland because it is still in the state socioeconomic interest. So innovations are the best tools allowing improvement of the branch competitiveness.

Various types of innovations are described in the literature. International standards referring to the definition and measurement of the innovativeness determined in Oslo Manual 2005 (Działalność innowacyjna, 2014), (Černecký et al., 2015) have been considered in this study. Product, process, as well as organizational and marketing innovations, are distinguished in this manual. With respect to the subject matter of this study, authors paid particular attention to process innovations considered as changes of used production methods, as well as changes of the manner of hunting customers of the product or service. The process innovations are aimed at reduction of the unit costs of the product or delivery and improvement of the product quality. They can comprise an implementation of suitable changes in the scope of the hardware and software, as well as changes related with procedures and techniques used in the provision of services.

Authors of the present study presented an example of process innovation aided with experiment conducted in industrial conditions, comprising application of suitably selected (for concrete conditions) construction and kinematic parameters of worm-type milling heads causing reduction of process energy consumption, reduction of dustiness and appearance of the winning with greater amount of coarser grade, what considerably influences the product price. Taking it under consideration, the authors presented an example of innovation. Method of the selection of parameters both of milling heads and milling process is aimed to tailoring them to concrete working conditions, i.e., properties of mined rock body and parameters of the longwall shearer.

[1] *Łukasz Bołoz,* AGH University of Science and Technology, Department of Mining, Dressing and Transport Machines, A. Mickiewicza Av. 30, 30-059 Krakow, Poland, boloz@agh.edu.pl

[2] *Katarzyna Midor,* Silesian University of Technology, Faculty of Management and Organization, Institute of Production Engineering, Roosevelta 26, 44-800 Zabrze, Poland, katarzyna.midor@polsl.pl

Research methods described in the study are based on quantitative examinations and research techniques. Research methods comprise observation and data analysis, such as desk research. Observation and experimental methods were applied in part referring to the application of the innovation.

Process innovations in Polish mining branch

Analyzing innovative action of industrial plants of the branch comprising hard coal and brown coal excavation according to classification Polish Classification of Activities (PKD) in the period 2008-2014, which is shown in Fig. 1, we can observe that innovative activity of Polish mining plants in the analyzed period was kept at the level of 45%, that means that every second plant did not introduce any innovative changes with respect to product quality, work organization or marketing. It is definitely an unprofitable situation for a branch being in difficulty with low profitability. It also results from Fig. 1 that in case of innovatively active companies this activity was mostly directed for process innovations, comprising among the others implementation of new, improved production methods. However, the rest of the innovation groups, the innovations were realized in small percent by companies belonging to the extractive branch.

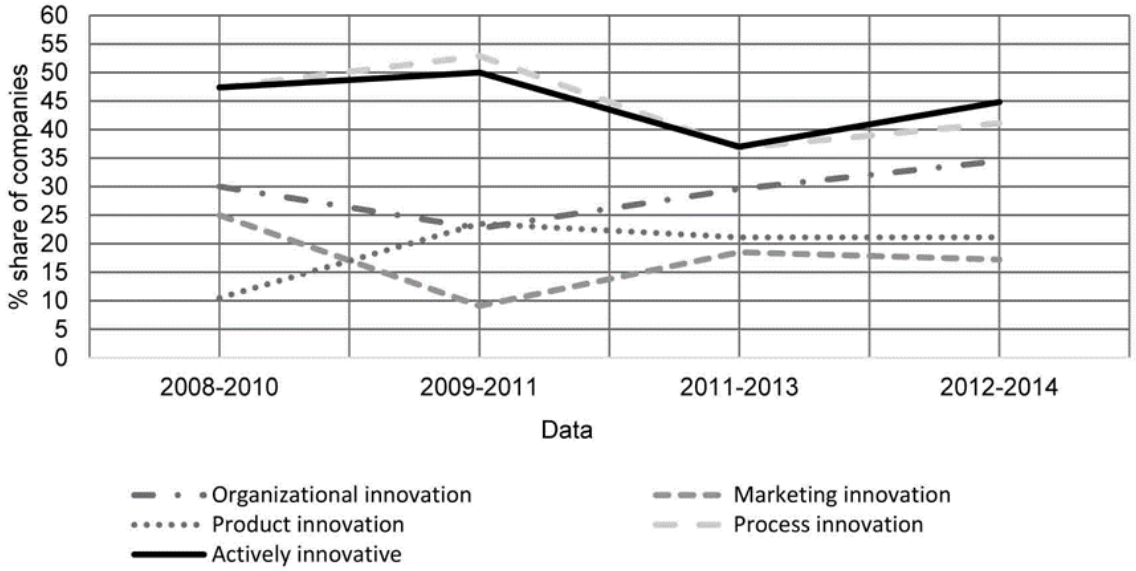

Fig. 1. Innovative actions of Companies – PKD.

Because process innovations very often are implemented simultaneously with product innovations, with respect to direct their mutual bonding, the participation of these two types of innovations is presented in Table 1. Analyzing data from this table, we can note that if the innovative activity is implemented, it is directed onto process innovations.

Tab. 1. The innovative activity of Companies belonging to PKD. Hard and brown coal extraction - product and process innovations.

	Total	**New, or considerably improved products**		**New, or considerably improved processes**
		Total	**New for market**	
	in % of all Companies			
Period 2008-2010	47.4	10.5	-	47.4
Period 2009-2011	52.9	23.5	5.9	52.9
Period 2011-2013	36.8	21.1	5.3	36.8
Period 2012-2014	47.3	21.1	10.5	42.1

Source: *own elaboration on the basis of* (Roczniki branżowe, 2005-2015)

Based on Fig. 1, one can conclude that Companies from the extractive branch are innovatively active first of all in the process field, whereas in other areas this activity is kept on a low level. It is also confirmed by data from Table 2, in which inputs for the innovative activity of companies from mining branch are presented.

Statistical data comprising innovation investments, with respect to their destination can be grouped into four basic areas (Franik, 2015; Nauka, technika, 2014; Midor et al., 2017):

Group A – research and development activity (B+R),

Group B – knowledge buy from external sources and software,

Group C – investment for machines and technical devices,

Group D – personnel training and marketing, or crucial improvements of products.

Tab. 2. Investments for innovative activity - hard and brown coal extraction in a million (mln) PLN in the period 2006-2014.

Year	Investments for innovative activity in the scope of product and process innovations in mln PLN					
	Total	Research and development activity (B+R) Group A	Knowledge buy from external sources and software Group B	Investments Group C		Personnel training, marketing related with new or considerably improved products Group D
				Buildings and installations and lands	Machines, technical devices, tools, and transport means	
2006	187,3	7,4	0,9	34	137,4	0,2
2007	226,8	5,4	0,3	85,3	113,3	0,6
2008	193,4	7,8	0,2	72,9	108,8	0,7
2009	*	*	*	*	*	*
2010	64,8	10,4	0,0	7,8	40,9	no data
2011	*	9,3	4,6	11,5	*	*
2012	67,0	13,2	*	*	*	0,2
2013	85,9	19,6	*	2,3	63,6	*
2014	80,5	5,4	*	1,5	63,3	*

* it means that the data can not be published with respect to the statistical secret - public statistics act.
Source: *own elaboration on the basis* (Roczniki branżowe, 2005-2015)

As results from analysis of data in Table 2, investments in machines and technical devices purchase have the greatest part in four groups of investments spent for innovative activities. Since the year 2006, their part in total investments is kept on a very high level when investment spent on machines and technical devices amounted for 73.3% of total investment spent on innovations. This situation was changed in the period 2007 to 2008. In this period, investment spent on buildings and grounds considerably increased, however in the year 2010 came back to high investment spent on machines and technical devices. In general, we can state that group C related with investment inputs constitutes the main direction of innovations in companies of the mining branch, what is related with process innovations. Example of introducing process innovation in the Polish mining industry will be discussed in the next part of the present study.

Method of longwall milling heads selection as an example of the process innovation

Longwall excavation commonly known as longwall is equipped with a set of machines and technical devices forming the so-called longwall system. Depending on the type of mining machine is used (shearer, plow) the system is called as shearer system or plow system. Longwall systems are commonly used for hard coal, brown coal, rock salt, and potash chloride exploitation. Actually, longwall shearers are the most commonly used, plow shearers are used rarely, although works on implementation of modern longwall systems in thin coal beds are conducted (Biały, 2014; Bołoz, 2013; Bołoz, 2018; Brodny, 2011). Except for the longwall shearer, the longwall system consists of mechanical longwall support, longwall scraper conveyor and chain conveyor, which transports the winning stream onto band conveyor (Krauze, 2000).

Longwall shearers are equipped with two worm-type milling heads, which realize processes of cutting and loading. These elements are in direct contact with mined rock body. The milling process is realized by milling tools, and loading is realized by worm vanes (Wydro, 2015).

Parameters of the cutting head influencing milling quality can be divided into the following groups:

- design parameters and resulting pick system, as well as the type of cutting tools,
- shearer operation parameters (kinematic and energy performance).

Both groups of parameters influence shearer load, the durability of the mining machine and winning grade, as well as dustiness. Parameters influencing the quality of loading process can be divided into the following groups:

- shearer design parameters and resulting shape of loading instruments,
- shearer operation parameters (kinematic and energy performance).

Also, in this case, both groups of parameters influence shearer load, the durability of the mining machine, winning grade and dustiness.

Parameters of machines of the shearer system should be selected in such manner that for definite excavation and mining and geological conditions, targeted V_d and winning grade (grain-size) were reached. That is why the application of the shearer in longwall excavations requires:

- determination of rules of machines and devices selection, with respect to conditions and hazards,
- determination of the coal properties in a coal seam in question,

- analysis of coal seam and longwall excavation parameters (length *l*, height *h*, longwall coasting area, dip),
- determination of required daily output V_d,
- determination of design, kinematic and energy parameters of the longwall shearer system,
- design of worm-type milling heads,
- assessment of the possibility of obtaining coarse coal grades.

Realization of mentioned tasks allows decision if the shearer or plow system can be operated in the given coal seam, as well as what parameters are required to obtain targeted daily output and satisfactory winning grain-size.

The mined material consists of grains of different granulation, which is classified in the enrichment process. In consequence mining plants offer coal of different grade (bricks, chestnut coal, pea coal, pea coal, fine coal) in different price depending on the coal grain-size and quality. In this classification, fine coal is the cheapest, and the most expensive is coal brick. Thus it is important to obtain from given excavation the winning consisting of the possibly great amount of coal grains with a diameter exceeding 8 mm, with a possibly small amount of fine coal (Krauze et al., 2016).

Obtaining of coal of coarse granulation should be analyzed both in technical and economical aspect. The technical aspect is related to mining and enriching power consumption, and it is related to coarser winning. Bigger coal grain-size is accompanied with smaller dustiness, what also is an advantageous feature (Krauze et al., 2016).

From the other side, economical aspect favors coarser coal grain-sizes because their price is considerably higher than the price of the fine coal. Coarser coal grade also generates low exploitation and transport costs. Thus one should consider if obtaining coal of courser grain-size from given excavation is possible, as well as what conditions and requirements must be satisfied. In the case of excavation equipped with full set of machines the problem comprises design of dedicated milling heads, as well as the determination of kinematic parameters of the shearer and its cutting head.

Proper cooperation of longwall system machines forces their compatibility, what is a condition sine qua non of obtaining targeted efficiency. However, generation of assumed daily output is not equivalent to optimal selection of these machines. Each element of the longwall system is characterized by a definite range of parameters, for which operation of the whole system is proper. That is why, in practice, there is at least one machine constituting the weakest element of the system, thus in definite operation conditions it reduces daily output (Krauze, 2000), for example with respect to conveyor efficiency, loading performance of cutting head (Wydro, 2015) or time of the section re-arrangement. That is why the determination of proper and optimal parameters of these machines, including conditions occurring in the machine operations place is needed.

Having in mind the upper conclusions we may suggest that for an assumed output level, accepted exploitation technology, and its parameters, the milling longwall shearer should possess the following design and kinematic parameters:

- advance rate-regulated from zero to maximal value, which should not exceed the smallest rate resulting from the cooperation of the longwall system machines,
- cutting height range soul be bigger than the longwall height *H* resulting from the coal bed thickness,
- two cutting heads of web *Z* (usually 0,8 m ÷ 1,1 m) and diameter D_s (recommended $D_s \approx 2/3\ H$).

Value of the assumed daily output and the longwall parameters allow determination of the support and longwall conveyor parameters. Thus we can also select proper parameters of the worm-type cutting heads. Method of the selection of design, kinematic and energy parameters of machines and devices of the longwall shearer system has been elaborated in the Department of Mining and transport Machines of the AGH University of Science and Technology. On the basis of this method, a suitable computer program allowing the determination of these parameters has been elaborated (Krauze et al., 2016).

The starting point of the selection of cutting head parameters is coal workability measured by mining capacity *A*, side crushing angle ψ, compressive strength R_c and compactness factor *f*. Compactness factor *f* is determined according to Protodiakonow's jr method (cracking method). Coal beds geological structure is also determined.

Method of determination of coal mining capacity *A* has also been elaborated in the Department of Mining and Transport Machines of the AGH University of Science and Technology, and it comprises measurement of milling resistances directly in longwall face during execution of rectilinear cuts (Krauze et al., 2016). The measurement cuts are made on an aligned surface with use of 2 cm wide model pick, which is moved along the face of the coal longwall. From the measurement of pressures occurring during cutting with use of a model pick on the depth of 2 cm, after suitable handling of the measurement signal, mean value of cutting force *P* is obtained. In result of these tests, mining capacity factor *A* and angle of side crushing ψ are obtained.

The ratio of mean cutting force P and measured cutting depth g_s is defined as mining capacity factor A, and it may be calculated from the following relation:

$$A = \frac{P}{g_s}\left[\frac{\mathrm{N}}{\mathrm{cm}}\right] \Rightarrow P = A \cdot g_s \ [\mathrm{N}] \tag{1}$$

where:

P–mean value of cutting force, N

g_s –cutting depth, cm

This factor is comparable for various coal beds, and the bigger the value it has, the more difficult is the bed mining capacity. In order to determine coal compactness (compact/weakly-cohesive), in parallel with the measurement of the mining capacity factor, the angle of side crushing is determined.

$$\psi = arctg\left(\frac{b_s - b}{2g_s}\right)[°] \tag{2}$$

where:

b_s – cut width

b – cutting pick edge width.

According to classification CMG KOMAG, coal of angle in question smaller than 60° is classified and strongly-cohesive coal, whereas coals having this angle bigger than 60° are classified as weakly-cohesive ones. On the basis of the mining capacity factor A and angle of side coal crushing ψ, taking under consideration classification of Polish coals also elaborated by CMG KOMAG, we are able to determine type and category of tested coal.

On the basis of parameters A, ψ, R_c and f we can determine coal mining capacity and its brittleness. On this base cutting method (milling, plowing), type of cutting picks and their arrangement in cutting head and kinematic parameters are selected, and the possibility of obtaining bigger amount of coarse material is assessed (Biały 2016), (Krauze et al., 2016). It should be noted, that worm-type cutting heads and picks used should be selected not only with respect to their design but also the high quality of their manufacturing, as well as compatibility of real parameters with those assumed in the design phase of the project in question (Krauze et al., 2015).

Properties of the tested rock body determined during executed examinations allow such selection of the cutting head parameters that improvement of the coal grade is possible, including reduction of dustiness and cutting process power consumption. In particular, selection of cutting scale (distance between individual cutting lines) and cutting depth (ratio of the shearer advance rate and the rotary speed of the cutting head with taking into consideration number of picks in cutting line), are very important. Both cutting scale and cutting depth directly influence the winning grain-size. It should be noted that obtaining profitable winning granulation and optimization of the power consumption directly influence the proper cutting process.

Pick fastened in its holder is a part of the cutting head (Fig. 2). Thus operational pick angles α_r and pick rake angle γ_r depend not only on design pick parameters but also on parameters of its holder, as well as on cutting rate v_s and advance rate v_p. Thus we can conclude that for the cutting head of diameter D_s, cutting rates v_s and advance rates v_p, holder height H_u and holder angle δ_u, the tangential rotary pick of required length L_n and pick angle $2\beta_u$ should be selected. The proper course of the cutting process is conditioned by such selection of these parameters that operational pick rack angle α_r was always positive. Dislocation of the pick holder along the tangential line marked as b is a parameter allowing correction of the operational cutting angles. Because of the tool wear and developed hazards, the maximal linear speed should be controlled and suitably limited. Moreover, the limitation of the shearer movement with respect to cutting depth resulting from the length of picks and their number in cutting line is needed (Krauze, 2000; Bołoz, 2012).

The pick torsion angle φ can describe the pick position on the cutting head. For the pick set shown in Fig. 2, angle φ has a value of geometrical pick torsion angle φ_g. Geometrical pick torsion angle is defined as an angle between radius passing the pick edge and radius, which is perpendicular to the holder base. Value of this angle is constant independently on the pick position during cutting. Angle φ_g can be calculated from the formula:

$$\varphi_g = arctg\left(\frac{b - b_{u1}\cdot sin(\delta_u) + L_r \cdot cos(\delta_u)}{0{,}5\cdot D_b + H_n}\right)[°] \tag{3}$$

The diameter of the cutting head $D_s$can be determined from the relation:

$$D_S = \frac{D_b + 2\cdot H_n}{cos(\varphi_g)}[°] \tag{4}$$

Whereas the angle of repose αamounts for:

$$\alpha = \delta_u - \beta_u + \varphi_g [^\circ] \tag{5}$$

A pick rake angle γequals to:

$$\gamma = 90 - \delta_u - \beta_u + \varphi_g [^\circ] \tag{6}$$

In result of a combination of advance rate v_p and cutting rate v_s the pick rake angle and pick edge range are changed by values of angle δ according to the following relations:

Operational pick rake angle:

$$\alpha_r = \alpha - \delta [^\circ] \tag{7}$$

Operational pick edge angle:

$$\gamma_r = \gamma + \delta [^\circ] \tag{8}$$

Value of the angle δ is changed during cutting in function of angle φ. Value of angle δ can be calculated from the formula:

$$\delta(\varphi) = arcos\left(\frac{v_s + v_p \cdot cos(\varphi)}{\sqrt{v_s^2 + v_p^2 + 2v_s \cdot v_p \cdot cos(\varphi)}}\right)[^\circ] \tag{9}$$

Value of angle δ is changed due to pick position during cutting, and it reaches its maximum when the pick passes horizontal axis of the cutting head.

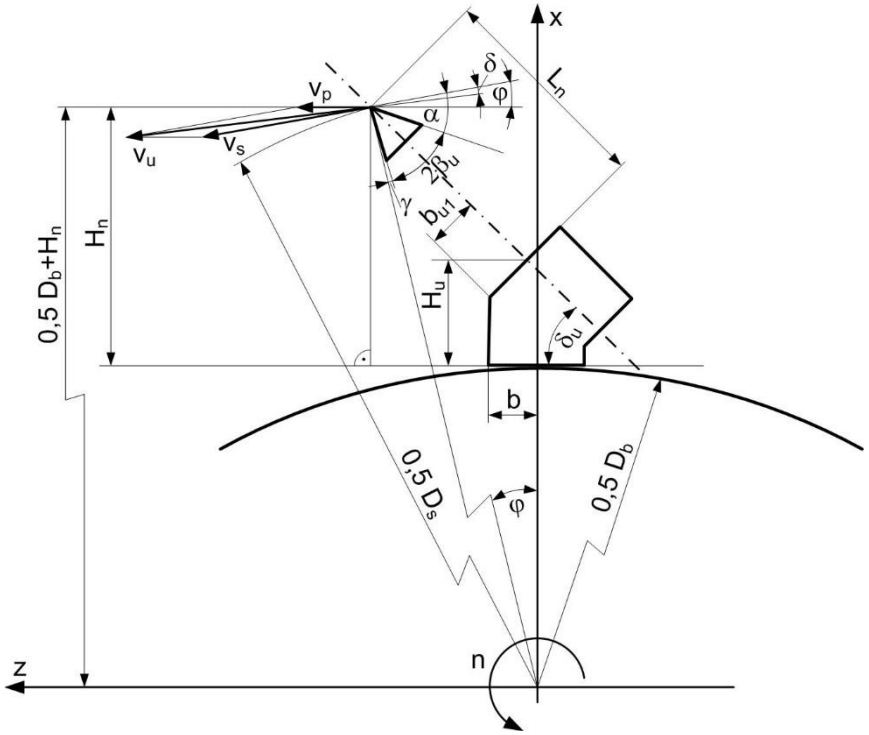

Fig. 2. Geometrical and kinematic parameters of pick during milling (Bołoz, 2012).

Example of the process innovation application within chosen coal longwall

The assumption of targeted output level from the excavation of defined geometrical parameters, settlement of coal mining capacity and crushing resistance and selection of support, conveyor, shearer and cutting head parameters allow realization of the project of dedicated cutting heads. Consequently, the longwall exploitation with a possibly small dustiness and power consumption, as well with increase of production of coarse coal grades call for empirical verification, which has been executed in one of the longwall excavations of chosen hard coal mining plant in Poland, within coal seam 501 at the exploitation level 830.

Theoretical base presented in the first part of the present study allow selection of worm-type milling heads for head KSW-880 EU/kV in the aspect of obtaining advantages. Thus, for chosen by the mining plant coal

longwall of the height H = 3 m, length L = 200 m and longitudinal inclination α_{pod} = 2° and transverse inclinationα_{pop} = 3.5°, the procedure of the cutting head selection have been executed. The procedure in question comprises the following activities:

- determination of coal mining capacity in the coal bed on the basis of underground examinations for two parallel cuts (marked as I and II),
- conduction of the analysis of mining and geological conditions, as well as longwall technical equipment in the aspect of obtaining the assumed daily output,
- selection of parameters of the shearer worm-type milling head in order to increase production of coarse coal grades.

Determination of the coal mining capacity requires conduction of suitable tests, and that is why the following activities have been executed:

- measurement of the mining capacity factor A and angle of side crushing ψ for coal occurring in examined coal bed (Fig. 1 and Fig. 3),
- measurement of cohesiveness factor f according to Protodiakonow's method on the basis of samples taken from places of determination of factors A and ψ,
- laboratory determination of the coal geological structure.

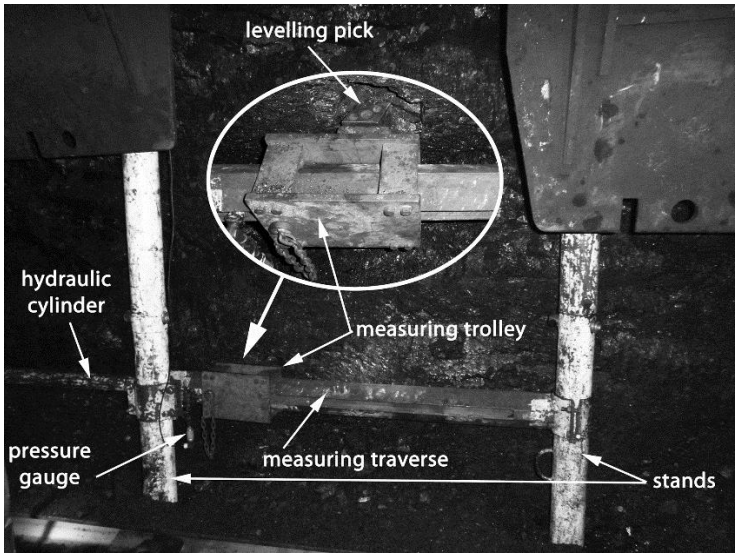

Fig. 3. Testing stand during examinations

Results of underground examinations (factor A, angle ψ, formulas 1 and 2) and results of laboratory tests (factor f, coal structure) constituted a base, on which the following conclusions have been drawn (Krauze et al., 2016):

- within the tested coal bed, occurrence of the coal classified to VII ÷ VIII class of mining capacity was proved – cohesive and particularly hardy mined coal (cut I - A_I = 4 045 N/cm, ψ = 18°31', cut II - A_I = 3 790 N/cm, ψ = 38°27', f = 1.76),
- cutting of this coal is possible only with the application of the milling method, with use of tangential-rotary picks,
- coal occurring in tested bed is classified as weakly crushed coal,
- the coal consists of vitrinite, clarite and fusain laminae and a minor amount of inert parts.

The upper conclusions indicate that coal occurring in this coal bed can be mined with use of worm-type milling heads equipped with tangential-rotary picks. Good mining capacity of this coal forces application of small variable scales between milling lines. From the other side, small brittleness indicates high coal resistance to degradation.

Coal occurring within the coal bed in question is classified as steam coal of symbol 32.2 (gas-flame coal). The coal is exploited by the longwall system, transverse, with use of hydraulic support. The shearer works in two-way technology and is equipped with worm-type cutting heads without shielded loaders.

Taking under consideration the longwall height, shearer technical parameters, coal mining capacity and shearer permissible advance rates resulting from cooperation with support and conveyor, as well as on the basis of used procedures, the following parameters of worm-type cutting heads were determined:

- cutting head rotary speed n = 36,2 rpm,
- drum diameter D_b = 1690 mm,
- vane inclination $\alpha_p = 23°$,
- number of vanes $i_p = 4$,
- hub diameter d_p = 900 mm,
- vane thickness $b_p \leq 50$mm,
- disc thickness $b_t \leq 80$mm,
- the width of the body $B \geq 720$ mm.

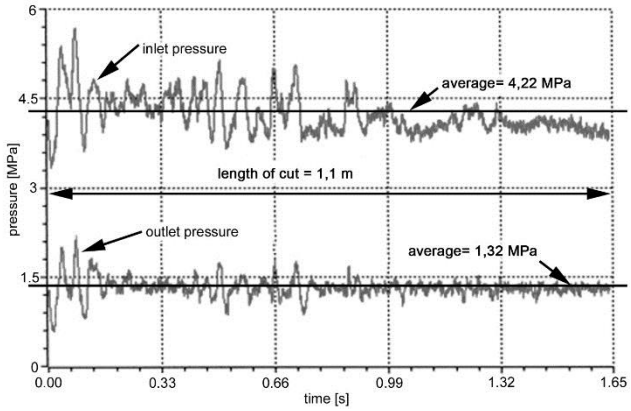

Fig. 4. Course of measurement signals during coal milling (g = 1.7 cm, b_s = 4.7 cm).

Pick arrangement with tangential-rotary picks was designed for a cutting head ϕ2000 x 800. Picks arrangement allowing obtaining changeable scale between milling lines and the moveable cut is characteristic for this cutting system. A small number of picks (disc – 20 pieces, cutting-loading part – 16 pieces) with combination with a changeable scale between milling lines and moveable cut allows obtaining increased part of the coarse coal grade, as well as dustiness reduction if the permissible advance rates are used. It should be noted that the reduction of some picks accompanied by the rock body parameters (mining capacity factor, brittleness factor)will allow the reduction of the power demand of the cutting head motors. Based on relations (3-9), values and courses of changing angle δ for pick position during the single cut of the shearer, have been determined. Courses of movable pick edge angle γ_r and pick rake angle α_r are shown in Fig. 1. These angles change their values, however, pick rake angle must always be positive. If the negative values of pick rake angle occur, crushing instead milling is observed.

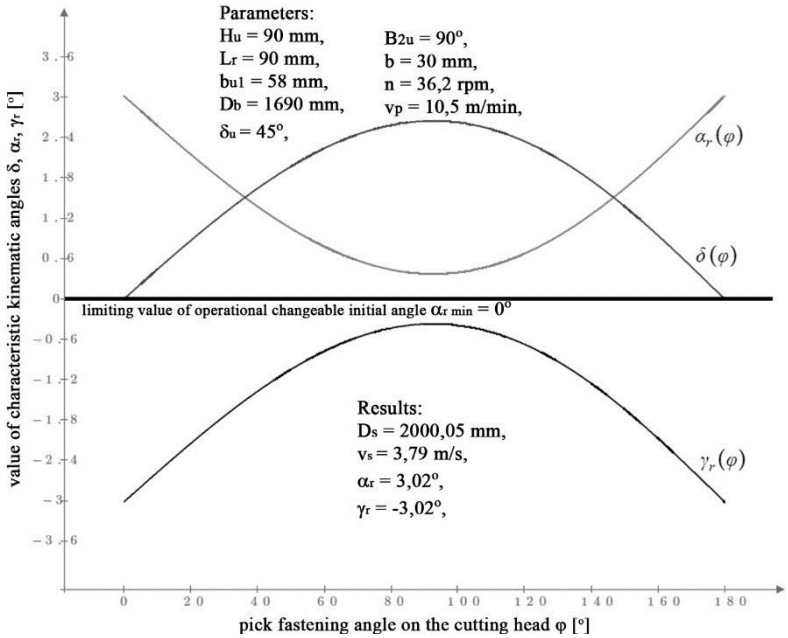

Fig. 5. Courses of pick edge angles and pick rake angles in function of the pick position of the designed cutting head.

Assessment of coal grade and dustiness reduction improvement

Effectivity of the proposed method of the selection of worm-type milling head parameters can be verified by assessment of the winning generated by factory-made milling heads (marked as old) and designed milling heads(marked as new). Thus two-stage analysis of the winning grain-size and analysis of the dustiness both for factory-made milling heads and for the designed milling heads was made. In order to assure the same operational conditions of both milling heads, the measurements were made right before and right after their replacement.

The winning grain-size was measured in the longwall outlet (sieve analysis), where coal samples were manually sieved and classified into fine coal (below 8 mm) and coarse coal (over 8 mm). Winning samples were also taken from these places, and they were exposed to classification in the coal processing plant for sieve mesh ranging from 8 mm to 80 mm.

Dustiness for factory-made and designed milling heads was also measured. The results are presented in Fig. 6. On the basis of data in the diagram shown in Fig. 6, we can conclude that application of the new milling heads reduced dustiness level in the longwall by 36%. Thus we can assume that use of the new milling heads resulted in a reduction of the dustiness, what is considered as the great advantage (Černecký et al., 2015).

Results of the analysis of winning grain-size obtained with the use of new and old milling heads are shown in Fig. 7. The milling heads used so far in this longwall produced winning characterizing with the greatest percentage for grain-size of classes 8÷0, 16÷6, 25÷16. Whereas, the new milling heads produced winning with the greatest percentage of grains over 80 mm, whereas this percentage for grains below 8 mm was the smallest. On the basis of executed tests and obtained results, it was proved that new milling heads satisfy the assumed target, i.e., production of the winning having the most profitable grain-size, what consequently results in smaller dustiness.

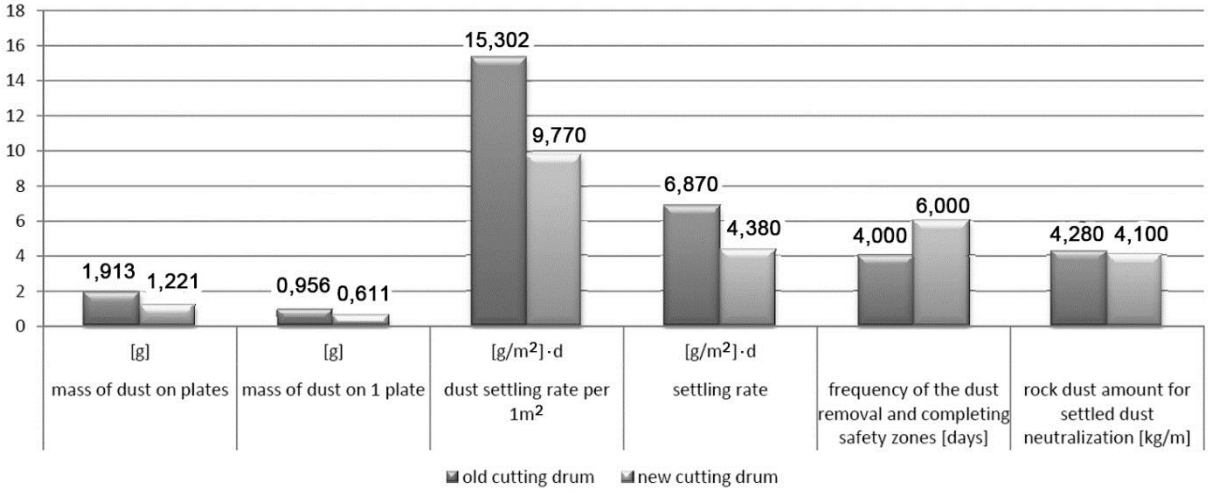

Fig. 6. Test measurement results obtained for mining with use of factory-made (old) and selected (new) milling heads.

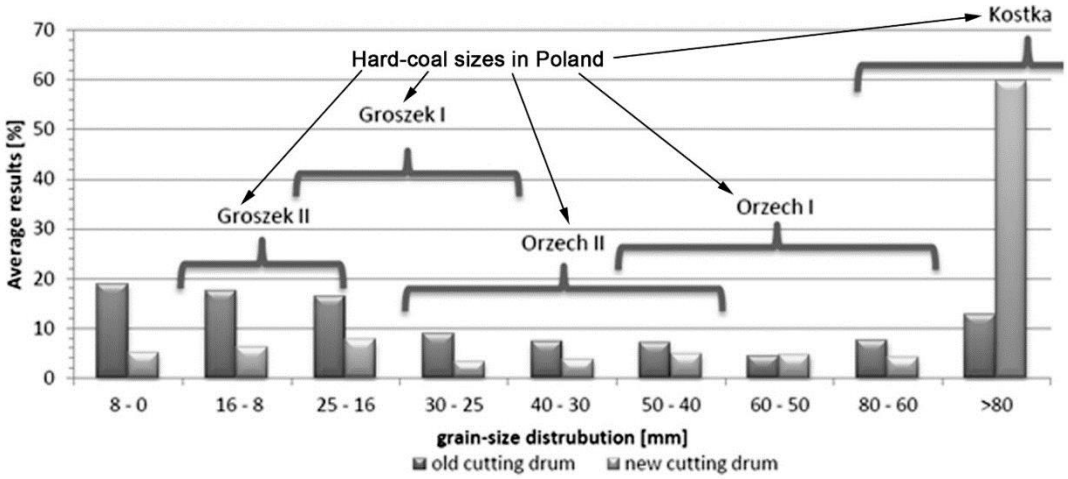

Fig. 7. Results of the sieve analysis of coal produced with the use of old and new milling heads.

Conclusions

Innovative processes have an essential influence on the competitiveness of the domestic economy. In Poland, the expenditures for research works and development amount for only 0,87% Gross Domestic Product (GDP), whereas in the Czech Republic – 1,91%, Germany – 2,85% and in Finland 3,31%. The document named as „Europe 2020" assumes that by the year 2020 the member countries will be investing 3% GDP in research and development activities (HTTP, 2016). In Poland, it is expected that this limit should amount for 1,7% and it is assumed that half of these expenditures will be paid by entrepreneurs. Thus if the Polish domestic mining plants want to survive on the market, they must contribute considerable part in this innovation level of Polish industry (Midor et al., 2015).

Current examination and practice prove that the market is the best verifier of business activity forcing suitable reaction of the company, i.e., it determines the profitability of the innovative programs. Thus market economy forces flexibility and adaptability of given company, an increase of entrepreneurship and ability of adaptation to not only already existing marked changes but also to predicted or expected changes. Thus we can conclude that the activity of the company in a time of the market globalization, and circumstances of a free economy is equal, or even bigger than this what happens in the company itself. The company, which is not intended or not able to tailor to the market and new economic challenges is also not able to develop, in time it loses the ability to satisfy local environment needs and is exposed for collapsing.

The economy of our country is in the specific development phase. For example, current competitive advantages based on monopoly loose their position. Thus developing new advantages based on knowledge and innovativeness is necessary for long distance economic development. Thus the development of innovation activities of companies, including research and development activities, are the major factors of competitiveness (Święcicka, 2012; Tkocz, 2012; Zioło, 2009). These postulates in great extent refer to mining branch and particularly hard coal mining industry which is responsible for state energy safety accompanied by reaching high effectiveness on difficult primary fuel market.

Winning (coal, salt) of increased grain-size is a great challenge both for shearer and cutting head Manufacturers and mining plants. Worm-type cutting heads are commonly considered as typical and standard equipment of longwall shearers. It should be noted that they are considered as main elements responsible for mining and loading process and are characterized with great sensitivity to mining and geological conditions and kinematic parameters. Coarse-grained winning brings a lot of technical and economical advantages for mining plants. The procedure of selection of worm-type milling heads refers both to mining and loading function, and the selection is conducted with respect both to longwall shearer parameters and mining and geological conditions occurring in the longwall excavation. Effect of this procedure depends on its regular application due to new conditions or a new type of the shearer used. Positive empirical verification of the innovation in question will result in considerable economical benefits.

The presented method is applied especially in underground hard coal mines in order to increase grain-size. Nowadays grain size is crucial in terms of a coal price. Additional benefit related to dust reduction enhances working conditions.

References

Biały, W. (2014). Coal cutting force measurement system – (CCFM). 14th SGEM GeoConference on Science and Technologies In Geology, Exploration and Mining, *SGEM2014 Conference Proceedings, Vol. III*.

Biały, W. (2016). Determination of workloads in cutting head of longwall tumble heading machine. *Management Systems in Production Engineering, 1(21). doi: 10.12914/MSPE-08-01-2016*

Bołoz, Ł. (2013). Model tests of longwall shearer with string feed system. *Archives of Mining Sciences, 63(1).*

Bołoz, Ł. (2013). Unique project of single-cutting head longwall shearer used for thin coal seams exploitation. *Archives of Mining Sciences, 58(4).*

Borowiecki, R. (2011). Przedsiębiorstwo w obliczu wyzwań współczesnej gospodarki. *Nierówności Społeczne a Wzrost Gospodarczy/Uniwersytet Rzeszowski, 20.*

Brodny, J. (2011). Tests of friction joints in mining yielding supports under dynamic load. Arch. *Mining Sci., 56(2).*

Černecký, J., Valentová, K., Pivarčiová, E. and Božek, P. (2015). Ionization Impact on the Air Cleaning Efficiency in the Interior. *Measurement Science Review, 15(4).*

Drucker, P.F. (1992). Innowacja i przedsiębiorczość. Praktyka i zasady, *Warszawa, PWE*.

Działalność innowacyjna przedsiębiorstw w latach 2008-2010, 2009-2011, 2011-2013,2012-2014. Główny Urząd Statystyczny. *Informacje i Opracowania Statystyczne. Warszawa*.

Franik, T. (2015). Ocena wykorzystania nakładów na działalność innowacyjna w górnictwie. *Przegląd Górniczy, 18.*

Gembalska-Kwiecień, A. (2016). Innovative forms supporting safe methods of work in safety engineering for the development of specializations. *Management Systems in Production Engineering, 4(24*).

Kołodziej, S. and Maruszewska, E.W. (2015). Economical effectiveness and social objectives in corporate social reports - a survey among polish publicly traded companies. In: 2nd International *Multidisciplinary Scientific Conference on Social Sciences and Arts SGEM.*

Krauze, K., Bołoz, Ł. and Wydro T. (2015). Parametric factors for the tangential-rotary picks quality assessment. *Archives of Mining Sciences, 60(1), 2015*.

Krauze, K., Bołoz, Ł. and Wydro T. (2016). Projektowanie frezujących organów ślimakowych dla zwiększenia wychodu grubych sortymentów węgla. *Przegląd Górniczy, 6*.

Krauze, K. (2000). Urabianie skał kombajnami ścianowymi. *Katowice, "Śląsk"*.

Midor, K. and Michalski, K. (2015). Górnictwo węgla kamiennego. Inteligentne rozwiązania. Gliwice, *P.A. NOVA.*

Midor, K. (2015). Innowacje w przedsiębiorstwach branży górniczej w Polsce. In*:* Górnictwo węgla kamiennego. Inteligentne rozwiązania (pod red) Midor K., Michalski K, Gliwice, *P.A. NOVA.*

Midor, K., Klimecka-Tatar, D. and Chybowski, L. (2017). Innowacje w przemyśle – wybrane aspekty. Gliwice, *P.A. NOVA.*

Nauka, technika, innowacje i społeczeństwo informacyjne w Polsce. (2014). *GUS, Urząd Statystyczny w Szczecinie. Warszawa.*

Roczniki branżowe. Rocznik statystyczny przemysłu. *Warszawa. Lata od 2005 do 2015*.

Święcicka, Z. (2012). Innowacje w zarządzaniu przedsiębiorstwem górniczym. *Współczesne Zarządzanie, 2*.

Tkocz, M. and Heder, A. (2012). Działalność innowacyjna upadającej branży przemysłowej na przykładzie górnictwa węgla kamiennego. *Prace Komisji Geografii Przemysłu Polskiego Towarzystwa Geograficznego, 20.*

Wydro, T. (2015). Influence of the plow filling and thread angle onto the plow head efficiency. *Archives of Mining Sciences, 60(1).*

Zasadzień, M. and Midor, K. (2015). Innovative application of quality management tools in a hard coal mine. In: 15th *International Multidisciplinary Scientific GeoConference SGEM*.

Zioło, Z. (2009). Rola przemysłu w procesie kształtowania społeczeństwa informacyjnego. *Prace Komisji Geografii Przemysłu Polskiego Towarzystwa Geograficznego, 13*

http://ec.europa.eu/polska/news/140304_innowacje_pl.htm (2016).

Influence of vibrations on structures

Zdeněk Kaláb[1]

One type of occasional structural load is a seismic load. Earthquakes and blasts are typical sources of vibrations, but vibration generated during urban tunnel construction can represent a significant problem. Evaluation of the harmful impact of vibrations transmitted through rock massif into buildings is solved using experimental measurements, detailed analyses of measured signals, knowledge of geological pattern and constructional analysis.

Seismic load of structures due to earthquakes is solved using the EUROCODE 8 standard. The earthquake movements at a certain location on the surface are determined by an elastic response spectrum to the ground acceleration. Eurocode 8 puts emphasis especially on the robust foundations and simplicity of construction systems. It is also mentioned vibration effect on historical buildings and effect under the surface, for example, in mine spaces. Historical structures are usually even more prone to vibration damage than, for example, typical wood-frame homes. The greater concerns over historic structures arise from the design, structure age, building materials and building methods used. The peak values of vibration generated by earthquake decrease with depth; the decrease is faster in shallow layers compared with the deeper part. Technical vibrations differ from natural earthquakes, for a comparable value of maximum vibration amplitudes, especially in the frequency range of the signal and mostly its duration. Evaluation of technical seismicity is more complicated because there are usually used national standards.

To document some common information about vibration effects on structures, some experimental measurements are presented. Examples of real wave patterns document common shapes and also signals with significant resonant vibrations. Very interesting is an example of resonant vibration that was generated as the influence of basin structures on the shape of wave patterns due to quarry blasts. To obtain complete information, measurement system has to keep sufficient parameters, especially the frequency range of the whole seismic channel, sampling frequency, and proper anchoring of the sensor. The basic methodology for evaluation of vibration on structures is outlined.

Keywords: *seismic load, seismic standard, Eurocode 8, earthquake, technical seismicity*

Introduction

The basic objective of all activities in the designing and realisation of structures must be to create a quality environment suitable for the intended purpose of the structure, while this quality should be maintained over the entire expected life of the structure. The basic requirements for structure construction are (according to Merritt and Ricketts, 2001; Macdonald, 2001; Chudley and Greeno, 2014):

- Architectural requirements;
- Structural static requirements;
- Resistance to external influences;
- Welfare and hygiene requirements for the indoor environment;
- Operational safety requirements;
- Technology requirements;
- Economic requirements;
- Environmental requirements.

A load of structures can be classified as follows:

- Occasional loads (long-term, short-term, extraordinary)
  - Payloads;
  - Climate loads;
  - Snow load;
  - Wind load;
  - Frost load;
  - Load from forced strains;
  - Temperature load;
  - Load by rheological material changes;
  - Load by deteriorating support;
  - Mounting load;
  - Seismic load;
  - Pressure waves;

[1] *Zdeněk Kaláb*, VŠB – Technical University of Ostrava, Faculty of Civil Engineering, L. Podéště 1875, 708 00 Ostrava – Poruba, Czech Republic, zdenek.kalab@vsb.cz , Institute of Geonics of the CAS, Ostrava – Poruba, Czech Republic

- Emergency load.

- Permanent loads
  - Load by the weight of the structure;
  - Pressure load;
  - Preloading.

In order to assess the seismic load (vibrations) of structures, we need to determine the safe boundary that does not break the object or release the rock. The occurrence of new cracks or the widening of existing cracks, in the case of structures such as a drop of mortar or plaster or falling-off rock fragments, is considered a failure in both cases mentioned above (for example, Tripathy et al., 2016; Zeigler, 2018). It is necessary to prevent catastrophic failure, i.e., collapsing the structure (Fig. 1) or rocking off, at all times (for example, Towhata, 2008; Villaverde, 2009). On the other hand, cosmetic (light) damage is allowed in some cases if it does not compromise the safety of the structure. To do this, it is necessary to know the appropriate criterion for assessing the vibration effects that can be measured and potentially extrapolated on the endangered structure. Further, the degree of violation must be distinguished more precisely, and finally, we should have the possibility of a preliminary estimate of the vibration effects. The assessment of seismic load of structures often results from the measurement of vibrations at the reference standing place (for example, standard ISO 4866). In order to assess the response of structures, records should be obtained for such intensity of vibrations that evoke measurable effects on the structures. Vibration records have to be realised in an adequate time and frequency ranges (for example, Scherbaum, 1994).

Fig. 1. A man walks past a collapsed building in Dabandikhan in Sulaimaniya Governorate, Iraq. (Photo by Ako Rasheed, Reuters; Received from http://www.interaksyon.com/toll-from-iran-iraq-quake-breaches-450/).

As an example, typical damages in a masonry building are presented in Fig. 2 (according to www.earth-auroville.com/index.php). Structural elements, such as walls, columns, and beams, are only bearing the weight of the building and the live load under normal conditions: mostly compression forces for the walls and columns, and vertical bending for the beams. Under dynamic load, they also have to withstand horizontal bending and shear forces, and extra vertical compression forces. Several types of cracks are possible to define (Fig. 2). It is necessary to point out that small amounts of cosmetic cracking can arise from slight settling, ground movement, temperature, and humidity cycling, and even, in extreme cases (hurricanes, tornadoes), wind loading (Zeigler, 2018).

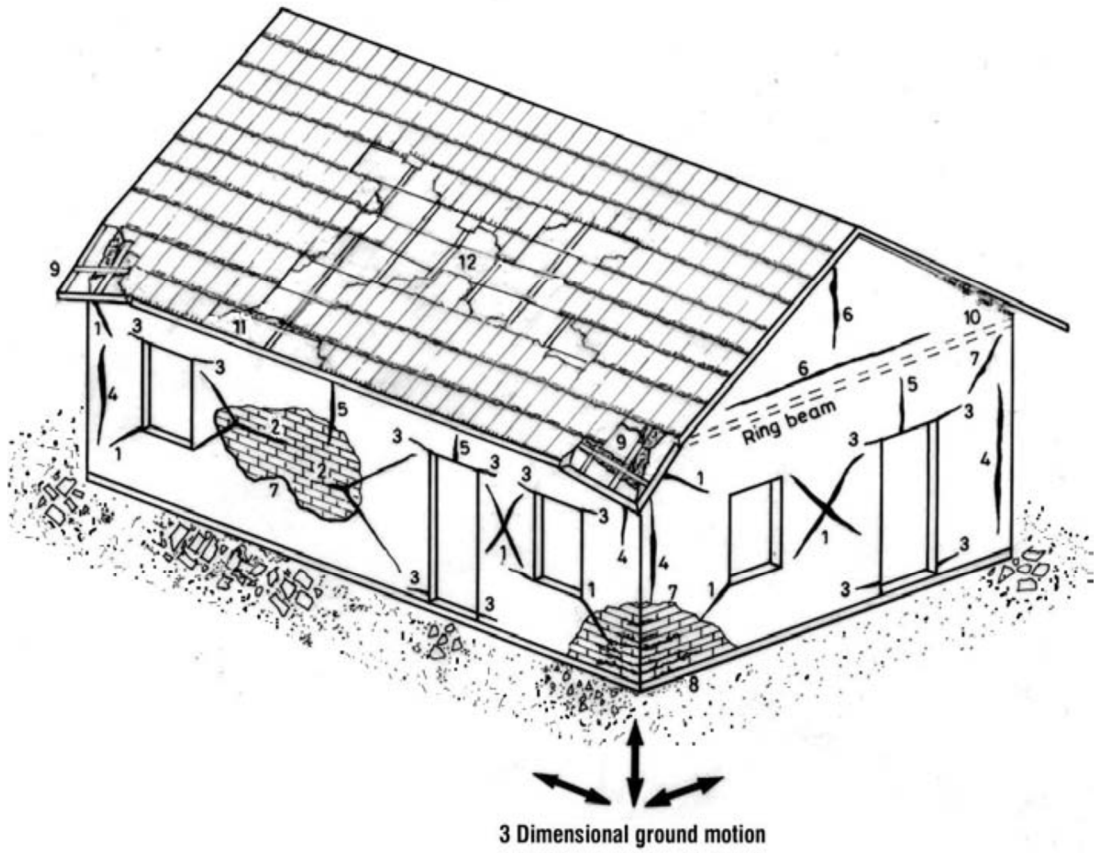

Fig. 2. Typical damages in a masonry building (according to www.earth-auroville.com/index.php)
1: Diagonal shear crack of piers, 2: Horizontal shear crack of long pier, 3: Bending cracks at feet and lintels, 4: Bending crack of wall (bad corner bond), 5: Bending crack of spandrel, 6: Bending crack of gable, 7: Plaster peeling off, 8: Crushing of weak masonry under vertical ground motion, 9: Damage of corner eaves under vertical ground motion, 10: Badly anchored roof, pulled out by vertical ground motion, 11: Falling of tiles from the roof eave, 12: Damage of tiles roof with shear (roof not braced).

To properly support a structure in response to whatever loads may be applied to it, a structure must possess four properties: it must be capable of achieving a state of equilibrium, it must be stable, it must have adequate strength, and it must have adequate rigidity (Macdonald, 2001). The achievement of stable equilibrium has been shown to be dependent largely on the geometric configuration of the structure and is, therefore, a consideration which affects the determination of its form. A stable form can almost always be made adequately strong and rigid, but the form chosen does affect the efficiency with which this can be accomplished. Therefore, collaboration has always been required between architects and those who have the technical expertise to realise building construction (for example, Merritt and Ricketts, 2001; Chudley and Greeno, 2014).

Every structure has vibration frequencies and mode shapes that are called "natural frequencies“ that can be found by using analytical methods. Calculation of these frequencies and their mode shapes are important to solve the vibration induced engineering problems. However, complex shaped objects can only be analysed by numerical methods. In particular, finite element methods (FEM) and boundary element method (BEM) enable to investigate the natural frequencies and mode shapes of complex structures by idealising them into computable small parts (for example, Berr, 2003; Hori, 2006; Chakraverty et al., 2012). Vibration analyses can be divided into two main parts. These are natural frequency and mode shape extraction and forced vibration analysis. By natural frequency analysis, the object's natural frequencies are obtained. A frequency of a periodic force which is applied to this object could be near to one of the object's natural frequencies. If so, that frequency is excited, and the structure starts to vibrate in its mode shape and natural frequency. If excitation frequency comes across the structure's natural frequency, "resonance" event occurs. In many case resonance is undesirable, and either excitation frequency or structure's natural frequency should be changed (http://www.mesh.com.tr/vibration-analyses.html).

The examples of analysis of the impact of vibrations on structures are presented in this paper, which is based mainly on the Eurocode 8 standard. Although this standard deals with the design of earthquake resistant structures, general rules apply to technical vibrations too. It is also necessary to point out the most common fundamental differences between natural and technical vibrations (at comparable amplitude values), which is especially the frequency range of the signal and mostly its duration. International standard ISO 4866 introduces

frequency range 0.1 – 30 Hz and velocity amplitude range 0.2 – 400 $m.s^{-1}$ for earthquakes. For quarry blasts, it introduces frequency range 1 – 300 Hz and velocity amplitude range 0.2 – 500 $m.s^{-1}$, and for other technical sources frequency range usually 1 – 100 Hz (up 1 kHz for machines) and velocity amplitude range up 0.2 – 50 $m.s^{-1}$.

Several examples of vibration records realised in a different type of structures, as mentioned at the end of this paper, document variability of structure responses.

Vibration movement

Theory of vibration movement, especially harmonic vibration, is commonly known and it is described in many textbooks, including seismological literature (for example, Bullen and Bolt, 1985; Kulhánek, 1990; Doyle, 1995; Udías, 1999; Shearer, 2009). The ground motions that are produced by earthquakes can be completely described by six components of motion, i.e., three translational components and three rotational ones, and by deformation (for example, Båth, 1979; Teisseyre et al., 2006; Graizer, 2006). Usually, only translational components are used for interpretation. Rotational components have been known for several centuries. However, it is only during the last two decades that greater attention has been dedicated to precise measurements of these. Although rotational components usually have small values, several studies have shown the importance of these components in seismological analyses and engineering applications (for example, Lee et al., 2009; Knejzlík et al., 2012; Kaláb et al., 2013).

Seismic movement can be described by the time variations of the ground acceleration and its associated parameters (velocity, displacement). The maximum (peak) ground acceleration, duration, and frequency content of earthquake can be obtained from an accelerogram. The seismic movement must be composed of three simultaneously acting accelerograms (calculated, actual, and simulated) in the case when a spatial model is to be considered. If particular constructions are evaluated, it is possible to describe the ground movement as a function of location and time. The damage potential of a given vibration is often assumed, even by those who do vibration monitoring, to be governed only by the maximum ground velocity of the vibration. However, the detailed frequency component makeup of the vibration, its duration and the number of times it is repeated all contribute to its potential for causing damage (for example, Lyubushin, 2007; Lyubushin et al., 2012; Zeigler, 2018).

We distinguish primary and secondary members as regards vibration of structures. A certain number of supporting elements can be designed as secondary seismic members, which do not form part of a seismic load-bearing structure. These are all parts of structures that hold something up but are not crucial to the building's structural integrity. The strength and stiffness of these members against seismic actions shall be neglected. These members and their connections shall be designed and constructed to maintain support of gravity load when subjected to the displacement generated by the most unfavourable seismic design condition. All structural elements that are not designed as secondary are considered as primary seismic members (see Eurocode 8). It means everything without which the structure will not stand up (typically columns, braces, and beams in steel constructions, add shear walls and slabs in concrete constructions). It is considered to be part of the load-bearing system that is resistant to transverse forces (for example, Iervolino et al., 2008).

As mentioned above, vibration load can be expressed in several ways. The earthquake movement (i.e., natural origin) at a certain location on the surface is determined by an elastic response spectrum to the ground acceleration (for example, Gupta, 1992; Viskup et al., 2005). The shape of the response spectrum is assumed to be the same for both seismic loads levels (i.e., the ultimate limit state and damage limitation state). The horizontal load is described by two independent perpendicular components (but with identical spectra). One or more different response spectra are used for all three components (occasionally a vertical component is also used) of the seismic load depend on the source parameters and magnitude of the earthquake. Also, more than one spectrum should be considered if earthquakes threatening the evaluated locality can come from directionally different source areas (for example, Bolt, 1999; Udías, 1999). In the last mentioned situation, different values of design acceleration values a_g will have to be defined for each spectrum type and earthquake. Response spectra (Fig. 3) are used to provide the most descriptive representation of the influence of a given earthquake on a structure (for example, Ali et al., 2017).

The guiding principles governing this conceptual design are (Eurocode 8):

- Structural simplicity;
- Uniformity, symmetry, and redundancy;
- Bi-directional resistance and stiffness;
- Torsional resistance and stiffness;
- Diaphragmatic behaviour at storey level;
- Adequate foundation.

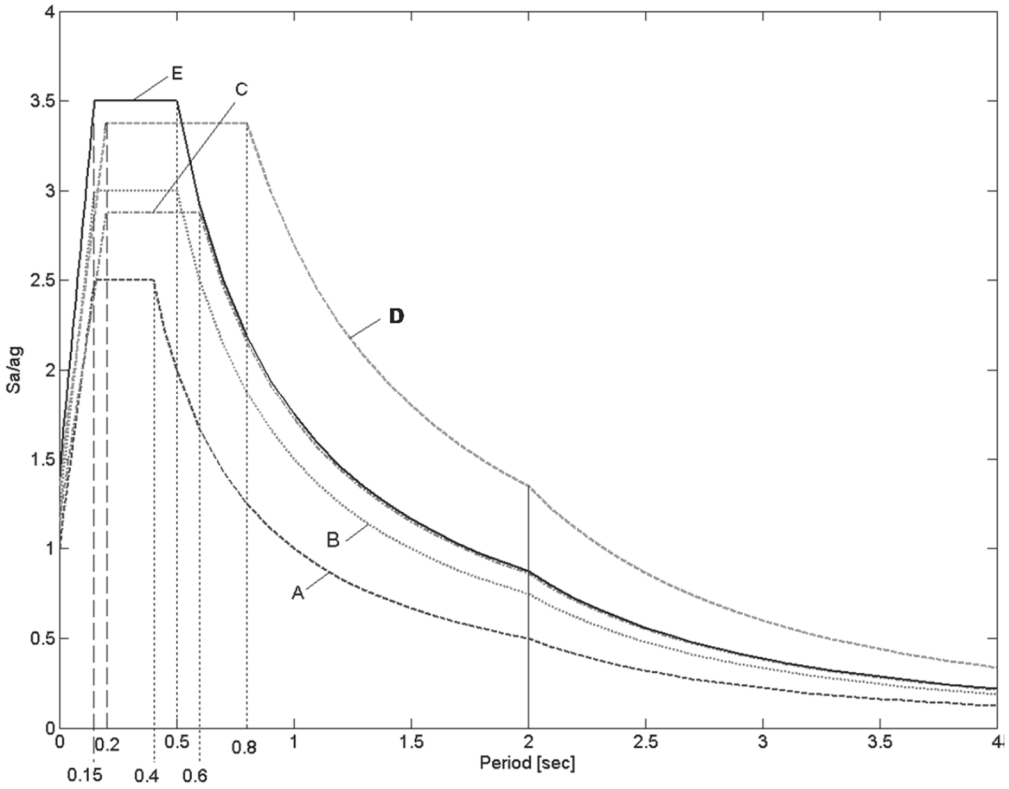

Fig. 3. Spectral shapes for main site classes (labelled as A – E). (Received from Iervolino et al., 2008).

In design calculations, structures are to be modelled, designed and modified according to the Eurocode rules. In terms of seismic design, the structures are categorised into regular and non-regular (which have an impact on the design model, the calculation method and the coefficient of ductility). The criteria for regularity in plan and elevation are defined.

Buildings are classified in 4 importance classes, depending on the consequences of a collapse for human lives, on the importance for public safety and civil protection in the immediate post-earthquake period, and the social and economic consequences of collapse (Eurocode 8). In the Czech Republic (National annex of the Eurocode 8), the following values of the importance factor γ are used: I = 0.8; II = 1.0; III = 1.2; IV = 1.4.

The Eurocode 8 puts emphasis especially on the robust foundation and simplicity of construction systems. This standard also allows differentiation of constructions according to their importance, their dimensions, and their mechanical action. Among other things, the standard specifies conditions for building site selection, soil parameters and also criteria that ground and foundation systems have to complete in seismic design situations. Eurocode 8 provides a simple quasi-static solution for ordinary buildings; seismic forces that already include the effect of motion are determined. Generally, horizontal excitation is used because vertical excitation is usually smaller, and structures are even more resistant to this direction because the design of structures respects their weight. Vertical loads can be of use both in the areas near the epicentres and in the case of long brackets or beams loaded with non-pillar columns.

It is also necessary to take into account that loads of buildings and structures by technical seismicity and their responses are evaluated according to, for example, Czech Technical Standard 73 0040 or Slovak Technical Standard STN EN 1998-1/NA/Z1. This evaluation is established using a class of resistance (A – F) and class of economic and social significance of buildings (U, I – III). Structures of A type are usually historical monuments and buildings, the oldest and poorly structures and also buildings with large plastic decoration; structures of B type are common masonry buildings, usually up to three levels and surface up to 200 m^2. Determination of resistance class depends also on the constructional technology and material used. From the constructional point of view, there are monolithic structures with resistance class E, framed structures with class D, half-timbered structures with class D, buildings up to three stories with class B and prefabricated panel structures with class C. Resistance class can be determined based on material used: stone - resistance class A, masonry - resistance class A, B, C, concrete - resistance class C, D, steel - resistance class D, E and steel concrete – E. Class of significance U represents structures with extraordinary economic and/or social significance (for example, dams, significant bridges …), following class I is represented by structures with great significance (for example, schools, churches…), classes II and III include structures with medium and small significances, respectively.

Historic structures (class A) are usually even more prone to vibration damage than typical wood-frame homes. The greater concerns over historic structures arise from the design, structure age, building materials and building methods used. Maintenance can be an issue in some cases, as well (Johnson and Hannen, 2015; Bongiovanni et al., 2017). For example, tower structures were often built by Romans to celebrate military victories. They played an important role in the reconstruction of some historical periods, but also in the study of the historical seismicity (for example, Bongiovanni et al., 2014). And further example, Clemente et al. (2002) analysed the experimental seismic behaviour of a bell tower damaged by the 1996 Reggio Emilia earthquake. Naturally, engineered, steel-reinforced buildings are more resistant to vibration damage than engineered, non-reinforced structures. All authors, not only describing historical structures loading, pointed out the importance of a multidisciplinarity approach to analyse and preserve given structure.

A most important article on amplitude versus depth relationship was published by Chinese researchers Hu and Xie in 2004. The following information was extracted from this article. The ratio of the amplitudes in the observed depth (underground) and the surface is used for the examination of changes in the value of vibration relative to depth (underground amplitude/surface amplitude). The amplitude ratio is calculated from the maximum values, which can be measured as the peak ground acceleration (PGA), the peak ground velocity (PGV) or the peak ground displacement (PGD). The reason for choosing the surface value as a comparative value is the following. In general, the value of the maximum surface amplitude is greater than in the underground, so if we use a larger value in the denominator, the relative error is reduced. Further, the surface records are much more frequent than from underground; therefore the values for the underground can be determined using statistical regression curves. The evaluation procedure is as follows: Firstly, we issue from the data recorded by a network of seismic stations; to study the effects of earthquakes depending on the depth, the recorded data are split into groups depending on the magnitude of the earthquake and peak amplitude. Secondly, it is possible to calculate the value of amplitude ratios for earthquakes of the same group. Based on this, the average size ratio of all the earthquakes of the same depth can be determined, thus obtaining the average amplitude ratios at different depths. Thirdly, the curves of average amplitudes for each group of earthquakes are determined using non-linear regression analysis. For research purposes, the value of the horizontal component amplitude is determined as the average of two components (NS and EW in the geographic positioning of seismometers).

The Dowding´s and Rozen´s study (1978 in Varnusfaderani et al., 2015) divides the damage to underground structures into three categories according to the effects of the earthquake: damage caused by vibrations, damage caused by faults and damage caused by disturbances due to the earthquake, for example, soil liquefaction or landslides. Varnusfaderani et al. (2015) also pay attention to the source mechanism of earthquakes. Manifestations of underground seismic activity can be divided into two categories:

- Vibration - changes in stress-strain conditions;
- Loss of stability - soil liquefaction, a fault in the rock massif, landslides.

Three types of deformation caused by seismic vibration appear in linear structures located in the underground (Owen and Scholl, 1981):

- Longitudinal axial deformation caused by pressure or tension;
- Bending of the direction axis of a tunnel;
- Deformation of the circular section into oval or frame deformation (racking).

Although the variation characteristics of PGA in different sites share some common features, as shown in Fig. 4, there are still some differences which can be summarised as follows. What is needed to say is that although the events are not quite enough in soil/rock site to account for the specific reduction characteristics of PGA, in order to illustrate the essential characteristics between different site conditions we still compared the two sites.

- The PGA decline velocity for soil/rock site is the most rapidly, for rock site it is the least rapidly, and for soil site, it is in the middle of the two sites.
- The variation of PGA with depth is affected by the magnitude of earthquakes and site geology. For soil site, the PGA decreases with the increasing of magnitude or intensity; for rock site, the declining extent of the larger earthquakes is more rapidly than that of the smaller's.
- Different from rock site, for soil site, there is a dramatic declination in the shallower layer.

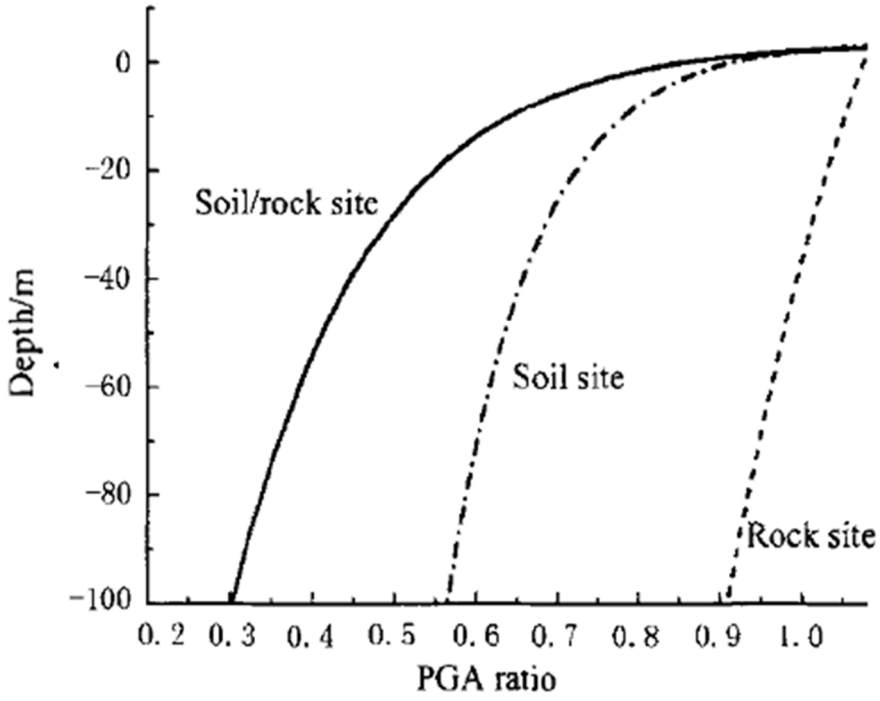

Fig. 4. The comparison of PGA ratios in different sites (from Hu and Xie, 2004).

Based on the results of Hu and Xie (2004), it drew some general conclusions:

- In general, the earthquake amplitude (PGA, PGV or PGD) decreases with depth, and the declining extent is more dramatic in shallower layers than that in deeper ones.
- The reduction of amplitude with depth is affected by the magnitude and site geology. In general, for soil site, the declining extent decreases with the increment of magnitude as well as the amplitude.
- For soil site, as shown in Fig. 5, the decline velocities of PGA, PGV and PGD decrease in sequence. For soil/rock site, the decline velocities of PGA, PGV, and PGD are similar to each other.

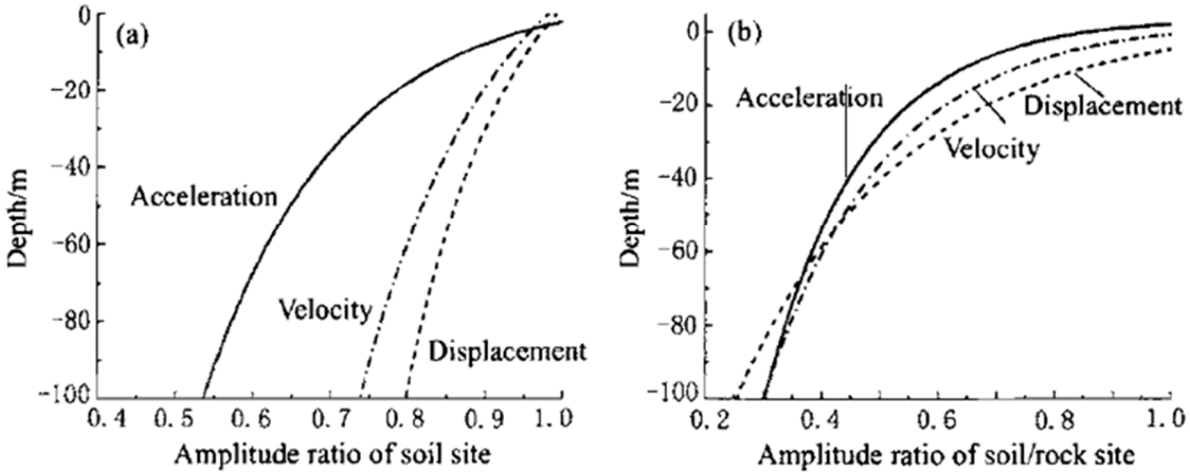

Fig. 5. The comparison of PGA, PGV and PGD ratios in soil sites (a) and soil/rock sites (b) (from Hu and Xie, 2004).

Results imply that PGA decreases with depth and the decline mainly focus on shallower layers. For example, the PGA in depth of 25 m decreases to 1/2 that of the surface. Moreover, as we all known in seismic response analysis, the input motion for structures are generally deduced from the design intensity of surface, and then the surface motion, like PGA, PGV, PGD or time histories, are put to the bottom of the buildings. Obviously, it is inappropriate for that the depth of burial of underground structure or high-rise buildings are always more than 10 m, and the general ideas of doing so are that it would lead to an overestimate of seismic response.

The issue of manifestations of earthquakes in underground mines is in the interest of responsible workers for many years. As an example, we present the findings which were published in a comprehensive study already in 1978 by Pratt, Hustrulid and Stephenson of Utah.

Stevens (1977 in Pratt et al., 1978) summarises the nature of earthquakes and lists numerous examples concerning the earthquakes manifestations on underground structures. He has several general conclusions:

- Effects on mines are less severe than surface effects.
  - Severe damage is inevitable when a mine or tunnel intersects a fault along which movement occurs during an earthquake;
  - Mines in the epicentre region of strong earthquakes but not crosscut by fault movement may suffer severe damage by shaking. Stevens did not define the word severe quantitatively;
  - Mines outside of epicentre regions are likely to suffer little or no damage from a strong earthquake;

- Damage to mines is most insignificant when they are located in highly competent, unweathered rock; greatest damage occurs in mines found in loose unconsolidated or incompetent rock. This is due to the diminished effect of shaking in competent rock; unconsolidated sediment is much more susceptible to damage caused by vibration.

Principal conclusions developed in this study are:

- There are very few data on damage in the subsurface due to earthquakes. This fact itself attests to the lessened effect of earthquakes in the subsurface because mines exist in areas where strong earthquakes have done extensive surface damage.
- More damage is reported in shallow tunnels near the surface than in deep mines.
- In mines and tunnels, large displacements occur primarily along pre-existing faults and fractures or at the surface entrance to these facilities.
- Data indicate vertical structures such as wells and shafts are less susceptible to damage than surface facilities.

Parametric studies were carried out to investigate the influence of the desired variables on the dynamic behaviour of an underground structure while earthquake loading (Serati and Moosavi, 2010). To perform a sensibility analysis of a particular parameter, a suitable model based on all important concepts of dynamic analysis was created. Then by changing the desired parameter in the selected range and keeping all other conditions of the model (such as model dimension, element size, etc.) constant, acceleration, displacement and velocity histories around the underground structure were calculated. Finally, the spectrum was obtained so that its independent variable was the desired parameter and its dependent variable was the maximum amplitude of velocity, displacement or acceleration history. Examining the obtained spectrum shows how changing in the desired parameter can affect dynamic records amplitude around the basic model of the underground structure. The greatest impact on the dynamic behaviour of the underground of structures during an earthquake in terms of geotechnical parameters is seen on the elastic modulus and density of the rock massif. The most important parameters, however, are the geometric parameters, i.e., the depth and diameter (the size) of underground structures.

According to Dowding and Rozen (1978), damage to shallow tunnels due to earthquakes occurs upon the excess of the certain value of acceleration (ground velocity) measured on the surface. The "no damage" limit lies below the level of 1.9 $m.s^{-2}$ (approx. 0.2 $m.s^{-1}$); the level of lesser damage lies in the range of 1.9 m. s^{-2} (approx. 0.2 $m.s^{-1}$) to 5.0 $m.s^{-2}$ (approx. 0.91 $m.s^{-1}$). The authors consider the values of the influence of vibrations in shallow underground areas as about half the value measured on the surface. Then the limit values for underground spaces are approximately 0,9 $m.s^{-2}$ (0,1 $m.s^{-1}$) for no damage zones, and limit values for lesser damage in the range of 0,9 $m.s^{-2}$ (0,1 $m.s^{-1}$) to 2,5 $m.s^{-2}$ (0,45 $m.s^{-1}$). Singh (2002) documents different limit values for the occurrence of damages in a mine as a result of vibrations induced by blasting explosives on the surface. According to this study, the first damage can arise after reaching a ground velocity of 0.05 $m.s^{-1}$ in rocks of very poor quality (RMR = 20 - 30). Different limit values refer to different underground structures and different sources of vibration, i.e., particularly to the frequency range of vibrations, local geological pattern, the shape and geometry of the underground spaces, reinforcement of underground structures and other parameters. Model experiments in various underground structures have shown that they are resistant to vibration. However, the existence of seismic discontinuity makes these structures exceptionally susceptible to collapse, especially in the case of shallow underground structures. Numerical modelling of the dynamic response of underground gas storage in caverns after the seismic load is stated in Wang et al. (2014). They use the modelling program FLAC3D, and they consider the size of the induced acceleration and the duration of vibrations as main factors.

New findings of the effect of technical vibrations

As mentioned in the introduction, technical vibrations differ from natural earthquakes, as regards the comparable value of maximum vibration amplitudes, especially in the frequency range of the signal and mostly its duration. The most usual attribute of technical vibrations is that they are often repeated shocks or periodical signals. In case of corresponding damage of construction, it is necessary to take into account the fact that repeated load, even if it does not reach critical values, can seriously debase the technical conditions of the structures, especially if they are already fissured and/or cracked. In addition, it is necessary to consider higher frequencies, whether the generated frequencies do not match the eigenfrequency of some of the primary or secondary seismic members of the structure. Then, resonant vibration is generated, and a significant increase in the probability of cracks occurring is expected.

The most intensive vibration effect is generated by a blast of explosives (Fig. 6). Blasts are represented by short but usually very intense impulses. As referred in ISO 4866 Standard, the frequency spectrum of the seismic records is continuous and includes frequencies ranging from lower values to very high values - usually 1 to 300 Hz. Wide frequency range of blasting depends on the properties of the disintegrated material, explosive properties, and blasting technology. The frequency spectrum of the seismic record of blasting is further significantly influenced by the environment, in which the waves pass through; higher frequency components are in the rock mass attenuated faster with increasing distances (for example, Barton, 2006; Banerjee and Kumar, 2016).

Fig. 6. Blast in Dewon quarry, Jarnoltowek, Poland, 2012. (Photo: author).

The evaluation of the effect of technical vibrations is usually based on measured values of ground velocity or acceleration; the maximum values can be calculated from empirical relations in some types of technical seismicity. To obtain experimental values, sensors are placed in the evaluated structures, either in cellars or on the lowest floor, and the enclosure load-bearing wall.

Usually, the load of structures generated by blasting vibrations is evaluated according to the maximum ground velocity amplitude (or acceleration) and the frequency of the prevailing vibrations (for example, CSN 730040 – Czech Republic, STN EN 1998-1/NA/Z1 – Slovak Republic, DIN 4150 – Germany, PN-B-02170:2016-12 – Poland …). An empirical relationship is formed which represents the dependence of the maximum ground velocity amplitude V_{max} on the total weight of the charge (or the weight of the charge fired at the one-time stage) Q and distance l (for example, Dojčár et al., 1996; Tripathy et al., 2016). At a sufficient distance from the source of vibrations, the so-called Langefors (or also Koch) formula is used (in the general form)

$$V_{max} = K \,.\, Q^m \,.\, l^{-n}\,, \tag{1}$$

where V_{max} - maximum ground velocity [mm.s^{-1}],
Q - weight of the charge [kg],
l - distance from blasting site [m],
K, m, and n are empirical parameters.

The empirical parameters are determined from the results of the experimental measurements, and they depend on the geological pattern of the area, on the distance between blast and structure, as well as on the method of blasting (for example, Spathis and Noy - eds, 2010, Kondela and Pandula, 2012). There are known locations where this relation shows a very high or conversely very low correlation coefficient (for example, Pandula and Jelšovská, 2008, Kaláb et al., 2013). Often, also in Czech Republic (CSN 73 0040), parameters $m = 0.5$ and $n = 1$ are recommended; the formula then takes the form:

$$V_{\max} = K \frac{\sqrt{Q}}{l}. \tag{2}$$

The value of the K parameter (it depends on geological pattern and distance, it reflects attenuation of seismic waves) is calculated from the experimental measurements; the tables of the K values are often part of standards, and it can be used for the orientation evaluation. From this empirical relation, it is possible to estimate the weight of the charge so that the maximum values of the ground velocity do not exceed the limit ground velocity defined in the standard. These limit values are defined by the permissible load on the construction to take into account local geological pattern and classification of the evaluated structure.

Blasting operations produce seismic waves with a wide frequency spectrum, which depends on properties of the material being disintegrated, properties of the explosive and the blasting technique. The frequency spectrum in a seismic record of a blasting operation is further significantly affected by the environment which the waves propagate through; components of higher frequencies are more rapidly attenuated with the growing distance in the groundmass. Isaac (1991) introduced a reference chart of dependencies of' the frequency range of a seismic signal on the distance from the blasting point. It follows from the chart that, if we wish to have an undistorted seismic record, it is necessary for the frequency range of the seismic channel, especially in the case of small distances from the blasting point, to be as wide as possible (first of all as far as higher frequencies are concerned). The frequency spectrum of seismic signals induced by close-distance blasting in rock and semi-rock may contain frequencies up to 250 Hz. In addition, higher frequencies in the record may be affected by the resonance of the rock mass, the dimension of which is compared with the wavelength. All of these effects cause that the relationship mentioned above between the value of the maximum ground velocity, the weight of a partial charge and the distance can be determined only approximately, using statistical methods. The actual maximum vibration velocities have to be determined by monitoring (according to Kaláb et al., 2011). Many examples contained in technical literature show significant dispersion of the measured values.

To sum up, it is possible to state that the intensity of blasting induced vibrations depends on many parameters (for example, Kaláb, 2004, Spathis and Noy – eds, 2010, Pandula and Kondela, 2010), first of all on the manner of the vibration generation, vibration intensity (radiated vibration energy), the epicentral distance or the depth of the source, the structure of the groundmass which the seismic waves propagate through and the local geology in the location of the manifestation being monitored. The wide diversity causes affecting the value of seismic manifestation on the ground surface is the reason why it is impossible to obtain more credible results without a significant quantity of measurements and why the simple relationships cannot be derived, first of all for small distances. Mathematical modelling using various program systems is today an inseparable part of assessing the impact of technical seismicity on structures.

Examples of vibration effects on structures

The first example describes an analysis of vibration effect in a shallow mine - Jeroným Mine located in West Bohemia, the Czech Republic. Experimental geomechanical and seismological measurements are performed in the mine so that geomechanical stability of the whole underground complex may be evaluated (for example, Kaláb and Lednická, 2016; Knejzlík et al., 2011; Kaláb et al., 2010). Permanent seismological monitoring has been carried out since 2004 using a seismic station JER1, installed in the mine about 35 m below the surface in one of the largest chambers. From 2004 to 2006, the seismic station JER 1 monitored especially effects of blasting operations during the reconstruction of drainage adit. From 2008, more than 2000 earthquakes in West Bohemia were recorded at the station JER 1 during three intensive seismic swarms in 2008, 2011 and

2014. Other sources of vibrations, recorded at the JER1 station, represent quarry blasts from nearby quarries, and vibrations generated by traffic on the road situated above the mine. Detailed analysis of the vibration effect caused by individual seismic load sources is performed in time and frequency domain (for example, Lednická and Kaláb, 2013; Kaláb et al., 2015). Some fractures are observed also using glass markers (Fig. 7).

Fig. 7. A glass marker in a fracture in the underground space of the Jeroným Mine. (Photo: Lednická).

The Jeroným Mine is located at a distance of about 25 km southeast of Nový Kostel focal zone, where seismic activity occurs in the form of seismic swarms. Maximum vibration effect in the mine is caused by these earthquakes. Maximum measured velocity values reached up to 0.8 mm.s^{-1} for an earthquake with magnitude M_L = 3.6 (Fig. 8). Technical seismicity also causes vibration effect in underground spaces. It was documented that maximum velocity values and prevailing frequencies of records from individual sources change significantly. Maximum values from the nearest quarries Vítkov (Fig. 9) and Krásno are usually within the range of 10^{-3} – 10^{-2} mm.s^{-1} (not too significant for stability assessment). The prevailing frequency range of recorded waves is 1 – 6 Hz. The passage of vehicles produces some weak vibrations; component values of maximum velocity are up to 10^{-2} mm.s^{-1} measured at the seismic station JER1. The frequency range of prevailing waves is very narrow at 9 – 15 Hz. This information is important especially for stability assessment and numerical modelling of a seismic load of the underground spaces. Based on current results (for example, Kaláb et al., 2015) we can state that the Jeroným Mine, as the whole complex of underground spaces, should be stable from the viewpoint of damage caused by vibrations. No sudden changes of convergence measurement and measurement of movement along fractures were detected in places with continuous monitoring during the seismic swarms. It is necessary to add that weathering of rock massif is a more important question (Lednická and Kaláb, 2016).

Vibration effect was also measured in different parts of Jeroným Mine. During the 2011 seismic swarm in Nový Kostel, more than 200 earthquakes with local magnitude $M_L \leq 3.3$ were recorded in the underground spaces (Lednická and Kaláb, 2016a); one permanent and five temporary seismic stations were used for the measurement and data analysis. These stations were placed in the mine at the depth ranging from 24 m to 53 m. The lowermost station was selected as the reference station for the analysis of vibration effect changes in comparison with other stations. The peak ground velocity during the phase of S-wave was determined for each recorded earthquake at each station. According to obtained results, it was found that the vibration effect in the mine is decreasing with increasing depth. Vibration effect at a depth of 30 m is approximately two times higher than at a depth of 53 m for vertical and both horizontal components. The calculated peak ground velocity ratio was plotted depending on depth under the surface (Fig. 10). Ratios from all seismic stations correlate with depth except one station at a depth of 24 m. This station was located near the surface in complicated geological and geomechanical conditions. The discrepancy of vibration effect at this place can be connected probably with the jointed rock massif and collapsed overburden consisted of rock blocks. It was also found that the ratio is almost the same for the local magnitude ranging from the 0.9 to 3.3.

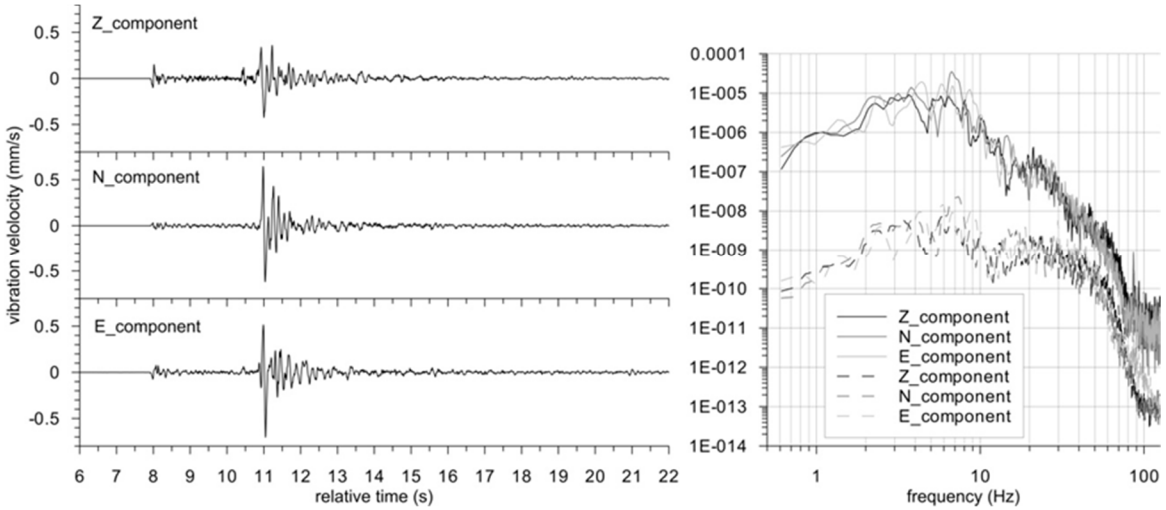

Fig. 8. Wave patterns and spectra of the earthquake from the Nový Kostel focal zone recorded at the seismic station JER1; left – wave pattern of M_L 3.6 earthquake on 4 August 2014; right – spectra of M_L 3.6 earthquake (solid line) and spectra of M_L 2.1 earthquake (dashed line).

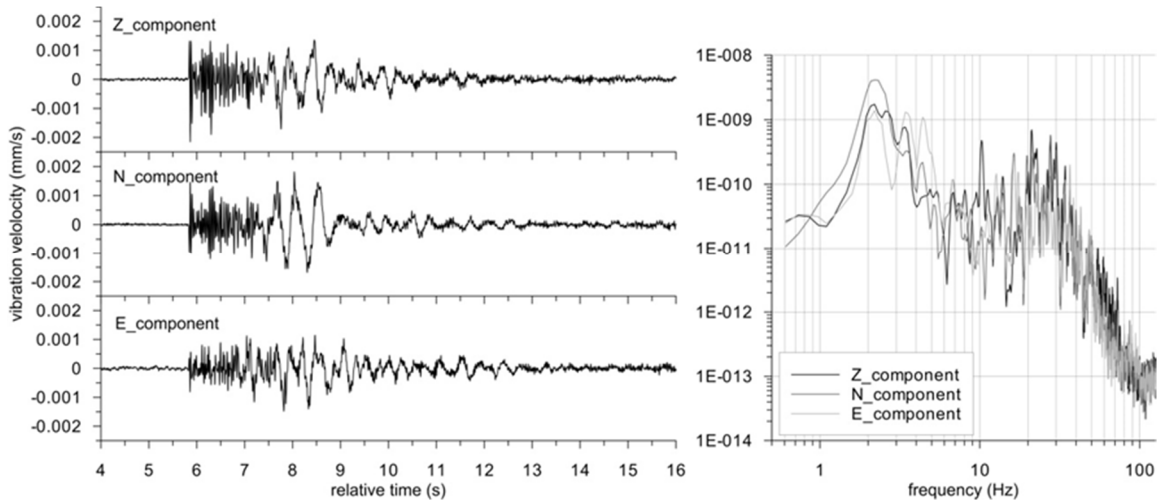

Fig. 9. Wave patterns and spectra of a quarry blast at Vítkov recorded at the seismic station JER1.

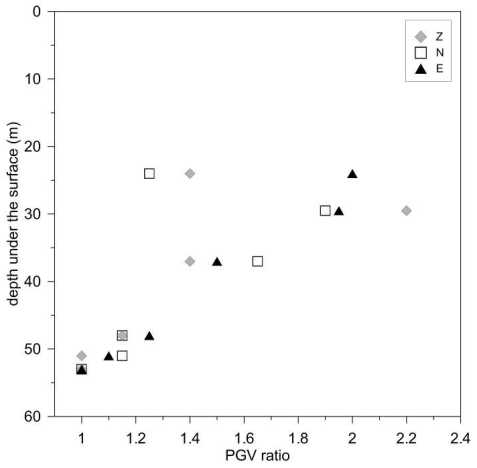

Fig. 10. PGV ratios depending on depth under the surface; depth of 53 m below the surface represents the reference depth for peak ground velocity ratio calculation (Lednická and Kaláb, 2016a).

Phyllite is excavated in the open pit mine near Jarnoltowek (Poland). This next experimental measurement documents resonant vibration generated on geotechnical structures – rock waste deposit that is located directly in the mined part of the quarry at a distance approximately 150 m from the quarry face. Blasting operations are used as mining technology so the rock waste dump might be influenced by these vibrations significantly. The first blast marked as BLAST1 was located on the nearest mined level, the second blast marked as BLAST2 was located on the higher level on the opposite side of the quarry (see Fig. 6); technological parameters of blasts were not published (Lednická and Kaláb, 2015). First presented seismic station (R) was also located in front of the dump on rock basement, second presented seismic station was located on given level of the embankment (D2 – twelve meters above basement). Obtained wave patterns are presented in Figure 10. Due to the short distances frequency range of seismic channel was set in the range 2 Hz – 200 Hz with sampling frequency 500 Hz; these values were sufficient for the measurement of blast-induced vibrations and the resonant vibration of the dump. Analysis of dump response in amplitude and frequency domains was performed by spectral ratio method and by detailed frequency analysis together with continuous wavelet (Morlet transform) time-frequency spectra method (for example, Lyubushin et al., 2014).

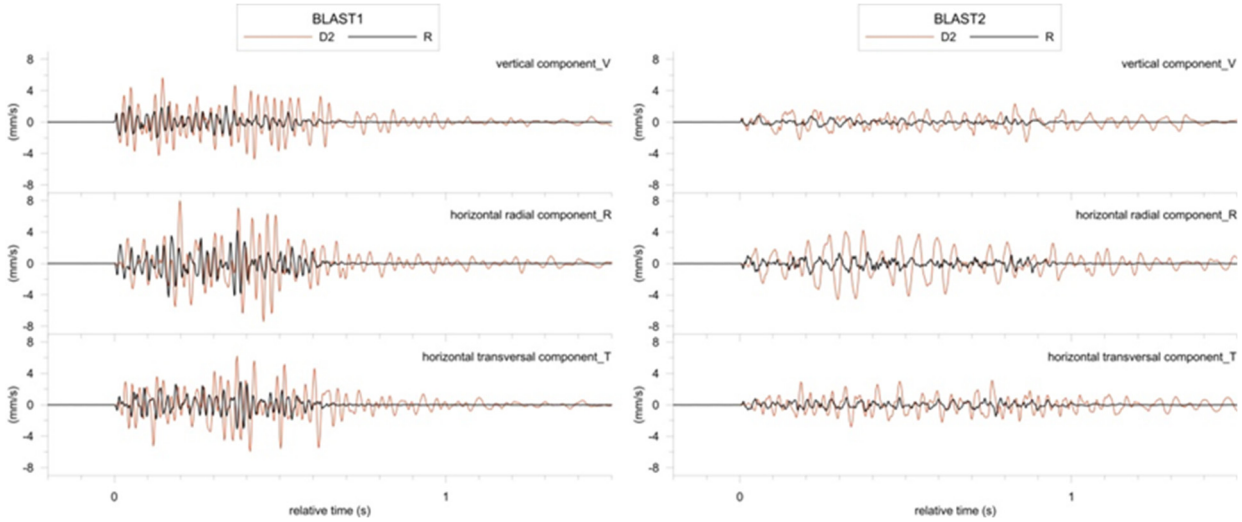

Fig. 10. Wave patterns of two blasts recorded on given seismic stations (R – rock basement, D2 – embankment). More details are described in the text.

The measurement was performed on four levels of the embankment of the rock waste (very fine material). Horizontal components of the ViGeo2 sensors were directed to radial (R) and transversal (T) directions; the third component was vertical (V). To obtain good contact of D1 – D4 sensors with the ground, they were placed into shallow holes. The maximum value of ground velocity during blasting reached 8 $mm.s^{-1}$ on the radial component at the embankment´s height approximately 12 m. Spectral analysis proved a difference in the prevailing frequency range of two measured blasts, i.e. 40 - 50 Hz during the first blast and 15 - 25 Hz during the second one. It was also found that the prevailing frequency content of input ground motion probably influences the dynamic response of the dump, especially in the phase of the dump´s resonant vibration. Both analysis methods mentioned above proved that the resonant frequency determined at the different level of the embankment is decreasing with the increasing elevation of the embankment, which means that the thicker is the waste rock layer, the lower is the fundamental frequency. The maximum amplitude of resonant vibration was detected on the top of the embankment with the resonant frequency equal to approximately 4.0 Hz.

The last example is the evaluation of the influence of basin structures on the shape of wave patterns of induced seismic events. These vibrations are induced by blasting operations that are practised as a part of exploitation technology. A data set of interpreted wave patterns was collected from the data that were obtained during experimental measurement in the open pit Nástup Tušimice Mines in the North Bohemian Brown Coal Basin in 1996 and 1997 (for example, Kaláb and Knejzlík, 1999). Seismic stations were located both in the mine and in buildings the surrounding villages (an example of failure on buildings are in Figure 11).

Fig. 11. Two examples of cracks in buildings damaged by vibrations in the surrounding of open pit Nástup Tušimice Mines. (Photo: Kaláb).

The wave field that is generated after blasting operations is very complicated. The set of recorded wave patterns from positions with different geological conditions shows influences of basin structures on the shape of wave patterns. The wave patterns in this locality made in the distances in range 2 - 5 km are marked with the 3 - 7 s duration of the group of body waves. After that, the record of the group of surface waves manifesting themselves in a vibration of the harmonic type for 15 - 35 s follows in the wave patterns (example on Fig. 12). In this second group of waves with the prevailing frequency of about 2 Hz, the maximum recorded value of ground velocity occurs in the majority of records too. The obtained type of record in the discussed area is similar to some records of near shallow earthquakes. These records are also characterised by intensive surface waves whose amplitudes can exceed the amplitudes of body waves as well.

On the whole, in terms of evaluation of seismic load on buildings in surroundings of the discussed open pit mine according to the values defined in the Czech standard (CSN 73 0040) it can be stated that the value of 3 $mm.s^{-1}$, which is a minimum limit value at the "0" degree of damage (i.e., without any damage) was never reached during any blasting. If we admit the "1" degree of damage (i.e., the first damages – small failures), we can present that the minimum limit value of 8 $mm.s^{-1}$ is three times higher. The maximum recorded value of velocity amplitude in buildings was 2.8 mm $s^{-1,}$ but seismic loading is often repeated which then results in debasing of the technical conditions of the buildings.

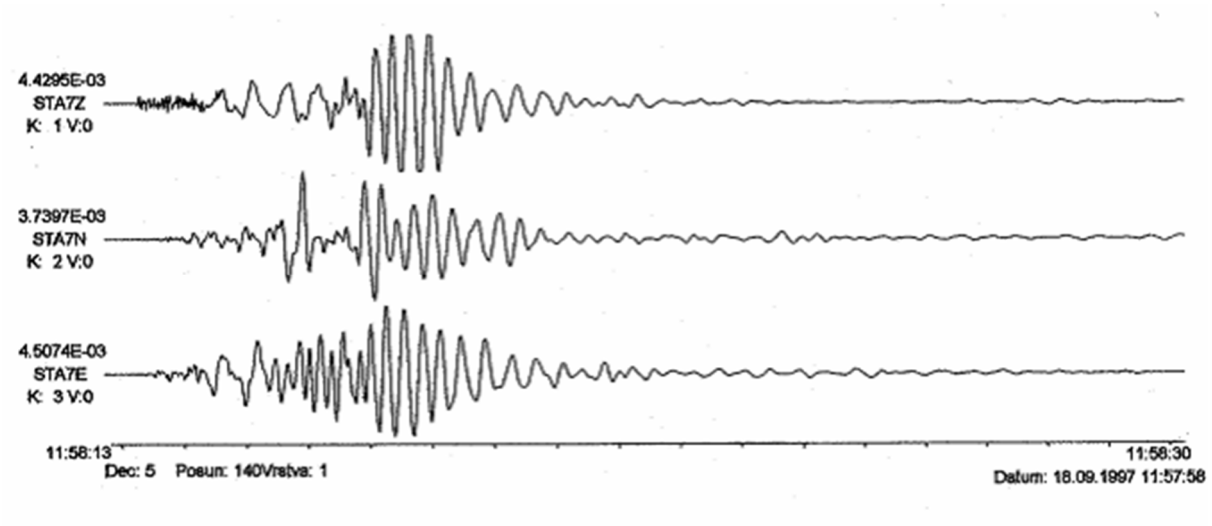

Fig. 12. Wave patterns of blasting operation recorded on concrete pillar located on the boundary of open pit Nástup Tušimice Mines (epicentre distance about 1.5 km).

Discussion

It is possible to find a large number of papers and books that described the main topic of this paper, i.e. influence of vibrations on structures (for example, Bolt, 1999, Towhata, 2008, Chudley and Greeno, 2014). Generally, three main parameters are necessary to take into account for comprehensive evaluation of this physical process: a source of vibration, the geological medium through which the seismic waves propagate, and local condition in evaluated point (geological and/or engineering problems). To obtain complete information, measurement system has to keep sufficient parameters, especially the frequency range of the whole seismic channel, sampling frequency, and proper anchorage of the sensor.

Methodology for evaluation of vibration on structures usually includes the following steps:

- Determination of acceptable load;
- Prognosis of the load;
- Determination of risk, eventually safe distance and other parameters;
- Description of failures including their photographs, with special view of historical and fissured structures;
- Measurement of seismic effects;
- Evaluation of safety for the obtained (from measurement) load, correction of the current state;
- Observing existing fissures and failures.

At present, permanent seismic monitoring with automatic data acquisition and primary interpretation of basic parameters is favoured in urban regions when significant vibrations are generated. Realisation of temporary seismic stations that will operate in suitable buildings during the whole period of seismic loading (generally weeks or first months) is supposed. Obtained results are at disposal to civil engineers, fire-fighters and also to custodians and occupants of influenced buildings. Usually, the web application is available with different access authority levels.

Lu (2014) defined major steps in the detailed analysis of ground-borne vibrations of building structures (engineering approach):

- Develop estimates of the force density. Can be based on previous measurements or a special test program. Adjustments for factors such as traffic speed, road surfaces, track support system, and vehicle suspension.
- Measure the point-source transfer mobility at representative sites. The transfer mobility is a function of both frequency and distance from the source. (mobility: velocity; inheritance: acceleration, displacement: receptance).
- Use numerical integration to estimate a line-source transfer mobility from the point-source transfer mobilities.
- Combine force density and line-source transfer mobility to project ground-surface vibration.
- Add adjustment factors to estimate the building response to the ground-surface vibration and to estimate the weighted sound level inside buildings.

It is also necessary to point out the second-hand influences of a seismic event on structures. The main discussed topics are influences on properties of the medium:

- Change of physical-mechanical behaviour of the subsoil of buildings;
- Change of stress conditions;
- Change of slope (downhill) stability.

Dynamic loading, even though its effect on underground structures is usually much smaller than that produced by the rock pressure, has been given greater attention of late, especially when dimensions of utility tunnels are designed. This type of load belongs among indirect loads, i.e., imposed deformation or limited deformation or constrained vibration. The problem of determining the magnitude of the affection of lining by dynamic loading is not simple to solve; the following methods are most frequently used:

- Recalculation from a wave pattern (usually a record of longitudinal and transverse waves) to tensile stresses and compressive stresses or shear stresses (Bulyčev, 1982); however, the complexity of the calculation together with the great number of constants and unknown quantities, makes this method impracticable.
- The use of calculation programs, which are capable of mathematical modelling of the dynamic action. The input parameters consist of basic characteristics of the dynamic action, for example, prevailing frequency of vibration, the maximum amplitude of ground velocity or acceleration, etc. Among such programs, we can name Plaxis, Cesar, ANSYS and other systems.
- The possibility of introducing a "dynamic coefficient" γ_a, which makes it possible to allow for the dynamic loading by means of adjustment of the value of gravitational acceleration (for example, Kaláb, 2007). The relationship between gravitational acceleration and the induced acceleration at the location of the structure, which is to be designed, is defined in the form of

$$\gamma_a = \frac{(a_d + g)}{g}, \tag{3}$$

where a_d is dynamic acceleration [m.s^{-2}]
and g is gravitational acceleration [g = 9.80665 m.s^{-2}].

The latter method is based on the method of partial coefficients used in the ultimate load design concept. This principle is commonly used in Eurocodes. The method of partial coefficients is based on the verifying in all design situations whether the values for limit states are not exceeded if the design values are assumed in all design models to be applied to the loading, material properties, and geometrical data. The partial coefficients are partially based on the theory of reliability and partially on historical and empirical experience.

Problems of measurements and interpretation of vibrations originating at small distances during shallow tunnel excavation are paid great attention, first of all in settled areas (for example, Qui et al., 2008; Kaláb et al., 2011). Special attention is even devoted to the impact of vibration on vibration-sensitive devices.

Conclusion

Influences of earthquakes and quarry blasts on the structure are traditionally discussed and solved. Presently, vibrations generated by commercial explosives in tunnel construction may cause structural damage in urban areas. Therefore, suppressing the vibration effects and mitigating the possible hazard after blasting is important. The duration and also the number of explosives were carefully controlled. Urban tunnel construction induces not only changes in rock massif, but buildings and inhabitants in the nearest surroundings above a tunnel or underground working can be affected too. At present, permanent seismic monitoring with automatic data acquisition and primary interpretation of basic parameters is favoured in urban regions when significant vibrations are generated. Realisation of temporary seismic stations that will operate in suitable buildings during the whole period of seismic loading (generally weeks or first months) is supposed. Obtained results are at disposal to civil engineers, fire-fighters and also to custodians and occupants of influenced buildings. Usually, the web application is used with different access authority levels.

Generally, it is necessary to point out that disturbed objects, even without visible signs (for example, cracks), are more vulnerable. It is reflected by the resonance vibration of the smaller or larger building element and the acceleration of the "ageing" of the object. It is appropriate to include this fact in the assessment of a load of a structure by means of a coefficient (similar use as a construction reliability factor) if the discussed effect is proven by the passporting of the structure.

This paper summarises common information about the influences of vibrations on structures. The paper shows differences of vibration evaluation for earthquakes and technical events, esp. blasts. Examples of real wave patterns document common shapes (Fig. 8 and Fig. 9) and also signals with significant resonant vibrations (Fig. 10 and Fig. 12). Also, the wave field of high frequencies of seismic signal significantly interferes on the surface, and an important part of this field is also a response of the buildings' constructional elements.

Acknowledgement: *The paper has obtained financial support for conceptual development of science, research and innovation in 2018, assigned to VSB-Technical University of Ostrava, The Ministry of Education, Youth and Sports in the Czech Republic. This research is partly sponsored by Research Program of Academy of Sciences of the Czech Republic, OZ30860518.*

References

Ali A., Abu-Hayah N., Kim D., Cho G. S. (2017) Design response spectra-compliant real and synthetic GMS for seismic analysis of seismically isolated nuclear reactor containment building. *Nuclear Engineering and Technology,* 49, 4, 825-837, https://doi.org/10.1016/j.net.2017.02.006

Banerjee S., Kumar A. (2016) Determination of seismic wave attenuation: A Review. *Disaster Advances*, 9 (6), 10-27.

Barton N. (2006) Rock quality, seismic velocity, attenuation and anisotropy. *CRC Press*, Taylor & Francis Group.

Båth M. (1979) Introduction to seismology. *Birkhauser Verlag*, Basel.

Berr G. – ed. (2003) Numerical simulation in tunnelling. *Springer*.

Bolt B.A.: Earthquakes. *W. H. (*1999) *Freeman and Company*, New York, fourth ed..

Bongiovanni G., Buffarini G., Clemente P., Rinaldis D., Saitta F. (2017) Experimental vibration analyses of a historic tower structure. *J Civil Struct Health Monit, Vol. 7,* 601–613. DOI 10.1007/s13349-017-0245-4

Bongiovanni G, Buffarini G, Clemente P, Saitta F. (2014) Dynamic characterization of the Trajan's Column. In: Pen˜a F, Cha´vez M (eds), Structural analysis of historical constructions. *Proc. SAHC2014,* Mexico City.

Bullen K.E., Bolt B.A. (1985) An Introduction to the Theory of Seismology. *Cambridge University Press*, Cambridge 4th edition.

Bulyčev H.C. (1982) Mechanics of underground objects. *NEDRA*, Moscow.

Clemente P., Bongiovanni G., Buffarini G. (2002) Experimental analysis of the seismic behaviour of a cracked masonry structure. *Proc. of 12th European conf. on earth. eng. (12ECEE,* London), Elsevier Science Ltd.

Dojčár O., Horký J., Kořínek R. (1996) Blasting technology. *Montanex, a.s.,* Ostrava.

Dowding CH, Rozen A (1978): Damage to rock tunnels from earthquake shaking. *J Geotech Eng Div*, 104, 15–20.

Doyle H. (1995) Seismology. *John Wiley & Sons Ltd*., Chichester.

Chakraverty S., Sahu A., Keong Ch.K., Hassan S.M. (2012) Recent trends of computational methods in vibration problems. *Advances in Acoustics and Vibration,* Vol 2012, http://dx.doi.org/10.1155/2012/645981.

Chudley R., Greeno R. (2014) Building Construction Handbook. *Routledge*, Taylor & Francis Group, eleven ed.. http://www.simardartizanfarm.ca/pdf/Building_Construction_Handbook.pdf

Graizer V. (2006) Equation of pendulum motion including rotations and its imlifications to the strong-motion. In: Teisseyre R., Takeo M., Majewski E. – eds: Earthquake source symmetry, structural media and rotation effects. *Springer-Verlag*, Berlin, 471-485.

Gupta A. K. (1992) Response spectrum method in seismic analysis and design of structures. *CRC Press*, Taylor & Francis Group.

Hori M. (2006) Introduction to computational earthquake engineering. *Imperial College Press*, London.

Hu J., Xie L (2004) Variation of earthquake ground motion with depth. *Acta Seismologica Sinica*, 18, 1, 72-81, DOI 1000-9116(2004)01-0072-10.

Iervolino I., Maddaloni G., Cosenza E. (2008) Eurocode 8 compliant record sets for seismic analysis of structures. *Journal of Earthquake Engineering*, 12, 54–90, http://www.reluis.it/doc/pdf/AccelerogrammiEC8/Eurocode_8_Compliant_Real_Record_Sets_for_Seismic_Analysis_of_Structures.pdf

Isaac I.D. (1991) Effect of constructional vibrations upon an urban environment. In: Earthquake, blast and impacts: Measurements and effect of vibration. *Elsevier Applied Science*, 442-462.

Johnson A.P., Hannen W.R. (2015) Vibration limits for historic buildings and art collections. *Journal of Preservation Technology,* Vol. 46:2-3, 66-74.

Kaláb Z. (2004) Impact of seismicity on surface in mining affected areas: General description. *Acta Geod. Geomat.,* Vol. 1. (133), 35-39.

Kaláb Z. (2007) Shallow underground construction and vibration. *Tunnel*. Magasine of the CTC and STA ITA/AITES, 2, 16, 12-20.

Kaláb Z., Knejzlík J. (1999) The influence of basinal structures on the shape of wave patterns of induced seismic events: An example from the North Bohemian Brown Coal Basin. *Bulletin of the Czech Geological Survey*, 74/2, Prague, 185-190.

Kaláb Z., Knejzlík J., Lednická M. (2013) Application of newly developed rotational sensor for monitoring of mining induced seismic events in the Karvina region. *Acta Geodyn. Geomater*., Vol. 10, No. 2(170), 197-205. http://www.irsm.cas.cz/materialy/acta_content/2013_02/acta_170_09_Kalab_197-205.pdf

Kaláb Z., Lednická M. (2016) Long-term geomechanical observation in the Jeroným Mine. *Acta Geophysica*, 64, 5, 1513-1524, DOI: 10.1515/acgeo-2016-0054.

Kaláb Z., Lednická M., Knejzlík J., Telesca L. (2010) First results from long-term monitoring of distance using a laser distance meter in shallow medieval mine. *Acta Geodyn. Geomater.,* 7, 4 (160), 469-475.

Kaláb Z., Lednická M., Kaláb T., Knejzlík J. (2015) Evaluation of vibration effect in shallow mine caused by natural and technical seismicity. *15th International Multidisciplinary Scientific Geoconference SGEM 2015,* Albena, Bulgaria, Conference proceedings, Science and Technologies in Geology, Exploration and Mining, III, 855 – 862. DOI: 10.5593/sgem2015B13

Kaláb Z., Pandula B., Stolárik M., Kondela J. (2013) Examples of law of seismic wave attenuation. *Metalurgij*a, 52, 3, 387-390. http://public.carnet.hr/metalurg/Metalurgija/2013_vol_52/No_3/MET_52_3_387-390_Kalab.pdf

Kaláb Z., Stolárik M., Kukutsch R., Němeček J. (2011) Olbramovice Tunnel – Experimental seismic measurements in a near zone. *Tunnel - Magazine of the Czech Tunnelling Association and the Slovak Tunnelling Association ITA-AITES,* Vol. 20, No. 1/2011, 93-99.

Knejzlík J., Kaláb Z., Lednická M., Staš L. (2011) Investigation of the medieval Jeroným Mine stability: Present results from a distributed measurement network. In Idziak, A.F., Dubiel, R. – editors: Geophysics in Mining and Environmental Protection. *Ser. Geoplanet: Earth and Planetary Science*, Vol. 2, 59-70. DOI 10.1007/978-3-642-19097-1.

Knejzlík J., Kaláb Z., Rambouský Z. (2012) Concept of pendulous S-5-S seismometer adaptation for measurement of rotational ground motion. *Journal of Seismology*, Vol. 16, No. 4, 649-656. DOI 10.1007/s10950-012-9279-6.

Kondela J., Pandula B. (2012) Timing of quarry blasts and its impact on seismic effects. *Acta Geodyn. Geomater*., 9, 2(166), 155-163.

Kulhánek O. (1990) Anatomy of Seismograms. *Elsevier Science*, Amsterdam.

Lednická M., Kaláb Z. (2013) Vibration effect of earthquakes in abandoned medieval mine. *Acta Geod Geophys.*, 48/3, 221-234,. DOI 10.1007/s40328-013-0018-4.

Lednická M., Kaláb Z. (2015) Vibration response of waste rock dump in open pit mine caused by blasting operation. *Acta Montanistica Slovaca*, 20, 2, 71-79, http://actamont.tuke.sk/pdf/2015/n2/1lednicka.pdf

Lednická M., Kaláb Z. (2016) Determination of granite rock massif weathering and cracking of surface layers in the oldest parts of medieval mine depending on used mining method. *Arch. Min. Sci.*, 61, 2, 381-395. DOI 10.1515/amsc-2016-0028.

Lednická, M., Kaláb, Z. (2016) Vibration effect of near earthquakes at different depths in a shallow medieval mine. *Acta Geophysica*, Vol. 64, No. 6, 2244-2263, 2016a. DOI 10.1515/acgeo-2016-0085

Lee W.H.K., Celebi M., Todorovska M.I., Igel H. (2009) Introduction to the special issue on rotational seismology and engineering applications. *Bull. Seismol. Soc. Am*., 99, 2B, 945-957.

Lu Y. (2014) Structural vibration: Overview, modelling and evaluation. *NTU Public Seminar*. http://www.cee.ntu.edu.sg/NewsnEvents/EPres/Documents/Sem20Aug14/Structural%20vibrations_NTU%20public%20seminar_LY.pdf, May 2018.

Lyubushin A.A., Kaláb Z., Lednická M. (2014) Statistical properties of seismic noise measured in underground spaces during seismic swarm. *Acta Geod Geophys.,* 49, 2, 209-224. DOI 10.1007/s40328-014-0051-y.

Lyubushin A.A. (2007) Data analysis from geophysical and ecological monitoring. *Nauka*, Moscow.

Lyubushin A.A., Kaláb Z., Lednická M. (2012) Geomechanical time series and its singularity spectrum analysis. *Acta Geod. Geoph. Hung*., Vol. 47, No. 1, 69-77.

Macdonald A. J. (2001) Structure and architecture. *Architectural Press,* University of Edinburgh*, s*econd ed..

Merritt F. S., Ricketts J.T. (2001) Building design and construction handbook, *The McGraw-Hill Companies, Inc., s*ixth ed.

Owen G.N., Scholl R.E. (1981) Earthquake engineering of large underground structures. *Report no. FHWA RD-80 195.* Federal Highway Administration and National Science Foundation.

Pandula B., Jelšovská K. (2008) New criterion for estimate of ground vibrations during blasting operations in quarries. *Acta Geodyn. Geomater.,* 5, 2(150), 147-152.

Pandula B., Kondela J. (2010) Methodology of seismology of blasting operations. *SSTVP, Banská Bystrica*, Slovakia.

Pratt H.R., Hustrulid W.A., Stephenson D. E. (1978) Earthquake damage to underground facilities. *Savannah River Laboratory Report*, DP-1513, 20-25.

Qui W., Gong L., Zhang J., Hu H. (2008) Study on vibration influence on existed tunnel by blasting construction of underpass dispersion tunnel in short distance. *Proceedings of World Tunnel Congress 2008*, India, 1139-1147.

Shearer P.M. (2009) Introduction to seismology. *Cambridge University Press*, Cambridge, second edition.

Scherbaum F. (1994) Basic concept in digital signal processing for seismologists. *Springer-Verlag*.

Serati M., Moosavi M. (2010) Analysis of influencing factors in response spectrum of underground structures using numerical method. In: *Rock stress and earthquakes*, Proceedings of the Fifth International Symposium on In-situ Rock Stress. 5th International Symposium on In-situ Rock Stress and Earthquakes, Beijing, China, 579-583.

Singh P.K. (2002) Blast vibration damage to underground coal mines from adjacent open-pit blasting. *Int J Rock Mech Min Sci*., 39, 959–973.

Spathis A. T., Noy M. J. – eds. (2010) Vibrations from Blasting. *CRC Press*, Taylor& Francis Group.

Teisseyre R., Takeo M., Majewski E. – eds (2006) Earthquake source asymmetry, structural media, and rotation effects. *Springer-Verlag*, Berlin.

Towhata I. (2008) Geotechnical earthquake engineering. *Springer*, Verlag Berlin Heidelberg.

Tripathy G. R., Shirke R. R., Kudale M. D. (2016) Safety of engineered structures against blast vibrations: A case study *Journal of Rock Mechanics and Geotechnical Engineering,* 8, 2, 248-255, DOI: 10.1016/j.jrmge.2015.10.007

Udías A. (1999) Principles of seismology. *Cambridge University Press*.

Varnusfaderani M.G., Golshani A., Nemati R. (2015) Behavior of circular tunnels crossing active faults. *Acta Geodyn. Geomater.*, 12, 4 (180), 363–376. DOI 10.13168/AGG.2015.0039

Villaverde R. (2009) Fundamental concept of earthquake engineering. *CRC Press*, ninth ed., Taylor & Francis Group.

Viskup J., Pandula B., Leššo I., Jelšovská K. (2005) Spectra of seismic response. *Acta Montanistica Slovac*a, 10(2005), 2, 380-386.

Wang T., Yang Ch., Yan X., Li Y., Liu W., Liang Ch., Li J. (2014) Dynamic response of underground gas storage salt cavern under seismic loads. *Tunnelling and Underground Space Technology,* 43, 241–252.

Zeigler J.M. (2018) Vibration and damage. http://vibrationdamage.com/vibration_and_damage.htm, May 2018.

The abandoned mines rehabilitation on the basis of speleotherapy: used for sustainable development of the territory (the case study of the single-industry town of mining industry)

Zhanna Mingaleva[1], Evgeny Zhulanov[1], Natalia Shaidurova[2], Michał Molenda[3], Albina Gaponenko[4] and Marieta Šoltésová[5]

The depletion of mineral resources and the increasing complexity of mining conditions (including the strengthening of environmental legislation) lead to a reduction in mining activities. This causes serious problems for towns and cities where mining was the main activity of their residents. The problem's solution to such settlements is seen in the development of new types of economic activity on the basis of abandoned mines. The most common is currently caving, eco-tourism and historical tourism. The sustainable development of the territory depends on the economic activities of agents and the ecological safety of the region. Rehabilitation of abandoned mines makes it possible to implement new ways of use of closed mines and improve economic and ecological situation in "mining cities". Russia has good experience in the use of salt mines with the rest of their minerals for their application as speleoclinics. The article aims to analyze the possibilities of organization of speleotherapy on the basis of waste mines of the mining industry. The developed economic and mathematical model allowed to estimate the economic effect of the development of speleotherapy on the basis of salt mines of Berezniki potash deposit. The analysis proved the positive effect of the development of speleotherapeutic services for the socio-economic system of the city of Berezniki as a whole.

Key words: *Mining industry, salt mines, speleotherapy, economic and mathematical model, sustainable development*

Introduction

An acute problem in the development of mono-cities built on the mining industry is the search for ways to preserve the socio-economic system of the territorial settlement and its development after the mining of minerals has been reduced or completely stopped. In many countries, including central Europe, "the mining exploitations have led to the birth of communities, and for some, they have been a growing source. Therefore abandoned mining sites have a huge impact on economic, social, ecological and urban terms" (Biały, 2014; Midor and Zasadzień, 2015; Pascu, 2013). The negative social and economic implications of mining restructuring is exacerbated by such cause as mono-professional specialization and low educational level of the labor force (Costache and Pehoiu, 2010).

After the cessation of mining activity, the population faces a difficult choice (Schejbal, 2011; Demirović et al., 2018). In this case, the task of effective interaction between mineral developers, local authorities, local community, the population at the choice of a specific direction of restructuring closing mines is to ensure the sustainable development of the territory arises among all members of the society (Shekov and Shekov, 2016).

The first option is to change the region of residence. This has been actively used in European countries: "After stopped of mining activities in developed countries at the end of 20 century, mining work removal, as well as standard technological procedures of reclamation brought removal of unique mining works and machinery, and abandonment of former mining settlements. These solutions were correct, for they put an end to hard work and unsuitable living conditions in mining settlements" (Hronček and Rybár, 2016). However, this path is a difficult task in Russian conditions, since it requires significant capital investments.

The second option is the re-profiling of city-forming activity under a new look. The development of mining, mountain, and speleological tourism is widely used in the world as the implementation of such direction. As many modern researchers have noted: "Paradoxically, attenuation of mining activities has brought about greater importance and popularity of mining tourism" (Hronček and Rybár, 2016).

It is possible to combine different types of tourism: mountain, ecological, historical and cultural. After the termination of mining and removing of the inhabitants to other places, the mines are abandoned, and the technologies, mechanisms, and tools used in mining are destroyed. At the same time mining technology is a kind of cultural and historical heritage in those countries where mining has been developed for centuries. Researchers from Slovakia, Romania, Poland (Biały, 2014; Biały & Mroczkowska, 2015; Midor & Zasadzień, 2015) the

[1] *Zhanna Mingaleva, Evgeny Zhulanov,* Perm National Research Polytechnic University, Department of Economics and management in industrial production, 29 Komsomol'skii ave., Perm, 614990, Russia, mingal1@pstu.ru, zeepstu@yandex.ru.

[2] *Natalia Shaidurova,* Kalashnikov Izhevsk State Technical University (Votkinsky branch), Department of Economics and Organization of Production, 1 Shuvalov str., Votkinsk, 427433, Russia, Shaydurovans@gmail.com

[3] *Michał Molenda,* Silesian University of Technology, Faculty of Organization and Management, Institute of Production Engineering, ul. Roosevelta 42, 41-800 Zabrze, Poland, e-mail: michal.molenda@polsl.pl

[4] *Albina Gaponenko,* Russian State Social University, Department of the Technosphere Safety and Ecology, st. Wilhelm Pick, 4 Building 1, Moscow, 129226, gaponenko69@mail.ru

[5] *Marieta Šoltésová,* Faculty of Mining, Ecology, Process Control and Geotechnology, Institute of Geodesy, Cartography and Geographical Information Systems, Park Komenského 19, 040 01 Košice, Slovakia

Czech Republic emphasize the importance of preserving the mountain heritage for the comprehensive support of the development of the former mining areas. They note that in Central Europe, after the decline of mining activities, their historical significance has been recognized, as well as a «willingness to recognize social, economic and technological relations of mining increase» (Rybár & Gómez, 2014). G. Pascu, J. Bayon, and T.O. Gheorghiu present three possibilities of tourism regeneration of waste mines and their impacts in Romania (Pascu et al., 2013).

The third way is a combination of medical and sanatorium-resort treatment on the basis of waste mines. This option is possible in case if the mine contains ore reserves, which can be used for medicinal purposes.

However, there can be some problems. In particular, dumps taken to the surface or waste rock, dips in the soil after the extraction of minerals, faults and washouts and other negative phenomena that spoil the natural landscape remain in the environment after mining. "Dumps after underground mining usually remain like stars on the appearance of the landscape" (Hronček and Rybár, 2016). "The open craters filled with water and garbage, having steep, unstable slopes represent most of the abandoned quarry sites, raising public health and safety concerns additionally to unpleasant environments" (Jayawardena et al., 2018). For example, Figure 1 shows the photographs of two craters from the failures of the mines of the Bereznikovsky mine department (Russia, Perm region). The first crater is located right in the city center between the buildings threatening their safety. The second crater is located outside the city above one of the mines that were flooded by the earthquake.

Fig.1. The craters from the failures of the mines of the Bereznikovsky mine department

In Italy in the region of Sardinia "abandoned tailing dumps from mining industry represent important sources of metal contamination in the surrounding environments" (Bacchetta et al., 2015). A similar problem is in Romania: "Abandoned mining sites contain large quantities of mineral processing wastes stored in dumps that are characterized by high concentrations of heavy metals" (Gherman et al., 2012). "Disturbed lands with traces of old mines in different regions of Russia, both in use and abandoned mining-industrial territories" (Shekov et al., 2017) are scientific and practical objects of modern research of the Russian scientists such as V.V. Zapariy, (Zapariy, 2009), G.D. Pershin (Pershin, 2014), A.L. Potravnov and T.Y. Khmelnik (Potravnov and Khmelnik, 2015), K. Shekov, V. Shekov (Shekov et al., 2017).

A particular problem is the presence of large quantities of heavy metals in the dumps and the metal accumulation in wild plants surrounding mining wastes (Angiolini et al., 2005; González and González-Chávez, 2006) and in the crop plants at different levels of soil contamination (Zubkova et al., 2016).

Sometimes such dumps or spills contain toxic chemicals that cause significant environmental damage and have negative environmental effects on the environment for a long time. The development of tourism and other activities in such areas is unacceptable. For such situations requires a large and long-term rehabilitation of the soil. However, "the traditional rehabilitation methods are rarely applicable for such circumstances due to unique socio-economic conditions and stakeholder aspirations" (Jayawardena et al., 2018) and mine ecological closure costs are rather big (Sorensen, 2007; Sorensen, 2008). A. Paulo wrote about the environmental limitations in possible directions of post-mining land use (Paulo, 2008). The environmental hazard in the mining district for southern Iglesiente (Sardinia, Italy) has been described by M. Boni and colleagues (Boni et al., 1999).

The forming of the landscape of post-mining areas in Poland (Biały, 2014; Biały & Mroczkowska, 2015; Midor & Zasadzień, 2015) and an inactive basalt quarry in Strzegom was analyzed in the works by K. Tokarczyk-Dorociak, K. Skolak, and M.W. Lorenc (Tokarczyk-Dorociak et al., 2010; Tokarczyk-Dorociak et al., 2015), K. Zych-Głuszyńska (Zych-Głuszyńska, 2011). Tourist possibilities of using the closed marble quarry in the Republic of Karelia (Russia) were revealed and presented in the works of I.V. Borisov (Borisov, 2014), A.B. Artemyev and A.A. Yushko (Yushko and Artemyev, 2015), K. Shekov and V. Shekov (Shekov and Vitali, 2017). A.E. Kurlaev (Kurlaev, 2015), Yu.S. Lyakhnitsky, A.A. Yushko, O.A. Minnikov, I.Yu. Khlebalin

(Lyakhnitsky et al., 2015), Zh. Mingaleva and O. Bunakov (Mingaleva and Bunakov, 2014), N.S. Solonina and O.A. Shipitcina (Solonina and Shipitcina, 2015) engaged in identifying other opportunities for the development of mountain tourism in Russia.

Finally, some modern authors (but they are few) are considering the possibility of transforming dying mountain villages on the abandoned mining sites in alternative industrial production parks. The implementation of this direction "would have an enormous positive impact both nationally and internationally" (Pascu et al., 2013). However, this direction of the renovation of mine towns is still poorly disclosed in the scientific literature, although the creation of industrial production parks and technoparks in various areas of the economy is studied widely in world science and Russia (Shaidurova et al., 2017; Mingaleva and Shaidurova, 2018). Conclusions and recommendations on the possibility of using old mines should be based on an assessment of the general and special characteristics of the mine and the stock of mineral raw materials in it, based on an assessment of the state of the transport and social infrastructure of the mine settlements and the ability to create new products or services on it, based on an assessment of environmental risks.

Theoretical and methodological background

International studies of the mining heritage and speleotourism development

The development of various types of tourism associated with mountains, mines, caves has recently been widely discussed by the scientists in the countries where mining of mineral resources is becoming more and more costly and less profitable, and mines are being closed.

A comparative analysis of the world scientific literature on the renovation of former mining areas showed a certain concentration of research on certain areas of their development. Thus, scientists from Slovakia and Slovenia are primarily focused on the study of opportunities for the development of mountain tourism, including historical, industrial and other types of tourism: "historical mining monuments processed have become the main attraction in the still-developing of both - geo and mining tourism in Slovakia" (Hronček and Rybár, 2016). In their studies, they widely use the term "mining heritage". Mining heritage can also cover the territory, which has long depended on mining. In territorial terms, we may assign mining heritage in different categories. In general, the concept of heritage can be defined by cultural, natural and mixed categories, what is a case that covers the most areas where mining existed for a long time" (Hronček and Rybár, 2016). As for the term "Mining heritage" itself, it can be applied even in general to the territory "which has long depended on mining" (Hronček and Rybár, 2016).

«Mining tourism offers visitors a chance to see and get to know a follows: mining tools, devices and technologies, minerals, ores and rocks accessible in the region, technologies applied in ore extractions, as well as technologies used to enrich produced ores; historical personalities who used to secure and support mining process, just like conditions in the area after shut-downs of the operations» (Rybár and Hvizdák, 2010).

Also the study of geotourism and mining tourism in different countries, including UK, Southern Spain, Serbia, Romania and all European countries, devoted work by J. Swarbrooke (Swarbrooke, 2002), C. Schejbal (Schejbal 2005, 2011), E.R. Ballesteros and M.H. Ramírez (Ballesteros and Ramírez, 2007), P. Rybár (Rybár 2010), M.D. Petrović, N. Vuković, T. Gajić, D. Vuković and their colleagues (Petrović et al., 2017; Petrović et al., 2018), G. Mairescu, V. Timotin, N. Grudnicki, C. Zup, (Mairescu et al., 2014), Iu. Simionca (Simionca, 2013), P. Różycki1and D. Dryglas (Różycki1 and Dryglas, 2017). About the remediation for historical mining and smelting sites written by A. Dybowska and colleagues (Dybowska, 2006). P. Hronček and P. Rybár studied the relics in historical underground spaces and the possibility of their presentation in mining tourism (Hronček and Rybár, 2016).

The development of mining tourism is becoming more and more common in the world. Development of these types of tourism is economically attractive in Russia also. However, it is the practically untapped field of activity in Russia. Ruskeala Mining Park Phenomenon (the Republic of Karelia, RF) is currently the only good example of the active development of mountain tourism in Russia (Borisov, 2014; Shekov and Vitali, 2016).

Another direction of the use of waste mines is their use for medical purposes for sanatorium-resort treatment. When choosing this option to harmonize transformation processes, the industrial heritage of the region should be used, if possible, that could be successfully applied to a new type of city-forming activity. With regard to the mining industry, there are numerous mine workings, the existing transport, and urban infrastructure, which can be used for health purposes, in case if the developed field contains ore reserves, which can be used for medicinal purposes.

Many works by scientists from Romania and the Czech Republic are dedicated to the development of caving and speleotherapeutic services on the basis of salt mines. "The microclimate of some caves and salt mine can beneficially affect respiratory disorders and should be considered as an optimal environment for complex respiratory rehabilitation" (Munteanu, 2017). Biological evaluation of the therapeutic properties of salt mines was examined by N. Cl. Bilha and S. Bilha (Bilha and Bilha, 2015), N. Cl. Bilha and I. Simionca Iu (Bilha and Simionca, 2013), C. Munteanu, D. Munteanu et al. (Munteanu et al., 2013), D. Sas, O. Navrátil and P. (Sas et al.,

1999). S. P. Beamon, A. Falkenbach, G. Fainburg and K. Linde based on a statistical database of clinical reviews of patients with asthma, have proven the effectiveness of speleotherapy for the treatment of this disease. (Beamon et al., 2001). Iury Simionca with his colleagues, they studied the speleotherapeutic and balneoclimatic tourism potential of salt mines in Romania (Simionca et al., 2010, 2012; Simionca, 2012, 2013). L. Thinová, A. Froňka and K. Rovenská studies the environmental and medical characteristics in the Czech caves (Thinová et al., 2015). V. Debevec published the encyclopedia of caves and karst science in the areas of speleotherapy (Debevec, 2003).

The study of different aspects of speleotherapy in conditions of sylvinite-halite mines was lead by scientists from Belarus (Levchenko et al., 2014).

Scientists from Russia are also focused on the study of the development of speleotherapy (Nevzorov and Mukhina, 2013; Fainburg, 2017; Bessmertnyy et al., 2018). The good experience of Perm region in the use of salt mines for the speleoclinics is described in the writings of the Perm researchers (Fainburg, 2005, 2017; Speleotherapy in potash mines, 2017). A significant level of development of karst and salt caves in Russia, as well as the accumulated therapeutic experience of the use of salt mines for medical and recreational purposes, has determined this direction of research and re-profiling of the activities of mining enterprises.

Opportunities for the development of speleotherapeutic activities based on salt mines

Speleotherapy as a scientific direction was developed in the middle of the XIX century. Several directions of speleotherapy appeared at this time. The use of the climate of salt mines and caves – speleotherapy, "is an accepted but not widely known therapeutic measure in the treatment of chronic respiratory diseases" (Munteanu, 2017).

Studies have shown that the use of sylvinite caves in waste mines for medicinal purposes can improve health among people with asthma and bronchitis by 76 %, sinusitis and depression by 71 %, tinnitus by 43 %, various types of allergies 89-92 %, rheumatism by 80 % and fatigue syndrome by 94 %. This improvement comes after passing a 3-week course of treatment with a daily two-hour stay in salt caves. In addition, patients improve sleep and performance. All this is achieved thanks to:

- the shielding effect of the mountain range or patient protection from the effects of human-made electromagnetic radiation;
- neutralization of radiation;
- saturation with air ions and the caving medium itself (without allergens and microbes) (Černecký et al., 2015).

Firstly, it is the use of underground mineral and hot springs (underground balneotherapy and hydrotherapy), which was developed in Italy in the XIX century in the form of speleotherapeutic hospitals.

Secondly, in the Mammoth Cave (Kentucky, USA) an attempt was made to use the air of the caves for the treatment of patients. However, this hospital existed only a few months and, after the death of one of the patients, was closed.

Fig. 2. The photos of the speleological hospital on the basis of 1st Berezniki mine

The history of modern speleotherapy dates back to the 50s of the XX century. At this time, speleotherapeutic hospitals appear in a number of countries of Eastern and Central Europe, which had numerous

mountain caves and waste mines. Speleotherapeutic hospitals in the natural environment of karstic caves were organized most actively in Hungary, Czechoslovakia, and Romania.

An underground hospital was organized in the potash mine of the 1st Berezniki mine at a depth of 280 m from the earth's surface. In the thickness of potassium salt at a distance of 200 m from the shaft of the mine, which has a crate descent, used for the descent and ascent of people, the main workings were passed, from which 14 dead-end workings of 6-8 m length were made, intended for the stay of patients and the staff (Vishnevskaya et al., 1987). In 1994-1997 the Ministry of Health of Russia approved the special treatments (Manual for physicians) about the using of the speleo-climatic chamber of natural potassium-magnesium salts of the Verkhnekamskoye deposit (Treatment in the speleo-climatic chamber, 1994; Treatment of respiratory allergies, 1997).

It should be noted that the approximate cost of designing and constructing a speleological chamber with an area of 25 square meters in the Russian Federation currently amounts to 240 thousand rubles or 3.65 thousand dollars (Design and construction of salt caves throughout Russia; downloaded on 10. September 2018, available online: http://saltwaves.ru). Taking into account that these chambers are already built in the process of mining activities and do not require significant capital investments for conversion, it can be argued that competition on the national and international market of medical services under consideration will be minimal. In addition, the existing salt mines have a number of advantages: low gas content, centralized ventilation system for ventilation of chambers, launching system and transportation system, which can be converted for the transportation of patients. In 1982 the USSR took another important step in speleotherapy: the first climate chamber was patented, equipped with a salt filter-saturator and recreating the conditions of salt mines on the earth's surface (Qazizada et al., 2016). Thus, Russia has a good experience in the use of salt mines with the rest of their minerals for their use as speleo clinics.

Such cities as Berezniki and Solikamsk in the West-Ural region of the Russian Federation are an example of such cities and such mining enterprises, where the Verkhnekamskoye potash salt deposit (Fig. 3), which has large deposits of sylvinite and carnallite, is being developed.

Fig. 3. The location of the Verkhnekamskoye potash salt deposit on the map of the Perm region (Perm Krai).

The deposit area is about 8.1 thousand km^2, 205 kilometers long in the meridional direction, and up to 55 kilometers in the latitudinal direction (Baturin et al., 2012). Figure 4 shows the border of potash deposit in the salt deposit boundary and the location of functioning potash mines.

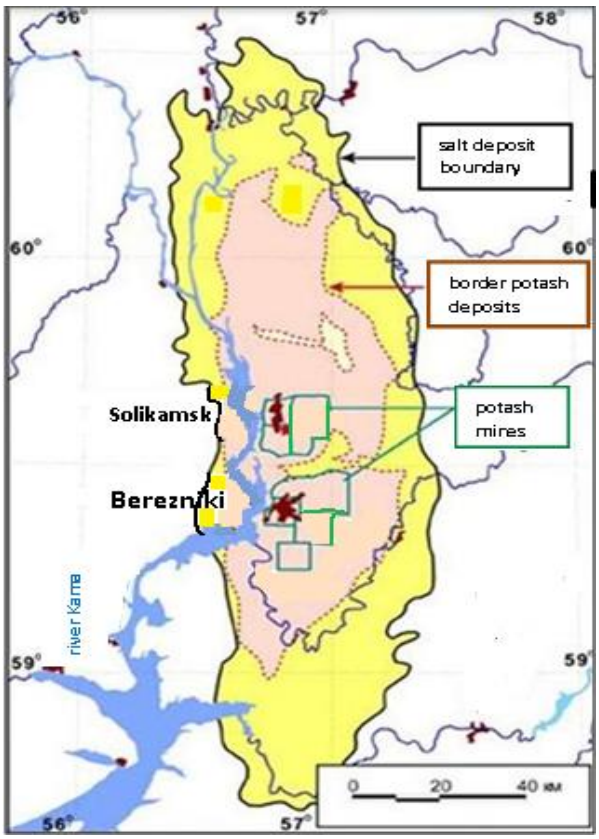

Fig. 4. The location of the salt deposit boundary, the border of potash deposit and the location of functioning potash mines of the Verkhnekamskoye potash salt deposit.

The development of the field is conducted by the town-forming enterprise OJSC Uralkali. The mine workings pass through salt beds, extending in one direction up to 10 km. The corridors and rooms of the mines have incredible beauty, not just healing properties (Fig. 5).

Fig.5. Walls and ceiling of the Uralkali's mine in Berezniki and Solikamsk

Materials and methods

Methods of analysis of the economic efficiency of the mining enterprises conversion

We carried out a rapid analysis of the economic benefits of reprofiling the mining enterprises in Berezniki after exhausting the saline reserves and stopping the enterprise activity.

At the first stage, an assessment of the potential consumer demand was made - the potential capacity (throughput) remaining after the development of the mines. To do this, we have proposed the following formula:

$$D = \frac{R*T_v*(1-\frac{Z}{100})}{N*P}, \quad (1)$$

where D is the carrying capacity of the mines remaining after development or the number of people who could undergo speleotherapy treatment at the same time, people;

T_v - total area of the existing salt mine workings suitable for rendering speleotherapeutic services, m^2;

R - mode of operation of speleological chambers in the mine workings, hours;

Z - the percentage of laying voids mining, %;

P - duration of stay of each patient in the speleological chamber in the mine workings, hours;

N - conditional norm of the area in the speleological chamber per person, m^2/ person.

As the experience of specialized speleotherapeutic organizations shows, average N value is equal to 17 m^2.

At the second stage, an assessment was made of the need for investment in the development of the urban hotel business to ensure speleotherapy tourism. For this calculation the following formula is used:

$$Q_o = K * \left(\frac{D}{O_c} - Q_d\right), \quad (2)$$

where Q_o is the number of additionally required hotels for the settlement of patients, people;

Q_d - the number of operating hotels in the region;

O_c - the average capacity of one hotel in the city, people/hotel;

K - specific capital investment in the construction of a hotel building according to a typical project characteristic of the given city.

At the third stage, the annual economic effect obtained by the city from the provision of a new service was assessed. The aggregate income of participants of the market for speleotherapeutic services was determined, its technological interconnections with other territorial markets were highlighted.

The calculation of income is made according to the formula:

$$V = D * S, \quad (3)$$

where S is the cost of a three-week treatment course.

Based on existing international experience, the minimum value of S is 2,760 euros (Healing salt caves of Berchtesgaden, 2018) or 208380 rubles.

Method of calculating the technological relationship between the complex of municipal markets

The technological relationship between the complex of municipal markets was determined on the basis of the available data of the Federal State Statistics Service according to the "Cost - Output" tables in monetary terms, which was formed on the basis of the well-known Leontiev's inter-sectoral balance method in 2015 (National Accounts, 2018)

In accordance with this method the following identities are fulfilled:

$$X_i = \sum_{j=1}^{n} a_{i,j} * X_j + Y_i; \qquad i = \overline{1,n}, \quad (4)$$

where X_i is the gross production of the good of type i;

$a_{i,j}$ - the coefficient of direct material costs of the good i for the production of a unit of good j;

Y_i - the volume of final consumption of the good i.

$$X_i = \sum_{j=1}^{n} b_{i,j} * Y_j; \qquad i = \overline{1,n}, \quad (5)$$

where $b_{i,j}$ - the ratio of full material costs, calculated as a result of the transformation matrix of coefficients of direct material costs:

$$S = (E - A)^{-1}, \quad (6)$$

where a is the matrix of coefficients of direct material costs; E - the identity matrix of the same order as the matrix A.

On the basis of the study of the above mentioned actual data, the interrelations determined by speleotherapeutic tourism between the following urban markets were determined:

- hotel and restaurant services (1);
- agricultural products and services (2);
- food and beverages (3);
- pulp and paper products (4);
- electricity, gas, steam and hot water (5);
- construction services (6);
- wholesale trade (7);
- financial intermediation services (8);
- transport services (9);
- other goods and services supplied to the city from other territories (10).

Also, the coefficients of direct material costs were determined, which are presented in Table 1 in the context of these markets. In the table, markets are numbered in accordance with the above list.

In the *i*-th row of the table, there are the markets of the manufacturers (suppliers) of intermediate goods and services to the *j*-th consumers market described in the columns. These factors characterize the rate of consumption of good *i* for the production of a unit of good *j*.

This table also shows the rates of value-added and investments, which are formed when production increases for a good *j* by 1 ruble.

Tab. 1. Ratios of direct material costs, norms of value-added and investments per product (service) by markets.

Consumer markets / Manufacturers markets	1	2	3	4	5	6	7	8	9	10
Coefficients of direct material costs										
1	0,0022	0,0001	0,0005	0,0005	0,0005	0,0013	0,0009	0,0026	0,0011	-
2	0,0296	0,2012	0,3255				0,0008		0,0000	-
3	0,1537	0,0628	0,1712				0,0015		0,0001	-
4	0,0067	0,0032	0,0214	0,1725	0,0002	0,0007	0,0019	0,0010	0,0002	-
5	0,0281	0,0150	0,0150	0,0590	0,3540	0,0058	0,0040	0,0056	0,0456	-
6	0,0222	0,0027	0,0022	0,0036	0,0107	0,0267	0,0028	0,0009	0,0165	-
7	0,0413	0,0392	0,0621	0,0898	0,1139	0,0553	0,0304	0,0023	0,0172	-
8	0,0296	0,0097	0,0151	0,0189	0,0124	0,0141	0,0133	0,0833	0,0139	-
9	0,0065	0,0079	0,0083	0,0335	0,0123	0,0136	0,1329	0,0005	0,0481	-
10	0,2121	0,1001	0,1537	0,2760	0,1971	0,3996	0,2211	0,2030	0,3423	-
The rate of value added per ruble of finished products (services) in each market										
Payroll fund	0,1903	0,1018	0,0817	0,0931	0,1417	0,1858	0,1575	0,3244	0,1692	-
Sinking fund	0,0383	0,0272	0,0174	0,0392	0,0385	0,0079	0,1238	0,0618	0,0632	-
Tax deductions	0,0112	0,0036	0,0090	0,0128	0,0115	0,0104	0,0069	0,0353	0,0187	-
Net profit	0,2304	0,4256	0,1174	0,2017	0,1077	0,2801	0,3029	0,2818	0,2649	-
The specific amount of investment per ruble of finished products (services)										
Investments in machinery and equipment	0,0048	0,0189	0,0078	0,0272	0,0145	0,0369	0,0064	0,0017	0,0228	-

Source: own processing

Tab. 2. The coefficients of the total material costs per product (service) by markets.

Consumer markets / Manufacturers markets	1	2	3	4	5	6	7	8	9	10
1	1,0026	0,0003	0,0010	0,0010	0,0011	0,0014	0,0011	0,0029	0,0013	0
2	0,1167	1,2919	0,5077	0,0004	0,0005	0,0003	0,0021	0,0003	0,0003	0
3	0,1949	0,0980	1,2455	0,0005	0,0006	0,0004	0,0023	0,0006	0,0005	0
4	0,0139	0,0077	0,0345	1,2088	0,0009	0,0010	0,0026	0,0014	0,0005	0
5	0,0545	0,0350	0,0471	0,1159	1,5530	0,0116	0,0173	0,0099	0,0751	0
6	0,0249	0,0047	0,0058	0,0072	0,0184	1,0282	0,0057	0,0013	0,0189	0
7	0,0695	0,0640	0,1101	0,1273	0,1845	0,0606	1,0369	0,0041	0,0288	0
8	0,0395	0,0173	0,0295	0,0294	0,0247	0,0173	0,0177	1,0913	0,0178	0
9	0,0207	0,0213	0,0324	0,0619	0,0462	0,0234	0,1452	0,0013	1,0559	0
10	0,3093	0,1804	0,3050	0,4150	0,3756	0,4387	0,2897	0,2265	0,3943	1

Source: own processing

On the basis of the data of Table 1 and formula (6), the coefficients of the total material costs are counted and presented in Table 2.

Further, the proposed method estimates the change in the urban socio-economic system as a result of the emergence of a new type of health services that gives impetus to the development of these markets. In equation (5), only *Y1* is taken into account - the total cost of their consumption. The determination of the increase in production volumes by interconnected urban markets was carried out on the basis of using the indicator *Y1*, the coefficients of full material costs (Table 2) and formula (5).

Results of the study

The estimated calculations carried out according to the presented methodology allowed us to obtain the following results:

To assess consumer demand (potential capacity (throughput) remaining after the development of mines), the following assumptions were made:

- the total area of the existing salt mine workings T_v was taken on the basis of the length of the excavation in one direction only - 10 km and width 5.1 m. Its value was 51000 m^2;
- the operation mode of speleological chambers is *R* - 12 hours per day;
- the percentage of laying voids mine workings is equal to *Z* - 70%;
- the duration of each patient's stay in the speleological chamber in the mine working *P* is 2 hours;
- conditional area norm in the speleological camera per person *N* is equal to 17.2 m^2 / person.

On this basis, consumer demand (throughput of salt mines in Berezniki) is:

$$D = \frac{8 * 51000 * (1 - \frac{70}{100})}{17 * 2} = 3600\ person$$

As can be seen from the presented calculations, the prospective consumer demand for only one mine working is very large and significantly exceeds the capacity of the hotel complex of the city of Berezniki. Currently, it has 10 hotels with an average capacity of 350 people, which will allow only 3500 people to be accommodated.

Tab. 3. Calculation of additional production volumes of goods and services, value added and investments in urban markets, (mln. rub.)

Consumer markets / Manufacturers markets	1	2	3	4	5	6	7	8	9	10
Commodity flows between the markets according to the "Cost - output" model										
1	1,61	0,01	0,08	0,01	0,02	0,02	0,04	0,08	0,02	-
2	21,68	17,13	46,26	0	0	0	0,04	0	0	-
3	112,36	5,34	24,34	0	0	0	0,08	0	0	-
4	4,93	0,27	3,04	1,75	0,01	0,01	0,10	0,03	0	-
5	20,54	1,27	2,13	0,60	14,08	0,11	0,20	0,16	0,69	-
6	16,25	0,23	0,31	0,04	0,42	0,48	0,14	0,03	0,25	-
7	30,19	3,33	8,83	0,91	4,53	1,00	1,54	0,07	0,26	-
8	21,63	0,83	2,15	0,19	0,49	0,26	0,67	2,40	0,21	-
9	4,73	0,67	1,18	0,34	0,49	0,25	6,73	0,01	0,73	-
10	155,08	8,52	21,84	2,80	7,84	7,25	11,20	5,86	5,18	-
Value-added per ruble of finished products (services) for each market										
Payroll fund	139,17	8,67	11,60	0,94	5,64	3,37	7,98	9,35	2,56	-
Sinking fund	27,98	2,31	2,48	0,40	1,53	0,14	6,27	1,78	0,96	-
Tax deductions	8,22	0,30	1,28	0,13	0,46	0,19	0,35	1,02	0,28	-
Net profit	168,46	36,23	16,68	2,04	4,28	5,08	15,35	8,13	4,01	-
Total gross output										
X_i	731,21	85,11	142,11	10,13	39,78	18,15	50,67	28,84	15,13	225,58
The specific amount of investment per ruble of finished products (services)										
Investments in machinery and equipment	3,49	1,61	1,11	0,28	0,58	0,67	0,33	0,05	0,35	-

Source: own processing

The websites of travel companies offering speleotherapeutic tourism and speleotourism were used to calculate the minimum cost of a speleotherapy treatment (21 days) in the salt mines of Western Europe (Austria, Germany) (Healing salt caves of Berchtesgaden, downloaded on 21. August 2018, available online: *http://www.ost-westeuropa.com/resort/salzheilstollen.php*).

Hence, the maximum level of income from the provision of speleotherapeutic services will be:

$$V = Y_1 = 3600 * 2760 = 9\,936\,000\ Euro\ (775\ \text{mln. rub.}),$$

Based on the estimated income received, the possibilities for developing a complex of urban markets were calculated (Table 3).

Thus, in case of a mining enterprise ceasing its activities and converting it to speleotherapeutic services with the available facilities of the Berezniki hotel complex, it would be possible to ensure the growth of:

- incomes of economic entities in all interconnected markets in the amount of 1346.72 million rubles,
- profits of economic entities in all interconnected markets in the amount of 260.26 million rubles.
- tax revenues to the budgets of all levels by 12.22 million rubles;
- investment in production equipment by 8.45 million rubles.

All those prove that implementing new ways of use of waste mines for speleotherapeutic purposes provides the sustainable development of such urban territory as Berezniki.

Conclusions

The developed method of analyzing the economic efficiency of the conversion of mining enterprises makes it possible quickly, in detail and accurately assess the prospects for the transformation of territorial economic processes as a result of the conversion of the mining city-forming industry to the goals of recreational activities.

The example of the city of Berezniki, Perm Region of Russia, shows how such a redevelopment of closing salt mines makes it possible to maintain reproduction processes in the socio-economic system of a single-industry mining city. Reprofiling implies the transformation of the existing economic model and is the preferred option compared with the complete closure of production and bankruptcy of the city. It is economically most rational in terms of public welfare and development. Such a transformation involves the restructuring of the economic relationships between the state, social (non-productive), financial, and industrial sectors of the territorial economy with a new type of industrial city-forming activity. This should provide sustainable development of cities, urban agglomeration, and region on the whole.

The proposed method of assessment allows the city authorities and management to appreciate the overall increase in financial and economic indicators received by business entities of the city and the potential total income of the city.

Further studies suggest a more detailed analysis of the definition of specific salt mines developed for their transformation into speleological chambers for rendering medical and recreational procedures to the population.

The further direction of research development is the analysis of technical possibilities of development of speleotherapy in the salt mines of Berezniki potash deposit. The complexity of the project is the need to combine the organization of speleotherapy and speleotourism with the ongoing industrial development of salt plateau.

The second further direction of research development is the analysis of possibilities of the abandoned mining sites in alternative industrial production parks.

Acknowledgments: *The work is carried out based on the task on fulfillment of government contractual work in the field of scientific activities as a part of base portion of the state task of the Ministry of Education and Science of the Russian Federation to Perm National Research Polytechnic University (the topic № 26.6884.2017/8.9 "Sustainable development of urban areas and the improvement of the human environment").*

References

Angiolini, C., Bacchetta, G., Brullo, S., Casti, M., Giusso Del Galdo, G., Guarino, R. (2005) The vegetation of mining dumps in SW-Sardinia. *Feddes Repertorium, 116 (3-4), pp. 243-276.*

Bacchetta, G., Cappai, G., Carucci, A., Tamburini, E. (2015) Use of native plants for the remediation of abandoned mine sites in mediterranean semiarid environments. *Bulletin of Environmental Contamination and Toxicology, 94 (3), pp. 326-333.*

Ballesteros, E. R., Ramírez, M. H. (2007) Identity and community - Reflections on the development of mining heritage tourism in Southern Spain. *Tourism Management, 28 (3), pp. 677-687.*

Barannikov V. G., Chekina N. L., Chernyshev V. A. (1981) Underground hospital in a potash mine. *Perm.*

Baturin E. N., Menshikova E. A., Blinov S. M., Naumov D. Yu., Belkin P. A. (2012) Problems of development of the largest potash deposits in the world. *Modern problems of science and education, 6,. http://www.science-education.ru/ru/article/view?id=7513*

Beamon, S. P., Falkenbach, A., Fainburg, G. and Linde K. (2001) Speleotherapy for asthma. *Cochrane Database of Systematic Reviews, 2. DOI: 10.1002/14651858.CD001741*

Bessmertnyy, N. A., Volodina, N. E., Brylyakov, L. A. (2018) Application of potassium and Speleotherapy in prevention and treatment of bronchial diseases. *In the collection: Actual problems of labor protection and safety of production, extraction and use of potassium-magnesium salts Materials of the I International scientific-practical conference. Ed. G.Z. Fainburg. pp. 491-497.*

Biały, W. (2014) Post-mining areas reclamation – case study. *14th SGEM GeoConference on Science and Technologies In Geology, Exploration and Mining, SGEM2014 Conference Proceedings*, June 17-26, 2014, Vol. III, BUŁGARIA ISBN 978-619-7105-09-4/ISSN 1314-2704. s. 443-450.

Biały, W., Mroczkowska P. (2015) Influence of coal waste heaps on water environment in upper silesian borderland areas – case study. *15th SGEM GeoConference on Science and Technologies In Geology, Exploration and Mining, SGEM2015 Conference Proceedings*, June 18-24, 2015, Vol. III, BUŁGARIA ISBN 978-619-7105-33-9/ISSN 1314-2704. s. 675-682.

Bilha, N.-Cl. v Bilha, S. (2015) Wich salt mine do you recommend for speleotherapy? Interdisciplinary project proposal. *Balneo Research Journal, 6 (3), pp. 172-175. DOI: 10.12680/balneo.2015.10101*

Bilha, N.-Cl., Simionca, I. (2013) General remodeling in the rehabilitation process through salt mine speleotherapy, *European Respiratory Journal, 42 (Suppl 57), pp.22-26.*

Boni, M., Costabile, S., De Vivo, B., Gasparrini, M. (1999) Potential environmental hazard in the mining district of southern Iglesiente (SW Sardinia, Italy). *Journal of Geochemical Exploration, 67 (1-3), pp. 417-430.*

Borisov, I.V. (2014) Ruskeala Marble Quarries, *Mining Road, Russia, Mining Road, Russia. Petrozavodsk: Karelian Scientific Center of RAS, 165 p.*

Costache, A., Pehoiu, G. (2010) Social and economic effects of mining industry restructuring in Romania - case studies. *World Academy of Science, Engineering and Technology, 42, pp. 600-604..*

Černecký, J., Valentová, K., Pivarčiová, E., Božek, P. (2015) Ionization Impact on the Air Cleaning Efficiency in the Interior. *Measurement Science Review*, Volume 15, Issue 4, pp 156-166, 2015.

Debevec, V. (2003) Speleotherapy. Encyclopedia of Caves and Karst Science / *John Gunn. Routledge*.

Demirović, D., Radovanović, M., Petrović, M., Cimbaljevic, M., Vuksanović, N., Vuković, D.B.: Environmental and community stability of a mountain destination: an analysis of residents' perception. *Sustainability, 10(1), pp.70, 2018. doi:10.3390/su10010070.*

Design and construction of salt caves throughout Russia. *Downloaded on 10. September 2018, available online: http: //saltwaves.ru*

Dybowska, A., Farago, M., Valsami-Jones, E., Thornton, I. (2006) Remediation strategies for historical mining and smelting sites. *Science Progress, 89 (2), pp. 71-138,.*

Fainburg, G. (2017) Salty Air Therapy The new effective method for treatment and healing. *Perm, Russia: The publishing house of the Perm National Research Polytechnic University, 280 p..*

Fainburg, G. Z. (2005) Speleotherapy - treatment with underground air. Introduction to aerovaleology: Air environment and human health. *Perm: Perm State Technical University, 104 p.*

Gherman, G., Negrea, A., Ciopec, M., Teodor-Eugen, M.A.N., Motoc, M. (2012) Studies concerning the stabilization by phytoremediation of soils degraded by mining activities. *Revista de Chimie, 63 (3), pp. 324-329.*

González, R. C., González-Chávez, M. C. A. (2006) Metal accumulation in wild plants surrounding mining wastes. *Environmental Pollution, 144 (1), pp. 84-92.*

Healing salt caves of Berchtesgaden. *http://www.ost-westeuropa.com/resort/salzheilstollen.php*

Hronček, P., Rybár, P. (2016) Relics of manual rock disintegration in historical underground spaces and their presentation in mining tourism. *Acta Montanistica Slovaca, 21 (1), 53-66..*

Jayawardena, C. L., Thiruchittampalam, S., Dassanayake, A., Abeysinghe, A., Wimalarathna, W. (2018) A proximity based rehabilitation approach for abandoned quarries in rural Sri Lanka. *MERCon 2018 - 4th International Multidisciplinary Moratuwa Engineering Research Conference, pp. 247-252.*

Kurlaev, A. E. (2015) Industrial Heritage in the Protection and Preservation of Monuments of History and Culture in Russia: Problems and Prospects. *Russian Scientific Journal, Russia, 4, p. 79.*

Lyakhnitsky Yu.S., Yushko A.A., Borisov I.V., Minnikov O.A., Khlebalin I.Yu. (2015) The ancient mine workings of Karelia are the most important element of the tourist potential of the republic (on the examples of the Ruskeala Mountain Park and the Rogoselga mine). *The role of tourism in the sustainable development of the Russian North. Proceedings of the All-Russian Scientific and Practical Conference).Petrozavodsk, pp. 197–208.*

Levchenko, P. A., Dubovik, N. N., Delendik, R. I. (2014) Some aspects of speleotherapy in conditions of sylvinite-halite mines in the city of Soligorsk in the Republic of Belarus. *Asthma and Allergy, 3, pp. 27-29.*

Mairescu, G., Timotin, V., Simionca, I., Grudnicki, N., Zup, C. (2014) Existing and perspective arrangements to Salina Cacica in the context of tourism development in salt mines. *Balneo Research Journal, 5 (1), pp. 25-36.*

Midor, K., Zasadzień, M. (2015) Directions of post-mining areas revitalization in a selected area of Polish-Czech borderland. *15th International Multidisciplinary Scientific GeoConference SGEM 2015. Science and technologies in geology, exploration and mining*, 18-24 June 2015, Albena, Bulgaria. Conference proceedings. Vol. 3, Exploration and mining, applied and environmental geophysics. Sofia: STEF92 Technology, 2015, s. 219-227.

Mingaleva, Z., Bunakov, O. (2014) Competitiveness assessment of Russian territories in terms of inbound tourism. *Life Science Journal, 11 (SPEC. ISSUE 6), pp. 318-321.*

Mingaleva, Zh., Shaidurova, N., Prajová, V. (2018) The role of technoparks in technological upgrading of the economy (using the example of agricultural production). *Management Systems in Production Engineering, 26 (4), pp.241-245.*

Munteanu, C., Munteanu, D., Simionca, I., Hoteteu, M., Cinteza, D., Lazarescu H. (2013) Biological evaluation of therapeutic properties of salt mines. *16th International congress of speology, 343,.*

Munteanu, C., Munteanu, D., Simionca, I., Hoteteu, M., Mera, O. (2012) Therapeutical evaluation of Turda Salt Mine microclimate on pulmonary fibroblasts cultures. *Balneo Research Journal, 1 (1), 24-29.*

Munteanu, C. (2017) SPELEOTHERAPY - scientific relevance in the last five years (2013 - 2017) - A systematic review. *Balneo Research Journal, 8 (4), pp. 252-254. DOI: 10.12680/balneo.2017.161.*

National Accounts, 2018. *http://www.gks.ru/wps/wcm/connect/rosstat_main/rosstat/ru/statistics/accounts* .

Nevzorov, A. Yu., Mukhina, M. Yu. (2013) Speleotherapy as a form of alternative medicine. *Bulletin of medical Internet conferences, 3 (2), p. 177.*

Pascu, G., Bayon, J., Gheorghiu, T.O. (2013) Strategies of regeneration of former mining sites in Romania. *CESB 2013 PRAGUE - Central Europe Towards Sustainable Building 2013: Sustainable Building and Refurbishment for Next Generations, pp. 257-260.*

Paulo, A. (2008) Environmental limitations in possible directions of post-mining land use. *Mineral Resources Management, 24 (2-3), pp. 8-40.*

Pershin, G. D. (2014) Raw Material Base of Ural's Stone Industry, Stone around Us, *Russia, p. 28.*

Petrović, M. D., Radovanović, M., Vuković, N., Vujko, A., Vuković, D. (2017) Development of Rural Territory under the Influence of Community-Based Tourism. *Ars Administrandi, 9 (2), pp. 253–268..*

Petrović, M. D., Vujko, A., Gajić, T., Vuković, D., Radovanović, M., Jovanović, J. M., Vuković, N. (2018) Tourism as an Approach to Sustainable Rural Development in Post-Socialist Countries: A Comparative Study of Serbia and Slovenia. *Sustainability, 10(1), p.54.*

Potravnov, A. L., Khmelnik, T. Y. (2015) Research and Development Work Peculiarities When Preparing Mining-and Industrial Heritage Sites to be Shown to Tourists. *Role of Tourism in Sustainable Development of Russian North, Russia, pp. 237-242.*

Qazizada, M.E., Sviatskii, V., Božek, P. (2016) Analysis performance characteristics of centrifugal pumps. In *MM Science Journal*. October 2016, pp 1151-1159.

Różycki1, P., Dryglas, D. (2017) Mining tourism, sacral and other forms of tourism practiced in antique mines - analysis of the results. *Acta Montanistica Slovaca, 22 (1), 58-66.*

Sas, D., Navrátil, O., Sládek, P. (1999) Monitoring of natural factors in Czech speleotherapeutic centres. *Czechoslovak Journal of Physics, 49 (1), pp.103—106. DOI:10.1007/s10582-999-0013-8.*

Schejbal, C. (2011) Possibilities of using of abandoned mining sites in tourism. *Acta Geoturistica, 2 (2), pp. 17–25.*

Shekov, K., Shekov, V., Kurlaev, A. (2017) The issue of abandoned open mining workings: Reclamation of the territories or…? *International Multidisciplinary Scientific GeoConference Surveying Geology and Mining Ecology Management, SGEM, 17(53), pp. 947-954. DOI: 10.5593/sgem2017/53/S21.118*

Shekov, V. A., Shekov, K.V. (2016) Mineral developers and local community: On the way toward mutual understanding, Hereditas Minariorum. *Poland, 3.*

Shekov, K., Vitali, S. (2016) Ruskeala mining park phenomenon. *International Multidisciplinary Scientific GeoConference Surveying Geology and Mining Ecology Management, SGEM, 3, pp. 515-522. DOI: 10.5593/SGEM2016/B53/S21.066*

Shaidurova, N., Mingaleva, Zh., Davydov, I., Livenskaya, G. (2017) Features of Functioning of Technoparks in Russia and EU Countries. *Acta Logistica, 4 (4), pp. 1-6. DOI: 10.22306/al.v4i4.52*

Simionca, Iu., Enache, L., Calin, M.R., Hoteteu, M., Bunescu, Iulia, Zup, C., Ietcu, I., Grudnicki, N., Dincu, I. (2010) Preliminary data related to underground microclimate in Cacica and Dej salt mines with speleotherapeutic and balneoclimatic tourism potential. *Romanian Journal of Physical and Rehabilitation Medicine, 20 (2), Supplement, pp.68–69.*

Simionca, Iu., Hoteteu, M., Lazarescu, H. (2012) Halotherapy-descendant of speleotherapy in salt mines; Realities and perspectives of scientific halotherapy in Romania. *Casa Cartii de Stiinta, 56-57.*

Simionca, Iu. (2012) Complex medical-biological study for the innovative use of potential therapeutic environmental factors from salt mines and caves in health and balneoclimatic tourism; modeling solutions theirs (Salt mines-Salina Ocna-Dej, Salina Cacica; Cave Fundata). *Project 2250, Financing contract nr. 42120/2008, National Plan of Research-Development-Innovation 2, Program 4. Partenerships in priority areas, 4. Health, Romania Published.*

Simionca, Iu. (2013) Speleotherapy development in Romania on the world context and perspectives for use of some salt mines and karst caves for speleotherapeutic and balneoclimatic tourism purposes. *Balneo Research Journal*, 4 *(3), 133-139.*

Schejbal, C. (2011) Possibilities of using of abandoned mining sites in tourism. *Acta Geoturistica, 2 (2), pp. 17–25.*

Solonina, N. S., Shipitcina, O. A. (2015) Historical-And-Architectural Potential of the Industrial Heritage of the Middle Part of Ural. *Architecton: News of Higher Educational Institutions, Russia, 50. http://archvuz.ru/2015_2/8*

Sorensen, P. (2008) Financial provision for mine closure. *2nd Mine Closure and Rehabilitation Conference 2008. Sorensen. Southern Sun Garden Court, OR Tambo International Airport*

Sorensen, P. (2007) Mine closure costs. *Mine Closure and Rehabilitation Conference 2007. Sorensen. Southern Sun Grayston, Sandton.*

Speleotherapy in potash mines and speleoclimatotherapy in sylvinite speleochamber: theoretical foundations and practical achievements. On the 40th anniversary of the use of potash for speleotherapy: Ed. I.P. Koryukina and G.Z. Fainburg. Perm: *Perm, Russia: The publishing house of the Perm National Research Polytechnic University, 256 p.* (2017).

Swarbrooke, J. (2002) Heritage Tourism in the UK: A glance at things to come. *Sheffield Hallam University, Department of sociology. http://www.insights.org.uk/articleitem.asp*

Tokarczyk-Dorociak, K., Lorenc, M. W., Jawecki, B., Zych-Głuszyńska, K. (2015) Post-industrial landscape transformation and its application for geotourism, education and recreation - an example of the wide mt. Near strzegom, lower Silesia/Poland. *Zeitschrift der Deutschen Gesellschaft fur Geowissenschaften, 166 (2), pp. 195-203.*

Tokarczyk-Dorociak, K., Skolak, K., Lorenc, M. W. (2010) Abandoned basalt quarry in Strzegom - A chance for reopening. *Geoturystyka, 3 (22), pp. 59-64.*

Treatment in the speleo-climatic chamber of natural potassium-magnesium salts of the Verkhnekamskoye deposit: Guidelines. Approved Ministry of Healthcare of the Russian Federation April 28, 1994. *Moscow, 20 p.*

Treatment of respiratory allergies and the rehabilitation of children with the living air of sylvinite speleoclimatic chambers (Manual for Physicians). Approved by the Ministry of Health of Russia. *Moscow-Perm, 20 p.* (1997).

Thinová, L., Froňka, A., Rovenská, K. (2015) The overview of the radon and environmental characteristics measurements in the Czech show caves. *Radiat Prot Dosimetry, 164(4), pp.502-509, doi: 10.1093/rpd/ncv337.*

Vishnevskaya, N. L., Barannikov, V. G., Startsev, V. A., Nokhrina L. M. (1987) Hygienic Studies of Natural Factors of the Air Environment of the Potash Mine P. *Integrated Exploration of the Subsoil and Environmental Protection. Perm, pp. 65-66.*

Yushko A.A., Artemyev A.B. (2015) Ruskeala Mountain Park: Ten Years of Successful Innovations. *Museum. Education. Tourism. Prospects for development: a collection of materials of the All-Russian Scientific and Practical Conference on Museum Pedagogy "Educational Tourism and Historical and Cultural Heritage: Museum Practices and Prospects for Development". Petrozavodsk: IDU, pp.183-189.*

Zapariy, V.V. (2009) Industrial Heritage and Its Modern Interpretation, (1). *Academic Bulletin, Russia. http://cyberleninka.ru/article/n/industrialnoe-nasledie-i-ego-sovremennoe-tolkovanie*

Zubkova V. M., Gaponenko A. V., Belozubova N. Y., Voskresenskaya O. L., Zubkov N. V. (2016) The accumulation and distribution of heavy metals in crop plants at different levels of soil contamination. *International Journal of Ecology and Development. 31 (2), pp.1-9.*

Zych-Głuszyńska, K. (2011) Forming of the Landscape of Post-mining Areas Illustrated with an Example of an Inactive Basalt Quarry in Strzegom. *M.Sc. thesis, Wrocław University of Environmental Life and Sciences, (unpubl.), pp. 1-64,.*

A novel approach to estimate systematic and random error of terrain derived from UAVs: a case study from a post-mining site

***Rudolf Urban*[1], *Martin Štroner*[1], *Tomáš Křemen*[1], *Jaroslav Braun*[1] and *Michael Möser*[2]**

In recent years, there has been a major development in the field of Unmanned Aerial Vehicles (UAVs) as well as a significant increase in the use of aerial photogrammetry, which is an affordable alternative to using LiDAR. However, the nature of the data obtained from photogrammetry differs from LiDAR data. Photogrammetry using the Structure from Motion (SfM) method is however computationally complicated, and results can be affected by many influences. In this paper, data from two UAVs were compared. The first one is a commercial eBee system produced by SenseFly equipped with a Sony Cyber-shot DCS-WX220 camera. The other is a home assembled solution consisting of EasyStar II motorised glider and 3DR Pixhawk B autopilot equipped with Nikon Coolpix A camera. The area of spoil heap was measured by both systems in the leaf-off period. Both systems were set up identically for data acquisition (overlapping, resolution), which made a comparison of the output quality possible. The ground control points (GCPs) were placed in the study area and their position determined by GNSS (RTK method).

A traditional approach for point clouds accuracy validation is their comparison with data of greater accuracy. Unfortunately, the photogrammetry is often validated using GNSS points, the position of which is determined under different conditions than GCPs (different daytime, number, and visibility of satellites, etc.). The magnitude of photogrammetry errors is theoretically the same as that of GNSS. Therefore, in this study, we suggest a novel approach that can be used to compare the accuracy of UAV point clouds without the need for additional validation data (for example, GNSS survey). To exemplify this approach, we used data gathered by two UAV systems (eBee and Easy Star II). Particularly, we statistically estimated the accuracy of the UAV point clouds; used two approaches to estimate standard deviations (one of them using estimated dependencies between data); and investigated the influence of the vegetation cover.

To determine the systematic and random errors of the UAV systems data, three areas were selected, each with a typical example of vegetation on the spoil heap (forest, grass, bush). A comparison of the individual data in a grassy area suggests that the accuracy of the differences is about 0.03 m, which corresponds to the actual pixel size. Average shift (systematic error) ranged from 0.01 m to 0.08 m. In the forest terrain, the accuracy of data differences is about 0.04 m, which is slightly worse than in the grassy area. Bushy terrain data achieves precision values between a grassy area and a forest area.

Keywords: *digital terrain model (DTM), UAV, photogrammetry, spoil heap*

1. Introduction

Mining has a significant impact on the environment. From this point of view, the surface mines are particularly problematic with the original arrangement of the landscape completely disturbed and the fertile field taken away. Although the regeneration of these areas is usually incorporated into mining plans, the actual effect of these activities is still being investigated through scientific research.

Published studies typically use measurement data to model the current state of the landscape or to analyse terrain stability (for example, Close et al., 2016; Stephenne et al. 2014; Zalesky and Capova, 2017). Such data represent the basis, the frame, and their quality is conditional for the quality of the study results. Data are acquired in a variety of ways, including terrestrial geodetic techniques such as total station and/or GNSS measurements (for example, Hogarth et al., 2017; Zalesky et al., 2008). Such common methods are however more appropriate for targeting a limited number of individual points rather than to capture a larger natural area at the stage of standard bio-chaos. A great benefit of remote sensing over more traditional techniques lies in its ability to provide continuous information over a large area. However, references to the use of remotely sensed data for monitoring or restoration success assessment of post-mining sites are scarce (Ćmielewski, 2018; Cordell, 2017).

For such purposes, mass data acquisition technologies such as laser 3D scanning, photogrammetry, and satellite imagery are preferable to traditional techniques. Laser 3D scanning is especially suitable in its airborne variant known as Airborne Laser Scanning (ALS) or LiDAR (Light Detection And Ranging), where multiple reflections of a single signal/flight allow a comprehensive analysis of the condition of the vegetation and creation of a quality digital terrain model, used for example by (Koska, 2017) or by (Wężyk, 2015) for landscape monitoring.

Recently, extensive research into the use of UAVs carrying a digital camera has been performed. Data processing through photogrammetric methods based on Structure from Motion and/or Patch-based Multi-View

[1] *Rudolf Urban, Martin Štroner, Tomáš Křemen, Jaroslav Braun*, Czech Technical University in Prague, Faculty of Civil Engineering, Department of Special Geodesy, Thákurova 7, Prague 6, 166 29, Czech Republic, rudolf.urban@fsv.cvut.cz, martin.stroner@fsv.cvut.cz, tomas.kremen@fsv.cvut.cz, jaroslav.braun@fsv.cvut.cz

[2] *Michael Möser* , Technical University Dresden, Faculty of Environmental Sciences, Department of Geosciences, Geodetic institute. Hülsse-Bau, Westsight Helmholtzstraße 10, 01069 Dresden. Germany, michael.moeser@tu-dresden.de

Stereo is investigated, along with the use of a wide range of carriers and digital cameras from professional and costly to very inexpensive and simple. For example in (Pukanská, 2014) photogrammetry was used for mapping of a surface quarry and compared with the 3D scanning method, rock outcrops documentation by the UAV photogrammetry was studied by (Blišťan, 2016). Low-cost UAVs can also be successfully used for digital terrain modelling as shown by (Kršák, 2016). The digital terrain model built in this way can subsequently serve for various purposes such as for the monitoring of rock slides (Fraštia, 2014), a case of the monitoring of the Super-Sauze landslide is described by (Niethammer, 2012). Degradation of the coastal areas is another field of research where the UAVs can be successfully used according to (Goncalves, 2015). Roads detection is another of UAV applications (Zhou, 2015). Monitoring of the dynamic natural processes with a focus on reproducibility of the Earth topography is described in (Claypuyt, 2016). A similar topic focusing on a river channel evolution is investigated in (Flener, 2013) combining mobile laser scanning and low-altitude unmanned aerial vehicle photography for creating both a bathymetric model and DTM of a meandering Sub-arctic River. The disadvantage is the need to take pictures or perform the measurement during the leaf-off period to be able to obtain a terrain model as documented in (Hogson, 2005)

Numerous UAV platforms equipped with various cameras are increasingly available on the market, differing in their suitability for mapping of mining areas (Thoeni et al., 2014; Boon, Drijfhout, and Tesfamichael, 2017; Torresan et al., 2017). Surveyors then often face a question which UAV platform to buy. The ever-increasing use of UAVs for mining industry makes the knowledge of the precision of resulting point clouds very important. Experimental flights over typical areas with various UAVs are often performed before committing to the purchase.

A traditional approach for point clouds accuracy validation is their comparison with data of greater accuracy. Unfortunately, the photogrammetry is often validated using GNSS points, the position of which is determined under different conditions than GCPs (different daytime, number, and visibility of satellites, etc.). The magnitude of photogrammetry errors is theoretically the same as that of GNSS. The point cloud accuracy can be greatly affected by the accuracy of the GCP for the GNSS. Due to the size of the image overlays and flight height (actual pixel size), the internal accuracy of the photogrammetric model may be higher than the accuracy of the GCP determination. Another disadvantage when comparing a point cloud with the GNSS point is that the collection of validation data is often limited to hard surfaces and easily accessible places. Another option is to compare point cloud with airborne laser scanning data; those are however also affected by a GNSS error. Ideal data for comparison would be data identifying both GCPs and validation points in random cloud places, determined with significantly higher accuracy than that expected of the model itself. Such validation data can be obtained using a total station method that has a significantly higher accuracy than GNSS but is quite a time-consuming and thus economically demanding.

Therefore, in this study, we suggest a novel approach that can be used to compare the accuracy of UAV point clouds without the need for additional validation data (for example, GNSS survey). To exemplify this approach, we used data gathered by two UAV systems – a commercially available eBee and home–assembled Easy Star II fixed wing system. Particularly, we (1) statistically estimated the accuracy of the UAV point clouds; (2) used two approaches to estimate standard deviations; and (3) investigated the influence of the vegetation cover

2. Materials and Methods

2.1 Hornojiřetínská spoil heap

Spoil heap (Fig. 1) is located in north-west Bohemia, Czech Republic, in the Most mining district (50°34’N, 13°34’E). The study area of 68 ha is located in the southern part of Hornojiřetínská spoil heap, which has not been technically reclaimed. The terrain morphology has, as a result, remained rugged with a typical undulated terrain formed by heaping (for example, Doležalová et al., 2012). It has been observed that rough terrain and dense vegetation negatively affect the accuracy of point clouds (for example, Meng et al., 2010). Therefore, such a challenging environment provides an ideal location for exploring the quality of point clouds and DTMs.

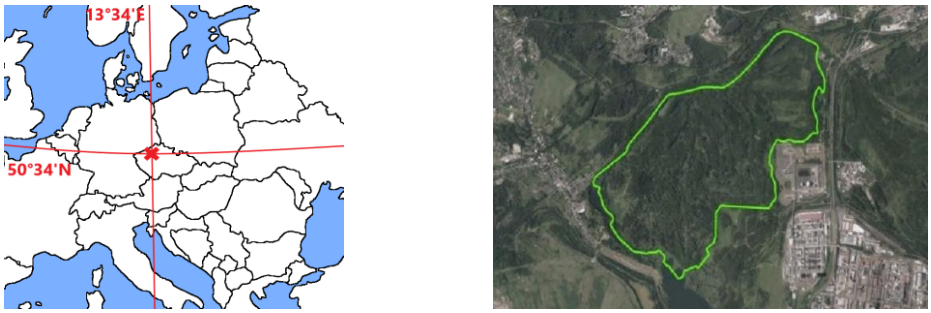

Fig. 1. Location of the Hornojiřetínská spoil heap.

Before the UAV flights, twenty ground control points (GCPs) were established within and in the vicinity of the study area (Fig. 2, yellow dots with blue flags). GCPs were made of white wooden boards (dimensions 0.40m by 0.40m) with a black circle of 0.15m diameter in the centre. The expected pixel dimension of the circle in the image at the intended resolution and flight height was approximately 5 x 5 pixels. GCP coordinates were surveyed using a Trimble GeoXR 6000 handheld GNSS receiver with Zephyr 2 external antenna mounted on a pole, by the dual-frequency real-time kinematic (RTK) method with a 15 seconds observation time, with a connection to the CZEPOS permanent GNSS network. All GCPs were transformed to the Datum of Uniform Trigonometric Cadastral Network (S-JTSK; EPSG: 5514) and Baltic Vertical Datum - after adjustment (Bpv; EPSG: 5705). Relative precision of GCPs can be estimated at 0.02 m (for example, Štroner et al., 2013).

Fig. 2. Location of the study areas (red rectangles - forested area (central part), bushy area (upper left corner) and grassy area (lower left corner); GCPs marked as yellow dots with blue flags.

The whole area of the spoil heap consists of distinctly different zones with regard to surface cover, ranging from dense forest through low bushes to surface solely covered by grass. Three zones with those three types of vegetation were selected as study areas (red rectangles at Fig. 2).

2.2 UAV systems

Two UAV systems were used for image collection. A commercial system EBee (Fig. 3) produced by the SenseFly company is a fixed-wing aircraft with removable wings and a push propeller. It allows an automatic flight with a flight time of up to 40 minutes. It is a commercially available mapping and monitoring system for data acquisition, equipped with a complete control unit. For the experiment, the aircraft was equipped with a SenseFly provided Sony Cyber-shot DSC-WX220 camera (pixel size 1.25 μm) with a resolution of 18.2 MPix and a focal length of 4.45 to 44.5mm (was set to 4.45 mm during acquisition, a 35mm equivalent 25mm).

Home-assembled drone EasyStar II is a commercially available motor glider (Fig. 3), which can be combined with a commercially available 3DR Pixhawk autopilot. This autopilot can convert any type of model into an autonomous system. The system also features a Nikon Coolpix A (pixel size 1.19 μm) camera with a 16.2-megapixel resolution and a fixed focal length of 18.5mm (35mm equivalent 28 mm).

Fig. 3. Ebee (left) and Easystar (right).

2.4 UAV surveys

UAV images were collected during March 2017. One flight with Easystar and two flights with eBee were performed to assess the effect of the image quantity on the accuracy and density of a point cloud. The eBee flights were mutually perpendicular and differed in flight trajectories (Fig. 4). From now on, we refer to these flights as Easystar, eBee[1,] and eBee[2]. For both systems, a forward overlap of 85 %, sidelap of 65 % and a ground

sampling distance of about 30 mm per pixel was set. The height and speed of the UAV flight, as well as the shutter speed (1/250 – 1/ 640 for Ebee and 1/1250 for Easystar), were set in both systems by the control program. For both systems, the flight height was about 100 m above the ground level. During the Ebee flights, the weather was sunny with a temperature of 19 °C, and during the Easystar flight, it was partly sunny with 8 °C. For the eBee system, two complete mutually perpendicular flights were performed. The first flight yielded 1004 images (marked as eBee 1, Fig. 4 left) and the second one 903 images (marked as eBee 2, Fig 4 middle). Only one flight (940 images, Fig. 4 right) was performed with the Easystar II glider.

Fig. 4. Flight line trajectories (from left eBee[1](left), eBee[2](middle) and Easystar (right).

2.5 Image processing and 3D point cloud generation

To generate 3D point clouds, acquired images were processed in the Agisoft's PhotoScan Professional software, version 1.2.6. Processing was done separately for each individual flight (Easystar, eBee[1], eBee[2]) as well as for the combination of the two eBee flights (eBee[12]) to test the improvement in the terrain representation. The process consisted of alignment, iteratively refining external and internal camera orientations and camera locations through a least squares method, thus generating a sparse point cloud of tie points, followed by an application of a dense multi-view 3D surface reconstruction algorithm. The images, along with a text file containing camera positions estimated by the onboard GNSS during the flight, were loaded into PhotoScan software. The alignment was subsequently completed using the accuracy parameter set to "high" and pair pre-selection to "disabled". Accuracy set to "high" ensured that the original resolution of images was used while the "disabled" pair pre-selection ensured the most accurate image matching in all possible combinations. The limit for key points (indicating the maximum number of points sampled within each image) was set to 20,000 and for tie points (points used for image matching and relative orientation) to 5,000. The GCPs were loaded and identified in the images, their a priori accuracy was set to 0.02 m. Six ground control points were completely removed from the evaluation due to their physical displacement or complete destruction by animals. This devaluation was caused by a time gap between the measurement of the ground control points and the flights, which was in turn caused by the necessity to wait for the appropriate weather conditions (no snow cover, low wind speed, etc.). Bundle adjustments were computed in the S-JTSK and Bpv datum. Dense point clouds were built with a high reconstruction quality and mild depth filtering (set in software Agisoft for optimal results in our study area). To determine the accuracy of the photogrammetric model, the total coordinate error (TCE) was calculated for each point cloud as follows:

$$\Delta_{pi} = \sqrt{\Delta_{xi}^2 + \Delta_{yi}^2 + \Delta_{zi}^2}, \tag{1}$$

where Δ_{xi} , Δ_{yi} , Δ_{zi} are coordinate differences of ground control points.

$$TCE = \sqrt{\frac{\Delta_{p1}^2 + \Delta_{p2}^2 + \cdots + \Delta_{pn}^2}{n}}. \tag{2}$$

The point clouds were exported to the LAS format, and points representing ground surface were identified using LAS Ground tool in the ArcGIS software. We calculated point clouds density and height differences between point clouds in Cloud Compare 2.9.1. The entire workflow is illustrated in Fig. 5.

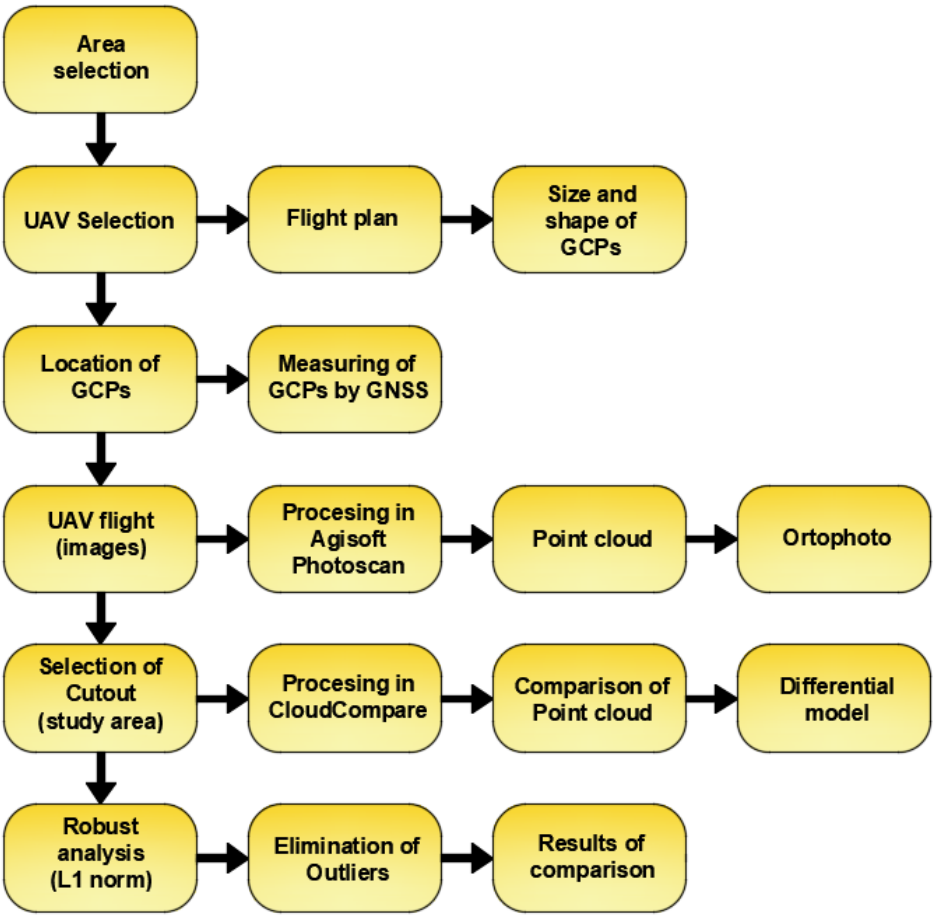

Fig. 5. The whole procedure diagram.

The total coordinate error of the point clouds in Agisoft Photoscan from eBee achieved worse results than Easystar, which was most likely caused by the lower quality of images. These results were published in (Moudrý, 2018) and are given in Tab. 1 for a general description of each flight and its processing.

Tab. 1. Precision overview of flights.

Flight	Total coordinate error [m]
Easystar	0.041
eBee[1]	0.081
eBee[2]	0.053
eBee[12]	0.050

Residual errors from the Coolpix A camera (Easystar) after calibration in a maximum of 0.2 pixels were very small, which is most likely due to the construction and superior quality of the lens. The DSC-WX220 camera (eBee) achieved a residual error after calibration in a maximum of 0.7 pixels.

2.6 Outliers filtering

Due to the presumed presence of outliers, we used a robust method (L1 norm). This method (Koch, 1999), as a function of the probability distribution, directly uses Laplace distribution that is more suitable for data with outlying values than a normal distribution. For nonhomogeneous measurements (measurements with the different standard deviation) a robust weight change is given by the function,

$$w_i = 1 / |v_i|. \quad (3)$$

Where w_i represents weights and v_i residuals. The calculation is done iteratively, residuals acquired from one calculation are used to calculate robust weights' changes in the next calculation. The outliers are determined by residuals exceeding the limit value (2.5 times the standard deviation calculated from residuals before the robust method use). After detection and exclusion of the first set of outliers, a new value of mean and standard

deviation is determined, followed by a new robust analysis of outliers. The algorithm of outliers' filtration is shown in Fig. 6.

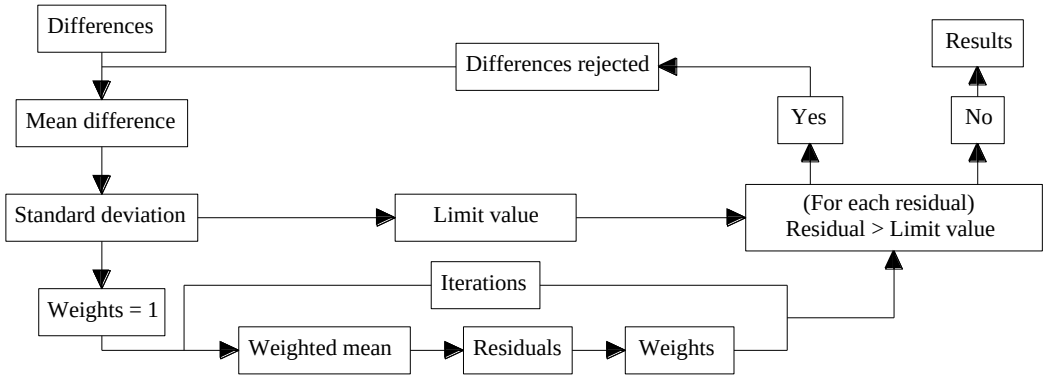

Fig. 6. Algorithm of outliers' filtration.

Ten iterations were typically used, and the number of outliers did not exceed 5 % of the dataset. From the point clouds representing the bare ground, the following vertical differences were calculated: EasyStar - eBee1, Easystar – eBee2, Easystar – eBee12, eBee1 – eBee2, eBee1 – eBee12 and eBee2 – eBee12. These differences were used for calculating a mean difference (which is the difference between systematic errors) and the standard deviation of the differences (describing the random errors). The RMSE of the differences consists of systematic error and random error while the standard deviation contains only the random error component.

$$\text{Mean difference} = \frac{\sum_{i=1}^{N}(x_i - x_{REF})}{N} \tag{4}$$

$$\text{RMSE} = \sqrt{\frac{\sum_{i=1}^{N}(x_i - x_{REF})^2}{N}} \tag{5}$$

$$\text{Standard deviation} = \sqrt{\frac{\sum_{i=1}^{N}(x_i - \bar{x})^2}{N-1}} \tag{6}$$

where x_i is the elevation derived from the first point cloud, x_{REF} is the corresponding elevation in the second point cloud, and N is the number of differences. Differences were derived using 2.5D Delaunay triangulation from ten nearest points in the software Cloud Compare 2.9.1.

2.7 Evaluation of correlated data

In principle, it is not possible to calculate the absolute precision and accuracy characteristics just from the differences. In the presented experiment, the differences and their standard deviations were calculated in all six possible combinations (EasyStar - eBee1, Easystar – eBee2, Easystar – eBee12, eBee1 – eBee2, eBee1 – eBee12 and eBee2 – eBee12).

The fact that some of the differences were calculated from partly identical data (i.e., eBee12 is a combination of images also used for eBee 1 and eBee 2 point cloud, respectively), and are therefore self-correlated had to be taken into account. An equation describing the relation of the single standard deviations of individual point clouds (data "a" and "b") and the standard deviation of their difference is:

$$\sigma_a^2 + \sigma_b^2 = \sigma_{\Delta ab}^2 \tag{7}$$

Where σ_a^2 is stthe andard deviation of the first point cloud, σ_b^2 of the second point cloud and $\sigma_{\Delta ab}^2$ is a standard deviation of their difference. In our case, only the standard deviation of the difference was known. However, due to the existence of four point clouds in total, there are six of these equations with four unknowns to solve (standard deviations of each point cloud). Due to the possible correlation of the data (differences of point clouds) to the calculation, a variance - covariance matrix must be added. Formulas for the calculation of surface coordinate points from th eimagery is very complicated and the size of the correlation can therefore be only estimated.

Authors have chosen to use the multiple generation of three random files E1, E2, E3 (each containing 1000 randomly generated numbers). File E4 was created as a sum of E1 and E2 (like Ebee12 = Ebee1 + Ebee2), after which the differences L1 – L6 and standard deviations of differences were calculated.

$$\begin{aligned} &L1 = E1 - E2; \ldots s_{\Delta 12} \\ &L2 = E1 - E3; \ldots s_{\Delta 13} \\ &L3 = E1 - E4; \ldots s_{\Delta 14} \\ &L4 = E2 - E3; \ldots s_{\Delta 23} \\ &L5 = E2 - E4; \ldots s_{\Delta 24} \\ &L6 = E3 - E4; \ldots s_{\Delta 34} \end{aligned} \tag{8}$$

The data are only subtracted, each difference L1 … L6 is characterised by the standard deviation s, which is the result of the real data subtraction. The dependence of the data thus determined can be characterized by a correlation coefficient, which can easily be converted to covariance. If the standard deviation of the individual variables is equal to 1, the correlation coefficient is directly the covariance.

The correlation coefficient ρ can be easily calculated using a definition formula:

$$\rho = \frac{s_{xy}}{s_x \cdot s_y}, \tag{9}$$

where

$$s_x = \sqrt{\frac{v'^2_x}{n-1}}, \; s_y = \sqrt{\frac{v'^2_y}{n-1}}, \; s_{xy} = \frac{v'_x \cdot v'_y}{n-1}. \tag{10}$$

The v_x and v_y are corrections from the mean within individual files L1 … L6 and n is the number of differences for each dataset L1 … L6. Due to the relatively small dataset and pseudo-randomness of computer-generated random numbers (common rand() function), generation and computation were performed 1000x, and the mean was used as a result. The resulting correlation matrix **M** shows considerable dependencies:

$$\boldsymbol{M} = \begin{pmatrix} 1 & 0.50 & 0.51 & -0.50 & 0.50 & 0.51 \\ 0.50 & 1 & 0.51 & 0.50 & 0.50 & 0.49 \\ 0.51 & 0.51 & 1 & 0 & 1 & 1 \\ -0.50 & 0.50 & 0 & 1 & 0.01 & -0.01 \\ 0.5 & 0.50 & 1 & 0.01 & 1 & 1 \\ 0.51 & 0.49 & 1 & -0.01 & 1 & 1 \end{pmatrix} \tag{11}$$

This correlation and covariance matrix were used for the calculation of the solution of the system of equations for the determination of the individual standard deviations. A plan matrix **A**:

$$\boldsymbol{A} = \begin{pmatrix} 1 & 1 & 0 & 0 \\ 1 & 0 & 1 & 0 \\ 1 & 0 & 0 & 1 \\ 0 & 1 & 1 & 0 \\ 0 & 1 & 0 & 1 \\ 0 & 0 & 1 & 1 \end{pmatrix} \tag{12}$$

The measurement vector **l** is given by the standard deviations of the differences in the square, and thus:

$$\boldsymbol{l} = \begin{pmatrix} s^2_{\Delta Easystar,eBee1} \\ s^2_{\Delta Easystar,eBee2} \\ s^2_{\Delta Easystar,eBee12} \\ s^2_{\Delta eBee1,eBee2} \\ s^2_{\Delta eBee1,eBee12} \\ s^2_{\Delta eBee2,eBee12} \end{pmatrix} \tag{13}$$

The weight matrix $\boldsymbol{P}$ is acquired according to the formula:

$$P = M^{-1} \tag{14}$$

The system of equations is then solved by the least squares method easily, as it is in a linear form (unknown standard deviations are also solved in square):

$$\begin{pmatrix} s^2_{Easystar} \\ s^2_{eBee1} \\ s^2_{eBee2} \\ s^2_{eBee12} \end{pmatrix} = (\mathbf{A}^{\mathrm{T}} \cdot \mathbf{P} \cdot \mathbf{A})^{-1} \cdot \mathbf{A}^{\mathrm{T}} \cdot \mathbf{P} \cdot \mathbf{l}\,. \tag{15}$$

To show the advantage of our method, we also tested the approach without the use of a weight matrix (no correlation calculation).

3. Results and discussion

3.1 Comparison of point clouds

The density of point clouds for the acquired data sets varied significantly (Tab. 2). The densest point cloud was achieved with Easystar in all areas.

Tab. 2. Mean point density of study areas (points per m^2).

Flight	Forest	Grass	Bushy
Easystar	313	275	309
eBee^1	249	250	266
eBee^2	185	181	196
eBee^{12}	217	223	239

Tab. 3 shows a comparison of data in a height component for a grassy area. The mean difference values (systematic shift) are about 0.05 m higher for Easystar data in comparison to all eBee data. Ebee data shows similar parameters with very small systematic shift, which corresponds to the size of one pixel in reality. The values of the standard deviations for all data combinations show similar values up to 0.03 m.

Therefore, the quality of the camera does not have a significant effect on the relative accuracy of the model but directly affects the systematic shift of the whole model (determination of the points) and the number of correctly evaluated points (Tab. 2).

It is also interesting to note that on the grassy surface, a very small number of outlying points were detected in comparison to other surfaces, although the surface is very compact, has a uniform colour and the correlation of individual pixels in the picture may not be unambiguous.

Tab. 3. Grass area.

Data difference	Mean difference [m]	RMSE [m]	Std. deviation [m]	No. of differences	No. of outliers
Easystar - eBee^1	0.077	0.082	0.029	496757	2201 (0.44 %)
Easystar – eBee^2	0.046	0.054	0.029	365160	1225 (0.34 %)
Easystar – eBee^{12}	0.057	0.063	0.026	448186	1428 (0.32 %)
eBee^1 – eBee^2	0.029	0.041	0.029	365223	484 (0.13 %)
eBee^{12} – eBee^1	0.018	0.031	0.024	496508	1079 (0.22 %)
eBee^{12} – eBee^2	0.010	0.018	0.015	365044	1812 (0.50 %)

Fig. 7 shows a significant local distortion of the difference model between EasyStar and eBee 1 data (in the middle). On the right side, a comparison of the eBee 12 and eBee 2 is shown, which displays very small differences without significant deformation.

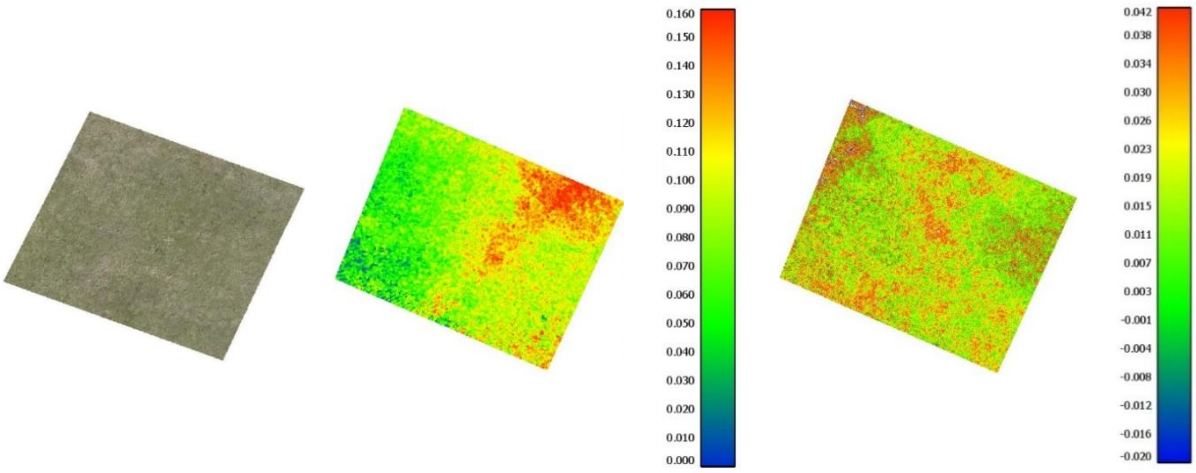

Fig. 7. Height differences of grassy area (Ortophotomosaic - left, Easystar vs. eBee1 – middle, eBee12 vs. eBee2 – right).

Tab. 4 shows a data comparison for a forested area. Values of mean differences point to a large systematic shift between both eBee 1 and 2 data, which reaches about 0.1 m. The values of the standard deviations of all data differences show values of about 0.04 m, which is slightly worse than in the grassy area. The number of outlying values is much higher, probably due to considerable filtration and generally worse evaluation quality due to the vegetation cover of the area. Despite these negative aspects, it is surprising that the coverage of the points (shown in Table 2) is not significantly worse than for the remaining surfaces.

Tab. 4. Forested area.

Data difference	**Mean difference** [m]	**RMSE** [m]	**Std. deviation** [m]	**No. of differences**	**No. of outliers**
Easystar - eBee^{1}	0.043	0.062	0.044	541920	9321 (1.72 %)
Easystar – eBee^{2}	0.062	0.074	0.039	413272	4942 (1.20 %)
Easystar – eBee^{12}	0.022	0.044	0.039	470317	7347 (1.56 %)
eBee^{1} – eBee^{2}	0.103	0.116	0.055	415704	6380 (1.53 %)
eBee^{12} – eBee^{1}	0.065	0.078	0.043	545399	12449 (2.28 %)
eBee^{12} – eBee^{2}	0.034	0.052	0.039	416149	9462 (2.27 %)

Fig. 8 shows the comparison of Easystar and eBee 12 data (middle), characterised by very small differences and clearly visible holes after ground filtration (tree removal). Fig. 8 shows on the right the differences between eBee 1 and eBee 2 data; especially in places where trees obscured the ground, large systematic shifts up to 0.25 m were detected, probably due to the different directions of the flight.

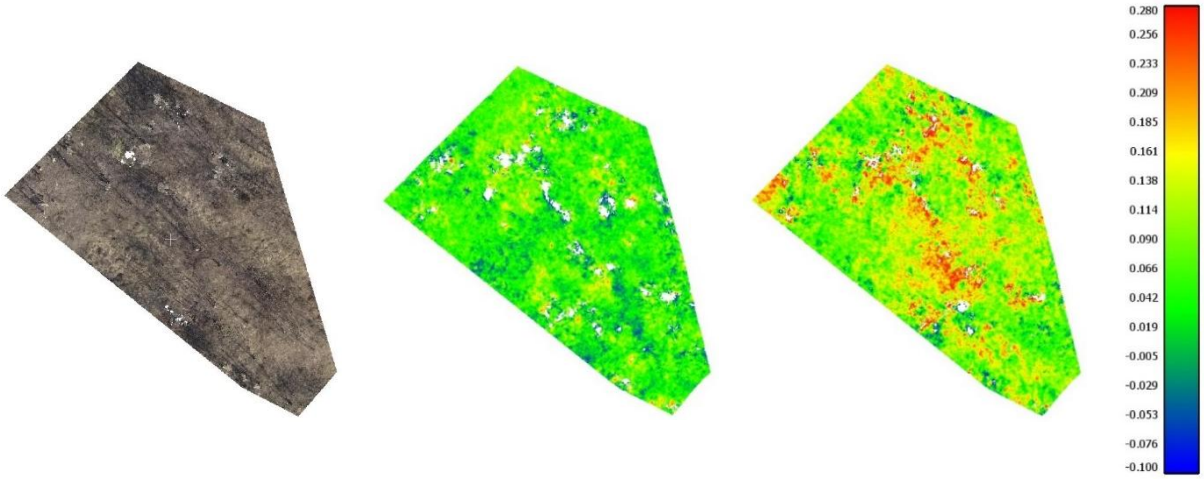

Fig. 8. Height differences of forested area (Ortophotomosaic – left, Easystar vs. eBee12 – middle, eBee1 vs. eBee2 – right).

Tab. 5 shows a comparison of data for the bushy area. The mean difference values are the smallest of all tested areas, which may be due to the proximity of three ground control points. Values of standard deviations are between the wooded area and the grassy area as expected. The number of outliers is similar to the forested area.

Tab. 5. Bushy area.

Data difference	**Mean difference** [m]	**RMSE** [m]	**Std. deviation** [m]	**No. of differences**	**No. of outliers**
Easystar - eBee^{1}	0.054	0.070	0.043	461261	9582 (2.08 %)
Easystar – eBee^{2}	0.013	0.037	0.034	339136	6419 (1.89 %)
Easystar – eBee^{12}	0.037	0.052	0.036	411331	6613 (1.61 %)
eBee^{1} – eBee^{2}	0.041	0.052	0.031	340180	5026 (1.48 %)
eBee^{12} – eBee^{1}	0.019	0.033	0.027	463081	8635 (1.86 %)
eBee^{12} – eBee^{2}	0.021	0.032	0.023	340566	4059 (1.19 %)

Fig. 9 shows in the middle the height differences of Easystar and eBee 1 data, where a greater height differences were found (red, yellow colour). Fig. 9 on the left, the height differences between Easystar and eBee 2 data are depicted, with fewer significant deformations or holes. So eBee 1 seems to be the worst in bushy and forest terrain.

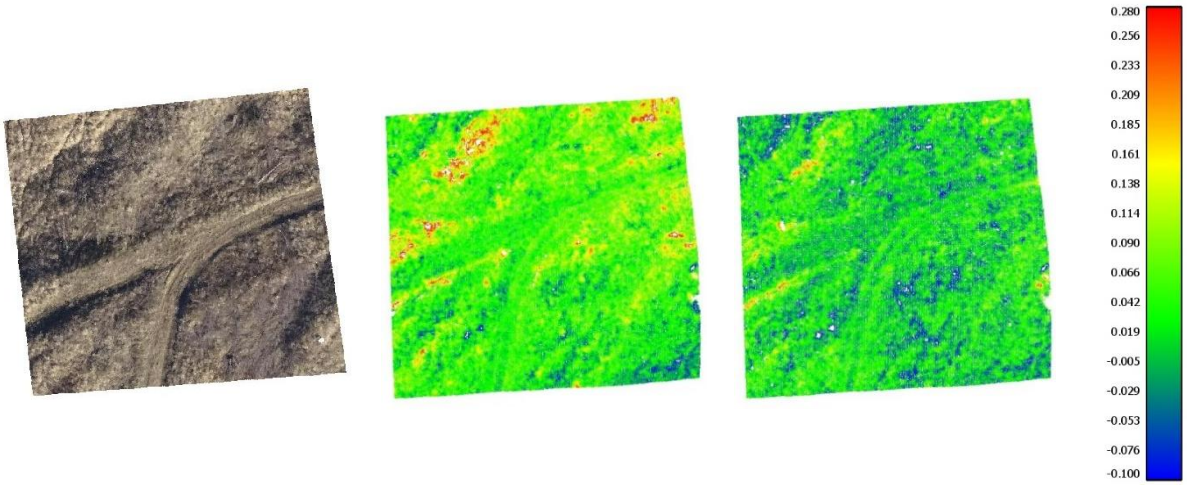

Fig. 9. Height differences of the bushy area (Ortophotomosaic, Easystar vs. eBee1 – left, Easystar vs. eBee2 – right).

3.2 Evaluation of data correlation

Results of the correlated data calculation, the estimates of the errors of each dataset are shown in Tab. 6, both variants (with and without the use of the weights and covariances) are presented.

Tab. 6. Estimation of the standard deviations from the correlated data.

Flights	**Forested area** [m]		**Grassy area** [m]		**Bushy area** [m]	
	No correlation used	Correlation	No correlation used	Correlation	No correlation used	Correlation
Easystar	0.024	0.038	0.023	0.023	0.033	0.037
eBee 1	0.039	0.041	0.022	0.021	0.026	0.029
eBee 2	0.034	0.037	0.017	0.009	0.015	0.025
eBee 12	0.023	0.031	0.008	0.010	0.014	0.018

The standard deviations determined by the adjustment with the use of the covariances are greater than the standard deviations determined without correlation usage, which is due to "false" internal compliance of (at least) a part of the data – in this case, a substantial part of the data. In addition, besides the increase of the values, their order in terms of accuracy changes, which is again caused by the dependencies (covariances). Covariances (or correlation coefficients) are estimates of the size dependencies, but their exact calculations are not possible in this case; on the other hand, but without the correction on covariances, the values can be considered to be more accurate than they really are since the data and its differences are highly dependent on each other. The values of standard deviations determined this way are also closer to realistically achievable values.

4. Summary

Here, we presented a comparison of data acquired through two UAV systems on a spoil heap in areas with various vegetation densities in the leaf-off stage. The first system was eBee (SenseFly), and the other was a home-assembled EasyStar II motor glider with 3DR Pixhawk autopilot. Images were processed in the same way using the same ground control points for both platforms to make the resulting data comparable in terms of random and systematic errors. These errors are, among other things, dependent on the used camera and its lens

distortion and internal imaging settings. For example, eBee keeps changing both shutter speed and ISO settings for the image capture while the Easystar system allowed the change of the aperture setting only.

To determine the systematic and random errors of the UAV-acquired data, three areas with typical examples of vegetation on the spoil heap were selected (forest, grass, bush). The density of the datasets was also determined for each area to compare the SfM efficiency of individual systems in different types of terrain. From the comparison of the densities of points in individual regions, it is evident that SfM yielded the best results in most cases in the bushy terrain. Interestingly, the density is the same or worse in the grassy area than in the forest area, where obscuring of the ground by the tree can be assumed. This phenomenon is probably caused by a worse matching of the relatively monochromatic grassy surface.

A comparison of the individual data on a grassy area suggests that the accuracy of the differences is about 0.03 m, which corresponds to the actual pixel size at the used flight height. However, individual data may show local deformations due to the worse quality of matching of points on the monochromatic surface. Average shift (systematic error) ranged from 0.01 m to 0.08 m. In the forested terrain, the accuracy of data differences is about 0.04 m, which is slightly worse than the in the grassy area. However, a large number of outlying values is present in the data, and the average value shows the greatest deviation of up to 0.12 m in the case of the two datasets acquired by the same system (eBee). Bushy terrain data achieves precision values between a grassy area and a forested area.

The evaluation of the data using simulated correlation values shows another side of the experiment. It indicates that such calculations can be treacherous if not calculated and interpreted well. Although the results achieved with and without the use of the simulated correlation data were relatively similar, these results differ in absolute values. When using the correlation data, standard deviations are higher, taking in account the inner dependence of individual used data. These standard deviations can be considered to be an estimate of the standard deviation describing the absolute precision of the data. It should be emphasised that this is only a statistical estimate, not the real values. Actual values of standard deviations cannot be determined in this way, a component of the mutual systematic error for both compared data will always be missing.

Acknowledgment*:This work was supported by the Grant Agency of the Czech Technical University in Prague, grant No. SGS18/067/OHK1/1T/11.*

References

Blišťan, P., Kovanič, Ľ, Zelizňaková, V., Palková, J. (2016) Using UAV photogrammetry to document rock outcrops. Acta Montanistica Slovaca, Volume 21, number 2, pp. 154-161, ISSN 1335-1788.

Boon, M. A., Drijfhout, A. P., Tesfamichael, S. (2017). Comparison of a Fixed-Wing and Multi-Rotor Uav for Environmental Mapping Applications: a Case Study. *The International Archives of Photogrammetry, Remote Sensing and Spatial Information Sciences, 42, 47.*

Clapuyt, F., Vanacker, V., Van Oost, K. (2016) Reproducibility of UAV-based earth topography reconstructions based on Structure-from-Motion algorithms. GEOMORPHOLOGY Volume: 260 Special Issue: SI Pages: 4-15.

Close, O., Stéphenne, N., Frippiat, C. (2016) Impact of DEM Processing on the Geotechnical Instability Analysis of Waste Heaps in Wallonia.GEOProcessing 2016: The Eighth International Conference on Advanced Geographic Information Systems, Applications, and Services. ISBN: 978-1-61208-469-5.

Cordell, S., Questad, E. J., Asner, G. P., Kinney, K. M., Thaxton, J. M., Uowolo, A. ... Chynoweth, M. W. (2017). Remote sensing for restoration planning: how the big picture can inform stakeholders. *Restoration Ecology, 25, S147-S154. ISSN: 1526-100X.*

Ćmielewski, B., Dabek, P. B., Patrzałek, C., Wilczynska, I. (2018). Potential of Using Unmanned Aircraft Systems for Landslide Monitoring: the Case of Janowiec Landslide in Poland. *Journal of Environmental Science and Management, 21(1). ISSN 0119-1144.*

Doležalová, J., Vojar, J., Smolová, D., Solský, M., Kopecký, O. Technical reclamation and spontaneous succession produce different water habitats: a case study from Czech post-mining sites. *Ecological engineering, 43: 5-12. doi:10.1016/j.ecoleng.2011.11.017*

Flener, C., Vaaja, M., Jaakkola, A. et al. (2013) Seamless Mapping of River Channels at High Resolution Using Mobile LiDAR and UAV-Photography. *REMOTE SENSING Volume: 5 Issue: 12 Pages: 6382-6407.*

Fraštia M., Marčiš M., Kopecký M., Liščák P., Žilka A. (2014) Complex geodetic and photogrammet-ric monitoring of the Kraľovany rock slide. In *Journal of Sustainable Mining. Vol. 13, no. 4, s. 12-16. ISSN 2300-1364.*

Goncalves, J. A., Henriques, R. (2015) UAV photogrammetry for topographic monitoring of coastal areas. *ISPRS JOURNAL OF PHOTOGRAMMETRY AND REMOTE SENSING Volume: 104 Pages: 101-111*

Hodgson, M. E., Jensen, J., Raber, G., Tullis, J., Davis, B., Thompson, G., Schuckman, K. An Evaluation of Lidar-derived Elevation and Terrain Slope in Leaf-off Conditions. *Photogrammetric Engineering & Remote Sensing, 71(7), 817–823.* http://doi.org/10.14358/PERS.71.7.817

Hogarth, J., Hawley, M., Beale, G. (2017) Instrumentation and monitoring. In Hawley, M., & Cunning, J. (Eds.), Guidelines for Mine Waste Dump and Stockpile Design. *CSIRO PUBLISHING*.

Koch, K. R. (1999) Parameter Estimation and Hypothesis Testing in Linear Models. *Springer Verlag, Berlin Heidelberg New York, ISBN 3-5406525-74.*

Koska, B., Jirka, V., Urban, R., Křemen, T., Hesslerová, P., Jon, J., Pospíšil, J., Fogl, M. (2017) Suitability, characteristics, and comparison of an airship UAV with lidar for middle size area mapping, *International Journal of Remote Sensing. 38(8-10), 2973-2990. ISSN 0143-1161*.

Kršák B., Blišťan, P., Pauliková, A., Puškárová, P., Kovanič, Ľ. ml., Palková, J., Zelizňaková, V. (2016) Use of low-cost UAV photogrammetry to analyze the accuracy of a digital elevation model in a case study. *Measurement. Vol. 91, p. 276–287. ISSN 0263-2241*.

Meng, X., Currit, N., Zhao, K. (2010). Ground filtering algorithms for airborne LiDAR data: A review of critical issues. *Remote Sensing, 2(3), 833–860*. http://doi.org/10.3390/rs2030833

Moudrý, V., Urban, R., Štroner, M., Komárek, J., Brouček, J., Prošek, J. (2018) Comparison of a commercial and home-assembled fixed-wing UAV for terrain mapping of a post-mining site under leaf-off conditions. International *Journal of Remote Sensing. 1 – 18.*

Niethammer, U., James, M. R., Rothmund, S. et al. (2012) UAV-based remote sensing of the Super-Sauze landslide: Evaluation and results. *ENGINEERING GEOLOGY Volume: 128 Special Issue: SI Pages: 2-11*

Pukanská, K., Bartoš, K., Sabová, J. (2014) Comparison of Survey Results of the Surface Quarry Spišské Tomášovce by the Use of Photogrammetry and Terrestrial Laser Scanning. In: *Inżynieria Mineralna. Vol. 33, no. 1, p. 47-54. ISSN 1640-4920.*

Stephenne, N., Frippiat, C., Veschkens, M., Salmon, M., Pacyna, D. (2014). Use of a LiDAR high resolution digital elevation model for risk stability analysis. *EARSeL eProceedings, 13(S1), 24-29.*

Štroner, M., Urban, R., Královič, J. (2013) Testing of the relative precision in local network with use of the Trimble Geo XR GNSS receivers. *Reports on Geodesy [online]. 94: 27-36*. https://doi.org/10.2478/rgg-2013-0004

Thoeni, K., Giacomini, A., Murtagh, R., Kniest, E. (2014). A comparison of multi- view 3D reconstruction of a rock wall using several cameras and a laser scanner. In Proceedings of ISPRS Technical Commission V Symposium, Riva del Garda, Italy, 23–25.

Torresan, C., Berton, A., Carotenuto, F., Di Gennaro, S. F., Gioli, B., Matese, A., ... , Wallace, L. (2017). Forestry applications of UAVs in Europe: A review. *International Journal of Remote Sensing, 38(8-10), 2427-2447.*

Wężyk, P., Szostak, M., Krzaklewski, W., Pająk, M., Pierzchalski, M., Szwed, P., Ratajczak, M. (2015). Landscape monitoring of post-industrial areas using LiDAR and GIS technology. *Geodesy and Cartography, 64(1), 125–137*. http://doi.org/10.1515/geocart-2015-0010

Zalesky, M., Zalesky, J., Kuklik, P., Hanek, P. (2008, May). Monitoring of a large slide and slope reclamation in a former Open-Pit Mine. In Proceedings of 13th FIG International Symposium on Deformation Measurements and Analysis and 4th IAG Symposium on Geodesy for Geotechnical and Structural Engineering.

Záleský, J., Čápova, K. (2017) Monitoring and assessment of remedial measures in closed open cast mine. In: Advancing culture of living with landslides, vol 3. *Springer International Publishing Switzerland. ISBN 978-3-319-53486-2*.

Zhou, Hailing, Kong, Hui, Wei, Lei et al. (2015) Efficient Road Detection and Tracking for Unmanned Aerial Vehicle. *IEEE TRANSACTIONS ON INTELLIGENT TRANSPORTATION SYSTEMS Volume: 16 Issue: 1 Pages: 297-309*.

Soil contamination by heavy metals at Libiola abandoned copper mine, Italy

***Giuseppe Buccheri*[1], *Peter Andráš*[1], *Emery Vajda*[2], *Pavol Midula*[1], *Zuzana Melichová*[1] *and* *Vojtech Dirner*[3]**

Exploitation of ores has surely represented a risk for contamination of environmental matrices for a long time. This paper reports the results of a study concerning soil contamination by heavy metals at Libiola abandoned copper mine (Italy). This deposit has surely got special importance in Italy because of its historical, environmental and mining features. From a historical viewpoint, Libiola deposit was known since Copper Age, with maximum exploitation at the end of the 19th century. Our investigation plan was elaborated in order to characterize the environmental matrices there, and it provided for inspection of the zones (included in the valley of Gromolo stream) which, according to our preliminary studies and according to literature, could be most affected by past mining activity. Within our selected zones, some soils (even cultivated) were collected in order to check their contamination by heavy metals. Results from the analysis of the collected soil samples showed that the content of heavy metals often exceeds limits provided by the Italian Law 152/06. The knowledge of situation concerning pollution can give useful indications about the influence of mining activities on the surrounding environment, and it can also be valid support in order to organize an optimal future use of the studied mining area, which has been abandoned since its closure (1962).

Keywords: *contamination, dump-field, heavy metals, soil, pollution, abandoned mines*.

Introduction

The abandoned Libiola sulfide ore deposit is located in the valley of Gromolo stream, near Sestri Levante (Liguria), and it is one of the several deposits whose mineralization is related to Jurassic ophiolites (gabbros and diabases, Vara Supergroup) of Northern Apennine (Faccenna et al., 2001; Buccheri et al., 2014; Andráš et al., 2016). Surface covered by mine is about 4 km^2, including more than 30 km of underground passages plus extensive open-cut mines that facilitate drainage of rainwater (Capello et al., 2016).

Libiola deposit may be classified as a strata-bound volcanic-associated massive sulfide deposit (VMS), and it occurs both as massive lens-shaped bodies which are concordant with pillow basalts and as scattered mineralization, done of small aggregates of sulfides, either filling vesicular cavities or concordant with pillows' textures (Andráš et al., 2017). Libiola ore deposit was formed because of convective circulation of seawater through hot rocks at spreading ridges; the successive metamorphic and tectonic processes because of Apennine orogenesis, caused the formation of this ore deposit (Scott, 1997). Sulfide mineralization at Libiola area is mainly associated to pillow basalts and basaltic breccia and, subordinately, to serpentinitic rocks of ophiolites of Internal Ligurian Units belonging to the Supergruppo della Val di Vara Unit (Fig. 1).

According to texture and setting (Andráš et al., 2017), we can distinguish three types of mineralization at Libiola mine:

a) massive mineralization with pyrite and chalcopyrite as strata and lenticular bodies in basaltic rocks;
b) mineralization in stockwork-veins, not economically important, with pyrite and chalcopyrite in pillow lavas;
c) scattered mineralization consisting of millimetric pyrite crystals inside a serpentine (lizardite and chrysotile), chlorite, and magnetite matrix, in basaltic and serpentinitic rocks (tectonically overlying basalts).

The sulfide mineral assemblages consist of pyrite and chalcopyrite, with minor sphalerite and pyrrhotite, in a gangue of quartz, chlorite, and minor to accessory calcite in both massive lenses and mineralized veins. Disseminated mineralizations within the serpentinites consist almost exclusively of millimetric pyrite crystals scattered in a serpentine (lizardite and chrysotile), chlorite, and magnetite matrix (Marescotti et al., 2010).

At Libiola mines, oxides and hydroxides show themselves as massive crusts of variable colors from ochre-yellow to intense red (Marescotti et al., 2010).

Ca^-, Mg^-, Al^-, Fe^-, Co^- and Cu^- sulfates show themselves as surface efflorescences, which are formed by water evaporation of interstitial water or by precipitation of circulating solutions. Besides hydroxides, sulfates, and phyllosilicates, it is also possible to observe some Cu^- and Ca^- carbonates, cuprite, native copper and secondary sulfides such as chalcanthite.

[1] *Giuseppe Buccheri, Peter Andráš, Pavol Midula*, Faculty of Sciences, Matej Bel University, Tajovského 40, 974 01 Banská Bystrica, Slovakia, giuseppe.buccheri@studenti.umb.sk, peter.andras@umb.sk
[2] *Emery Vajda*, Edison Spa, Foro Buonaparte 31, 20121 Milano, Italy
[3] *Vojtech Dirner*, VŠB-Technical University, 17. Listopadu 15; 708 33 Ostrava, Czech republic

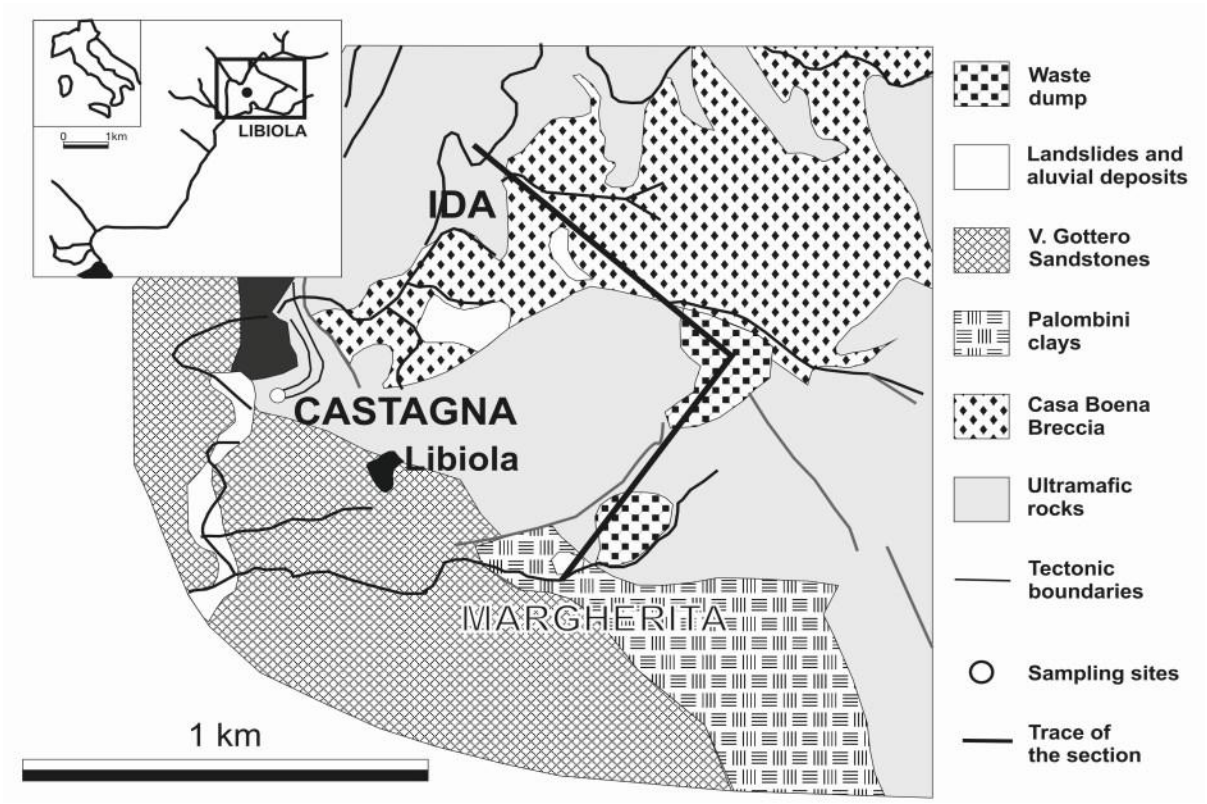

Fig. 1. Geological sketch map of Libiola mining area (Dinelli et al., 2007). About Ligurian Domain, it includes both tectonic units deriving from the Jurassic oceanic lithosphere (Ligure-Piedmont oceanic basin) and their sedimentary covers (Jurassic-Paleocene). The Internal Ligurian Units outcrop between the north-western side of Northern Apennine and the southern border of the western Alps. They are divided (from the bottom) as it follows: 1) a peridotitic basement (more or less serpentinized ultra-mafites) associated to gabbros; 2) a volcano-sedimentary complex, characterized by presence of tectonic and sedimentary ophiolitic breccias, and massive or pillow effusive basalts at its bottom, and by a cover of fine oceanic sediments; 3) torbiditic deposits; 4) schist.

From a historical viewpoint, Libiola mine is one of the most ancient and important heritage of copper extraction activity in western Europe, together with Monte Loreto mine (near Castiglione Chiavarese, Liguria). According to radio-carbon analysis on the discovered pre-historical tools, first excavations at Libiola were dated around 3500 B.C. (Marescotti et al., 2018). Such rests testify early exploitation of iron and copper from Jurassic ophiolitic succession.

Ligurians, the enemy of Romans, built their weapons with copper coming from Libiola. Libiola mine was also exploited during the Roman Age. Around 1840, the interest for mines got higher again because of funds from Savoia administration. Libiola mine was thus exploited at an industrial level (important enrichment plants were built), and this fact contributed to the cancellation of the most ancient extraction traces. Mining activity kept on flourishing until the first thirty years of the 20th century, and its maximum production was achieved at the beginning of the 20th century (Buccheri et al., 2014).

After the Second World War, mining activity at Libiola fell into a crisis. In 1955, after its passage to Montecatini Society, this mine was closed, and then it was abandoned (1962). Closure of the mine left a degraded and polluted landscape. As a matter of fact, such long exploitation left a considerable amount of waste as heaps without vegetation covering a total area of ~ 500,000 m^2. Mine waste is poorly sorted, either sterile or mineralized rock fragments, mainly serpentinites and basalts, and secondary mineral phases produced by weathering (mainly Fe oxy-hydroxides, brown-reddish-orange in color) (Marini et al., 2003; Marescotti et al., 2010; Carbone et al., 2005, 2013).

One of the most interesting aspects characterizing Libiola mines is due to water flowing out of the old galleries, which are a typical example of Acid Mine Drainage (AMD). Originated by oxidative dissolution of pyrite, and subordinately of other metal sulfides, as well as by processes of mixing, dilution, and especially neutralization through water-rock interaction, we can observe two distinct groups of water at Libiola: red and blue water, up to the color of the deposited solid phases. Red water is acidic (pH 2.4 – 3.5), whereas blue water pH is close to neutral (Andráš et al., 2017).

Libiola mining area is included in the hydrographic basin of Gromolo stream. Its path starts about 10 km from the coast and debouches in Mar Ligure, covering an area of about 21 km^2 (Provincia di Genova, 2013).

The hydrographic network is asymmetric with respect to the main river course. Distribution of rivers inside the network is rather homogeneous. Among the most important tributaries on the left bank, Rio Boeno and Rio

Cattan are the most important ones from our viewpoint because they represent confluence points of mining waters, continuously coming from the northern and the southern slopes of the mining area respectively. Hydrologic regime of the area including Libiola abandoned mine is very affected by mining activities. As a matter of fact, acid water is constantly flowing out of the several galleries (in particular in correspondence with downward galleries Margherita, Ida, Weirs, and Castagna) and discharged into Gromolo stream, thus representing a threat for the surrounding environment (Consani et al., 2017). This feature is due to the presence of an extended network of interconnected galleries and wells, which facilitates drainage of raining water. At higher quotes, extended open excavations (showing a sink-like morphology) are moreover present: they increase drainage of water and represent important artificial basins for water collection (Buccheri et al., 2014).

Precipitation of ferrihydrite and schwertmannite (Dinelli et al., 2001; Asta et al., 2015) takes place upon mixing between acid mine waters and surface waters. Most of these solid phases remain in suspension in river waters. Although precipitation of these minerals may scavenge some metals, river waters are heavily polluted, especially during the dry season, when their flow rate decreases.

The end of mining activity there left many questions about the probable pollution of environmental matrices there and the instability of excavations, galleries, and dumps. The waste-rock dumps are very heterogeneous from mineralogical and geochemical viewpoints, with significant lateral variations and vertical heterogeneity, because dumps were formed within a period of over 50 years, during which different exploitation techniques were used, and several lithotypes and economic minerals were extracted (both underground and by open-air excavations). Waste materials that were piled up during exploitation included both host rocks and not economic mineralization derived from handpicking, milling and other treatments (Marescotti et al., 2008).

Materials and methods

After studying past literature and after inspecting the interested mining area, we could confine our largest investigation area within the hydrographic basin of *Gromolo* stream, starting from identification of potential danger centers present in the area.

Potential danger centers can be related to: extraction activities (i.e. mining excavations, discharges for tracing deposit or for mining research), mineral processing (i.e. basins for mine steriles, banks of fine rests, steriles from gravimetry) and presence of different waste (i.e. reagents used at plants, oils, coverings or detritus with concrete-asbestos).

In the case of *Libiola* mining area, primary contamination sources are represented by dumps, excavations, and galleries. They can undergo erosion, powders emission and solid transport to soils and river sediments as well as infiltration, percolation and leaching, causing hydro-geological instability. Secondary contamination sources are there represented by hydro-geological instability and by soil (and sediments), which can move pollution to surface and groundwater (by solid transport or in solution) and wind/atmosphere (by the emission of powder).

After identifying the possible polluting sources present in the area, we could also identify the potential migration pathways of contaminants from sources to targets, according to features of the sources themselves and according to geologic, hydro-geologic and geomorphologic features of the site. It allowed us to build up a preliminary conceptual model (MCP).

We could thus realize our investigation plan in order to obtain a correct definition of features of danger centers and quality status of environmental matrices within our investigation area. We decided for a "reasoned" sampling strategy (Fig. 2), thus based on knowledge of the site itself (morphology, type of materials, active erosion, results of past investigations, etc.), which allowed us identification of the most vulnerable areas and the most probable contamination sources. Sampling operations were documented by pictures showing collecting points of each sample and the area in its context. Each sample was identified with univocal initials.

Soil and techno-soil samples (about 10 kg in weight) were collected by using manual tools down to 30-50 cm in depth. Samples were then saved in labeled containers, after taking out vegetable rests and roots, till laboratory analysis.

ICP-MS analyses of heavy metal content in soil and techno-soil samples were carried out by ACME Laboratories in Vancouver (Canada), starting from samples of 50 g in weight. Samples were homogenized and dried at laboratory temperature. The grinding in agate mill was realized in the laboratory of UMB, Banská Bystrica (Slovak Republic). We are reporting results in the following paragraph (Tab. 1, 2).

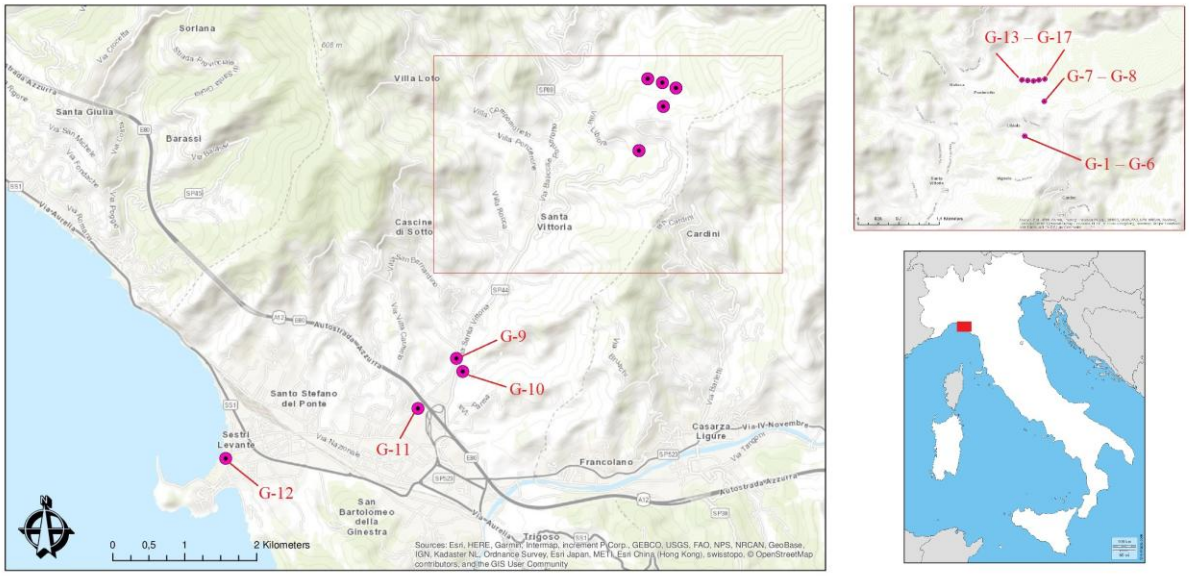

Fig. 2. Map with location of sampling points at Libiola mining area.

Results and discussion

Table 1 reports concentration values concerning soil and techno-soil samples collected at Libiola mining site, compared with Italian law limits provided by the Italian Law 152/06 (Decreto Legislativo 3/4/2006, n. 152, Norme in materia ambientale).

Tab. 1. Concentration values concerning soil and techno-soil samples collected at Libiola mining site, compared with Italian law limits provided by the Italian Law 152/06. Concentration values exceeding the limit for residential/public green (A) are marked, whereas concentration values exceeding the limit for industrial/commercial sites (B) are both marked and underlined.

Soil Sample	Latitude	Long	Cu	Pb	Zn	Ni	Co	As	Cd	Sb	V	Cr	B
G-1	44.299763	9.445048	**1794**	44	**374**	**982**	**85**	5	0.9	<3	75	**961**	**36**
G-2	44.299763	9.445048	**1624**	47	**328**	**732**	**73**	5	0.8	<3	65	**752**	**36**
G-3	44.299763	9.445048	**1765**	27	**402**	**1115**	**101**	4	1.1	<3	**121**	**989**	**43**
G-4	44.299763	9.445048	**>10000**	14	**2851**	**574**	**87**	3	**5.3**	<3	**185**	**444**	**39**
G-5	44.299763	9.445048	**323**	**137**	22	9	2	10	0.7	<3	**231**	86	<20
G-6	44.299763	9.445048	3343	40	**219**	18	7	**110**	1.0	<3	**202**	117	<20
G-7	44.303712	9.448071	**>10000**	**476**	**354**	**308**	**34**	**266**	<0.5	**84**	**176**	**1121**	<20
G-8	44.303712	9.448071	1383	38	113	32	**10**	12	0.8	<3	**266**	**190**	<20
G-9	44.281134	9.422246	**284**	55	**228**	**560**	**49**	5	<0.5	<3	53	**530**	**31**
G-10	44.280005	9.423046	**820**	**189**	**288**	**196**	**51**	3	<0.5	<3	**191**	**274**	**29**
G-11	44.276664	9.417445	**371**	98	**177**	**488**	**39**	8	<0.5	<3	43	**475**	**30**
G-12	44.273630	9.393970	**448**	32	**189**	**435**	**38**	6	<0.5	<3	73	**455**	**36**
Law limit A [mg/kg]			**120**	**100**	**150**	**120**	**20**	**20**	**2**	**10**	**90**	**150**	**2**
Law limit B [mg/kg]			**600**	**1000**	**1500**	**500**	**250**	**50**	**15**	**30**	**250**	**800**	**10**

Sample G-4 is a detritus containing blue patina near *Margherita* Gallery. It shows the highest values for copper (there, in fact, chalcanthite is present) and zinc. Nickel also a little exceeds limit B. Cobalt, cadmium, vanadium and chromium exceed limit A. Content in cadmium in the sample G-4 could be due to the simultaneous presence of greenockite and sphalerite.

G-7 (southern dump, upper layer, Fig. 3) shows, together with G-4, the highest value as far as copper is concerned. It also shows high values as far as arsenic (over five times the allowed limit B), antimonium (almost three times) and chromium are concerned. About the sample G-7, all elements are shown in Table 1, also exceed limit A (except for cadmium).

We can also underline that horizons of cultivated soil near *Margherita* Gallery (G-1, G-2 e G-3) show values over limit B as for copper (almost three times), nickel, chromium (only G-2 shows a value that is a little lower than the limit B) and boron. About high values in boron (between three and four times the allowed limit B), we must remember that ophiolites (basaltic volcanic rocks which were erupted in the submarine environment about 150 million years ago and which are present in the scaly clays) show high resistance against erosion in

comparison with clays. During their long geological story, lava flows were fractured. Mineralized waters could thus deposit on them salts with calcium, silicon, boron, and aluminum: thus, several minerals could be formed, also containing boron, i.e., datolite - $CaB(OH/SiO_4)$, a silicate, associated to basic ophiolitic rocks, which is formed by the action of hydrothermal fluids containing boron.

We must also underline that in samples G-1, G-2 e G-3 (collected under an olive tree), zinc and cobalt also exceed limit A (Law 152/06).

Fig. 3. Libiola southern dump.

G-5 (detritus from the dump, upper layer) is the least contaminated sample: only copper, lead, and vanadium exceed limit A. No metal there exceeds limit B.

Vanadium (together with copper) exceeds limit B only in the sample G-8 (lower layer, -50 cm, the sediment of the southern dump). As for G-8, cobalt and chromium exceed limit A.

About the sample G-6 (detritus from the dump, -50 cm), copper (over five times) and arsenic (more than twice) exceed limit B. Zinc, and vanadium exceed limit A.

If we move away from the mining area to the sea, while following *Gromolo* stream, the situation seems safer, even though, in the sample G-10 (orographic left of *Gromolo* stream, along with Provincial Street SP44), copper and boron (almost three times) exceed limit B. About G-10, lead, zinc, nickel, cobalt, vanadium, and chromium exceed limits A.

The situation of the sample G-9 (orographic right of *Gromolo* stream, locality *Villa Scorza*) results a little safer, on the average, but limit B for nickel shows low exceed. In G-9, copper, zinc, cobalt, and chromium also exceed limit A.

The sample G-11 (orographic right of *Gromolo* stream, *via Fabbrica a Valle*) shows a content in boron that is three times higher than limit B (Law 152/06). Moreover, copper, zinc, nickel, cobalt, and chromium also exceed limit A. Limit A concerning lead is almost reached there.

About the sample G-12 (sediments at the mouth near hotel "Grande Albergo"), copper, zinc, nickel, cobalt, and chromium exceed limit A.

An interesting high concentration of boron was found in many samples. It could also be due to the presence of datolite (to be confirmed by successive analysis), at least partially. Datolite is a mineral that we could mainly find in gabbro, and that could also be easily found in *Bargonasco* Valley (i.e., *Gallinaria* mine and at other outcrops), a parallel and eastern valley with respect to *Gromolo* Valley. Though we cannot exclude that presence of datolite at *Libiola* mining area could be responsible for an increase of boron content in our soil samples, we

must, therefore, underline that diffusion of datolite in this mining area is not expected to be so large to justify such a high content in boron.

It is also interesting to notice that a high concentration of boron has been found near *Margherita* Gallery and in soil samples collected out of *Libiola* mining area (till the mouth of *Gromolo* stream, *Sestri Levante*), whereas we couldn't find such a high boron concentration in dump-soils and detritus from mining discharge near *Margherita* Gallery. We find interesting to deepen reasons for such high concentration of boron.

We also focused our attention on the northern side of the mining area (Table 2), in the surroundings of the main building. There, soil samples G-13 to G-17 were collected (Fig. 4). As for G-15, we also differentiated soil horizons (A, B, C).

Tab. 2. Concentration values concerning soil and techno-soil samples collected at the northern side of Libiola mining site, compared with Italian law limits provided by the Italian Law 152/06. Concentration values exceeding the limit for residential/public green (A) are marked, whereas concentration values exceeding the limit for industrial/commercial sites (B) are both marked and underlined.

Soil Sample	Latitude	Long	Cu	Pb	Zn	Ni	Co	As	Cd	Sb	V	Cr
G-13	44.305623	9.448771	**946**	75	**411**	81	**34**	11	1,0	4,0	**282**	**222**
G-14	44.305701	9.448023	**2992**	17	**228**	**511**	**62**	7	**9,5**	0,6	**139**	**702**
G-15 A	44.305741	9.447636	**>10000**	49	**606**	**1023**	**462**	8	**2,2**	1,7	**143**	**1118**
G-15 B	44.305741	9.447636	**>10000**	70	**691**	**908**	**541**	15	**2,7**	3,1	**151**	**830**
G-15 C	44.305741	9.447636	**7346**	31	**436**	**1115**	**197**	12	1,4	1,9	**99**	**1158**
G-16	44.305833	9.447268	**5639**	34	**435**	**714**	**109**	9	**3,6**	4,8	**142**	**1374**
G-17	44.305775	9.446834	**3239**	**114**	**265**	**668**	**82**	15	0,5	7,7	**196**	**1145**
Law limit A [mg/kg]			**120**	**100**	**150**	**120**	**20**	**20**	**2**	**10**	**90**	**150**
Law limit B [mg/kg]			**600**	**1000**	**1500**	**500**	**250**	**50**	**15**	**30**	**250**	**800**

Fig. 4. Dumps on the northern side of Libiola mining area.

Among these samples, G-15 is the one showing the highest contamination because of copper, nickel, cobalt, chromium, and zinc. It also shows a high concentration of vanadium. High concentrations of copper, cobalt, chromium, and zinc can also be due to the presence of a small creek river draining a part of the dump-field and flowing in a small channel upstream of the main building (Fig. 5). As a matter of fact, it joins *Rio Boeno* stream more or less where G-15 is located. It could justify high concentrations of copper, cobalt, chromium, and zinc, which, on the contrary, should decrease westwards from sample G-13 to sample G-17, as sampling points are farther from *Rio Boeno* stream, with the consequence that dilution could be expected.

Fig. 5. Map (from Google) representing the northern side of Libiola mining area, also showing the location of Weirs Gallery. The arrow indicates water flow from Weirs Gallery, through a small channel, in the direction of the area where samples G-13 to G-17 were collected (fig. 4).

With regard to it, it is necessary to underline that some pools for copper cementation were present in the surroundings of the main building in the past: as a matter of fact, some iron shavings can be found in the surroundings of the area (probably used to activate oxido-reduction processes to water flowing out from Weirs Gallery). It is thus plausible that defluxe interesting this area shows very high concentrations that, without pools, can reach *Rio Boeno* stream and justify higher concentrations in that point. Whereas, in the past, water flowing out from *Weirs* Gallery passed though pools, nowadays this water directly reaches *Rio Boeno* stream.

G-16 shows high contamination of copper, nickel, cobalt, chromium, zinc, and vanadium. Copper, nickel, and chromium exceed limit B. A little bit better situation is shown by the sample G-17 as far as values over the limit are concerned, with the difference that in G-17 cadmium remains under the thresholds provided by Law 152/06, whereas lead shows there higher contamination in comparison with the sample G-16.

In the sample G-14, closer to the main building, most of the analyzed metals (especially copper and nickel) exceed. Zinc, cobalt, cadmium, vanadium, and chromium exceed limit A (Law 152/06). It must be noticed that G-14 shows the highest content in cadmium among all analyzed samples.

In the sample G-13, copper and vanadium show high values, whereas nickel remains under the thresholds provided by Law 152/06. Zinc, cobalt, and chromium also exceed.

Conclusion

After results from analysis of soils collected in *Libiola* mining area and at surroundings, we can observe that:

- The content of heavy metals often exceeds limits provided by the Italian Law 152/06, and it is known that presence of heavy metals at abandoned copper mines, given by ore composition assemblage, can become a very important source of contamination for the surrounding environment. We must easily notice, for example, that sample G-12 (collected at the mouth of *Gromolo* stream) shows a content in chromium that exceeds three times the limit value provided by the Italian Law 152/06 for residential houses/public green.
- Sample G-7 is the only one in which antimonium exceeds according to the Italian Law 152/06 (limit B) and in which lead shows the most important deal. In any case, it is easy to obtain very different values when soils are collected from discharge, even within small distances, because of the extraordinary irregularity of the dumps, where concentrations of minerals are connected to the several extractive phases and the logistic points besides to the crossed lithotypes.

- We still find necessary to integrate our investigation plan by including other sampling points, in order to isolate anomalous compositions from the "average" ones, also taking into account that soils collected downstream of the mining area show concentration related to fluids that, after interacting with crossed materials, transport elements far away from the mine. Furthermore, transportation capability of these fluids depends on a) their physical and chemical properties, b) contribution of additional water streams not interacting with the mining area and c) seasonal fluctuation of stream flows. Additional sampling campaigns will have to consider all these variables in order to investigate better the area and related dynamics.
- About concentration values on the northern dumps, G-15 is the one showing the highest contamination because of copper, nickel, cobalt, chromium, and zinc. A cavity, upstream of the main building, acts as a drain for mineralized waters. As the leachated part of the dump is a source for metals in solutions, we should expect that physical conditions gradually change westwards (pH, in particular, because of the confluence with secondary and neutral channels and because of interaction with more neutral soils), causing precipitation of part of metals. On the contrary, in our case, concentrations show an anomalous trend from G-13 and G-17, because they show a peak with the sample G-15. This anomalous trend can be caused by the presence of a source (i.e., the above mentioned small drain), flowing into *Rio Boeno* stream, that could also collect (because of infiltration) defluxe water from *Weirs* Gallery which, in the absence of the pools that were used for cementation of copper, directly flow into *Rio Boeno* stream.

References

Andráš, P., Turisová, I., Buccheri, G., Matos, J.X., Dirner, V. (2016). Comparison of heavy-metal bioaccumulation properties in Pinus sp. and Quercus sp. in selected European Cu deposits. *Web Ecol., 16, 81–87, 2016*; www.web-ecol.net/16/81/2016/ doi:10.5194/we-16-81-2016.

Andráš, P., Turisová, I., Matos, J.X., Buccheri, G., Andráš, P. Jr., Dirner, V., Kučerová, R., Castro, F.I.P., Midula, P. (2017). Potentially toxic elements in the representatives of the genus Pinus L. and Quercus L. at the selected Slovak, Italian and Portuguese copper deposits. *Carpathian Journal of Earth and Environmental Sciences, February 2017, Vol. 12, n. 1, 95 – 107.*

Asta, M.P., Calleja, M.L., Pérez-López R., Auqué, L.F. (2015). Major Hydrogeochemical processes in Acid Mine Drainage affected estuary. *Marine Pollution Bulletin, Vol. 91, Issue 1, 295-305. 10.1016/j.marpolbul.2014.11.023*

Buccheri, G., Andráš, P., Astolfi, M.L., Canepari, S., Ciucci, M., Marino, A. (2014). Heavy metal contamination in water at Libiola abandoned copper mine, Italy. Rom. J. *Mineral Deposits, ISSN 1220-5648, vol. 87, No. 2, 65-70.*

Capello, M., Cutroneo, L., Consani, S., Dinelli, E., Vagge, G., Carbone, C. (2016). Marine sediment contamination and dynamics at the mouth of a contaminated torrent: The case of the Gromolo Torrent (Sestri Levante, north-western Italy), *Marine Pollution Bulletin, 2016, 109, pp. 128 – 141*.

Carbone, C., Di Benedetto, F., Marescotti, P., Martinelli, A., Sangregorio, C., Cipriani, C., Lucchetti, G., Romanelli, M. (2005). Genetic evolution of nanocrystalline Fe oxide and oxyhydroxide assemblages from the Libiola mine (eastern Liguria, Italy) structural and microstructural investigations. *European Journal of Mineralogy, Vol. 17, n. 5, 785-795. Editor: E. Schweizerbart'sche Verlagsbuchhandlung Science Publishers*.

Carbone, C., Dinelli, E., Marescotti, P., Gasparotto, G., Lucchetti, G. (2013). The role of AMD secondary minerals in controlling environmental pollution: indications from bulk leaching tests. *Journal of Geochemical Exploration, Vol. 132, 188-200. Elsevier.*

Consani, S., Carbone, C., Dinelli, E., Balić-Žunić, T., Cutroneo, L., Capello, M., Salviulo, G., Lucchetti G. (2017). Metal transport and remobilisation in a basin affected by acid mine drainage: the role of ochreous amorphous precipitates. *Environmental Science and Pollution Research International, ISSN: 0944-1344, doi: 10.1007/s11356-017-9209-9.*

Italian Law 152/2006. Decreto Legislativo 3/4/2006, n. 152, Norme in materia ambientale. In Italian language.

Dinelli, E., Lucchini, F., Fabbri, M., Cortecci, G. (2001). Metal distribution and environmental problems related to sulfide oxidation in the Libiola copper mine area (Ligurian Apennines, Italy). *Journal of Geochemical Exploration, 74(1-3), 141–152.*

Dinelli, E., Perkins, W.T., Pearce, N.J.C., Hartley, S. (2007). IMWA Symposium 2007: Water in Mining Environments, R. *Cidu & F. Frau (Eds), 27-31 May 2007. Cagliari, Italy*.

Faccenna, C., Becker, T.W., Lucente, F.P., Jolivet, L., Rossetti, F. (2001). History of subduction and back arc extension in the Central Mediterranean Geophys. *J. Int., 145, 809-820*.

Marescotti, P., Brancucci, G., Sasso, G., Solimano, M., Marin, V., Muzio, C., Salmona, P. (2018). Geoheritage Values and Environmental Issues of Derelict Mines: Examples from the Sulfide Mines of Gromolo and Petronio Valley (Eastern Liguria, Italy). *Minerals*, *8*, 229.

Marescotti, P., Azzali, E., Servida, D., Carbone, C., Grieco, G., De Capitani, L., Lucchetti, G. (2010). Mineralogical and geochemical spatial analyses of a waste-rock dump at the Libiola Fe–Cu sulphide mine (Eastern Liguria, Italy). *Environ Earth Sci (2010), 61, 187-199. DOI 10.1007/s12665-009-0335-7.*

Marescotti, P., Carbone, C., De Capitani, L., Grieco, G., Lucchetti, G., Servida, D. (2008). Mineralogical and geochemical characterization of open-air tailing and waste-rock dumps from the Libiola Fe-Cu sulphide mine (Eastern Liguria, Italy). *Environ Geol DOI 10.1007/s00254-007-0769-8*.

Marini, L. Saldi, G., Cipolli, F., Ottonello, G., Vetuschi Zuccolini, M. (2003). Geochemistry of water discharges from the Libiola mine, Italy. *Geochemical Journal, Vol. 37, pp. 199 to 216.*

Provincia di Genova (2013). Ambito Regionale di Bacino 17. Piano di Bacino Stralcio sul rischio idrogeologico (ai sensi dell'art. 1, comma 1, del D.L. 180/1998 convertito in L. 267/1998) - Torrente Gromolo - Relazione Generale.

Scott, S. (1997). Submarine hydrothermal systems and deposits. *Geochemistry of Hydrothermal Ore Deposits (Barnes, H. L., ed.), 3rd ed., 797–875, Wiley, New York.*